



ScuDo

Scuola di Dottorato ~ Doctoral School
WHAT YOU ARE, TAKES YOU FAR



Doctoral Dissertation
Doctoral Program in Energy Engineering (31st Cycle)

Study of hybrid electric architectures for industrial vehicle applications using Hardware In the Loop techniques

Francesco Mocera

* * * * *

Supervisor

Prof. Aurelio Somà

Doctoral Examination Committee:

Prof. Eugenio Dragoni, Referee, University of Modena and Reggio Emilia

Prof. Fabrizio Scarpa, Referee, University of Bristol

Politecnico di Torino
March 12, 2019

I hereby declare that, the contents and organisation of this dissertation constitute my own original work and does not compromise in any way the rights of third parties, including those relating to the security of personal data.

A handwritten signature in black ink that reads "Francesco Mocera". The script is cursive and fluid.

.....

Francesco Mocera
Turin, March 12, 2019

Summary

The current situation about air quality all around the world is pushing governments to ratify stricter and stricter regulations on pollutant emissions from the different fields of activity of the human kind. As reported from worldwide independent organizations, ground vehicles and manufacturing activities play a big role on the overall pollutants production. In the transportation field, several improvements have been introduced in the last years to meet these regulations as demonstrated by the emissions comparison between modern cars and older ones. These improvements highlighted a big gap with another group of vehicles: Non Road Mobile Machineries or NRMM. These machines are mainly used in commercial and industrial activities and are equipped with bigger and more robust Diesel engines which however are not so clean as demonstrated by a large number of research activities. Up to now OEM Diesel engine manufacturers for off-road applications mainly focused the attention on limiting the amount of pollutants by using gas after-treatment systems. However, recently stricter regulations pushed them and working machines manufacturers towards the evaluations of alternative ways to reduce the emissions of their vehicles. Vehicle electrification demonstrated in the automotive field how the overall performance of a vehicle can be improved reducing the amount of pollutant emissions. This process is slowing involving also working machines although very few applications are already available as commercial products.

This work wants to focus the attention on the electrification process that is involving the NRMM field to understand what are the main challenges that are preventing the wide diffusion of this technology on these machines. Chapter 1 proposes an analysis of the actual EU legislation on vehicles pollutant emissions which aim to meet international Air Quality agreements. In this scenario the role of the electrification is to improve performance of traditional engines in hybrid solutions or to replace them when possible. Chapter 2 focuses the analysis on the

electrification process that is currently involving the field of working machines. The main solutions proposed in the three major working fields (Construction, Handling and Agriculture) are reviewed to highlight the different design strategies required for the electrification of existing architectures as well as for the design of new machines.

Although full electric and hybrid solutions are well consolidated in the automotive field, the actual state of the art of energy storage systems prevents the widespread adoption of this type of architecture for working machines. Chapter 3 analyses the different energy storage technologies available today, focusing the attention on the battery-based ones. Among several chemistries, Lithium-Ion based cells represent today the most promising solutions for powering electric vehicles. However, their performance must be continuously monitored to keep them working in well defined limits Safe Operating Area. To improve the understanding of this technology and prepare the modelling base for the architecture proposed in the next chapters, a modelling and characterization activity was performed on a prismatic Li-Ion cell. The cell model obtained was then used in the battery pack model presented in Chapter 4. Here, starting from the general overview of the current situation given in the previous chapters, the design of a hybrid working machines was explored. Given the strong experience and history of the research group in the field of agricultural machineries, the vehicle considered as case study for this work was an orchard tractor. Since no standard working cycles are prescribed in the literature for orchard tractors (and in general there is still a gap in defining standard working cycle in each sector of working machines) an extensive measurement activity during on field operations was performed to determine its working scenarios and load conditions. From this data, a hybrid architecture was designed and simulated on a numerical model which allowed to replicate the same conditions. The main goal of the design process presented in this chapter was to think about a hybrid solution which could impact as less as possible on the actual architecture of the current vehicle. Performance of the traditional architecture were compared to those obtained with the proposed hybrid one both in terms of peak power capabilities and daily work capabilities. The hybrid solution was equipped with a downsized Diesel engine to improve the overall emissions performance of the system. The electric system of the model was powered using the numerical model of a lithium ion cell studied and characterized with an extensive experimental activity, presented in Chapter 3. The control system of the hybrid architecture was developed with the same design approach: the system should be easily integrated on an existing architecture. Thus, a Master-Slave control strategy was developed in order to pair the control strategy of the electric system to the actual control

architecture of the Diesel engine. To optimize the amount of electric energy used due to the downsized engine a Load observer function modulated the intervention of the electric system according to the actual engine load. Finally, Chapter 5 describes how the proposed architecture was developed and implemented both at mechanical and control level in a Hardware-In-the-Loop bench. The proposed configuration allowed to test the architecture both in terms of mechanical and electrical performance. The control architecture was developed on the bench both in terms of hardware and software which was deployed on an automotive like control unit. One of the goals of the proposed HIL bench configuration was to validate the control strategy previously simulated using loading scenarios modelled and derived from the analysis performed in Chapter 4. The specific management software developed for this bench allowed to test both the traditional architecture and the hybrid one on the same bench in such a way that the same loading conditions could be applied to the two of them. Thus, the tests aimed to prove the feasibility of a plug and play solution both in terms of hardware components and management strategies.

*I would like to dedicate
this thesis to my family
and closest friends*

To them and in particular to my nephews I would like to dedicate the following citation as a reminder for staying strong when things seem to go in the opposite direction they would like them to go.

“Let me tell you something you already know. The world ain’t all sunshine and rainbows. It’s a very mean and nasty place and I don’t care how tough you are it will beat you to your knees and keep you there permanently if you let it. You, me, or nobody is gonna hit as hard as life. But it ain’t about how hard you hit. It’s about how hard you can get hit and keep moving forward. How much you can take and keep moving forward. That’s how winning is done! Now if you know what you’re worth then go out and get what you’re worth. But you gotta be willing to take the hits, and not pointing fingers saying you ain’t where you wanna be because of him, or her, or anybody! Cowards do that and that ain’t you! You’re better than that!” [cit. Rocky Balboa film]

Contents

1. Overview on the electrification process of industrial vehicles	1
1.1 World scenario on pollutant emissions	1
1.2 Regulations on pollutant emissions	4
1.3 EU legislation on vehicles emissions.....	5
1.3.1 Emissions standards for light duty vehicles	5
1.3.2 Emissions standards for Non-Road Mobile Machineries.....	8
1.4 Emissions control on Diesel engines	12
1.5 The role of electrification on vehicles emissions.....	15
1.6 Conclusions.....	16
2. Electrified powertrains in industrial applications	18
2.1 Electric and hybrid topologies for working vehicles	19
2.2 Hybridization factor for powertrain classification.....	23
2.3 Review of electric powertrains on industrial vehicles	25
2.3.1 Construction	25
2.3.2 Handling.....	29
2.3.3 Agricultural tractors	31
2.4 Working vehicles electrification: limiting factors	34
2.5 Conclusions.....	35
3. Study and characterization of Lithium - Ion cells performance for heavy duty applications	38
3.1 State of the Art analysis on energy storage systems.....	39
3.2 Secondary batteries for electric vehicles	44
3.2.1 Lead-acid batteries	45
3.2.2 Nickel-based batteries	45
3.2.3 Sodium-beta batteries (ZEBRA).....	46

3.2.4	Lithium Ion batteries	47
3.3	Battery management for lithium ion cells.....	50
3.3.1	BMS architectures	51
3.3.2	Cell Balancing	52
3.3.3	State of Charge estimation	53
3.3.4	State of Health estimation	56
3.3.5	State of Power estimation.....	57
3.4	Battery thermal management systems	58
3.5	Battery pack design and in vehicle integration.....	60
3.6	Lithium - Ion cells modelling and characterization	62
3.6.1	Coupled thermo-electric model of a prismatic Lithium Ion cell..	66
3.7	Battery testing activities.....	68
3.7.1	Battery testing system setup.....	68
3.7.2	Description of the Li-Ion prismatic cell under test	71
3.7.3	Open Circuit Voltage Characterization.....	72
3.7.4	Parameters identification and model validation.....	73
3.8	Conclusions.....	78
4.	Modelling of an electrified architecture for agricultural applications	83
4.1	Use case definition: study of an agricultural tractor	84
4.2	Experimental analysis on tractor performance	87
4.2.1	Methods.....	88
4.2.2	Field tests and data processing.....	89
4.3	Modelling and performance analysis of an electrified architecture for an orchard tractor	94
4.3.1	Modelling of a tractor.....	95
4.3.2	Simulation and validation of the model	102
4.3.3	Identification of an electrified architecture for an orchard tractor 107	
4.3.4	Modelling of the electric hybrid architecture.....	109
4.3.5	Performance analysis of the hybrid architecture.....	113
4.3.6	Performance comparison on working cycles	119
4.4	Conclusions.....	122

5. Hardware – In – the – Loop bench testing for hybrid electric vehicles and control strategies	125
5.1 Design and development of the HIL bench	126
5.1.1 Electro-mechanical layout.....	129
5.1.2 Control architecture and CAN BUS implementation.....	131
5.2 The Hybrid Control Unit.....	138
5.2.1 Development and hardware implementation of the control algorithm	139
5.3 Experimental tests.....	144
5.3.1 HIL tests	146
5.4 Conclusions.....	152

List of Tables

Table 1.1 Main air pollutants and their characteristics	2
Table 1.2 Emission standards for light duty vehicles (passenger cars)[1.6]-[1.7].	6
Table 1.3 Engine categories for NRMM.	9
Table 1.4 NRSC 8-mode cycle ISO 8174-4	10
Table 1.5 Stage I – V emission limits for land based NRMM (NRE)	11
Table 2.1 HF classification for electrified automotive powertrains.	23
Table 2.2 HF for hybrid cars.	24
Table 3.1 Lithium Ion chemistries performance	48
Table 3.2 SoC estimation methods.....	53
Table 3.3 SoH estimation methods	56
Table 3.4 Battery testing system components.....	70
Table 3.5 CUT key specification	71
Table 3.6 Thermal model parameters.....	73
Table 3.7 Electric model parameters.....	75
Table 4.1 Main characteristics of the orchard tractor under test.	89
Table 4.2 Through and across variables in a physical network model. ...	97
Table 4.3 Statistics of the considered PTO working scenario – Power (kW).	106
Table 4.4 Electric motor characteristics.	110
Table 4.5 Power unit Energy consumption (kWh):	119
Table 4.6 Hybrid unit normalized energy consumption	120
Table 5.1 Electric machines characteristics	130
Table 5.2 Monitoring message structure	134
Table 5.3 Control message structure	135
Table 5.4 Plant model parameters	136
Table 5.5 ICE mechanical characteristics (75 kW equivalent)	145

Table 5.6 ICE mechanical characteristics (54 kW equivalent) 145
Table 5.7 EM mechanical characteristics (30 kW equivalent) 145

List of Figures

Figure 1.1 Emissions' levels in the EU zone. Eurostat [1.3]	3
Figure 1.2 Driving cycles for vehicle emission (passenger car) type approval: a) NEDC, b) WLTP [1.8]	6
Figure 1.3 Normalized Non-Road Transient Cycle (NRTC) schedule [1.11]	10
Figure 1.4 Emission control system layout.....	14
Figure 2.1 Full electric architecture for a working vehicle	19
Figure 2.2 Parallel hybrid architecture for a working vehicle.....	20
Figure 2.3 Series hybrid architecture for a working vehicle.....	21
Figure 2.4 Traditional power split configuration.....	22
Figure 2.5 Power split configuration with electric machines	22
Figure 2.6 Common hybrid architecture for hybrid excavators [2.19]....	26
Figure 2.7 Hybrid architecture: Hitachi wheel loader [2.31].....	26
Figure 2.8 Hybrid architecture: Volvo L220F wheel loader [2.32]	27
Figure 2.9 Hybrid architecture: Volvo LX1 wheel loader [2.33]	27
Figure 2.10 Hybrid architecture: John Deere 944K wheel loader [2.35] ..	28
Figure 2.11 Hybrid architecture: Merlo TF 40.7 telescopic handler [2.18]	29
Figure 2.12 Hybrid architecture: Belarus 3022e tractor	31
Figure 2.13 Hybrid architecture: Rigitrac EWD 120 tractor	32
Figure 2.14 Hybrid architecture: Claas Arion 650 Hybrid tractor	33
Figure 3.1 Daily electric energy demand	39
Figure 3.2 Energy Storage Systems overview	40
Figure 3.3 Electrochemical cell.....	41

Figure 3.4 Flow battery	42
Figure 3.5 Fuel Cell.....	43
Figure 3.6 Ragone plot: secondary batteries performance.....	44
Figure 3.7 Lithium-Ion electrochemical cell.....	47
Figure 3.8 Battery management system layout for an electric vehicle	51
Figure 3.9 Battery management system layout for an electric vehicle	52
Figure 3.10 Indirect SoH analysis: a) ICA, b)DVA.....	57
Figure 3.11 Battery performance at lower temperatures [3.28].	60
Figure 3.12 Lithium Ion discharge curve (1C): Voltage – discharge capacity.	62
Figure 3.13 Equivalent circuit models: a) Rint, b) Thevenin,	63
Figure 3.14 Thermo-electric battery model.	66
Figure 3.15 Thevenin model, 2RC.	67
Figure 3.16 Thermal model implementation	68
Figure 3.17 CC-CV charging procedure.	69
Figure 3.18 Battery testing system [3.67].	70
Figure 3.19 Graphical User Interface NI LabVIEW [3.67].	70
Figure 3.20 Constant Current discharge: capacity evaluation.	71
Figure 3.21 VOC discharge test.	72
Figure 3.22 VOC charge test.	72
Figure 3.23 Voc evaluation.	73
Figure 3.24 Model response and experimental data Voc test.	75
Figure 3.25 Model response and experimental data for a	76
Figure 3.26 RMS error on voltage estimation for several standard tests	77
Figure 3.27 RMS error on temperature estimation for	77
Figure 3.28 Model response and experimental data for a	78
Figure 4.1 A modern tractor and its main functions	84
Figure 4.2: a) Drawbar structure, b) Three points hitch system	85
Figure 4.3: a) PTO output, b) PTO coupling shaft	85
Figure 4.4: Connectors for hydraulic auxiliary tools	86
Figure 4.5 Data acquisition setup: a) CAN Bus protocol analyser, b) J1939 to DB9 adapter, c) Personal computer for data storage	89
Figure 4.6 Transportation test – empty trailer 1400 kg	91
Figure 4.7 Transportation test – fully loaded trailer 6000 kg	91
Figure 4.8 Shredding test – PTO 540 rpm	92
Figure 4.9 Rotary harrow test – PTO 540 rpm	93
Figure 4.10 Atomizer test – PTO 540	93
Figure 4.11 Numerical model of a traditional tractor architecture	96

Figure 4.12 1D longitudinal tractor dynamic model	98
Figure 4.13 Gearbox model with logic clutches	99
Figure 4.14 Equivalent polynomial engine map	100
Figure 4.15 Engine speed controller	101
Figure 4.16 Model input signals: transportation test – trailer 6000 kg.	102
Figure 4.17 Vehicle speed comparison: Model vs Experimental data	103
Figure 4.18 Engine performance comparison: Model vs Experimental data	103
Figure 4.19 Model input signals: transportation test – trailer 1400 kg.	104
Figure 4.20 Engine performance comparison: Model vs Experimental data	105
Figure 4.21 Engine performance comparison: Model vs Experimental data	106
Figure 4.22 PTO equivalent load	107
Figure 4.23 Physical network model of the hybrid parallel architecture	111
Figure 4.24 Physical network model of the battery pack	112
Figure 4.25 Electric motor controller	113
Figure 4.26 Power units performance comparison	115
Figure 4.27 Power units performance comparison	116
Figure 4.28 Power units performance comparison	117
Figure 4.29 Power units performance comparison	118
Figure 5.1 V-diagram and system engineering approach	126
Figure 5.2 Hardware-In-the-Loop simulations	128
Figure 5.3 HIL Bench	129
Figure 5.4 HIL Bench: mechanical couplings	130
Figure 5.5 HIL Bench Layout	131
Figure 5.6 ECU custom board: digital and analogue sections	132
Figure 5.7 PWM control signal	133
Figure 5.8 RC low pass filter of the control signal	134
Figure 5.9 PI speed controller response of the ICE electric drive (full load)	137
Figure 5.10 PI speed controller response of the ICE	137
Figure 5.11 Master-slave control strategy with	139
Figure 5.12 Hybrid Control Unit	140
Figure 5.13 HCU software architecture	142
Figure 5.14 HCU Application architecture	143
Figure 5.15 HCU Processing function	143

Figure 5.16 Atomizer test – Diesel 75 kW (equivalent)	149
Figure 5.17 Shredder test – Diesel 75 kW (equivalent)	149
Figure 5.18 Rotary Harrow test – Diesel 75 kW (equivalent)	150
Figure 5.19 Atomizer test – hybrid parallel	150
Figure 5.20 Shredder test – hybrid parallel	151
Figure 5.21 Rotary Harrow test – hybrid parallel	151

Chapter 1

Overview on the electrification process of industrial vehicles

Air quality is one of the most discussed topics since the 1970s when for the first time the problem was faced at international level. The transboundary nature of the problem pushed the most developed countries to sign agreements targeting the limits for the most harmful air pollutants. To meet these limits, special legislations for all the main activity fields of the human kind were required. In this chapter, the focus will be on the EU legislation on Road and Non-Road vehicles. These legislations must be known and clearly understood by the actors involved in the electrification process. The standards are becoming every year stricter and stricter to meet international regulations. For the traditional propulsion systems, gasoline and diesel engines, it will soon be impossible to meet both the power requirements of the application and the emissions limits. This is the main reason why manufacturers are seriously considering electrification as a viable solution to satisfy performance and future emissions requirements.

1.1 World scenario on pollutant emissions

The Human kind has continuously tried to pursue a better living condition from the beginning of its relatively long history. However, every action taken in this direction has always had an impact on the ecosystem we are living in. And now, this is clearer than ever. Environmental pollution can be declined in several ways depending on the physical form of the contaminants: air pollution, plastic pollution, soil contamination and water pollution are several faces of the same global problem. Air pollution has high impact both on the environment and the human kind itself. According to [1.1], its main effects on the environment can be classified in:

- Eutrophication of soil and water; it consists of an anomalous quantity of nutrients that helps the rise of new species (like algal blooms in water) that change the ecosystem and its biodiversity;

Pollutant	Description	Impact on	Precursor to
Particulate matter (PM)	Particles of various sizes and chemical compositions. PM ₁₀ (PM _{2.5}) are 10 (2.5) micrometres or smaller. These particles can be emitted by natural sources (volcanic ash, suspended dust, pollens) as well as by anthropogenic sources (combustion, heating, transport, industry, agriculture, etc.). Secondary PMs can form from emissions of SO ₂ , NO _x , and NVMOCs	Health Climate	-
Ozone (O ₃)	Is the result of chemical reactions involving some precursor pollutants (NO _x , CO, NMVOCs and CH ₄) and sunlight	Health Environment Climate	-
Nitrogen Oxides (NO _x)	Mainly refers to Nitrogen monoxide (NO) and Nitrogen dioxide (NO ₂). They come from fuel combustion in the energy industry and in transports (especially from diesel engines)	Health Environment	Ozone PM
Sulphur dioxide (SO ₂)	Mainly related to combustions of high sulphur fuels	Health Environment	PM
Ammonia (NH ₃)	Emitted mainly by fertilisers used in agriculture	Health Environment	PM
Non-Methane Volatile Organic Compounds (NVMOCs)	They come from anthropogenic sources like solvents, paints and road transports as well as from the vegetation itself	Health	Ozone PM
Benzene (C ₆ H ₆)	Volatile organic compound emitted by combustion of fuels and industrial processes	Health	Ozone
Carbon monoxide (CO)	Related to incomplete combustion	Health	Ozone
Methane (CH ₄)	Produced by anthropogenic sources (especially agriculture, waste and gas extraction) as well as by natural sources	Climate	Ozone
Metals (Pb, Cd, Hg, As, Ni)	Metals are usually the products of fuel combustions as well as industrial processes	Health Environment	

Table 1.1 Main air pollutants and their characteristics

- Acidification of soil and water with different pH levels that damage plants and animals
- Damage to vegetation, especially affecting plants growth rates.

Air pollution is an identifier to address a more complex problem related to the emission in the atmosphere of several dangerous substances. The ones directly emitted by human activities are called primary pollutants. However, they can react with other chemicals in the air leading to the formation of other harmful products called secondary pollutants. The former can be defined as the precursors to the latter. In Table 1.1 the main pollutants and their characteristics are shown, with the major anthropogenic sources highlighted in Figure 1.1 (for further details see [1.1]-[1.3]). Data show the fact that each field affects significantly the amount of at least one dangerous pollutant. Agriculture dominates the emission of ammonia. Industrial processes mainly affect the amount of NMVOC. Road transports have a huge impact on NOx production. Energy production and distribution produces both nitrogen and sulphur dioxides. It is worth to mention that because of heating, commercial activities and residential buildings have a quite significant role on the annual emission of most of the pollutants.

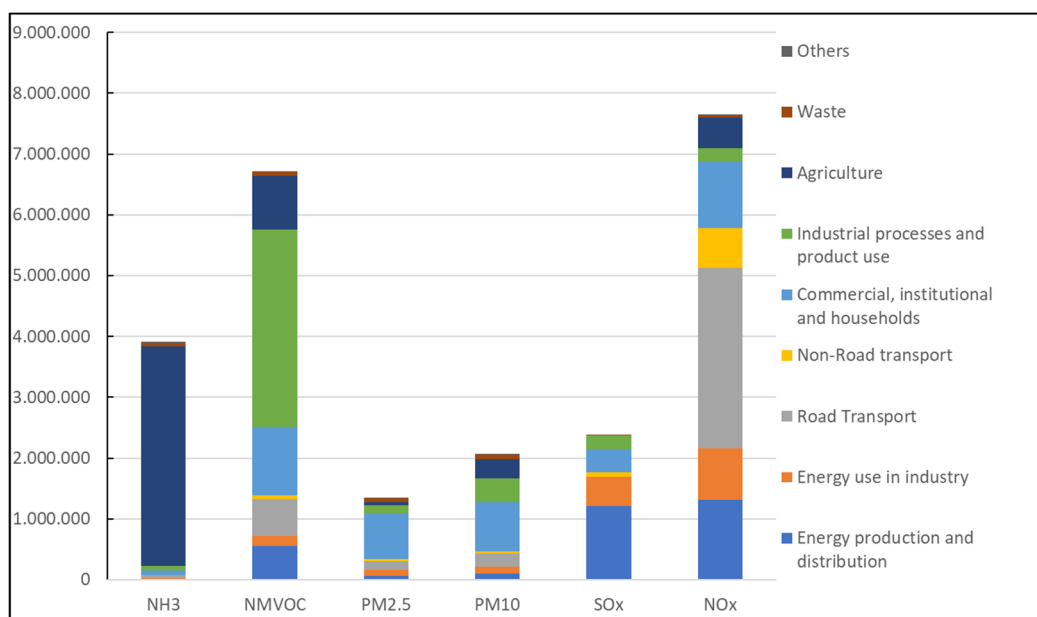


Figure 1.1 Emissions' levels in the EU zone. Eurostat [1.3]

Altering the ecosystem, we are living in irreversibly affects ourselves and threat human health. For the World Health Organisation (WHO) [1.4], the exposure to air pollution is the biggest environmental risk to human health increasing the incidence of respiratory and cardiovascular diseases. Moreover, the Agency for Research on Cancer has classified some pollutants as carcinogenic compounds. Involving human health, it is clear the huge economic cost associated as highlighted also in [1.5] by the Organisation for Economic Cooperation and Development (OECD). Not only there is an additional cost for public health, but also crop yields have lower productivity, and tourism is strongly influenced.

For all these reasons, air pollution has become one of the hottest topics since the 1970s when the transnational nature of the problem was officially acknowledged by several international conferences. The very first international agreement, the United Nation Framework Convention on Climate Change (UNFCCC), was signed in 1992 during the Earth Summit in Rio de Janeiro. The main outcomes of UNFCCC were to stabilize the greenhouse gases (GHGs) emissions at levels not dangerous for human health and with rates ecosystems could easily adapt to. This agreement was ambitious, but soon it appeared to be unpractical because resolutions adopted by all the UN members did not satisfy the signed timetable. To increase the effectiveness of action towards air quality protection, the Kyoto Protocol was approved in 1997. This protocol legally obliged developed countries to meet their emissions targets in the period 2008-2012. The extension to the period 2012-2020 was discussed in Doha, Qatar, on 8 December 2012. Although several years passed, by the end of 2018 only 122 countries out of the 144 required ratified the agreement, preventing its actual entry into force. The most criticized point of the Kyoto protocol, that prevented the ratification by the U.S government was and is still today the exception of some countries still considered developing as China and India. The protocol was considered too dangerous for the U.S economy in the moment of the economic explosion of China, thus was not ratified. Another important step within the UNFCCC was the Paris Agreement which set a long-term goal of holding the global warming below 2°C above the average temperature of the pre-industrial phase. This agreement, effective since November 2016, has been described as the first comprehensive climate agreement and the first driver towards fossil fuel divestment. International agreements set the main goals. Each signing country has the freedom to propose specific plans and legislations to achieve the goals.

It is worth to mention that climate change and air pollution are not exactly the same thing as discussed in [1.2]. The former is mainly related to the release into the atmosphere of GHGs while the second is related to the concentration of pollutants over a specific area. The phenomena are intimately related to each other since the main sources for both are combustion and other anthropogenic activities. However, some pollutants are actually slowing down global warming. Thus, each climate action and air quality legislation must consider that reducing the emission of some pollutants does not linearly relate to the overall temperature growth rate.

1.2 Regulations on pollutant emissions

Air quality is an international topic and worldwide measures are required to achieve the same shared goals. Historically, the two main actors have been the U.S and E.U with independent legislations voted to achieve air quality protection/improvements.

The first relevant step towards air pollution control of the U.S. was the Clean Air Act (CAA-1963). This federal law, updated in 1970, fixed limits for the six major air pollutants: SO₂, NO₂, CO, O₃, PM, and lead. Moreover, the Environmental Protection Agency (EPA) was assigned to watch over each federal

state implementation of the air quality standards in the CAA. If the implementation plan did not satisfy CAA standards, severe sanctions were applied. However, some states proposed Air pollution control plans even stricter than the CAA. This was the case of the California Air Resources Board (CARB) that set very stringent limits on vehicles emissions, considered one of the most influent contributors of particulate matter.

On the other side, the EU started its air quality activities in 1979 with the Long-Range Transboundary Air Pollution (LRTAP). From there, a long series of directives, amendments and recommendations were promoted on several pollutant elements. The very first comprehensive directive was ratified in 1996 by the EU. It was the Directive 96/62/EC, 1996 (Directive on Ambient Air quality Assessment and Management) which main contribution was to set limits for air pollutants that could affect human health above those levels. Then, more specific directives were introduced to regulate emissions from stationary sources and ground vehicles. The European Environmental Agency (EEA), established in 1990 with the Regulation 1210/90/EEC, has the role of watching over the air quality results of each state. The scientific analysis that the agency regularly must provide can be used by the European Commission (EC) to send warnings of legal actions to those Member States (MS) that were not able to meet certain standard limits and did not ask for prolongation of established deadlines. In these terms, the role of the EU is to put pressure on states that do not meet the requirements, but there is not enough power to directly promote legal sanctions as in the case of the U.S. EPA. In that case, if a state implementation plan does not satisfy some standard of the CAA, it can be directly persecuted by the law through EPA sanctions.

1.3 EU legislation on vehicles emissions

The EU is particularly committed in air quality protection. However, the different structure between the EU and the US reduce the effectiveness of each measure taken due to self-protective behaviour of the involved entities that want to protect their economic interests. In the following sections, a brief review of the current EU standards in force for automotive vehicles and Non-Road Mobile Machineries (NRMM) is given.

1.3.1 Emissions standards for light duty vehicles

The beginning of EU legislation on motored vehicles can be identified with the Directive 70/220/EEC del 1970. This document stated for the first time the need for type-approval tests on new vehicle focused on the amount of pollutants emitted. The attention was initially focused on carbon monoxide and hydrocarbons, but with a series of amendments up to 2004, the basic structure of the directive was expanded including also other pollutants as can be seen in Table 1.2. Today, Euro 5 and 6 standards (and related extensions) are based on the Regulation 715/2007 and its following amendments. These standards are defined for light duty vehicles (LDVs)

Stage	Date	CO*	HC*	HC+NO _x *	NO _x *	PM*	PN**
Gasoline							
Euro 1	1992	2.72		0.97			
Euro 2	1996	2.2		0.5			
Euro 3	2000	2.3	0.2		0.15		
Euro 4	2005	1	0.1		0.08		
Euro 5	2009	1	0.1		0.08	0.005	
Euro 6	2014	1	0.1		0.08	0.005	6x10 ¹¹
Diesel							
Euro 1	1992	2.72		0.97		0.14	
Euro 2	1996	1		0.7		0.08	
Euro 3	2000	0.64		0.56	0.5	0.05	
Euro 4	2005	0.5		0.30	0.25	0.025	
Euro 5a	2009	0.5		0.23	0.18	0.005	
Euro 5b	2011	0.5		0.23	0.18	0.005	6x10 ¹¹
Euro 6	2014	0.5		0.17	0.08	0.005	6x10 ¹¹
* measured in g/km							
** measured in number of particles/km							

Table 1.2 Emission standards for light duty vehicles (passenger cars)[1.6]-[1.7].

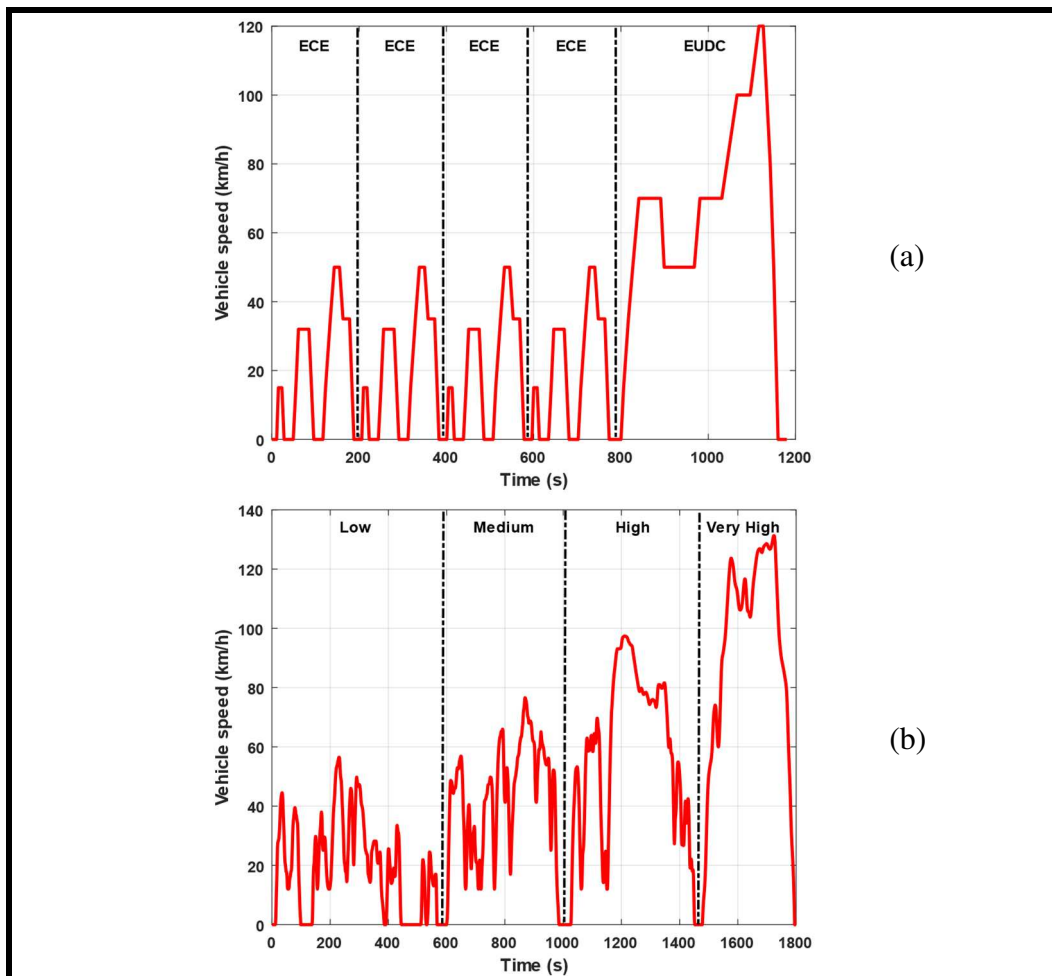


Figure 1.2 Driving cycles for vehicle emission (passenger car) type approval: a) NEDC, b) WLTP [1.8]

and apply to passenger cars (category M₁₋₂) and small commercial vehicles (category N₁, N₂).

The most critical and discussed part of these standards are the methodologies defined to assess the amount of emitted pollutants. For instance, from the very first directive in 1970 up to 2017, the official test for emissions evaluation of passenger cars was the New European Driving Cycle (NEDC) shown in Figure 1.2(a). It consists of a series of 4 Urban Driving Cycles (UDC) to simulate an urban like loading scenario followed by an Extra Urban Driving Cycle (EUDC) to simulate the extra urban loads. The test has a duration of 1180 s (267 s of idling time) for a total “equivalent travelled distance” of 10.93 km on flat road at 25 °C. Although the standardization of testing procedures helps for results repeatability and comparability, NEDC received lots of criticisms in the last years for its outdated vision of car performance and usage. Thus, in 2017 the new World Harmonised Light vehicle Test Procedure (WLTP) shown in Figure 1.2(b) came into force replacing the NEDC as type approval testing standard for light duty vehicles. It is defined as the combination of 3 or 4 smaller cycles representing a loading scenario (Low, Medium, High). The innovative approach of this testing procedure is that several loading scenarios are defined depending on which type of vehicle is under test. Based on the power to weight ratio and to its maximum speed, a passenger car category can be identified and consequently its testing procedure.

The adoption of a new standard testing cycle helps in improving the fidelity of laboratory tests but cannot prevent questionable approaches of car manufacturers. In 2015, the diesel gate that involved Volkswagen focused the attention towards a real deficiency in the legislation on emissions standards. If test standardization helps for repeatability and comparability, on the other hand it is relatively easy to hack in order to improve performance. What the diesel gate highlighted was the possibility to program Engine Control Unit (ECU) to identify specific working condition adapting engine performance to meet certain requirements. Thus, the ECU can recognize the loading cycle of the type approval test and change some calibration parameters in order to decrease engine performance and meet emissions requirements. As the International Council on Clean Transportation highlighted [1.9], a high number of vehicles tested on real driving conditions with Portable Emissions Measurement Systems (PEMS) resulted in pollutants emission above the manufacturer declared values. Together with the adoption of the WLTP, the diesel gate pushed the EU Commission to also consider the adoption of Real Driving Emissions (RDE) tests with PEMS to measure emissions on real working conditions. Although RDE seems the most promising solution several obstacles prevent to the full adoption of these tests in the type-approval procedure (together to the laboratory tests). The main reasons are related to the opposition that car manufacturers are moving due to objective lacks in the definition of these procedures and to the intrinsic variability that a road test would include on such a delicate measurement. Moreover, the actual state of the art PEMSs are not able to guarantee the same level of accuracy of laboratory equipment. What was dealt in the last years was the adoption of conformity factors that correlate results obtained on RDEs with those obtained with laboratory tests, taking into account variability

of the testing conditions and accuracy level of PEMS. Essentially, the RDE emissions are considered compliant to laboratory tests if the emission of a certain pollutant is CF (Conformity factor) times the quantity measured in controlled environments. Or in other terms, the test is considered valid if the measured quantity is below CF times the emissions limit for that pollutant.

It is clear that after the diesel gate, the EU is increasing pressure on car makers and trying to set up a US like emissions regulation. The introduction in the type approval process of an RDE already is a big step forward that is not considered in the US regulations. Moreover, it is still under discussion the proposal of including an in-service control test to make sure that wear and usage does not affect emissions above certain limits. This procedure is already established in the US and could represent a breakthrough on this topic, forcing manufacturers to design systems whose performance are reliable over an extended period of time. However, the diesel gate highlighted the lack of proper legislation on what the ECU software can and cannot do during testing procedures. The overcoming of these regulatory flaws will be the main goal of the European Commission in the upcoming years.

1.3.2 Emissions standards for Non-Road Mobile Machineries

According with the definition given in [1.10]-[1.12], a Non-Road Mobile Machinery (NRMM) is any vehicle with an internal combustion engine which is not mainly used in on road transportation of people and goods. Within this definition, are comprised:

- Small gardening and handheld equipment;
- Construction machineries;
- Handling machineries;
- Agricultural and farming machineries;
- Snow-plough equipment;
- Railcars, locomotives and waterway vessels.

Agricultural tractors and forestry machineries are directly included in this definition, because have specific regulations [1.13].

Several independent studies from all around the world [1.14]-[1.16] have recently demonstrated that due to the improvements in emissions in road transportation, NRMMs have climbed the ranking of the most relevant sources of pollutants. For this reason, several international organizations started to regulate emissions also on this type of machines. The European Commission first directive on the topic is dated 1997 [1.10], when the first restrictions on carbon monoxide, hydrocarbons, oxides of nitrogen and particulate matter were stated. One important difference between regulations for NRMMs and LDV ones is the focus not on the vehicle itself, but on its power unit. Emissions regulations are not strictly meant for NRMMs manufacturers but also for engines' OEMs. As shown in Table 1.3 the EU

Regulation in [1.12] defines 10 engine categories depending on their application and, in some cases, on their power range.

Category	Application	Power range
NRE	Mobile NRMMs	< 560 kW
NRG	Generating sets	> 560 kW
NRSh (SI)	Handheld machineries	< 19kW
NRS (SI)	Engines not in NRSh	< 56 kW
IWP	Inland waterway vessels	> 19kW
IWA	Auxiliaries engines	> 19kW
RLL	Locomotive propulsion	-
RLR	Railcars propulsion	-
SMB (SI)*	Snowmobiles	-
ATS (SI)*	All-Terrain Vehicles	-
*SI – Spark Ignition		

Table 1.3 Engine categories for NRMM.

The 2004 EU regulation for NRMM [1.11] prescribes two types of dynamometer test cycles for emissions evaluation:

- The NRSC (Non-Road Steady Cycle) where the warmed-up engine is loaded at several steps with a specific combination of speed and engine load Table 1.4. At each steady state condition emissions are measured. For each pollutant, the combination of the measured quantities weighted with factors different for each step must meet the emissions limits. The EU regulation prescribes this test especially for gaseous pollutants measurements.
- The NRTC (Non-Road Transient Cycle) where the engine is loaded with a high dynamic load profile (Figure 1.3). The test is run twice: with all the temperatures stabilised at room temperature (cold start); immediately after the cold cycle, when all the operating temperatures are near the nominal ones (hot start). The emissions are measured in both the tests and are combined with weighting factors (10% - cold, 90% hot). This combination must meet the emissions prescribed by the standard. Although these tests are prescribed for particulate matter measurements, the EU regulation admits its use also for gaseous pollutants.

In both tests, engine and dynamometer signals are stored. Emissions limits are prescribed in g/kWh so the work done by the engine (time integral of product between speed and torque) must be calculated and related to the amount of pollutants measured. The emissions limits are prescribed for each category, depending on the power range and in some cases, with differences between Spark

Ignition (SI) and Compression Ignition engines (CI). In Table 1.5, the evolution from stage I to the most recent stage V emissions limits for NRE engines is shown.

Mode	Engine speed	Engine load (%)	Weight factor
1	Rated speed	100	0.15
2	Rated speed	75	0.15
3	Rated speed	50	0.15
4	Rated speed	10	0.1
5	Intermediate speed	100	0.1
6	Intermediate speed	75	0.1
7	Intermediate speed	50	0.1
8	Idle	-	0.15

Table 1.4 NRSC 8-mode cycle ISO 8174-4

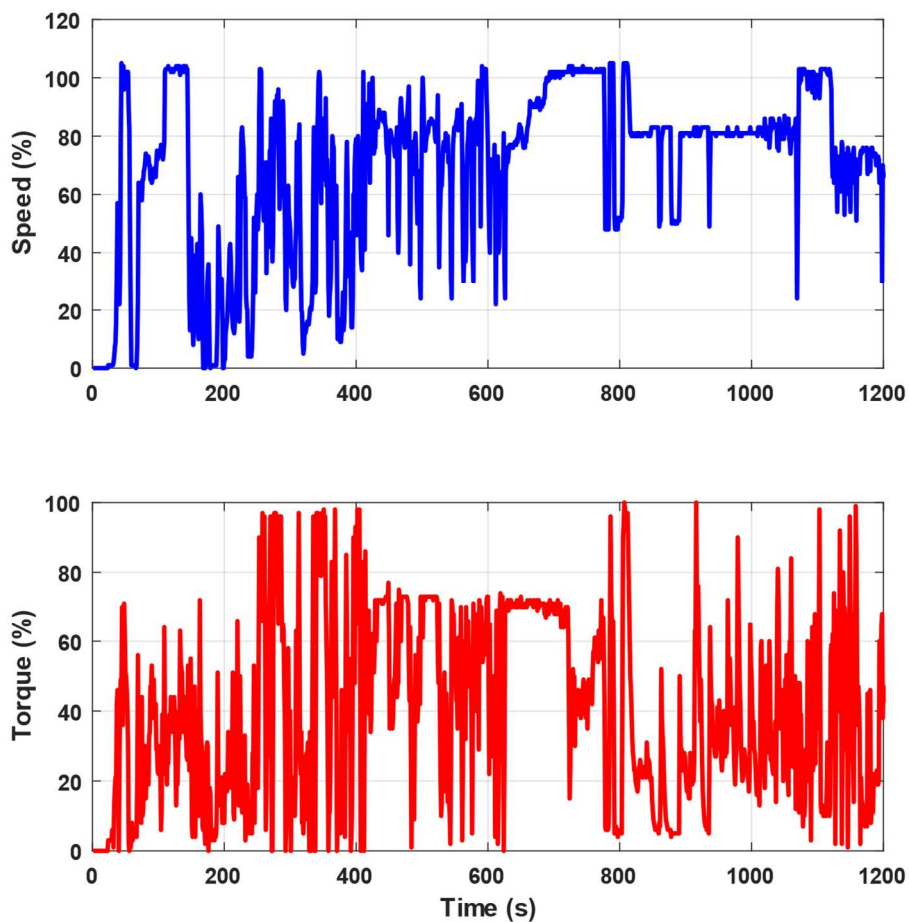


Figure 1.3 Normalized Non-Road Transient Cycle (NRTC) schedule [1.11]

Power range	Ignition type	CO	HC	NO _x	PM	PN
kW		g/kWh				#/kWh
Stage I (1999)						
35 ≤ P < 75	CI	6.5	1.3	9.2	0.85	-
75 ≤ P < 130	CI	5.0	1.3	9.2	0.70	-
130 ≤ P ≤ 560	CI	5.0	1.3	9.2	0.85	-
Stage II (2001-2004)						
18 ≤ P < 37	CI	5.5	1.5	8.0	0.8	-
37 ≤ P < 75	CI	5.0	1.3	7.0	0.4	-
75 ≤ P < 130	CI	5.0	1.0	6.0	0.3	-
130 ≤ P ≤ 560	CI	3.5	1.0	6.0	0.2	-
Stage III A (2006-2008)						
19 ≤ P < 37	CI	5.5	(HC+NO _x) ≤ 7.5		0.6	-
37 ≤ P < 75	CI	5.0	(HC+NO _x) ≤ 4.7		0.4	-
75 ≤ P < 130	CI	5.0	(HC+NO _x) ≤ 4.0		0.3	-
130 ≤ P ≤ 560	CI	3.5	(HC+NO _x) ≤ 4.0		0.2	-
Stage III B (2011-2013)						
37 ≤ P < 56	CI	5.0	(HC+NO _x) ≤ 4.7		0.025	-
56 ≤ P < 75	CI	5.0	0.19	3.3	0.025	-
75 ≤ P < 130	CI	5.0	0.19	3.3	0.025	-
130 ≤ P ≤ 560	CI	3.5	0.19	2.0	0.025	-
Stage IV (2014)						
56 ≤ P < 130	CI	5.0	0.19	0.4	0.025	-
130 ≤ P < 560	CI	3.5	0.19	0.4	0.025	-
Stage V (2019-2020)						
0 < P < 8	CI	8.0	(HC+NO _x) ≤ 7.5		0.40	-
8 ≤ P < 19	CI	6.6	(HC+NO _x) ≤ 7.5		0.40	-
19 ≤ P < 37	CI	5.0	(HC+NO _x) ≤ 4.7		0.015	1x10 ¹²
37 ≤ P < 56	CI	5.0	(HC+NO _x) ≤ 4.7		0.015	1x10 ¹²
56 ≤ P < 130	All	5.0	0.19	0.40	0.015	1x10 ¹²
130 ≤ P < 560	All	3.5	0.19	0.40	0.015	1x10 ¹²
P ≥ 560	All	3.5	0.19	3.5	0.045	-

Table 1.5 Stage I – V emission limits for land based NRMM (NRE)

Two considerations can be made looking at the limit values shown above. From Stage IIIB emissions limits have dropped consistently thanks to the advancement in exhaust after treatment technologies (see next section). However, these major constraints have been imposed always to engines with a rated power greater than 56 kW. The main reason can be searched in the costs of all the systems required to meet these emissions limits. Low power engines are usually installed in small

machines where the increase in the cost related to after treatment systems could determine the death of the product on the market. On the other hand, high power engines are usually installed on much bigger machines where the cost of the power unit is relatively smaller compared to the other on-board technologies. Thus, these machines can admit an increase of the overall cost to improve emissions performance.

The second consideration is related to the newest Stage V emission standard that will officially enter in force during 2019. Two major measures have been introduced: the particles counting in the exhaust gas for engines from 19 to 560 kW clearly derived from on road vehicles legislations; the extension of emissions limits also to Spark Ignition engines above 56 kW. The latter is related to the recent adoption of gasoline, gas (methane) or bi-fuel engines on several NRMMs. In the specific case of bi-fuel engines, a Gas-Energy-Ratio (GER) must be determined to identify how much of the energy supplied during the test was coming from the gaseous or liquid fuel source. The hydrocarbons emissions limit changes depending on the actual GER occurred during the cycle.

1.4 Emissions control on Diesel engines

As discussed in the previous sections, nowadays emissions regulations address most of the traditional propulsion systems (CI and SI). Historically, Diesel engines are known for their high efficiency, durability and reliability. For these reasons, they have been widely adopted in heavy duty transportation and off-road application, where low operating costs related to maintenance and fuel efficiency translate to high saves. Despite of the high performance over total cost of ownership ratio of this type of propulsion technology, the diesel engine has been addressed by many researcher and non-academic authorities as one of the greatest contributors to air pollution. The use of such propulsion system in heavy duty applications amplifies this aspect. As a matter of fact, NRMM emission regulations have historically addressed CI engines rather than SI engines, at least the oldest ones.

To meet emissions limits for Diesel engines, several strategies have been developed over the years to compensate the not perfect combustion of the fuel [1.17]-[1.18]. This can be related to several factors like the air fuel ratio, ignition timing, level of turbulence in the combustion chamber and so on. Among all the undesired products CO, HC, PM and NO_x are the most addressed by today emissions control systems. NO_x emissions reduction has been the driving element in the development of the most widely adopted emissions control systems since they have the highest percentage among all the undesired combustion products. Three main technologies can be mentioned for NO_x emissions management.

Exhaust Gas Recirculation (EGR). Some of the exhaust gas are sent back into the combustion chamber to be mixed with new fresh air. The result of this action is a worse combustion because of the lower percentage of free oxygen. Thus, the inefficient combustion reaches lower temperatures so lower NO_x production. The problem with this technology is that a worse combustion increases the production

of other pollutants (especially CO and HC) thus this system cannot work alone on a Diesel-powered vehicle.

Lean NO_x Trap (LNT). Lean burn engines and especially Diesel engines present a the relatively high amount of Oxygen available in the exhaust gas because of the excess of O₂ in the combustion chamber compared to the required stoichiometric quantity. A higher percentage of free O₂ leads to higher production of NO_x due to the presence in the intake air of free N₂. The LNT literally trap some of the NO_x available in the exhaust gas when the production is higher due to leaner mixtures required by the working condition. They are stored as barium nitrates (Ba(NO₃)₂) due to the presence of barium oxide (BaO) and barium carbonate (BaCO₃) in the base metal coating of the device structure. During heavy working conditions when a fuel-rich mixture is required (or periodically injecting a higher amount of fuel then required), the related excess of HC, CO, H₂, combines with the metals inside the device thus also the barium nitrates and releases the previously stored NO_x. It is worth to note that the fuel rich mixture determines also lower NO_x production. Thus, the results are lower NO_x emissions on fuel-lean mixtures, and slightly higher production with fuel-rich ones. A well-designed engine should not require fuel rich mixtures so often, thus the beneficial effect of the LNT that, however, would require periodically controlled regeneration with richer mixtures.

Selective Catalytic Reduction (SCR). This process prescribes the injection of a reductant element (ammonia, urea or others) into the exhaust stream before entering a specific catalyst element. Using ammonia (NH₃) as reductant, NO_x and O₂ combines leading to N₂ and H₂O as primary product but also to ammonium sulphate ((NH₄)₂SO₄) when there is an excess of sulphur contents in the exhaust stream (due to the use of a sulphur rich fuel). Similarly, the use of urea ((NH₂)₂CO) lead to N₂ and H₂O as primary products and CO₂ as undesired product. In both cases, the SCR process reduce the amount of NO_x emissions increasing the amount of other pollutants: ammonium sulphate can react in the atmosphere producing sulphuric acid that will affect landscapes; CO₂ have an impact on global warming.

Diesel Oxidation catalyst (DOC). It is a catalyst for oxidation of CO, HC and some organic compounds among all the PM. The main products from the oxidation of CO and HC are CO₂ and H₂O. The abundancy of oxygen in the catalyst helps also the oxidation of sulphur compounds (SO₂ and SO₃) and the formation of gaseous sulphuric acid. This, combined with water molecules leads to hydrated sulphuric acids or sulphate particulates which is considered also as PM.

On Diesel engines, Particulate matter is the second highest (in percentage) pollutant emitted. The most effective solution is physical filtration of exhaust gas. A Diesel Particulate Filter (DPF) is a honeycomb structure made by porous walls which mechanically filter the exhaust gas stream that goes towards the tailpipe. The porosity and shape of the filter walls are designed to trap PM on the filter surface without a relevant pressure drop. However, as the filter become saturated by the amount of PM trapped, an increase of the pressure drop is inevitable thus a backpressure is added at the outlet of the combustion chamber which decreases the overall performance. Thus, periodically the PM trapped must be burnt to not negatively impact on engine performance. Two possible regeneration modes of the

DPF are available. The nominal mode of operation, or passive regeneration, considers that during high load working conditions, exhaust gas temperatures are high enough to activate the combustion between the PM in the filter and a catalyst inside it. The worst-case scenario is when the load cycle is not demanding enough to increase exhaust gas temperatures at the point to “ignite” the passive regeneration. In this case, a controlled active regeneration is periodically scheduled. An external heater, the use of a fuel burner on the exhaust pipe and some latency in fuel injection into the combustion chamber are some of the possible active ways to increase gas temperatures. However, each active system comes with an increase in fuel consumption. In Figure 1.4 an implementation of a standard emission control system is shown.

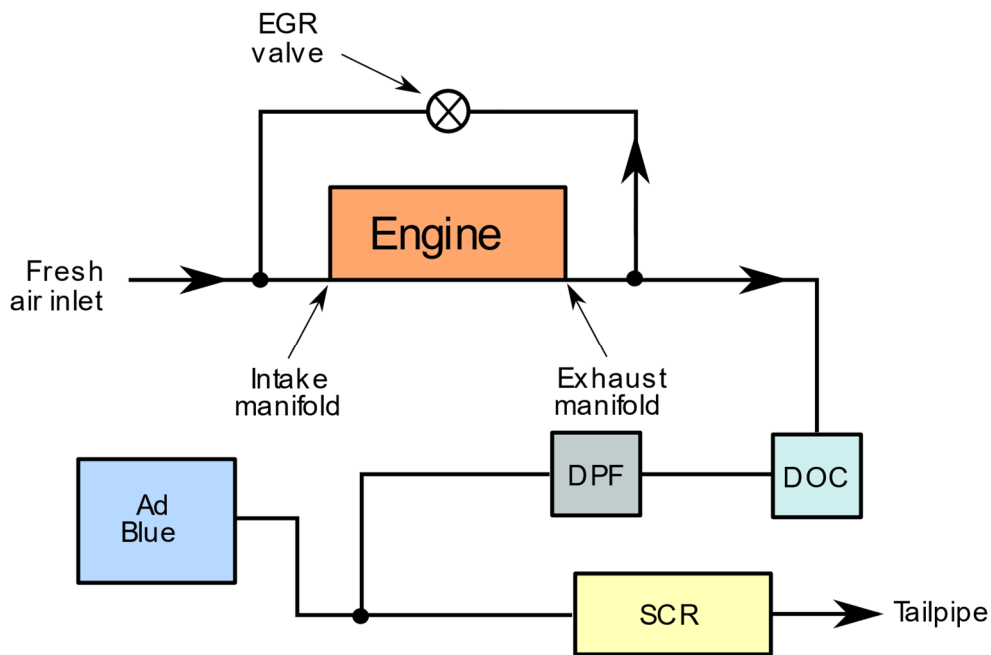


Figure 1.4 Emission control system layout

What was just described, considered mainly external aftertreatment devices which act on the overall products of the combustion happened inside the engine. However, the cleverest way to reduce pollutant emissions is to improve the combustion itself with proper calibration of the mixture quantities depending on the operating conditions, which translates in better engine efficiency. Or, depending on the actual condition and feedback from all the aftertreatment devices, a better air/fuel ratio can be adopted to improve on the emission side at the price of some performance loss. Nevertheless, the best absolute way to reduce emissions is to burn less fuel for the same work. Research activities at academia and industrial level are focused on engine optimizations in all its aspects. However, this technology is a very mature and consolidated one (it has more than a century of history), thus every improvement now comes at very high development price. This is the reason why, powertrain and machine optimizations are becoming more and more relevant to improve the overall performance of the vehicle.

1.5 The role of electrification on vehicles emissions

As previously discussed, the most effective way of reducing pollutant emissions is the overall improvement of machine performance. The better use of the energy the engine can provide reduce the amount of fuel, thus of combustion products, required to accomplish a certain task. For many years, the Internal Combustion Engine (ICE) has been the main source of mechanical power for almost any vehicle. The need for higher efficient “systems” has pushed towards alternative solutions where the ICE is no more the unique power source neither, in some cases, is considered as element of the power unit. This is the case for electrified powertrains.

The use of electricity to propel vehicles is not so innovative and it can be dated at the end of the 18th century with the invention of the electric motor itself. The low oil price and the greater investments in research and development, put the ICE in great advantage as propulsion system for almost one century. Nowadays, the need for more efficient power units is giving a new chance to this technology both for passenger vehicles and, more recently, for NRMMs. As further discussed in Chapter 2, powertrain electrification can take place on several levels. Electric components can just help an ICE during certain operating condition using the energy stored on a suitable storage system, can help it in more complex powertrains to achieve overall better performance or can totally replace it powering a vehicle in all its working conditions. Each level of electrification has its own advantages and disadvantages. However, it has been proved [1.19]-[1.20] how the use of more efficient and flexible components can help the overall machine performance. More recently researchers started to focus their attention also on real world emissions measurements of the very firsts electrified working vehicle [1.21]. These studies showed how higher overall machine efficiency has been achieved but still margins for improvements on emissions are available. Depending on the electrification level, some aftertreatment systems can be removed, others like the DPF still are necessary.

The higher is the degree of electrification, the bigger will be the impact of this technology once the production of electric energy from renewables and other cleaner sources (like nuclear fusion) will become ordinary. The electrification of standard powertrains is a step required to move away from fossil fuel dependency. At this moment, since the greater part of our energy availability is related to fossil fuels (oil and coal) electrified vehicles can improve air quality only in the measure of an increase in the tank-to-wheel efficiency. The higher is the degree of electrification of the powertrain, the higher is the amount of electric energy to be stored from the grid. At this moment, the availability of clean energy on the specific country has a major influence on the overall benefits of this type of technology. However, waiting for cleaner and cleaner energy production, electrification is a viable solution to improve air quality affecting the overall performance of the standard vehicles' power unit.

1.6 Conclusions

In the last decades, air quality has become a real concern due to the increasing evidences on the impact on global warming and human health. Although pollutant emissions come also from natural sources, it has been extensively demonstrated that every human activity affect more or less the emissions levels. We cannot effectively change the amount of pollutants emitted by natural sources, but we have to change the way we live and operate at least to reduce our impact. This is the main reason why organizations from all around the world converged on international agreements on air quality. Each macro region has the faculty to decide local legislation to meet internationally approved emissions limits. The US and the EU are the most active entities on emissions legislation. In this chapter, emissions from road and non-road vehicles have been analysed. Transportation represents one of the most influent sectors in pollutant emissions. The EU is actively promoting stricter and stricter standards both in road and non-road applications since the early 1990s. The most addressed pollutants are (in order of severity) NO_x , PM, HC and CO and in some measure, Diesel engines are the greater contributors of them. Several strategies to meet emissions limits are continuously under development. There are systems that act on the exhaust gas to reduce the amount of some pollutants (NO_x) increasing other less harmful ones. There are physical filters that limit the amount of particulate matter emitted blocking some elements and burning others before entering into the atmosphere. The most effective way of reducing pollutant emissions is indeed burning less fuel to do the same work or equivalently use the same fuel quantity to do more work. It is worth to mention all the hard work in research and development of more efficient power units that use as less as possible fuel per unit of work done. On the other hand, lot of work is done to develop machines (both for road and off-road applications) the require less and less energy to accomplish the same tasks. In this direction still room for improvements is available, especially in the field of working machines. Among the different solution available, the electrification of the machine can represent a good solution for efficiency improvements. The flexibility given by electric systems, allows also an internal combustion engine to work better if a proper combination between the two technologies is designed. The higher the level of electrification, the higher the benefits in terms of local fuel usage. In the case of those vehicles where the electric technology is the principal source of power, great simplification in the overall design of the machine can be achieved, lowering also costs both on the manufacturer and on the user side. With a high degree of electrification, the improvements on air quality increase depending on the amount of clean electric energy available on the local grid. The higher is this percentage, the higher is the effectiveness of this technology.

References

- [1.1]. D. Bourguignon, “Air quality- Pollution sources and impacts, EU legislation and international agreements”, *EPRS | European Parliamentary Research Service*, 2018.
- [1.2]. European Environment Agency, “Air pollution fact sheet 2014”, *European Environment Agency*, 2014.
- [1.3]. Eurostat Statistics Explained, “Air pollution statistics - emission inventories”, 2018. [Online] Available: https://ec.europa.eu/eurostat/statistics-explained/index.php/Air_pollution_statistics_-_emission_inventories. Accessed 03-Jan-2019.
- [1.4]. World Health Organisation, “Ambient air pollution: A global assessment of exposure and burden of disease”, *World Health Organisation*, 2016.
- [1.5]. WHO Regional Office for Europe, OECD, “Economic cost of the health impact of air pollution in Europe: Clean air, health and wealth”, *WHO Regional Office for Europe*, 2015.
- [1.6]. K. Kuklinska, L. Wolska, J. Namiesnik, “Air quality policy in the US and EU – a review”, *Atmospheric Pollution Research*, 6, 129-137, 2015.
- [1.7]. International Council on Clean Transportation (ICCT), “Co2 emission standards for passenger cars and light-commercial vehicles in the European Union”, *ICCT*, 2019.
- [1.8]. E. G. Giakoumis, “Driving and Engine Cycles”, *Springer*, 2017
- [1.9]. International Council on Clean Transportation (ICCT), “Test results confirm: Only 10% of Euro 6 cars meet emission limit in real-world driving conditions”, *ICCT*, 2017.
- [1.10]. European Parliament, Council of the European Union, “Directive 97/68/EC”, 1997.
- [1.11]. European Parliament, Council of the European Union, “Directive 2004/26/EC”, 2004.
- [1.12]. European Parliament, Council of the European Union, “Regulation (EU) 2016/1628”, 2016.
- [1.13]. European Parliament, Council of the European Union, “Regulation (EU) 2018/985”, 2018.
- [1.14]. United States Environmental Protection Agency, “Determination of PEMS Measurement Allowances for Gaseous Emissions Regulated Under the Heavy-duty Diesel Engine In-use Testing Program”, 2008
- [1.15]. L. Pirjola, T. Rönkkö, E. Saukko, H. Parviainen, A. Malinen, J. Alanen, H. Saveljeff, “Exhaust emissions of non-road mobile machine: real-world and laboratory studies with diesel and HVO fuels”, *Fuel*, 202, 154–164, 2017.
- [1.16]. F. Wang, Z. Li, K. Zhang, B. Di, B. Hu, “An overview of nonroad equipment emissions in China”, *Atmospheric Environment*, 132, 283–289, 2016.
- [1.17]. I.A. Reşitoğlu, K. Altinişik, A. Keskin, “The pollutant emissions from diesel-engine vehicles and exhaust aftertreatment systems”, *Clean Technologies and Environmental Policy*, 17(1), 15-27, 2015
- [1.18]. W.A. Majewski, H. Jääskeläinen, “Engine Emission Control” https://www.dieselnet.com/tech/engine_emission-control.php. Accessed 10-Jan-2019
- [1.19]. T. Banjac, F. Trenc, T. Katrašnik “Energy conversion efficiency of hybrid electric heavy-duty vehicles operating according to diverse drive cycles”, *Energy Conversion and Management*, 50, 2865–2878, 2009.
- [1.20]. X. Zeng, N. Tang, Y. Peng, Y. Zhang, J. Wang “Research on energy saving control strategy of parallel hybrid loader”, *Automation in Construction*, 38, 100–108, 2014.
- [1.21]. T. Cao, R.L. Russel, T.D. Durbin, D. R. Cocker, A. Burnette, J. Calavita, H. Maldonado, K.C. Johnson, “Characterization of the emissions impacts of hybrid excavators with a portable emissions measurement system (PEMS) based methodology”, *Science of the Total Environment*, 635, 112–119, 2018.

Chapter 2

Electrified powertrains in industrial applications

The growing demand for less pollutant vehicles is pushing manufacturers towards the evaluation of new architectural solutions to increase the overall efficiency and so decreasing the amount of fuel required per unit of work. Among all the possible architectural solutions, electrification has showed promising results considering the actual limitations related to the state of the art in energy storage. Electrification is an already well established trend in the automotive field where in the last three years (2015 -2018) the growth of electric and hybrid-electric cars on the market has been quite fast. However, to meet new and stricter emissions regulations, also Non-Road Mobile Machineries (NRMM) manufacturers are considering new solutions to increase the overall efficiency of their products and/or reducing the amount of pollutants produced per unit of work. Traditional exhaust gas after-treatment systems are able to reduce the amount of pollutants emissions but are expensive and, to meet new standards, are becoming more and more space consuming. This translates in a very difficult task when it comes to integrate those systems into the vehicle architecture. Moreover, the space used for those elements does not add any other benefit or functionality to the vehicle itself. On the contrary, the use of electric components for a certain degree of electrification would have the double effect to increase machine efficiency and add some extra features. The on-board availability of an electric power source opens the system to the adoptions of new tools and implements used together with the machine itself. Depending on the specific application, electric tools can increase productivity thanks to their better controllability. There are also some limitations in the widespread adoption of electric architectures. The energy density of the energy storage system required is still a major concern. Thus, great efforts are needed to optimize the overall system and to properly control electrified architectures to perform as well as traditional ones, without compromises on functionalities.

2.1 Electric and hybrid topologies for working vehicles

When it comes to vehicle electrification, a wide variety of architectural options can be considered. Combining several electrical, electronic and mechanical components the number of possible topologies allows a high level of optimization for the specific application. Especially for NRMM, there is not an optimal solution due to the high level of specificity of each application. In the working machine field, the knowledge on the characteristics of the application, on the type of working loads and working cycles is mandatory to design an electrified architecture able to accomplish the required tasks.

All the possible topologies for an electrified architecture derive from the proper combinations of these three basic structures: full electric, series hybrid, parallel hybrid [2.1]. As shown in Figure 2.1, a full electric system consists of just one source to provide power for mechanical loads as the driveline, hydraulic systems, auxiliaries and external implements. An electronic converter takes in input electric energy from a battery pack (DC voltage and current) and actuates an electric motor (EM) with alternate regulated voltage and current. Changing the characteristics of the electric energy delivered to EM it is possible to obtain high torque delivery or high speed, according to its characteristics and applied load. A full electric architecture is the simplest solution for vehicle electrification. Electric motors are very simple in their construction, with good power densities compared to Internal Combustion Engines (ICE). The amount of moving parts is reduced at the very essential, thus also failure probability. Electronic converters are now a well-established technology and the recent trends in power electronic components will improve the actual performance to volume ratio as well as reliability [2.2]. A full electric architecture would probably be the fit for all solution if battery packs would have better energy and power densities. The main constraining element of such topology can be identified with the actual state of the art technology of lithium ion batteries (the main adopted energy storage solution for electrified vehicles – see chapter 3). The energy density ratio between 1 litre of Diesel fuel ($\approx 10.9 kWh$) and 1 litre of lithium ion batteries ($\approx 0.25 kWh$) is currently 44. If the overall conversion efficiencies of an ICE (0.3) and an EM and its power converter (0.85) are considered, this gap can be reduced to 15 times, but still very in favour of thermal engines. Thus, only very specific applications (especially in the working machine field) can have satisfactory performance with this type of electric topology.

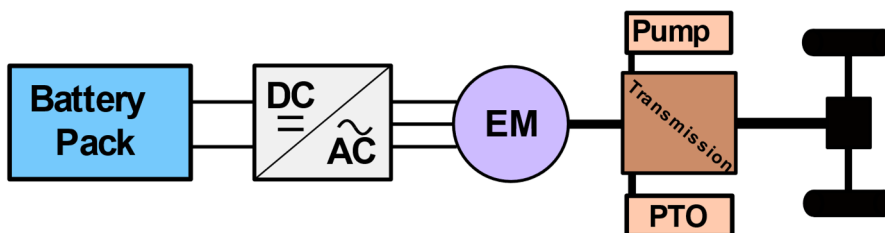


Figure 2.1 Full electric architecture for a working vehicle

To overcome limitations of basic full electric architectures, hybrid topologies combine two power sources to satisfy the power demand of the external load [2.3]-[2.7]. The parallel hybrid architecture shown in Figure 2.2 combines mechanically the power from an ICE and an EM. The main characteristics of this topology are:

- The possibility to satisfy the same peak power demand with a smaller ICE thanks to the mechanical power coming from the EM. This is called engine downsizing and has the benefit of reducing fuel consumption (smaller engines burn lower amount of fuel). Usually, the average power demand of the application is well below the nominal power of the ICE. If it is the main power source, it must be able to satisfy all the possible working loads. Thus, most of the time oversized engines are used to meet this requirement, leading to higher overall fuel consumption when the full power is not requested.
- The electric unit, thanks to its higher degree of controllability and fast response can easily help the ICE in highly dynamic working conditions where it is very inefficient. Quick variations in the external load or in the power demand from the driver can be satisfied by the joint work of the electric unit and the ICE.
- Only one electronic unit is required for the EM actuation. To smooth the ICE load, EM can be actuated both as a booster or as a generator to recharge the battery pack.

The combined use of the ICE and of the EM reduce the overall fuel consumption and improve, in some cases, peak power performance. However, this topology does not allow further improvement in energy management and efficiency of the ICE. The mechanical connection between the ICE and the external load force it to a rotational speed that will depend on the actual working condition. The rotational speed required by the application may not be in the region of higher efficiency of the engine, leading to a not optimized energy delivery. In the same way, a traditional gearbox and a clutch will always be required in this type of configuration to allow the engine to work in its rotational speed range while satisfying the rotational speed of the attached load. Thus, the overall efficiency of the gearbox still must be taken into account when evaluating the tank-to-wheel efficiency of the machine. From the architecture point of view, not being able to eliminate the traditional gearbox will complicate the on-board integration of the electric components in terms of available space (more components to be organized in the volume).

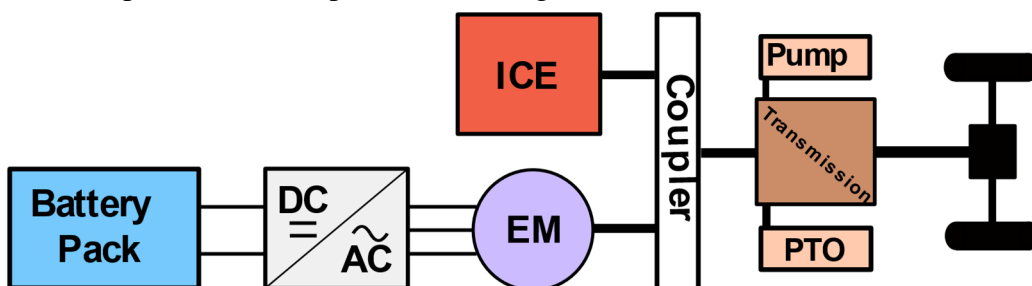


Figure 2.2 Parallel hybrid architecture for a working vehicle

Some of the drawbacks of a parallel topology can be addressed by a series architecture like the one shown in Figure 2.3. The main characteristics can be summarized as follows:

- The ICE is mechanically coupled with an electric generator (EG) to produce electric energy, but mechanically decoupled from the external load.
- If properly designed, this configuration may not require the battery pack. In this case ICE and EG are controlled to produce the amount of energy that EM must provide to satisfy the power demand. This solution (as shown in the following sections) is particularly indicated for those machines where power is currently delivered by mean of hydraulic circuits. In these machines, the ICE provides power to a hydraulic pump which delivers hydraulic power to one or more hydraulic motors in different places of the vehicles. This power transmission methodology has been widely adopted for many years, especially in the working vehicles field. However, the efficiency of the system drops due to hydraulic losses in the pump- motor elements and along the hydraulic line. From this point of view, electric power delivery is way more efficient.
- If the vehicle is equipped with a battery pack, some full electric operations can be performed. The mechanical decoupling of the driveline from the ICE allows the EM to propel the vehicle as long as the required energy is available in the battery pack. This feature is very important in some special working scenario and one of the reasons why this architecture was adopted on several hybrid working vehicles prototypes.
- The availability of stored electric energy allows also for ICE downsizing which can be sized according to the mean power demand of the application leaving the power peaks to the electric branch.
- Two separate electronic units are required to properly actuate the electric machines separately.

The presence of two electric machines and the mechanical decoupling of the ICE from the load allow for better optimization of the ICE working conditions but more complex energy management strategies are required, especially for self-sustaining configurations without a battery pack.

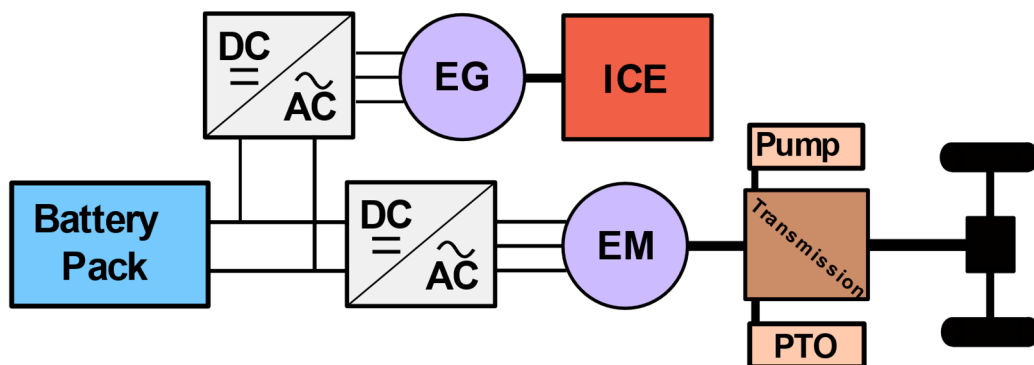


Figure 2.3 Series hybrid architecture for a working vehicle

An interesting application of the electric technology on working machine is in power split configurations. In a mechanical driveline, a power split happens when power coming from a single source is split in one point of the driveline and recombined later on according on some combination and optimization rules. One or more planetary gears are the mechanical devices in charge of splitting or recombining power. There are several examples of power-split transmissions in the working machine field where a mechanical path and hydrostatic transmissions like the one shown in Figure 2.4 work together to deliver power [2.8]-[2.9]. Depending on the working conditions and the driver demand, the hydraulic or the mechanical power path may be preferred to optimize the efficiency of the overall system. A more complex planetary gear system allows to recombine power previously split from the ICE shaft. A similar approach is used on several hybrid electric power split configurations (Figure 2.5) [2.10]-[2.12]. In this case, power is taken from a mechanical path and transferred to another electric machine where it can be delivered with a different combination of torque and speed. The planetary gearbox adds additional degrees of freedom to a traditional mechanical driveline and allows for better optimization of the power delivery. The use of an electric path instead of a hydrostatic transmission makes the process more efficient and more responsive but requires more space to account for motors and electronic controllers.

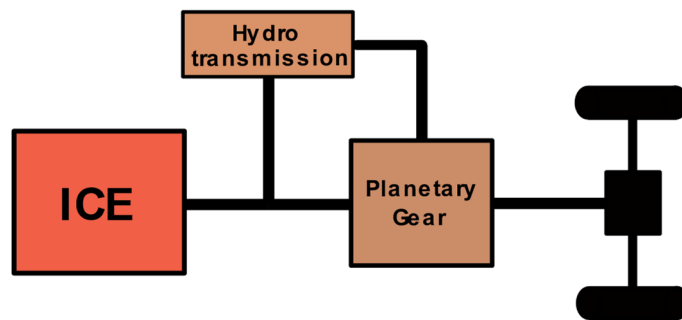


Figure 2.4 Traditional power split configuration with hydrostatic transmission

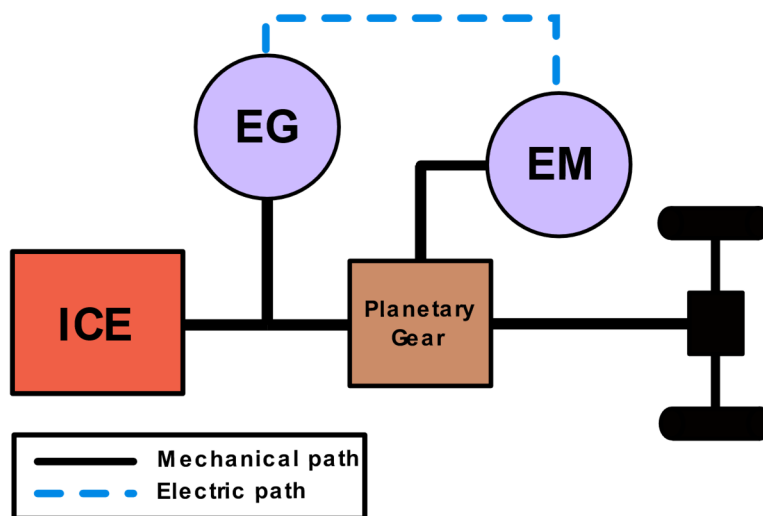


Figure 2.5 Power split configuration with electric machines

2.2 Hybridization factor for powertrain classification

When it comes to hybrid powertrains, the high number of possible architectures that can be obtained combining thermal and electric units makes it difficult to categorize them. In the automotive field it is common practice to define the degree of hybridization of a vehicle by mean of a Hybridization Factor (HF) [2.13]. Considering the amount of power delivered by the thermal and electric system, the HF is defined as

$$HF = \frac{P_{em}}{P_{ICE} + P_{em}} \quad (2.1)$$

where:

- P_{em} represents the power delivered by the electric motor/motors to propel the vehicle
- P_{ICE} is the nominal power of the thermal unit.

This definition allows to distinguish between vehicles where the contribution of the thermal engine is predominant from vehicle where the electric part is more and more prevalent. In fact, based on the HF classification, electrified powertrains can be organized as in Table 2.1 [2.14]. The lower the HF, the lower is the impact of the electric system on the overall vehicle architecture: HF=0 represents a traditional thermal engines architecture.

Electrification class	HF
Micro Hybrid	< 5 %
Mild Hybrid	5-10 %
Full Hybrid	
Parallel	10-50 %
Series	50-75 %
Full Electric	100 %

Table 2.1 HF classification for electrified automotive powertrains.

With the term micro hybrid, it is usual to indicate all those applications where the electric unit is an auxiliary element which helps the engine in some specific operating condition like start and stop operations. The electric system runs usually in the 12-48 V range, well below the safety voltage threshold against electric shock (50V [2.15]). Mild hybrids are vehicles where small electric motor/generator units connected in parallel to the engine are used to help it in transient operations. The power is provided by small battery packs with a voltage usually not greater than 200 V. With the category Full Hybrid, high performance parallel configurations are considered together with series hybrid solutions. In this last case, when the system has a small battery pack, the engine size must be capable of a charge sustaining strategy. With high capacity storage systems, high HF vehicles have smaller and smaller engines usually considered just as range extenders. The thermal unit is practically used to charge the system providing longer driving ranges. The electric

systems in the Full hybrid class work in the range between 200-400 V with trends that indicate a sooner increase of the DC bus voltage. Higher voltage allows for higher power delivery with lower electrical losses. The classification is headed by the Full electric class (HF=1) which of course represents vehicles with no on-board thermal engines. In this class, specifications of the battery pack strongly determine the overall vehicle performance. According to the expression in (2.1) some HF are shown in Table 2.2 for some hybrid cars available on the market on 2018.

Vehicle	Electric motor (kW)	ICE (kW)	HF
Chevrolet Volt	111	55	0.66
Toyota Prius	60	73	0.45
Kia Niro	32	77	0.29
Ford Fusion	79	116	0.32
Honda Civic	17	66	0.2

Table 2.2 HF for hybrid cars.

When dealing with electrified working machines classification, the automotive HF definition defined before is not comprehensive enough for this type of powertrains. As expressed in [2.16]-[2.18] the main difference between a car and a working machine powertrain is in the number of users to satisfy. The main user of a car power unit is the driveline, thus power goes into transportation of people or goods. In a working machine instead, power coming from the same power unit can be used by several utilities: some power can be used to propel the driveline (transportation); some can be used for hydraulic actuation of lifting arms and/or implements; some power can be absorbed by implements attached to the vehicle Power Take Off (PTO). Depending on the application, the power demand from all these different users can be comparable so that a different definition should be considered to account for all the power paths. In [2.19] the Hybridization Factor for a working machine (HF_{WM}) was defined as a function of the driveline hybridization factor (HF_{Drive}) and of the loading hybridization factor (HF_{Load}). Each of them was defined according to the same principle in (2.1). In the hypothesis of a comparable power demand between the driveline and the loading path,

$$HF_{WM} = \frac{1}{2}(HF_{Drive} + HF_{Load}) \quad (2.2)$$

To generalize this definition, it is convenient to include power used for external implements/tools by mean of another hybridization term, the HF_{PTO} . These devices can be actuated both hydraulically, mechanically or electrically. With this term, all those applications where the machine share its power output with external devices, as for tractors, can be included. Thus, the new definition proposed in this work can be expressed as

$$HF_{WM} = \alpha \cdot HF_{Driveline} + \beta \cdot HF_{Load} + \gamma \cdot HF_{PTO} \quad (2.3)$$

where α, β, γ are weighting factors that change depending on the average working load of the machine ($\alpha + \beta + \gamma = 1$). If no additional data are available regarding

the machine working cycle, it is reasonable to consider as first approximation an equal share of the power among the three subsystems.

2.3 Review of electric powertrains on industrial vehicles

The need for more efficient and less pollutant vehicles has pushed the industry and the scientific community towards the investigation of electrified powertrains applied to working machineries. The pioneer field in this electrification is the construction one where the very first prototypes were already presented back in the early 2000. From then, several companies in different fields proposed hybrid and electric prototypes of their machines. In the following sections, a brief review on the actual state of the art of hybrid and electric NRMM is presented. The analysis focused on the main three NRMM categories: construction, handling and agricultural tractors. The order to which each category is presented is not casual. It is indeed the result of the time evolution of the electrification process in the NRMM field. It started in the construction field (as said above), then it involved telehandlers which can be used both in construction and agriculture and nowadays (2018) is clearly extensively involving the agriculture field (tractors but also other types of machines).

2.3.1 Construction

The construction field was the first one which considered the possibility to use electric machines to improve machine efficiency as demonstrated and discussed in several studies [2.20]-[2.24]. The first research studies were published back in 1997. Excavators were the first working machines considered for electrification. Then, wheel loaders and bulldozers were involved by the same process [2.28]-[2.31]. Now, the major manufacturers have developed their own hybrid or electric machines. Some are also available on the market addressing the maturity of the technology in this field. A review of the major electrified construction machines is given below.

Excavators

Several manufacturers like Komatsu, Hitachi, Kobelco, and Doosan, have developed hybrid versions of their excavators which are already available on the market. The most common architecture is a series-parallel configuration like the one shown in Figure 2.6. The motor-generator unit attached to the ICE supplies electric power to the swing electric motor together with an Energy Storage System (ESS) which helps during acceleration and recovers energy during deceleration of the upper structure. Manufacturers like Komatsu [2.25], Hitachi [2.26] preferred the use of Ultracapacitors while companies like Kobelco[2.27] considered Lithium Ion batteries as ESS for their hybrid excavators. Usually the tracks, the arm, the boom and the bucket are still moved by hydraulic power. The pump connected to the ICE provides power to the tracks' motors and hydraulic actuators. However, the motor generator unit can help the engine in transient operating conditions using the

energy stored in the ESS. Since in this architecture the ICE is mechanically decoupled from the loads, a proper energy management strategy can optimize fuel efficiency.

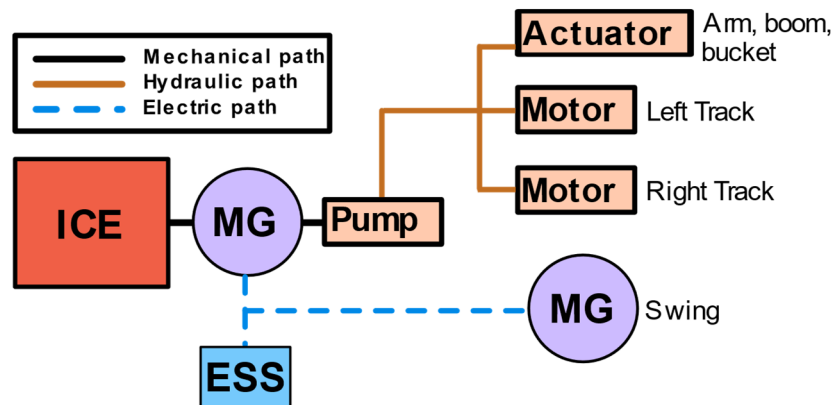


Figure 2.6 Common hybrid architecture for hybrid excavators [2.20]

Wheel loaders

Among wheel loaders' manufacturers, Hitachi, Volvo and John Deere have demonstrated a strong commitment in the electrification process. Compared to the excavator case, different hybrid topologies have been proposed for wheel loaders. Hitachi, for example, implemented in its ZW220HYB-5 wheel loader a series architecture like the one shown in Figure 2.7. A combined ICE-electric generator is in charge of the electric energy production for the two electric motors installed on the driveline. In this case, each motor propels independently the front and rear axle giving higher flexibility for traction control and power management. A supercapacitor-based storage system is in charge of energy recovery from regenerative braking. Energy which can then be released in transient operations in addition to the power delivered by the generator unit.

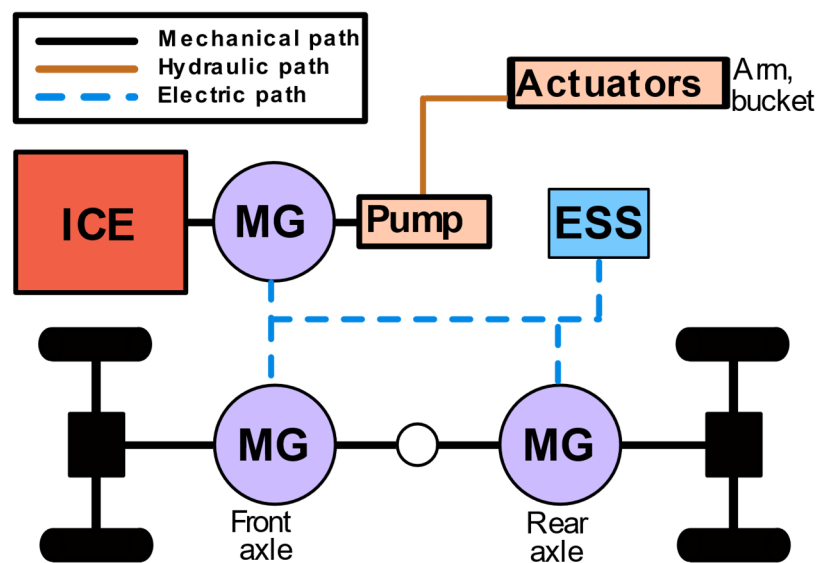


Figure 2.7 Hybrid architecture: Hitachi wheel loader [2.32]

Other interesting solutions for wheel loaders were developed by Volvo. The L220F Hybrid wheel loader represented the first result of a research and development program still in progress. The architecture of this machine (Figure 2.8)

consists of an electric generator in parallel to the engine shaft which help in frequent start and stop operations. Instead of leaving the engine idling, it can be easily turned off and quickly restarted thanks to the electric machine (with more power compared to standard engine starters). Moreover, thanks to a UC based storage, a power boost can be applied to the engine shaft on the most demanding working phases. The same ESS is used to store energy coming from the driveline during regenerative braking. The power unit is mechanically connected to the driveline by mean of a gearbox which split the mechanical power between the front and rear axle.

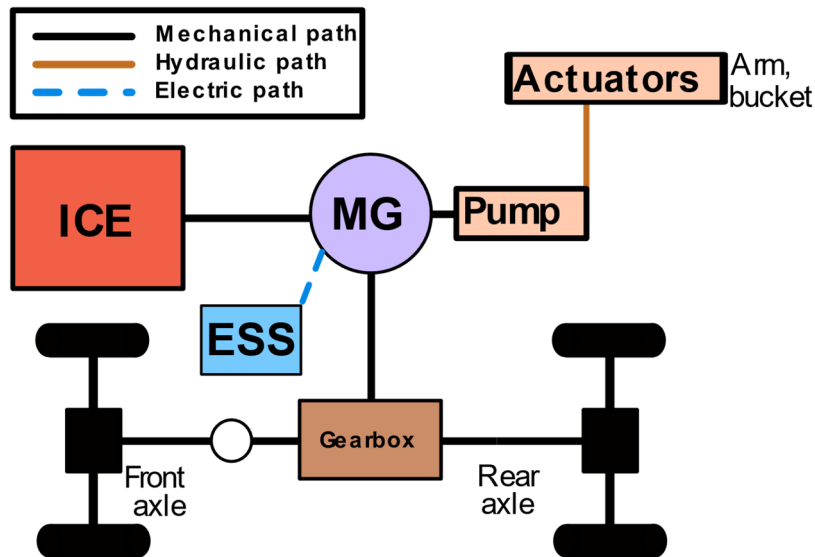


Figure 2.8 Hybrid architecture: Volvo L220F wheel loader [2.33]

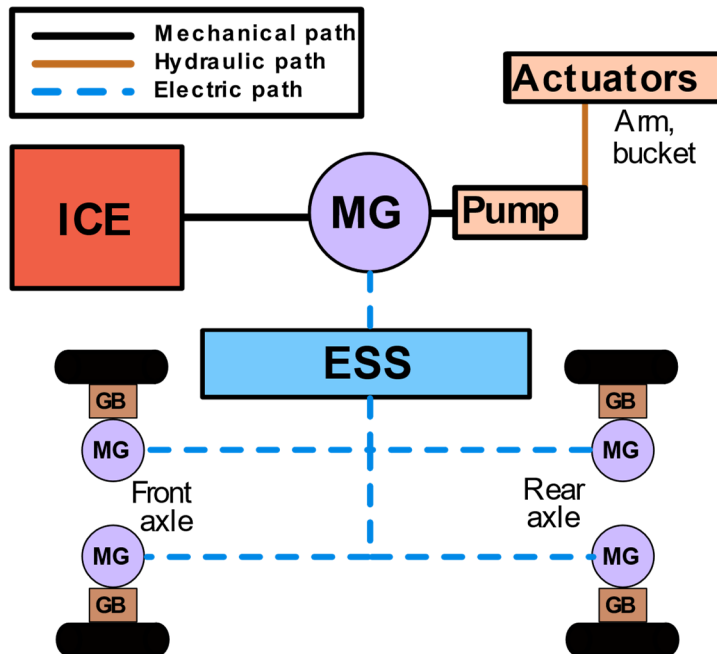


Figure 2.9 Hybrid architecture: Volvo LX1 wheel loader [2.34]

From the L220F project, the LX1 and LX2 projects were derived. The former is a totally new series architecture (Figure 2.9) [2.34] where the mechanical coupling of the ICE with the driveline is no more present. In this architecture, four electric drives are mounted on each wheel. A smaller ICE together with an electric generator

has to provide the average power requested by the application while the peak power capabilities are still provided by mean of a battery-based energy storage system. The combination of a smaller ICE and a more efficient driveline led to a drop in fuel consumption compared to traditional ICE driven wheel loaders. According to the manufacturer, up to 50% fuel saving was reached in field tests with this architecture. The LX2 project [2.35] is related to a smaller, full electric wheel loader, where the ICE left space to a larger battery pack to be able to complete an eight hour working day.

A full series hybrid wheel loader was developed by John Deere. The 944K hybrid wheel loader [2.36] (Figure 2.10) consists of a series configuration with 4 electric drives mounted on each wheel. What makes this solution different from the others presented above is the absence of an energy storage system. The combined power unit (ICE+EG) provides the electric energy required to propel the vehicle. In case of regenerative braking or of an excess of power that could negatively affect the DC bus of the electric system, this would be dissipated into heat by a set of water-cooled, electronically controlled, brake resistors. In this way, constant speed can be maintained also in downhill conditions increasing productivity and reducing the operator efforts.

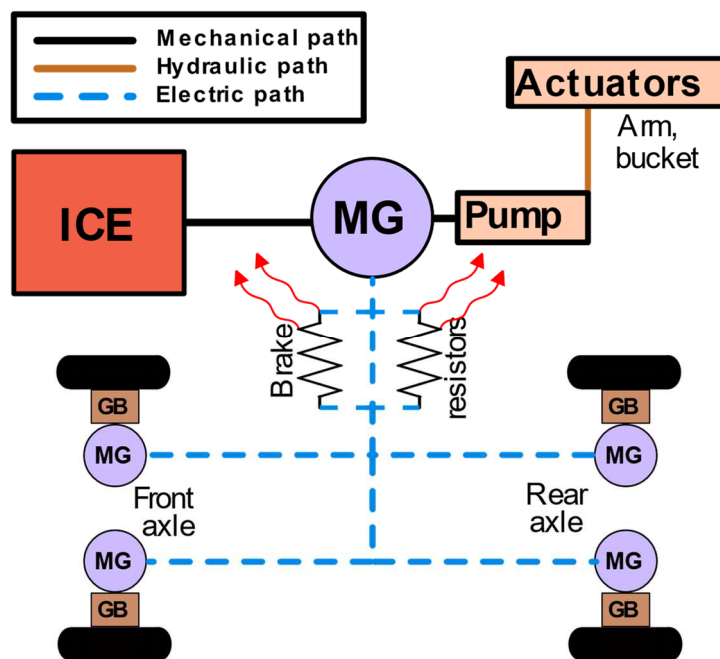


Figure 2.10 Hybrid architecture: John Deere 944K wheel loader [2.36]

Other hybrid wheel loaders were developed in the last decades. Kawasaki developed the 65Z Hybrid wheel loader. Joy (Komatsu group) developed the 22HD a hybrid wheel loader for mining applications. Several manufacturers are indeed considering switching to full electric architectures, especially for small loaders used primary in closed environments (Low Emissions Zone). Kramer, with its 5055e is the perfect example of this trend.

2.3.2 Handling

Below this definition it is possible to include machines from different fields of application. The common denominator is the use of the machine to lift loads and transport them between different places [2.37]-[2.39]. Most of the vehicles that will be described here have in common the versatility to be used for a wide range of tasks with the adoption of proper external tools.

Among the manufacturers involved in the development of hybrid electric solutions for telehandlers, the Italian manufacturer Merlo was a pioneer in the field. First in 2010 at Bauma, then in 2013 at Agrithecnica (relatively recently compared to the construction field) the hybrid turbofarmer TF40.7 was presented [2.19].

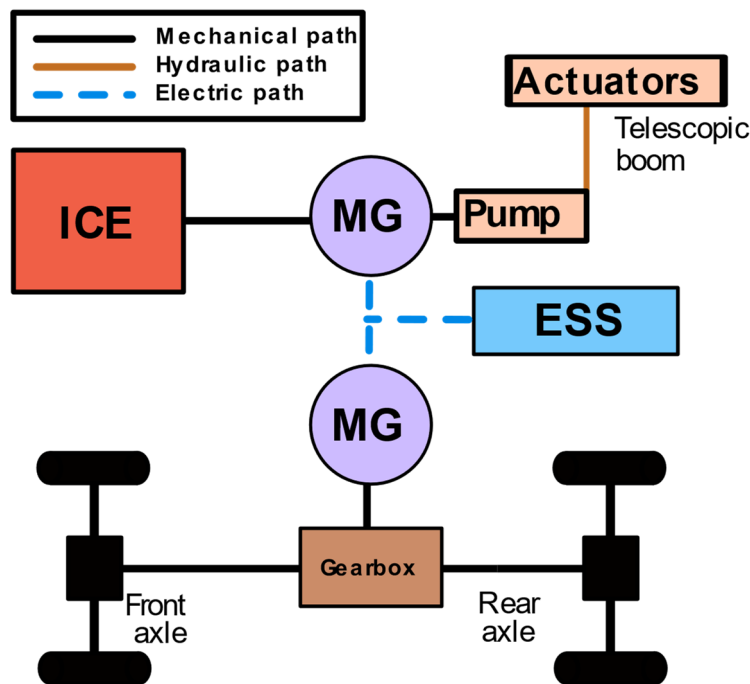


Figure 2.11 Hybrid architecture: Merlo TF 40.7 telescopic handler [2.19]

As shown in Figure 2.11, the architecture consists of a series topology for the driveline and a series-parallel configuration for the hydraulic system which actuates the boom. The mechanical decoupling of the internal combustion engine and the availability of battery based ESS allowed for engine downsizing: from the standard 90 kW diesel engine to a smaller 56 kW one. This was possible because of the typical working scenario of this type of machines. The average power demand for a telehandler is much lower than the nominal power of the standard engine equipped. The presence of a battery pack allows to cover with the electric subsystem the peak power demand still using a 37% smaller diesel engine. The hybrid architecture of this machine allows also for full electric operations (for a limited amount of time). In fact, the electric machines can be both controlled as generators and as motors in such a way that: the one in parallel to the ICE and the hydraulic pump can generate electricity when the engine is on and can power the pump when

the engine is off; the one connected to the driveline can propel the vehicle and recover energy during braking.

More recently (2018), other two hybrid electric telehandlers were developed: the Liebherr TL 432-7 and the Manitou MT1135. These two manufacturers share a common denominator: both the hybrid prototypes are powered by the E-Deutz power unit [2.40]. Deutz is an OEM manufacturer of diesel engines for off road applications. With the recent acquisition of the company Torqeedo GmbH, specialized in electric and hybrid systems for boats, Deutz started a clear industrial plan which wants to bring to the market more and more hybrid electric power units for Off road machines. The E-Deutz consists of an electric drive coupled with a special mechanical transmission to a diesel engine. The mechanical transmission allows to connect the electric motor in parallel to the engine for heavy operations, provides some full electric functionalities but also allows to recharge the battery when required. Another interesting common characteristic of the two hybrid prototypes is the fact that the electric system, characterized by a 20 kW electric motor, runs on a DC bus of 48 Volts. Despite the high current required to provide 20 kW of power at this low DC voltage ($\approx 400A$), it is worth to highlight the need for low voltage systems from both the manufacturers. It was not explicitly declared but safer electric systems against electric shock would probably reduce the scepticism of the final user in the adoption of electric technologies (author opinion). With that being said, it is reasonable to expect more low voltage hybrid systems in the near future.

Other interesting applications of electrification in the handling field are full electric prototypes developed especially for handlers which must operate in Low Emissions Zones (LEZ). Again, Liebherr and Manitou recently presented their full electric prototypes based on the E-Deutz full electric system. In this case, the diesel engine is dismissed to free space for a high power electric drive and a bigger battery pack which in this case runs at 400 V. Small telehandlers have the real possibility to be converted to full electric architectures. Usually, they operate in very limited areas; often, in closed environments (warehouses, farms,...). This would reduce range anxiety which often prevents the adoption of full electric systems by the end user. Liebherr and Manitou are not the first manufacturers which considered the full electric conversion of small telehandlers. Another Italian company, Galizia, presented several years ago a full electric telescopic handler: the Multi 636 electric. In this case, the machine is characterized by small electric drives (on for the front and one for the rear axle) which run at 48 V.

Finally, another interesting application can be found in the field of containers handling. Konecranes is the pioneer in its field. The hybrid SMV 4531 TB5 HLT reach stacker was presented back in 2013 [2.41]. Its hybrid architecture consists of a hybrid electric driveline and a hydraulic lifting system powered by an electric unit which takes power from the diesel electric generator and from a UC based storage system. The choice of UC for the on board ESS is particularly indicated in this case since the high power capabilities of UC allows for faster lifts and for energy recovery in the lowering phases. Similarly to Konecranes, the Italian manufacturer CVS Ferrari developed a hybrid UC based container handler. Their HY-Lift [2.42]

consists of two electric motors directly mounted on the wheels, powered in a series configuration by a diesel engine. Also in this case, the hydraulic lifting system is driven by an electric drive which can benefit of the high power capabilities of a UC based storage system.

2.3.3 Agricultural tractors

Tractors in agriculture are machines used mainly to mechanize agricultural or farming tasks. They can be used to pull and/or power external tools (also called implements) and to pull trailers for transportation of goods. Several attempts tried to electrify traditional tractors' architectures in the last two decades [2.43]-[2.44]. The first prototype was the Belarus/RuselProm 3022e presented at Agritechnica 2009 [2.45]. As shown in Figure 2.12 it consisted in a full series architecture which allowed to decouple the ICE from the wheels and to add a Continuously Variable Transmission (CVT) capability. Tractors have usually a high number of gear ratios to satisfy the user requirements in terms of vehicle working speed. An electric motor can be easily controlled to cover continuously a wide range of mechanical speeds. Thus, the need for mechanical gear ratios is lower and mainly related to the tractive force required by the application: if the electric motor has not enough torque, gear ratios can still be used to cover those working conditions. The prototype was not equipped with an ESS, thus the electric power generated by the ICE+EG unit was controlled to match the driver demand. After the presentation in 2009, no more official communications were released about the advancement of the project. In 2018, maybe considering the fast growth of electrification in working machines, the company announced to be ready for commercialization of the 3023e, but still no indications on the launch day are available.

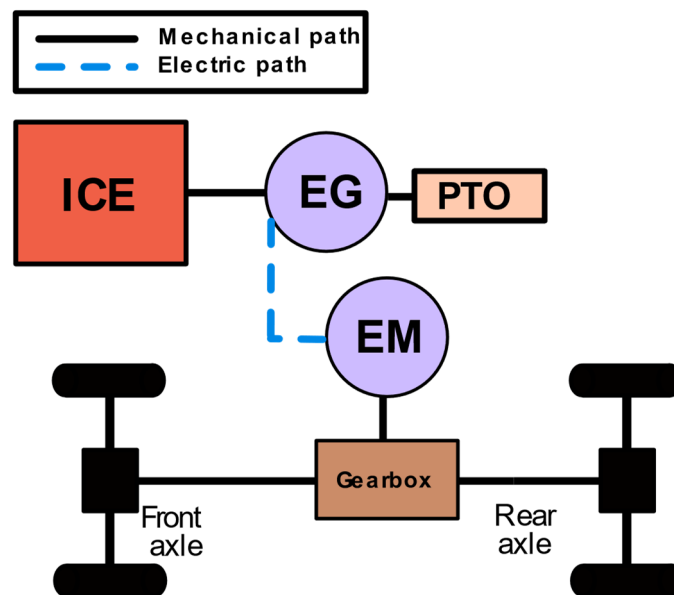


Figure 2.12 Hybrid architecture: Belarus 3022e tractor

Two years later, the company RigiTrac presented the EWD 120 at Agritechnica 2011 [2.46]. This prototype introduced two major differences compared to the previous example. The architecture (Figure 2.13) consisted of a full series hybrid with an ICE+EG unit which in charge of producing the required electric energy. This energy propels a set of 4 electric motors directly mounted on the wheels which, in this case, gives higher capabilities for traction control. The system was equipped with an electric interface to provide power (AC or DC) to attached implements. This was the major innovation in accordance to one of the major trends in agriculture is related to implements electrification[2.47]-[2.50]. Nowadays, implements are mainly propelled by the tractor PTO which is usually directly connected to the engine shaft. The problem is that this type of power delivery requires complex mechanisms to convert the rotational motion of the PTO shaft to the most convenient form for the implement. This introduce high variability in the actuation characteristics, which is fine for some implements but no more adequate for some working operations where high precision is required to improve productivity. Moreover, a pure mechanical implement mechanism is constrained to the engine rotational speed preventing for speed optimization if no gearbox is available. Modern tractors have hydraulic interfaces to propel external implements, but the precision obtained with such system is still not the best possible. Thus, the availability of an electric power source would be a major breakthrough for the advancements in this field because it would allow implements' manufacturers to develop more precise electrically driven devices.

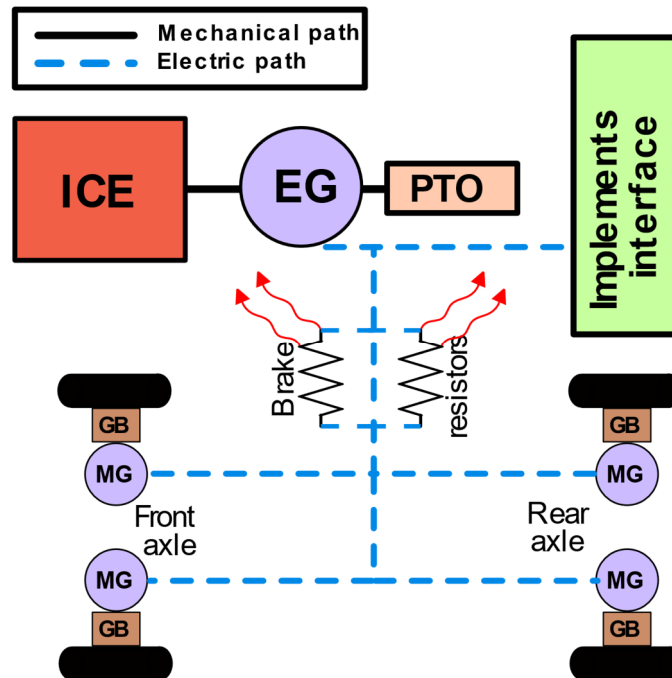


Figure 2.13 Hybrid architecture: Rigitrac EWD 120 tractor

In 2015, Claas developed the Arion 650 Hybrid an electrified, implement oriented, tractor architecture [2.49]. As shown in Figure 2.14, an electric

motor/generator is connected in parallel to the engine shaft. The electric machine has four main functions:

- To provide electric energy to the high voltage DC system when an implement is connected to the tractor interface
- To provide boost in some working conditions or to recover kinetic energy during regenerative braking
- To help the engine in frequent start/stop operations saving fuel during idling
- To allow a limited set of full electric operations disengaging the clutch at the input of the electric machine.

In this scenario, it is clear the main role of the energy management unit on the tractor side, but also of the implement controller on the other side which has to monitor the local work to optimize energy consumption and productivity. The Claas roadmap on tractor electrification expects a coexistence of PTO driven and electrical driven implements up to 2030. Then their plan is to fully switch to fully electrically driven implements.

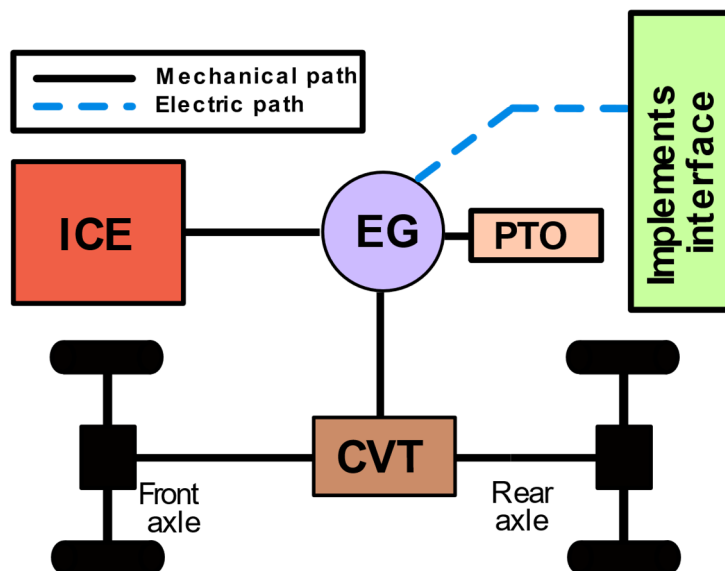


Figure 2.14 Hybrid architecture: Claas Arion 650 Hybrid tractor

In 2016 John Deere presented at SIMA a full electric prototype of the 6R Series, the first modern battery powered tractor. It is equipped with two electric machines which in standard mode propels the direct transmission and the PTO. Depending on the specific working condition, it is possible to couple the power of the two motors. The on-board battery pack is claimed to reach 4 hours of mixed work or 55 km of transportation.

One year later, in 2017 Fendt presented the e100 Vario at Agritechnica 2017, the first full electric specialized tractor. A single electric motor is used to propel both the rear and front axle (when the 4WD is required). The system is powered by a 100 kWh battery pack claimed by the manufacturer to accomplish an entire working

day with a single charge. However, the system is ready for fast charge which would recharge up to 80% of the total capacity in 40 minutes.

At the end of 2018, John Deere presented another electric project: A full electric, cable powered, autonomous tractor. There are traces of similar solutions designed in the Soviet Union when the tractor was directly connected to the grid [2.51]. At that time the benefits of the technological solution were not enough to validate the solution. Now, with the increasing need of more efficient vehicles and with the possibility to fully automatize some field operations thanks to autonomous technologies, this idea could regain interest. The solution could increase productivity, allowing for continuous day and night operations without the need of refuel the tank nor recharge the battery pack.

2.4 Working vehicles electrification: limiting factors

Nowadays, the need for more efficient and less pollutant working vehicles has increased the interest towards electric and hybrid solutions which have proven their capabilities in several field of application. The actual state of the art technology can well fit the working scenario of some fields of applications but is still not mature enough to cover all the different cases. The electrification of some construction machineries has proved better performance and reduction of the total cost of ownership. The successful adoption of hybrid architectures in excavators and wheel loaders demonstrated the feasibility of electric powertrains also for heavy duty applications. These machines are already available on the market, suggesting also the request for this type of machines. In the handling field, some machines have demonstrated their potential, especially in container handling. Several products are already available on the market, demonstrating also in this case a real interest for this technology. Agriculture has demonstrated to be the most conservative field when it comes to shifting towards new technologies. Several prototypes were presented in the past, both on agriculture handling and agricultural tractors. The feedback from the respective community of interest has always been positive as demonstrated by the prizes won by these machines. However, the technology still not meet the needs of these markets since almost any of these prototypes has become an official marketable product. Two elements can be addressed as responsible for this delay:

- The lack of knowledge about the real working scenario of the machines to be electrified
- The influences deriving from the automotive field.

The first point is crucial when it comes to define the performance, thus the design constraint of the electric system. Usually, standard agricultural machines are designed with oversized engine able to meet peak power demands in some specific working tasks. However, this leads intrinsically to higher fuel consumption for the normal use of the machine. This approach is winning for vehicles where the

refuelling is so fast to not interfere with the normal use of the machine but shows strong weaknesses when dealing with electric machines where a full charge must be well programmed to meet the full working day requirements. Moreover, an oversized electric system can increase a lot the total cost of electric and electronic components. Thus, the selling price can easily become too high to propose the machine to the market. Secondly, due to the recent explosion of electric vehicles in the automotive fields, it is clear that some expectations and some doubts and fears are intrinsically affecting the adoption of the electric technology in this field. If a working machine is not able to match the daily working tasks, the user can suffer of money losses due to delays in the production chain. Thus, the feeling recently defined as range anxiety in the automotive scenario, assumes more and more relevance when it comes to productive activities. Batteries play a big role in this scenario. The limited energy density of the actual state of the art of lithium ion batteries, intrinsically limits the amount of full electric operations that a machine can perform. However, this become a major issue only if the vehicle is designed to have a high HF. The more the electric architecture depends on the on board ESS, the higher would be the total cost (more battery would be required) and the range anxiety since the time required to fully recharge the vehicle is not even comparable to a traditional Diesel refuel. Some lithium ion technologies (LTO-see chapter 3) have demonstrated charging capabilities comparable to traditional refuelling but their current cost is too high for vehicle applications. Thus, as demonstrated by the construction, lower HF would minimize the amount of batteries required by the application still improving the overall efficiency of the machine.

2.5 Conclusions

Electrified architectures have demonstrated their potential when it comes to improve the overall efficiency of a vehicle. The automotive field is finally switching to electric and hybrid vehicles as demonstrated by the rapid growth of the electric car market in the last two years. To improve the overall efficiency of their machines thus reducing the amount of pollutant emissions (as required by the most recent legislations), working vehicles' manufacturers are considering the adoption of electric systems on their machines. In some fields of applications electric and hybrid machines are already a reality. The construction field was the pioneer towards electrification. More and more manufacturers are presenting their electrified solutions on the market as alternatives to traditional vehicles. However, some fields are still trying to successfully propose electric powertrains to their customers. In the agriculture field, the solutions proposed in the last decade were well accepted by the sector community. However, these products are still not considered mature enough to be proposed on the market. The key to unlock this impasse could be to rethink the HF of each specific machine according to the real working cycle, minimizing the amount of batteries required to reduce the costs but supplying a system able to satisfy the user needs.

References

- [2.1] C.C. Chan, "The State of the Art of Electric and Hybrid Vehicles", *In Proc. IEEE*, 90 (2), 247–275, 2002.
- [2.2] A. Emadi, M.Ehsani, J. M. Miller, "Vehicular Electric Power Systems: Land, Sea, Air and Space Vehicles", *CRC Press*, 1 edition, 2003.
- [2.3] T. Katrašnik, F. Tranc, S. R. Oprešnik, "Analysis of the energy conversion efficiency in parallel and series powertrains", *IEEE Trans. Veh. Technol.*, 56(6), 3649–3659, 2007.
- [2.4] J. Hong, L. ZhaoY. Lei, B Gao, "Architecture Optimization of Hybrid Electric Vehicles with Future High-Efficiency Engine", *Energies*, 11, 1148 – 1170, 2018.
- [2.5] K C Bayindir, M A Gözüküçük, A Teke, "A comprehensive overview of hybrid electric vehicle: Powertrain configurations powertrain control techniques and electronic control units", *Energy Conversion and Management*, 52, 1305-1313, 2011.
- [2.6] M. Mahmoud, R. Garnett, M. Ferguson, P. Kanaroglou, "Electric buses: A review of alternative powertrains", *Renewable and Sustainable Energy Reviews*, 62, 673–684, 2016.
- [2.7] A. Lajunen, "Energy consumption and cost-benefit analysis of hybrid and electric city buses", *Transportation Research Part C*, 38, 1-15, 2014.
- [2.8] Y. Xia, D. Sun "Characteristic analysis of a new hydromechanical continuously variable transmission system", *Mechanism and Machine Theory*, 126, 457-467, 2018.
- [2.9] P. Linares, V. Mendez, H. Catalàn, "Design parameters for continuously variable power split transmissions using planetary with 3 active shafts", *Journal of Terramechanics*, 47, 323-335, 2010.
- [2.10] W Wang, R Song, M Guo, S Liu, "Analysis on compound split configuration of power split hybrid electric vehicle", *Mechanism and Machine Theory*, 78, 272-288, 2014
- [2.11] W. Yang, J. Liang, J. Yang, N. Zhang, "Investigation of a novel coaxial power-split hybrid powertrain for mining trucks", *Energies*, 11, 172-189, 2018.
- [2.12] C. Rossi, D. Pontara, D. Casadei, "E-CVT power split transmission for off-road hybrid electric vehicles". *Vehicle Power & Propulsion Conference (VPPC) Coimbra*, 2014
- [2.13] T. Katrašnik, "Analytical framework for analyzing the energy conversion efficiency of different hybrid electric vehicle topologies". *Energy Conversion and Management*, 50(8), 1924-1938, 2009.
- [2.14] O.M. Govardhan "Fundamentals and classification of hybrid electric vehicles", *International Journal of Engineering and Techniques*, 3(5), 194-198, 2017.
- [2.15] European Parliament, Council of the European Union, "Directive 2001/95/EC" 2001.
- [2.16] A Somà, "Trends and hybridization factor for heavy duty working vehicles", *InTech*, Chapter 1, 2017.
- [2.17] A. Somà, F. Bruzzese, "Effects of driveline hybridization on fuel economy and dynamic performance of hybrid telescopic heavy vehicles", *SAE Heavy Duty Veh. Symp. Technol. High Efficiency Fuel Econ.*, 2013.
- [2.18] A. Somà, F. Bruzzese, E. Viglietti, "Hybridization factor and performances of hybrid electric telescopic heavy vehicles.", *2015 Tenth International Conference on Ecological Vehicles and Renewable Energies (EVER)*, 2015.
- [2.19] A. Somà, F. Bruzzese, F. Mocera, E. Viglietti "Hybridization Factor and Performance of Hybrid Electric Telehandler Vehicle", *IEEE Trans. on Ind. Appl.*, 52, 5130–5138, 2016.
- [2.20] J. Wang, Z. Yang, S. Liu, Q. Zhang, Y. Han, "A comprehensive overview of hybrid construction machinery", *Advances in Mechanical Engineering*, 8(3), 1-15, 2016.
- [2.21] D. Wang, C. Guan, S. Pan, M. Zhang, X. Lin, "Performance analysis of hydraulic excavator powertrain hybridization", *Automation in Construction*, 18, 249–257, 2009.
- [2.22] X He, Y Jiang, "Review of hybrid electric systems for construction machinery", *Automation in Construction*, 92, 286-296, 2018.
- [2.23] T Donateo, A. Nicolazzo, "Preliminary design of a hybrid electric powertrain for earthmoving machine", *Energy Procedia*, 148, 495-502, 2018.
- [2.24] M Edamura, S Ishida, S Imura, S Izumi, "Adoption of electrification and hybrid drive for more energy-efficient construction machinery", *Hitachi Review*, 62(2), 118-122, 2013.
- [2.25] Komatsu, [Online] Available: <https://www.komatsu.com.au/innovation/komatsu-hybrid-excavators/>.
- [2.26] Hitachi, [Online] Available: http://www.hitachi.com/environment/products/hybrid_excavator/index.html/.
- [2.27] Kobelco, [Online] Available: <https://www.kobelco-europe.com/innovation/hybrid/>.
- [2.28] K Oh, H Kim, K Ko, P Kim, K Yi, "Integrated wheel loader simulation model for improving performance and energy flow", 58, 129-143, 2015.
- [2.29] NW Zou, QL Dai, YH Jia, et al, "Modeling and simulation research of QL coaxial parallel hybrid loader." *Applied Mechanics and Materials*, 29, 1634-1639, 2010.
- [2.30] S Grammatico, A Balluchi, E Cosoli, "A series-parallel hybrid electric powertrain for industrial vehicles", *IEEE Vehicle Power and Propulsion Conference (VPPC)*, 2010.
- [2.31] A. Bertini, M. Ceraolo, G. Lutzemberger, "Systematic approach in the hybridization of a hydraulic skid loader", *Automation in Construction*, 58, 144-154, 2015.
- [2.32] Hitachi, 2015, [Online] Available: <https://www.hitachicm.eu/press-center/hitachi-unveils-hybrid-wheel-loader-at-intermat/>.
- [2.33] R Filla, "Alternative System Solutions for Wheel Loaders and other Construction Equipment", *1st CTI Forum Alternative, Electric and Hybrid Drive Trains*, 2008.
- [2.34] Volvo Construction Equipment, 2017, [Online] Available: <https://www.volvoce.com/global/en/news-and-events/news-and-press-releases/2017/lx1-prototype-hybrid-wheel-loader-delivers-50-percent-fuel-efficiency-improvement/>.

- [2.35] Volvo Construction Equipment, 2018, [Online] Available: <https://www.volvoce.com/global/en/news-and-events/news-and-press-releases/2018/volvo-ce-unveils-electric-compact-wheel-loader-concept/>.
- [2.36] John Deere, [Online] Available: <https://www.deere.com/en/loaders/wheel-loaders/944k-wheel-loader/>.
- [2.37] P. Immonen, P. Ponomarev, R. Aman, V. Ahola, J. Uusi-Heikkilä, L. Laurila, H. Handroos, M. Niemela, J. Pyrhonen, K. Huhtala, “Energy Saving in working hydraulics of long booms in heavy working vehicles”, *Automation in Construction*, 65, 125-132, 2016.
- [2.38] D Bertozzi, “Hybrid and fully electric powering technology for container handling lifttrucks: A look into the shortcoming future”, *Tec Europe*, 2018.
- [2.39] A Lajunen, P Sanio, L Laurila, JP Makelainen, K Tammi, “Overview of Powertrain Electrification and Future Scenarios for Non-Road Mobile Machinery”, *Energies*, 11, 1184-1206, 2018.
- [2.40] DEUTZ, [Online] Available: <https://www.deutz.com/en/e-deutz/>.
- [2.41] Konecranes, [Online] Available: <https://wayup.konecranes.com/tech/konecranes-pioneering-hybrid-reach-stacker-brings-multiple-advantages/>.
- [2.42] CVS Ferrari, [Online] Available: <http://www.cvsferrari.it/products/hybrid-empty-container-handler/>.
- [2.43] G. P. Moreda, M. A. Muñoz-García, P. Barreiro, “High voltage electrification of tractor and agricultural machinery - A review”, *Energy Conversion and Management*, 115, 117–131, 2016.
- [2.44] J. Karner, M. Baldinger, B. Reichl, “Prospects of hybrid systems on agricultural machinery”, *Journal on Agricultural Engineering (JAE)*, 1(1), 33-37, 2014.
- [2.45] Farmweekly, 2018, [Online] Available: <https://www.farmweekly.com.au/story/5670924/belarus-goes-electric/>.
- [2.46] Technische Universität Dresden, [Online] Available: https://tu-dresden.de/ing/maschinenwesen/int/ast/ressourcen/dateien/forschung/files/Datenblatt_Rigitrac.pdf?lang=de
- [2.47] KD Stoss, J Sobotzik, B Shi, ER Kreis, “Tractor power for implement operation – mechanical, hydraulic and electrical: an overview.”, *Agricultural Equipment Technology Conference*, 2013.
- [2.48] K Hahn, “High Voltage Electric Tractor implement interface”, *SAE International Journal Commercial Vehicle*, 1(1), 383-391, 2008.
- [2.49] S Tetzlaff, “System wide electrification and appropriate functions of tractor and implement”, *LandTechnik*, 70(5), 203-216, 2015.
- [2.50] S Florentsev, D Izosimov, L Makarov, S Baida, A Belousov “Complete Traction Electric Equipment Sets of Electro-Mechanical Drive Trains for Tractors”, *2010 IEEE Region 8 International Conference on Computational Technologies in Electrical and Electronics Engineering (SIBIRCON)*, 2010.
- [2.51] Jalopnik, 2011, [Online] Available: <https://jalopnik.com/when-the-soviets-built-an-electric-tractor-5796595/>.

Chapter 3

Study and characterization of Lithium - Ion cells performance for heavy duty applications

In a world where electric energy production satisfies the needs from manufacturing processes, commercial/residential buildings and more recently also propulsion Energy Storage Systems play a crucial role affecting research and development trends. Several physical principles can be used to store energy and use it in a separate moment when needed. Application requirements usually defines what is the best energy storage system among the others. At this moment, battery-based storage systems are considered a good solution for applications like grid storage plants, uninterruptible power supplies, vehicles propulsion. In this chapter, performance of a specific storage element will be studied: a lithium ion cell. Nowadays, this technology represents one of the most established but also still discussed solution for vehicles applications thanks to the good compromise between energy storage capacity, power capabilities, safety and stability of its chemical composition. These characteristics are extremely important in the automotive field where the weight/power ratio must be properly designed to optimize performance and costs.

The application of this technology in the industrial field is still at its primordial stage. Further investigations are required to study the behaviour under a wide variety of loading profiles with characteristics very different from the automotive case. High continuous power demand, very aggressive working environments in terms of vibrations, dust and temperatures may affect very differently battery behaviours. Thus, each field of application would require specific design strategies in order to use this new power source on board of their vehicles.

3.1 State of the Art analysis on energy storage systems

With the term Energy Storage System (ESS) [3.1] - [3.4] it is usual to address a device able to store energy at a certain time and release it whenever the user may need it. This capability is useful in several fields. ESSs for backup, also called Uninterruptible Power Systems or UPS, are particularly indicated for those critical systems where the loss of power due to grid problems cannot be accepted. UPSs come in different sizes, from the smallest ones used for electronic devices and personal computers to the biggest used as backup systems for entire buildings or manufacturing plants. A similar application is the use of ESS as grid storage. In this case, three possible scenarios can be considered. The first one is related to the electric energy production costs.

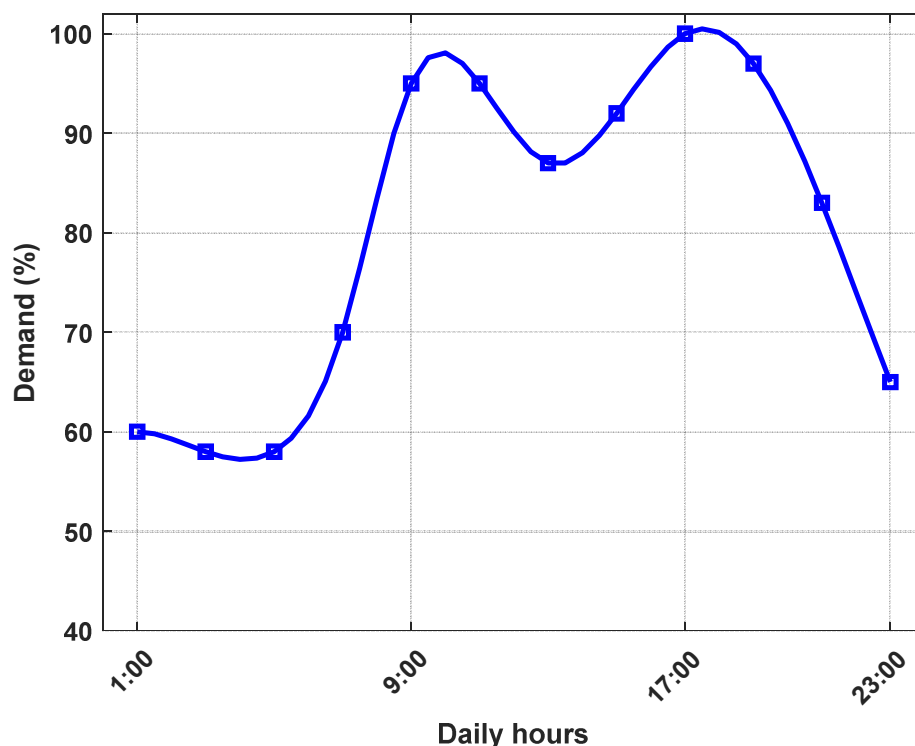


Figure 3.1 Daily electric energy demand

As shown in Figure 3.1, the typical electric energy demand during the day is not constant. Due to the higher demand, the energy cost increases thus an ESS capable of storing energy when the price is lower and releasing it during peak hours can lead to substantial savings. Typical examples are pumped hydro storage power plants that pump water back to their higher tanks during off peak hours and use it again during the day. Although the overall low energy efficiency of this operation, the lower energy cost makes it profitable. The rise of renewable energy adds complexity in the grid power management. The unstable availability of natural sources or the unpredictable behaviour of weather conditions feed the grid with an irregular amount of power which makes thermal generators work much inefficiently. For them to integrate with this unstable amount of power, power

plants must continuously change their operating conditions, working with workloads far from their nominal operating points. The availability of distributed ESSs allows to compensate the irregular power from renewable energy without a high impact on thermal power plants working conditions. Using ESS as grid storage systems also allows for more efficient backup against accidental events. With the same principle, distributed grid ESS allows for better performance of the grid itself, especially for those places far from the nearest power plant.

Energy can be stored in different ways. It is possible to have, mechanical, thermal, electrochemical, chemical and electrical ESS as shown in Figure 3.2.

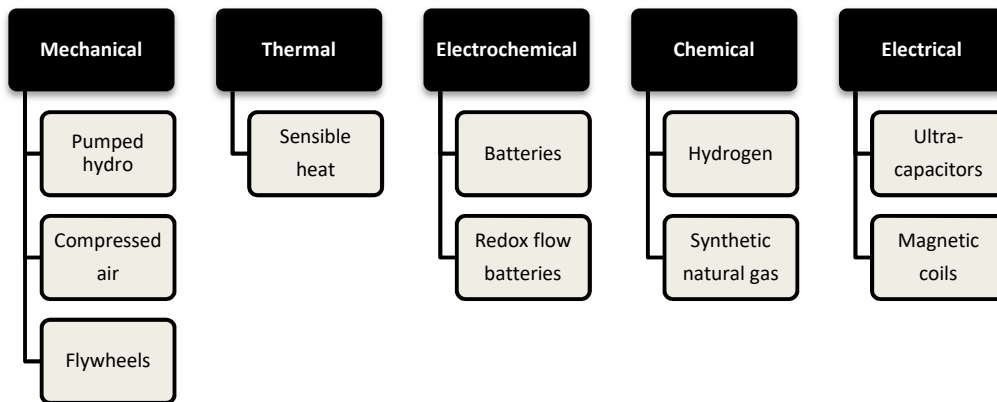


Figure 3.2 Energy Storage Systems overview

Pumped hydro storage systems store energy pumping water (or other fluids) between two or more reservoirs at different altitude. The stored potential energy can be then used adjusting the flow rate from the higher to the lower pond depending on the actual power demand. This process has an efficiency between 70 and 85% but is strongly related to the morphology of the environment.

Compressed air storage systems store energy compressing air at high pressure in underground caverns. When the power demand increases, the pressurized air is heated and expanded in a turbine-generator to produce electric energy for the grid. Depending on the thermodynamic cycle of the plant, the efficiency of this storage method can go from 40% (Diabatic method) up to 70% (Adiabatic method). As for pumped hydro storage systems, also in this case the morphology of the environment limits its feasibility.

Flywheels are often used as energy storage systems [3.5]. They consist of a rotating disk coupled with an electric motor/generator. When it is required to store energy, the motor uses the extra power to spin the disk whereas the use of the same electric machine as a generator allows to satisfy a peak in the power demand. According to Equation (3.1)

$$E = \frac{1}{2} I \omega^2 \quad (3.1)$$

the stored energy is proportional to the moment of inertia I of the rotating disk and to the square of its rotational speed ω . Thus, two different scenarios can be considered:

- big flywheels with low rpm;
- small flywheels but with very high rpm.

The first case is usually related to stationary applications while the second one is more suitable for mobile ones. There are several research activities that consider the use of small, high speed flywheel storage systems for vehicle applications. The main drawbacks are related to losses and safety. Small flywheels should have the rotating disk contained in a partial vacuum chamber to reduce windage losses and the use of magnetic bearings can help for friction losses. However, the high speeds (tens of thousands of rpm) involved require special reinforced containment structures to balance centrifugal forces acting on the disk to prevent catastrophic failures. Despite the small amount of energy that this system can provide in vehicle applications, they can deliver very high amount of power up to their complete discharge.

Sensible heat storage systems use phase change materials as storage element [3.6]. The heat can be “stored” when heating the material with very little temperature variations. The stored energy can then be released to a colder element. A common application of these systems in the automotive field is the pre-heating of several vehicle components during cold starts. Thermal energy coming from the engine is absorbed by the phase change material and stored in a thermally isolated heat accumulator. Then, the same energy can be used to pre-heat the engine or the catalytic converter at cold start according to the need.

Batteries are storage systems made by the connection of several electrochemical cells (Figure 3.3) [3.7]. Two electrodes, one positive (cathode) one negative (anode), reacts with an electrolyte solution leading to an electromotive force relative to a standard potential. These two halves of the electrochemical cell, due to the difference between their potentials, determine a current flow from the positive to the negative terminal when connected.

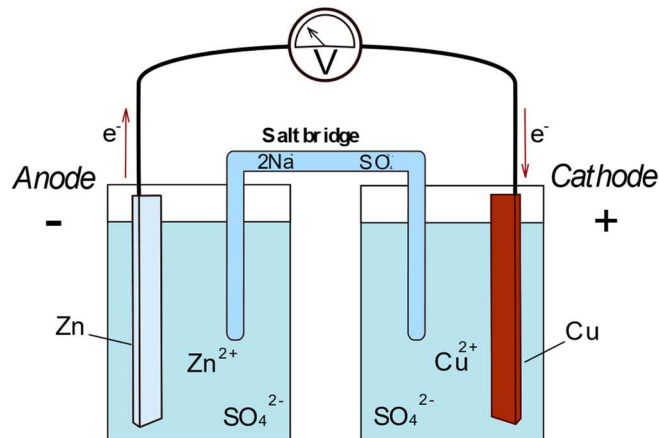


Figure 3.3 Electrochemical cell

Batteries can supply electric power to an external load (discharging phase) or they can store energy from an external power supply due to chemical reactions (charging phase). Based on these two operating modes batteries can be divided into two main groups: primary or “disposable” batteries that can be used just once due to the irreversible electrochemical changes in their electrodes when discharged; secondary or “rechargeable” batteries, often called accumulators, which can store and release energy several times thanks to the reversible electrochemical reactions that occur within the cells. Primary batteries are still preferred in those applications where very low self-discharge is required. Some reservoir batteries can essentially last tens of years having their physical component separated and assembled just when required. Secondary batteries have an overall lower cost due to the high number of cycles they can perform. This also limits the amount of waste products compared to first group. However, both battery categories represent today a good solution when portability is a requirement for the ESS.

Redox flow batteries are rechargeable storage systems where the energy is stored in electroactive species dissolved in electrolyte solutions within physical tanks (Figure 3.4) [3.8]. The active fluids are then pumped through an electrochemical cell that is responsible for the conversion of the chemical energy in electricity. The capacity of this type of battery is related to the tanks volume while the power capability depends on the flow rate and on the size of the conversion cell. Once the fluids are completely discharged in terms of active species, the battery can be recharged just by replacing them with new active solutions.

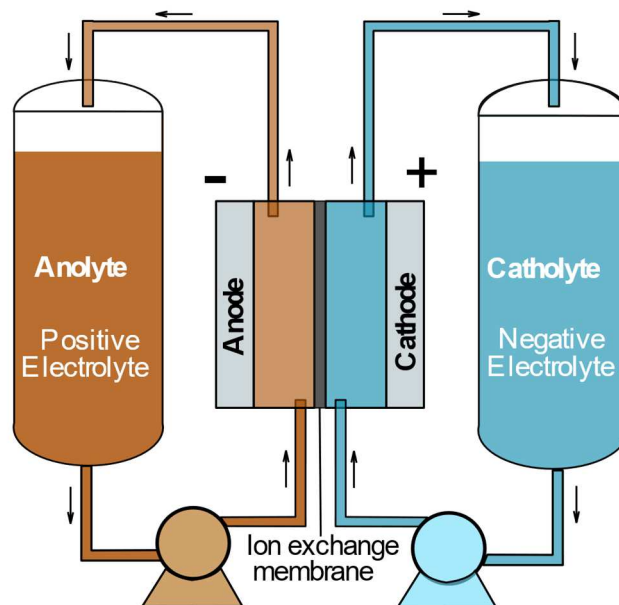


Figure 3.4 Flow battery

With the term chemical energy storage, it is usual to refer to *Hydrogen* or *Synthetic natural Gas* (SNG). In the first case, hydrogen is the storing element because it is obtained via water electrolysis using an excess of electric energy. Hydrogen storage systems usually consist of a hydrogen tank, an electrolyser and a fuel cell. The

electrolyser is the element responsible for hydrogen production from water and electric energy. Hydrogen can then be stored in tanks and used later with a fuel cell where it can combine again with oxygen to produce water and electric energy (Figure 3.5). In the second case, SNG can be considered as alternative to hydrogen as storing element. SNG are usually obtained in a two-step process: first, water can be split in oxygen and hydrogen with electrolysis using extra electric energy available. Then hydrogen and carbon dioxide can react with methane in a methanation reactor to produce SNG. This can be stored in tanks and then used as fuel in a power plant as well as in a fuel cell to produce electric energy. In both cases, if stored in suitable tanks, hydrogen and SNG are viable portable storage systems to be used in combination with fuel cells to propel vehicles [3.9].

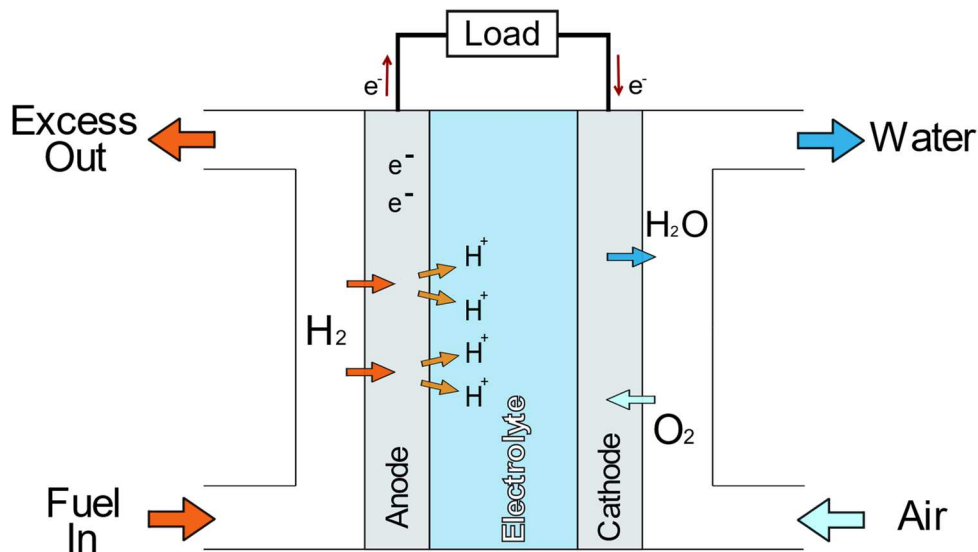


Figure 3.5 Fuel Cell

Ultracapacitors are systems able to store electric energy as standard capacitors but with much higher capacitance (thousands of Farads) and power capabilities [3.10]. Thanks to their low internal resistance, they can store and deliver energy in a very short time. These characteristics as well as their high reliability and durability, make them suitable as ESS for applications not compliant with standard battery performance.

Superconducting magnetic storage systems use a superconducting coil cooled below its critical temperature to store energy coming from a current flow [3.11]. The extra energy is stored in the magnetic field induced in the coil and can be quickly delivered when required. The fast responsiveness of these systems makes them suitable for critical applications as particle accelerators and nuclear fusion plants. The reliability of a magnetic storage systems depends mainly on that of the cooling system having theoretically an infinite lifetime in terms of charging/discharging cycles.

In the following sections, secondary batteries will be further explored especially for their applications as ESS for electric vehicle applications. A brief review on lithium batteries current state of the art will be proposed to understand strengths and weaknesses of their use in vehicles' applications.

3.2 Secondary batteries for electric vehicles

As discussed in the previous section, secondary batteries are ESS able to perform several charging/discharging cycles. This characteristic is crucial when the ESS must be portable and able to supply power several times. The main point is not to have a huge energy storage to satisfy the user during its all operating life but to always have enough energy when required. In these terms, it is possible to restore the depleted energy when the ESS does not have to work in order to be ready for the next working session. This is for example the main requirement that an ESS must have to be considered for vehicles applications [3.5],[3.12].

There are several types of secondary batteries depending on the chemistries of their elementary electrochemical cells. Each one comes with specific characteristics in terms of:

- Gravimetric and volumetric energy density;
- Gravimetric and volumetric power density;
- Lifetime in terms of maximum number of complete charging-discharging cycles before the energy storing capability drops below an acceptable threshold;
- Operating temperature ranges.

In Figure 3.6, an overview of secondary batteries performance is shown in the Ragone plot. Results refer to properties at electrochemical cell level. Remarkable differences arise when dealing with battery packs, where several components other than cells must be considered.

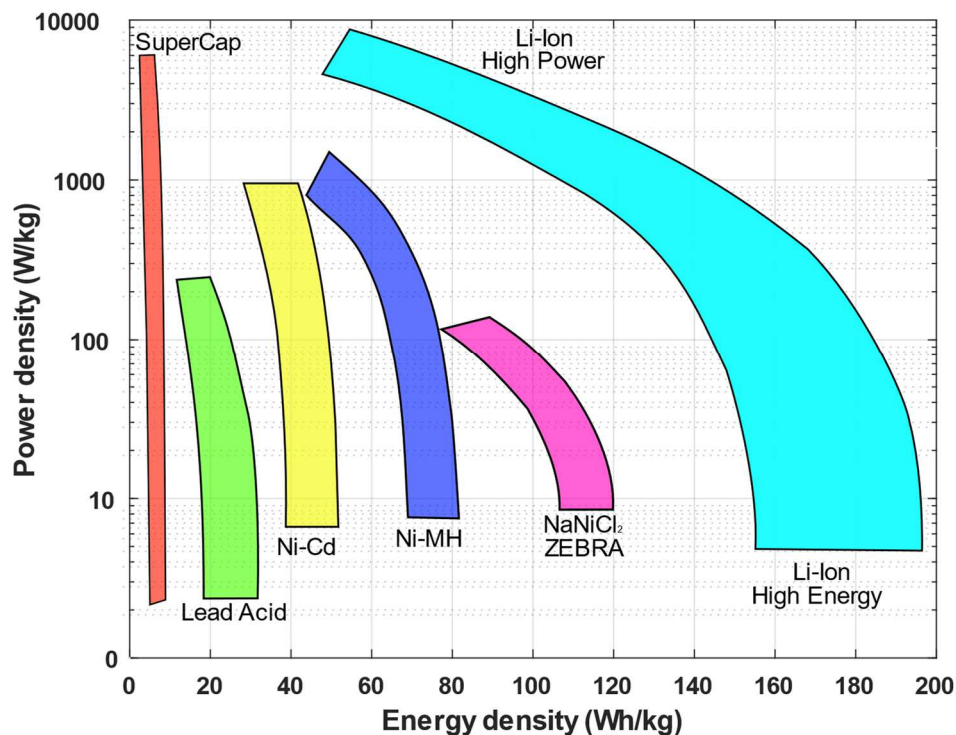


Figure 3.6 Ragone plot: secondary batteries performance

3.2.1 Lead-acid batteries

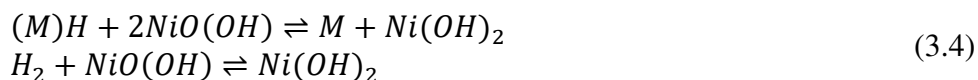
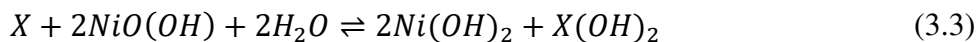
Lead-acid batteries (LA) [3.13] were invented in 1859 by the physicist Gaston Plantè. Due to the high weight of their active elements, the energy density is relatively low compared to other chemistries. However, these batteries can supply high power for short periods of time making them suitable as starter ESS for Internal Combustion Engines (ICE). The battery has an anode with lead (Pb), a cathode of lead dioxide (PbO₂) and sulfuric acid H₂SO₄ as electrolyte solution. The reversible chemical reaction shown in Equation (3.2) takes place during charging/discharging cycles within the electrochemical cell ($V_{\text{cell}}=2.05\text{V}$).



This class of batteries can operate up to 15 years or 2000 cycles at 80% Depth of Discharge (DOD). Usually, lead-acid batteries come in a 6-12 V packages suitable for starter and lighting application. However, the more recent development of valve regulated lead-acid batteries (VRLA) opened new scenarios for the application in small vehicles and industrial forklift. The main recognized solutions are absorbed glass materials (AGM) and GEL batteries. The former has a solid fiberglass separator able to absorb the electrolyte solution. The amount of liquid electrolyte in the battery is related to maximum absorption capability of the separator leading to less acid leakage in case of mechanical failure of the case. Moreover, the fiberglass matrix allows for better gas transportation through the separator leading to best performance during charging at high currents. On the other hand, Gel batteries are manufactured using a gel electrolyte solution. They perform as AMG batteries having also less leakage problems compared to standard LA. However, having an electrolyte solution in the form of a gel makes them less susceptible to electrolyte evaporation and freezing (which instead affects the liquid solution inside the fiberglass matrix of AGM batteries). The main drawback is the higher time required for charging due to the low currents allowed during this phase.

3.2.2 Nickel-based batteries

The electrochemical cell of Nickel-based batteries is composed by a nickel oxide hydroxide cathode, a metallic anode material (usually Fe, Cd, Zn or metal-hydride MH) and a potassium hydroxide solution as electrolyte [3.14]. The chemical reactions that take place during charging/discharging cycles are shown in equation (3.3) for X equal to one of the elements between Fe, Cd, Zn and equation (3.4) for MH.



Nickel-Cadmium batteries (NiCd) invented in 1899 by Waldemar Jungner, had been a competitive alternative to LA batteries for a long time showing better performance

especially on shelf life (amount of time of inactivity before the next use), reliability against hard working conditions and fast charging processes. These robust batteries are still considered in the aerospace industry as backup systems but require care in their use. They can be toxic in case of failure due to the presence of Cadmium. Although the good shelf life, the self-discharge rate is very high, so they frequently require to be charged. Finally, due to the so called memory effect, this chemistry requires periodic full discharge cycles to being able to use its full capacity. The relatively low capacity and voltage ($V_{\text{cell}}=1.20\text{V}$) needs proper design of the battery pack to meet the prescribed requirements of the application.

Nickel-Metal-Hydride is a relatively newer technology compared to NiCd that started to be considered as alternative solution in the 1980s. The very first chemistries showed one of the highest self-discharge rates at that time. The development of new hydride materials partially solved this problem at the price of lower specific energy. Ni-Mh batteries require special charging profiles to keep them stable. They show lower memory effect than NiCd but also lower cycle life. Nevertheless, the higher capacity (up to +40% than NiCd), robustness and the lower toxicity allowed them to slowly achieve the top position in the market of secondary batteries until the large scale commercialization of Lithium-Ion batteries (early 2000s). Actually, Ni-MH batteries were the first storage solution considered by big automotive manufacturers (Toyota, Mazda, Nissan, Mitsubishi, etc) for their first commercial electric and hybrid solutions.

Worth to mention are also *Nickel-Iron* (NiFe), *Nickel-Zinc* (NiZn) and *Nickel-Hydrogen* (NiH) batteries. They are alternatives to the chemistries shown before, preferred in certain applications depending on the specific requirements on life cycle, cell voltage, operating temperature ranges and costs.

3.2.3 Sodium-beta batteries (ZEBRA)

Batteries that have Na as anode material usually use a solid electrolyte as the beta-alumina that shows very good ion conductivity (Na^+) at high temperature [3.15]. The first electrochemical cell based on this principle was developed by Ford in the 1960s for electric vehicle applications. Sooner, *Sodium-metal halide* batteries of the form Na-MeCl₂ often known with the acronym of Zero Emission Battery Research Activity (ZEBRA) started to be developed for electric vehicles applications. These batteries usually operate at temperatures between 250 and 350 °C where the solid electrolyte activates itself. They are characterized by a relatively high energy density, good tolerance to overcharge, safety, long life cycle and lower cost compared to other chemistries. The main drawback is the need to heat constantly the battery to be able to use it, requiring up to 500W for an entire battery pack. Among ZEBRA batteries, Na-NiCl₂ are the most used for electric vehicles applications. The electrochemical reactions for this type of cells can be described by Equation (3.5) leading to a cell voltage of 2.58V at 300°C.



3.2.4 Lithium Ion batteries

Lithium-Ion batteries [3.16]-[3.18] were proposed in the 1970s by Michael Stanley who considered a pair of electrodes made of lithium metal and titanium sulphide. Although the promising characteristics this combination never had success due to its high instability. In fact, lithium-based battery chemistries have a strong potential thanks to the high lithium electro positivity or ability to donate positive charge. This characteristic is crucial when it comes to energy storage but makes the element highly reactive. Thus, great efforts are required to find the best electrodes and electrolyte combinations that balance performance, stability and safety. The breakthrough was reached in 1991 when the first stable configurations were finally commercialized.

As shown in Figure 3.7, a Li-Ion battery is essentially made by six components: a positive electrode (the cathode), a negative electrode (the anode), their corresponding current collectors (usually Aluminium and Copper respectively), an electrolyte which helps the Ion migration between the electrodes and a separator that physically prevents the contact between the electrodes.

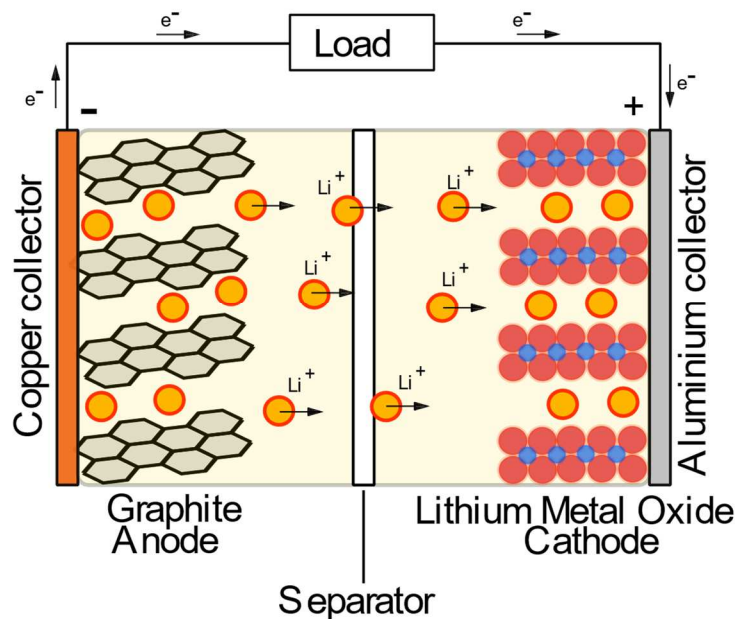


Figure 3.7 Lithium-Ion electrochemical cell

Lithium-Ion batteries are usually named based on the material of the cathode that donates lithium-ions. Nowadays, lithium metal oxides are preferred. The most commercially available solutions use lithium cobalt oxide (LCO), lithium manganese oxide (LMO), lithium iron phosphate (LFP), lithium nickel cobalt aluminium oxide (NCA) and lithium nickel manganese cobalt oxide (NMC). The anode is usually a graphite structure although recently lithium titanate (LTO) showed good performance as suitable alternative. The electrolyte is a solution of a lithium salt and an organic solvent that increases lithium-ion mobility between the

two electrodes. This characteristic is crucial when it comes to performance stability and cycle life. The electrolyte solution reacts with both the electrodes producing a thin layer called Solid Electrolyte Interface (SEI). This thin layer hinders the Ion movements and plays an important role in the total internal resistance of the cell. Moreover, the SEI increases at each complete charge/discharge cycle reducing the amount of usable charge (at the same voltage level). The separator physically prevents the contact between the two active electrodes. It is made by a polymeric material, usually polyethylene or polypropylene, permeable to lithium ions. Finally, two current collectors have the role of interfacing the active material to the external circuit. The use of copper for the anode and aluminium for the cathode is mainly related to chemical stability between them and the active material but also to the electrochemical stability at the electrode's voltage potentials. When dealing with stability and safety of a lithium-ion battery, thermal runaway is one of the greatest issues [3.19]. It is essentially a temperature threshold above which the battery starts to burn due to the reaction between the melted metal oxides and oxygen. This event can lead to the explosion of the cell if the high pressure coming from the gaseous products of these reactions cannot be controlled. The inherent safety of a chemistry can be related to the temperature threshold that identifies the ignition of thermal runaway events.

The proper combination between these components leads to remarkable differences in specific energy, power capabilities, cycle life (in terms of number of cycles for a certain Depth of Discharge -DOD) and safety. In Table 3.1 it is possible to appreciate the main differences in terms of performance among the most widely available chemistries.

	LCO	LMO	LFP	NCA	NMC
Nominal Voltage (V)	3.7	3.7	3.2/3.3	3.6	3.6/3.7
Gravimetric energy density (Wh/kg)	110-180	100-120	80-120	180-250	180-210
Discharge Rate (C)	1-2	3-15	1-15	1-10	1-10
Cycle life 60% DOD	300-500	1000-1500	2000-5000	500-1000	500-1000
Cost (€/kWh)	550	725	1300	490	415
Thermal Runaway (°C)	150	250	270	150	210

Table 3.1 Lithium Ion chemistries performance (graphite structure on the anode)

LCO was the first commercial Li-Ion chemistry in the 1990s with LiCoO_2 as cathode and graphite as anode. It was adopted for portable electronics and for some backup supplies in the aviation. The main problem of this chemistry relies in its thermal stability due to the low thermal runaway threshold. Although still used for

small electronics, this limitation together with a not great cycle life prevented the use of LCO batteries in stationary storage and vehicle applications.

LMO batteries (1996) use LiMn_2O_4 as cathode and graphite or LTO anodes reaching better performance in terms of cycle life but at the cost of a lower energy density. LMO cathodes show lower internal resistance which leads to higher power output and greater charging/discharging efficiency. Thermal stability is also remarkable with a thermal runaway temperature of 250 °C that allows the use in small vehicles (especially e-bike) and medical devices.

LFP batteries (1999) use LiFePO_4 as cathode and graphite as anode. They are designed for thermal stability and long cycle life at the compromise of relatively low energy density. This chemical configuration is also the most tolerant against full discharge, maintaining a quite constant voltage among all the working range. This also increases the amount of energy deliverable despite the lowest nominal voltage among the ones showed above. Actually, LFP is one of the most promising chemistry for the development of vehicle applications and stationary storage: it is a well consolidated technology and show the best compromise between performance and durability.

NCA batteries (1999) use LiNiCoAlO_2 as cathode and graphite anode. This combination leads to the best energy density and power capabilities as well as a good cycle life. These characteristics make this chemistry suitable for vehicle applications that require both power and enough energy as well as a good life span. The car manufacturer Tesla adopts this chemistry in their vehicles and, at the time of this research, is completing the building of the Gigafactory a production centre that will be mainly focused on NCA batteries.

NMC batteries (2004) use LiNiMnCoO_2 as cathode and graphite as anode. It is the most recent chemistry technology commercially available and yet gained a good market share for electric vehicle applications. Compared to NCA batteries, the chemical combination between these electrodes sacrifices energy density to increase cycle life. The most commonly used NMC cathodes have the same percentage of nickel manganese and cobalt also known as 1-1-1 (one third nickel, one-third manganese, one-third cobalt). Changing these proportions, custom solutions can be obtained. Considering the cost and toxicity of raw materials, especially cobalt, it is usual to increase the amount of nickel if energy density is the requirement or manganese to increase power density.

As shown in the Ragone plot (Figure 3.6) Li-Ion batteries properties make them suitable for high power and energy applications such transportation and grid storage but the gap with fossil fuels is still relevant. The higher efficiency of electric powertrains compared with ICEs reduces this gap, but still improvements in energy density are required. As stated in [3.17], actual chemical solutions have reached a certain saturation level. Still improvements in safety and cycle life can be achieved, but energy and power density are strictly related to the electrodes active materials and to the electrolyte characteristics. Safety can be improved if less toxic materials are considered as replacement of cobalt (as for LFP). The most futuristic scenario is to change entirely the paradigm of the energy storage mechanism, from Li-Ion insertion to their conversion. Further details can be found in the literature [3.17].

3.3 Battery management for lithium ion cells

Nowadays Lithium-Ion batteries are the most suitable solution both for stationary energy storage and electric vehicle applications. The electrochemical solutions shown in the previous section show good energy and power performance or cycle life depending on the electrodes' pairs considered. However, safety is a real concern for this type of batteries due to the inherent high reactivity of lithium with the involved chemical compounds. Catastrophic failures can happen due to imperfections in the design or manufacturing process as well as for a not proper monitoring and control during their operating life [3.20] - [3.22]. Overcharging and over discharging are very critical conditions where undesired reactions between the electrolyte and the active materials can be accelerated reducing the battery lifespan. As discussed, the most relevant concern for lithium ion batteries is thermal runaway. An increase of cell temperature above the thermal runaway temperature leads to irreversible chain reactions which increase internal pressure up to the final explosion. Moreover, it is not so rare to have events at cell level that propagate at the entire module and pack level, increasing the level of danger especially in vehicles applications. Thus, it is very important to continuously follow the evolution of the battery pack in all the operating conditions to promptly intervene when abnormal conditions are met. For these reasons, a dedicated management device must be designed for those applications where a lithium ion battery pack is involved.

Battery management systems (BMS) are electronic architectures designed to actively monitor battery pack operations [3.23] - [3.25]. Whenever an abnormal behaviour such as over-voltage or over-heating is detected, a properly designed BMS should warn the user and eventually execute predefined safe shutdown procedures. The main functions a BMS should perform are the following:

- Cell voltage, current and temperature acquisition and storage
- Cell state estimation
- Cell balancing
- Charging and discharging active control
- Safety features (shutdown procedures, power de-rating)
- Thermal management
- System/vehicle communication

Performing these tasks in Real-Time is quite an established point for modern BMS thanks to the advancements in processing capabilities of today's embedded systems. What is still discussed in the industrial and scientific community is the use of the data gathered over time to optimize battery performance and to predict what it is still capable to do as remaining operating life. As supervisor device, the BMS has always to be efficient, reliable, accurate and ready to intervene in case of failure events.

3.3.1 BMS architectures

The BMS architecture is strictly related to the battery pack layout. Due to the voltage requirements of the application, several elementary cells must be connected in series to sum their electric potential. The common practice is to group several cells (usually between 8 and 12) connected in series into a single low voltage module and then connect in series several modules to reach the desired voltage of the DC Bus. Within each module, it is also possible to connect several cells in parallel to increase the total capacity. Thus, the module will be identified by the array of $mp - ns$ cells where mp is the number of cells connected in parallel and ns is the number of cells (or groups of cells) connected in series. Once the battery pack layout is stated, the BMS architecture can be defined. It is usual to consider an architecture with several layers [3.25] of control units:

- Cell monitoring unit (CMU) is the lowest level of the architecture to which data acquisition is demanded;
- Module management unit (MMU) is the control unit that monitors and coordinates a group of several CMUs or several cells providing also balancing functionalities;
- Pack management unit (PMU) is the high-level control unit of the battery pack. It manages and coordinates several MMUs (Master-Slave configuration) and is responsible for communication with the external system with which the battery pack is working. PMU is also in charge of controlling signals for the thermal management unit, the pack safety devices and the external charging unit.

Depending on the number of cells and modules involved a centralized or decentralized BMS can be considered. For complex battery packs as those for electric vehicles, it is usual to consider decentralized structures with a Master/Slave configuration between the PMU and MMUs/CMUs. In Figure 3.8, a common layout for BMS systems in electric vehicles is shown

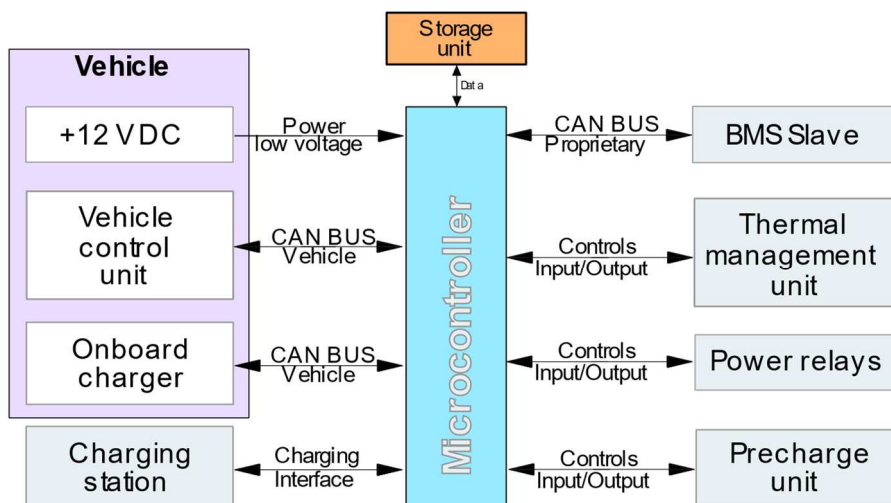


Figure 3.8 Battery management system layout for an electric vehicle

3.3.2 Cell Balancing

Lithium Ion cells come with intrinsic differences related to variations in the manufacturing process. Total capacity, initial capacity, internal resistance and self-discharge rates are the main characteristics affected [3.27]. The different temperatures that each cell experiences in the battery pack in operating conditions tend to emphasize possible inhomogeneities. For these reasons, balancing circuitry are integrated in a battery pack to smooth differences between each cell.

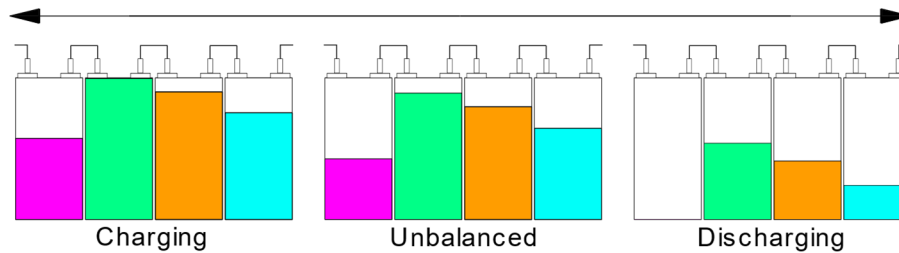


Figure 3.9 Battery management system layout for an electric vehicle

In Figure 3.9, the main drawbacks of an unbalanced group of cells connected in series is shown. Starting from an unbalanced condition, any charging process will be stopped once the most charged cell reaches the predefined charging voltage. Thus, all the other cells will remain partially charged. This condition results in a loss of available capacity. At this point, any discharging load applied will sink the same current from all the cells (series connection). At some point, the less charged cell will reach the over discharge voltage limit before the others and will define the empty status for the battery pack. This condition results in a loss of deliverable energy. To overcome this problem, three different strategies can be implemented:

- Passively dissipate energy from the most charged cells during charging
- Actively transfer energy from the most charged cells to the others
- Isolate each cell from the rest of the pack and controlling both the charging and discharging phase.

The first solution is the simplest and most reliable approach for cell balancing. Cells are connected to the shunt resistors in parallel by mean of electronic switches. During charging, all the switches can be simultaneously on in such a way that once the maximum capacity is reached, the excess charge is dissipated in the resistors. Otherwise, measuring each voltage cell, these switches can be controlled separately increasing the charging efficiency. The second solution consists in the adoption of complex capacitors topologies that can store the excess of energy and release it to cells with lower voltages depending on the specific connections realized with electronic switches. The last approach uses DC/DC converters for each cell controlling the amount of charging or discharging current depending on the actual cell conditions. This more complex solution gives more flexibility on the output voltage characteristic of the entire battery pack.

3.3.3 State of Charge estimation

The State of Charge (SoC) is an indicator used to describe the state of a battery in terms of how much electric energy it is still capable to deliver. It can assume values in the range 0-100% to address all the possible cases between the empty-full conditions. The same concept can be described by another indicator called Depth-of-Discharge (DoD) that addresses the reciprocal quantity of SoC. It represents the amount of electric energy delivered from the initial full condition. In principle, the SoC is like a fuel gauge of an ICE vehicle. Both describe the full-empty condition of the ESS but if on one end the fuel level in the tank represents well the amount of the stored energy, the SoC cannot be directly associated to one physical and measurable quantity. The amount of electric energy a battery can deliver is strongly affected by temperature and aging mechanisms [3.28], [3.29]. Nevertheless, several definitions have been proposed in literature for the SoC of a battery.

The SoC is a state of the battery, related to the actual composition of the active material on the electrodes and of the electrolyte solution. Thus, for a given thermodynamic equilibrium condition with constant temperature and pressure, a certain chemical composition of the active components corresponds to a value of the maximum electric energy still deliverable [3.30]. The physical quantity strictly related to the thermodynamic equilibrium condition is the Open-Circuit-Voltage (OCV) that is defined as the measured voltage between the two electrodes when the battery has reached the equilibrium condition. With no attached load, there are no charges movements towards the external circuit thus they can distribute inside the electrodes according to the lowest energetic condition. This is the best condition to evaluate the actual difference in the electrodes' electrochemical potential. Although the correlation between the OCV and the actual reservoir of electric energy, the measure of the OCV is not practical for real use cases due to the high amount of time required to reach the real thermodynamic equilibrium condition. This is the reason why several efforts have been made by the scientific community in order to find a way to estimate the actual SoC of a battery. According to the classification proposed in [3.31] there are several ways to practically estimate SoC. The current state of the art of SoC methods are shown in Table 3.2.

Conventional	Adaptive filter algorithm		Learning algorithm		Non-linear Observer	Others
OCV	KF	PF	NN	FL	SMO	MARS
EMF	EKF	UPF	ANN	ANFIS	ASGSMO	BI
CC	UKF	H ∞ filter	FNN	SVM	PIO	IR
Resistance	SPKF		RBFNN	GA	NLO	Hybrid
EIS	RLS					
Model based						

Table 3.2 SoC estimation methods

The conventional methods use measurable quantities to estimates the SoC. The *Open-Circuit-Voltage (OCV)* method as described before, relates the SoC of the battery to its terminal voltage after a certain amount of resting time. The method is relatively simple, but it is not practical for dynamic applications as electric vehicles

and energy storage where it is very unlikely to have no load applied (so no electric energy delivery) for a long period of time. Moreover, the accuracy of this method is strongly related to the accuracy of the voltage measurement devices used. In commonly adopted BMS, cell voltage accuracies of 5 mV are the standards. For some chemistries like LFP, the range between 20% and 80% of SoC is characterized by very flat voltage patterns. Thus, such standard accuracies can lead to high errors in SoC evaluation. As an alternative to the OCV method some researchers prefer to correlate the *Electromotive Force (EM)* to the SoC, but practically the evaluation is again based on the measurement of the OCV relaxation after the load is removed.

The *Coulomb Counting (CC)* method assumes that the electric energy stored in a battery is directly related to the amount of charges stored in the electrodes. Thus, integrating in time the battery current (I) as in Equation (3.7), and correlating it to its maximum capacity (Q_n nominal capacity) it is possible to obtain the estimation of the actual SoC.

$$SOC = \left(1 - \frac{\int Idt}{Q_n}\right) * 100 \quad (3.7)$$

This method is the easiest to implement but could lead to very inaccurate results. First, any not filtered noise on the current measurements reflects directly on the numerical integration as well as errors in the measurements themselves. Then, the most critical point is the correct value of Q_n to be used. At the beginning of its life, it is reasonable to use the nominal capacity measured with certain standard conditions. Aging affects the value of the maximum storable capacity over time thus, the value of Q_n should be periodically recalibrated. Of course, on a vehicle it is not possible to repeat the same testing procedure the manufacturer did on the initial cell so, an error on this recalibration reflects on the value of SoC estimated. Moreover, the amount of maximum stored capacity cannot be equal to the amount of usable charges due to the strong correlation with temperature. Higher temperatures allow to store and use more energy as well as cold temperatures prevent the full use of the charged capacity (at higher temperature).

Another approach consists in evaluating the *Internal Resistance (IR)* as the voltage drop after the application of a constant current I load. The measurements must be taken no more than 10 ms after the application of the load to consider just the ohmic effect and not Ion transfer or diffusion. It is demonstrated that the IR changes with the SoC. However, most Li-Ion chemistries show small IR variations within the 20-80 % SoC range making this method not practical for standard BMS. Similarly, the use of *Electrochemical Impedance Spectroscopy (EIS)* aim to correlate battery impedance to SoC measuring the frequency response of the battery under sinusoidal current loads at different frequencies. The low frequency response is practically dominated by the Ohmic resistance so measurements in that range allow the correlation with the SoC. The method is not practical for standard BMS hardware components, but it is often used for electrochemical models' characterization.

Model based methods use mathematical models to estimates the OCV and thus the SoC. There are two types of models: Electrochemical Models (EM) address the

main electrochemical dynamics and chemical thermodynamics; Equivalent Circuit Models (ECM) want to describe the battery dynamic behaviour using RC networks. These models are used to evaluate online the OCV and compare it to offline lookup tables OCV-SoC to evaluate the actual state of the battery. Recently, also new correlations between mechanical quantities (strain, stress) and SoC have been explored [3.32]. However, still a lot of work must be done to prove the feasibility under several working scenarios.

Adaptive filter algorithms usually are adopted to improve model-based methods in the estimation of unmeasurable quantities when measurements are also affected by noise. *Kalman Filter (KF)*, *Extended Kalman Filter (EKF)*, *Unscented Kalman Filter (UKF)*, *Sigma Point Kalman Filter (SPKF)*, *Particle Filter (PF)*, *H ∞ Filter*, are essentially methods that estimate unknown system states from time measurements of other system variable. The use of several noisy measurements related to the desired unknown state instead of using only one input-output model of just one measured quantity, can increase the final accuracy of the estimation. The mentioned methods start from this concept and then evaluate the desired unknowns from measurements and ECMs or more complex mathematical models to estimate the SoC.

Between learning algorithms *Neural Networks (NN)* methods want to train multi layered input-output models to represents the highly non-linear behaviour of a battery. Usually, NN takes current, voltage, and temperatures as input data in order to estimate the actual SoC of the battery. Similarly, *Fuzzy Logic (FL)* methods use sets of training dataset to draw up a series of input-output relationship and membership functions for each of them. Then, inputs are processed to understand to which set of rules they can be addressed obtaining as a result the unknown estimates. *Support Vector Machine (SVM)* and *Genetic Algorithms (GA)* are used changing the degree of complexity of the non-linear model to better estimates the unknown parameters.

Finally, Non-Linear Observers (NLO) like the *Sliding Mode Observer (SMO)*, the *Proportional-Integral Observer (PIO)* are methods derived from control theory that track the model response according to measurement data adjusting online model parameters to match the real behaviour of the system.

All the presented methods have demonstrated different degree of accuracy on the SoC estimation compared to the true CC of battery discharge in controlled environments. Some Hybrid version of the proposed methods have been recently explored by the scientific community. They show better performance compared to their base versions, but at the cost of a higher degree of complexity thus computational cost. However, still a lot can be done in SoC estimation research. Too often research activities are related to laboratory environmental conditions and workloads. More realistic working scenarios should be investigated especially for vehicles' applications where vibrations, dust, humidity and dirtiness can add variables that could affect the actual state of the battery.

3.3.4 State of Health estimation

The State of Health (SoH) of a battery represents its capability of storing and delivering electric energy over time. The best condition (SoH = 100 %) usually corresponds to the moment the cell is manufactured and tested for the first time. Depending on the application, a Li-Ion battery is considered to be functional until a certain SoH threshold is reached. At this point, the battery does not satisfy the design requirements of the application, but this does not mean that it cannot be used anymore. As an example, battery packs for EV applications are prescribed to be replaced when a SoH of 80% is reached. Very often, performance of these “exhausted” battery packs are still completely adequate for normal vehicle usage, but manufacturers do not guarantee anymore about their performance. These exhausted battery packs could fit also other applications like stationary grid storages where load profiles are lighter and adequate for aged batteries [3.33]. Thus, it is very important to continuously estimate the battery SoH to understand its actual capabilities.

The most considered SoH indicators are battery capacity and internal resistance [3.25], [3.34], [3.35] because can be directly related to the stored energy and power capabilities. Capacity fade is usually strictly related to the loss of Li-Ions availability, decomposition of the active material and other structural changes. The increase of internal resistance can be related to the growth of the SEI. Greater internal resistance with the same differential voltage between the two electrodes leads to less power capabilities due to the internal voltage drop. These considerations are valid if just aging mechanisms are considered. More complex behaviours can be triggered in case of abnormal use or mechanical/thermal abuse [3.36].

Considering standard aging mechanisms, methods for SoH estimation can be classified in Experimental Methods and Model Based estimation methods [3.25] as shown in Table 3.3.

Experimental Methods		Model Based Estimation Methods	
Direct measurement	Indirect Analysis	Adaptive algorithms	Data driven
Capacity test	Charging curve test	ECM based methods	Empirical models
Coulomb Counting	ICA	KF,EKF,UKF,	Data fitting
Internal Resistance	DVA	AEK,FPF,UPF	Optimization Algorithms
Impedance (EIS)	Ultrasonic inspection	H ∞ Filter, PIO,SMO,...	Machine Learning
Cycle number counting		EM based methods	Sample Entropy
Destructive methods		Hybrid methods	

Table 3.3 SoH estimation methods

As expected, most of the methods are strictly related to the ones already mentioned for SoC. What are worth to mention here are indirect analysis methods. The main reason is because the derived quantities considered are more sensitive to the characteristic small voltage variations of Li-Ion batteries. The *Incremental*

Capacity Analysis (ICA) [3.37] methods consider the actual capacity change rate with respect to voltage variations (the ratio dQ/dV). This quantity amplifies the phenomena occurring during the characteristic voltage plateau of several lithium chemistries. Moreover, researchers have demonstrated their good sensitivity to aging changes as shown in Figure 3.10. Similarly, *Differential Voltage Analysis (DVA)* [3.38], [3.39] methods consider the voltage change rates with respect to capacity to capture the two-phase transition in lithium chemistries. The distance between the typical two peaks of the DV curve represent the amount of electric charges involved in the transition. What makes this indicator particularly useful is its sensitivity to aging mechanisms that push the peaks toward the y axis as shown in Figure 3.10b [3.40].

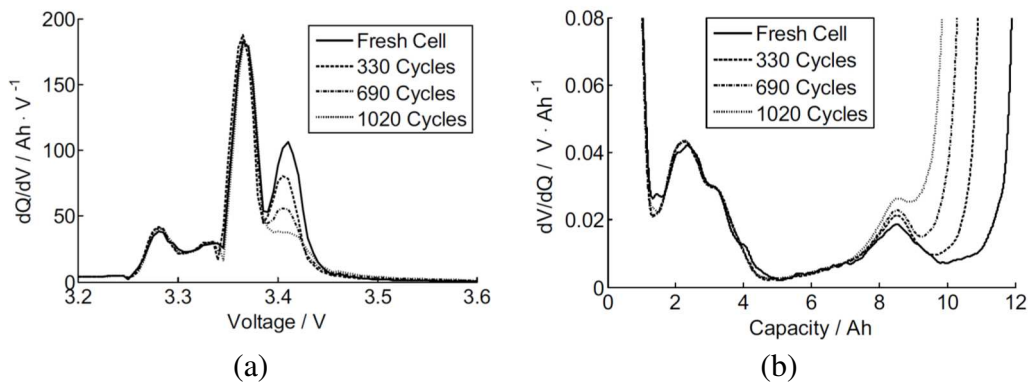


Figure 3.10 Indirect SoH analysis: a) ICA, b)DVA

Another interesting technique for SoH estimation involves the use of ultrasonic waves for inspection [3.41]. As in other the non-disruptive inspection methods, the goal is to identify any kind of defects looking at their interaction to the reflected waves. This technique is very promising for battery packs End-of-Life (EoL) inspection because can state clearly if the same batteries could be used or not for a second life application.

3.3.5 State of Power estimation

The idea of a State of Power (SoP) or State of Available Power (SoAP) indicator can be considered as belonging to a much larger battery state which is the State of Function (SoF) [3.42], [3.43]. There is no unique definition of the SoF. The most widely accepted, define the SoF of the battery as a parameter that states if it is able to perform the task/function it was designed for. This is the main reason why, for grid or vehicle's ESS it is usual to move from the general SoF definition to the SoP or SoAP. For those applications, it is necessary to know if the battery will be able to supply a certain power request or not depending on its operating conditions.

The main factor that can affect the SoP is the variation of the battery's internal resistance as it is shown in Equation (3.8) and (3.9).

$$P_{\text{discharge}} = V_{\text{batt}}(V_{\text{OCV}} - V_{\text{batt}})/R_0 \quad (3.8)$$

$$P_{charge} = V_{batt}(V_{batt} - V_{OCV})/R_0 \quad (3.9)$$

where the power needed to charge or discharge (not considering charge/discharge efficiency) is intrinsically related to the actual battery voltage (V_{batt}), its SoC (taken into account by V_{OCV}) and its internal resistance (thus practically temperature and SoH). The restriction on the maximum charging or discharging power is strictly related to the desire to keep the battery within the manufacturer specified Safe Operating Area (SOA). In operating conditions, battery voltage should always stay between the Cut Off Voltage ($V_{batt,min}$) and the maximum Charging Voltage ($V_{batt,max}$) to not damage the active material. Moreover, the battery temperature should not exceed the maximum temperature to not speed up irreversible ageing mechanisms nor should drop below certain cold temperature thresholds.

Although still lot of work must be done on the estimation of this parameter, it is clear how it is important for vehicles' applications, especially for working machineries. As it will be experimentally demonstrated in the next sections, the amount of power a battery can deliver it is not always the same so a Full EV it is not able to perform in the same way along all its SoC and SoH range. In case of automotive applications, these would lead to lower acceleration capabilities, while in the working machineries field it can prevent to accomplish a certain task leading to high money wastes.

3.4 Battery thermal management systems

It is well established that Li-Ion batteries show the best performance around room temperature, in the range between 15 and 35 °C [3.44]. Outside this window, their performance can change drastically and may affect irreversibly their cycle life. As demonstrated in [3.45]-[3.46], at lower temperatures batteries show a remarkable loss of available capacity. There are two main reasons for that. The first one is related to the decrease of electrolyte performance, especially in its ions transportation rate [3.47]. Lower temperatures slow down chemical reactions at the same voltage potential. The second reason is related to Lithium plating (or deposition) around the anode [3.48]. At low temperature it is easier for lithium ion to deposit on the anode surface rather than entering within its graphite structure. Thus, the SEI will increase in thickness. Both the phenomena are macroscopically felt as an increase in internal resistance. It is worth to mention that, if the battery is charged at higher temperature and discharged at lower ones it shows lower available capacity. However, the amount of charges stored in the electrodes can be used again if the battery is warmed up and discharged without another charging cycle as shown in Figure 3.11. So far, the main problems at low temperatures can be avoided if a certain pre-heating strategy is applied. Several (patented) solutions have been proposed both by the scientific community and automotive manufacturers (Toyota ahead) [3.49], [3.50]. They range from the basic and not so efficient self-heating where a certain amount of stored energy is used to increase internal temperature through the Joule effect, to more complex systems that consider electric heaters.

On the other hand, if the battery goes beyond the 40 °C threshold several phenomena can take place. First, high temperature speed up ions transportation and diffusion leading to a macroscopic reduction in internal resistance. More energy can be stored and more can be used. Thus, it may seem like better performance can be achieved warming up batteries. However, hot temperature speeds up also irreversible side reactions that lower the amount of Lithium ions in the electrolyte and the ones that increase the SEI growth rate [3.51]. Thus, the instantaneous increase in performance misleads from the truth of what is really happening.

The speed up of ageing mechanisms is an undesirable, but at least not dangerous, effect of working temperatures below 80 °C. At higher temperatures safety start to be a real concern. Around 85 °C the SEI starts to break down and dissolve in the electrolyte [3.52]. The anode is now exposed to the electrolyte which starts to corrode it. Moreover, side chemical reactions between the lithium ions stored inside the graphite structure and other compounds within the electrolyte and the anode active material may start as well. These reactions are exothermic and can lead to an increase in temperature up to 0.2 °C/min if a proper thermal cooling solution is used. When the battery temperature rises above 140 °C, exothermic reactions start also on the cathode releasing gasses rapidly (especially oxygen) and leading to increase in temperature growth rate up to 5°C/min. Above 180 °C the process is essentially irreversible. The separator starts to melt leading to possible short circuits and thus to another relevant source of heat. If a proper pressure release valve is not adopted, the high internal pressure can lead to the explosion of the battery with the spread of flammable hot chemical compounds all around. The described process is the so called Thermal Runaway.

Dealing with a battery pack, it is highly possible that thermal runaway happening on a single cell could spread also to its neighbours. This emphasizes the need for a proper Thermal Management System (TMS) that, coordinated by the BMS could cool down properly the cells inside a battery pack making them work within their SOA. Depending on their working principle, conventional TMS can be divided in [3.53]:

- Air cooled
- Liquid cooled
- Phase Change Materials (PCMs)
- Hybrid solution

Air cooled TMSs use unidirectional air flows to cool down cells' arrays. It is an active cooling solution because the heat extraction rate can be controlled based on the air flow rate thus, on the fans speed. It has been the most adopted solution for vehicles applications for a long time due to its inherent safety against short circuits. The efficiency of this solution depends on the amount of energy required to guarantee the proper air flow to cool down the cells.

Liquid cooled TMSs can rely on higher heat transfer coefficients than air thus, better cooling performance. They can be classified in direct and indirect systems.

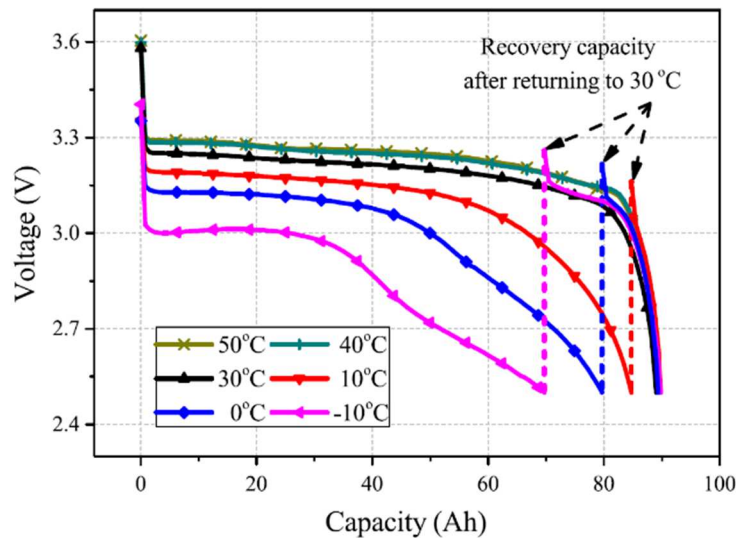


Figure 3.11 Battery performance at lower temperatures [3.28].

The first one is the case where the coolant is directly in contact with all the surfaces of the elements to cool down. This approach is more efficient but requires careful attention on the coolant choice that must be dielectric such as deionized water or mineral oils. It must be said that, although automotive manufacturers showed very little interest in this solution (maybe for electrical safety concern), several cases of oil cooled super computers show the feasibility of the solution at least from the electrical point of view. On the other hand, indirect liquid cooled TMSs are the most widely adopted solution among car manufacturers. Most of the time, they are tube or cold plate-based cooling solutions depending on the geometry of the cells and their configuration in the arrays in the battery pack.

Phase Change Materials TMSs is a well-known solution that is entering also in the industry market. They are much simpler systems compared to air or liquid cooling solutions and do not require special control algorithms. They are passive cooling systems that do not require maintenance and use the solid to liquid transition to extract heat from the cells. The heat will be released to the cells when they will cool down for lower external load. This is the main drawback of a passive solution. In fact, if frequent high rate charging or discharging cycle are performed with no resting periods, the material will melt and will prevent further heat extraction. This is the main reason why *hybrid solutions* are starting to be designed to take advantage from the simplicity of passive TMS and reliability of air or liquid cooling systems.

3.5 Battery pack design and in vehicle integration

Lithium Ion batteries come in different formats: cylindrical, pouch or prismatic with several options in terms of energy and power density [3.54] Historically, cylindrical and pouch cells have been widely adopted as ESS in electronics and personal computers thus their manufacturing process are quite consolidated. Prismatic cells are a more recent development where the electrochemical cells are stacked within a rigid prismatic case. However, voltage and capacity of the elementary cells are far from meeting requirements of a battery pack for vehicles'

applications. Thus, a certain combination of series and parallel connections between them must be realized to meet the design constraints.

Several aspects must be considered in the design of a battery pack. Cells format will strongly affect the module case shape and its cooling solution as well as the type of electrical connections and wiring between them [3.55]. Moreover, each of them leads to different energy density of the final pack due to size and weight of the required electrical connection as well as the proper cooling solution. Considering the same chemistry and the same total capacity, if all the required accessories are considered (connections, wiring, cooling solutions) cylindrical cells show the best packing density, thus the highest density (kg/m^3) of the battery pack.

The most important driving factor in the design of a battery pack surely is safety. As discussed in the previous sections, Lithium Ion batteries are inherently unstable if they work at high temperatures. Moreover, vibrations and mechanical abuse can irreversibly damage the cells starting undesired thermal runaways due to physical short circuits [3.56]. Vibrations coming from the vehicle chassis are transmitted down to elementary cells by the battery pack case and its mechanical connections to it. For an automotive application it is usual to have vibrations up to 50 Hz coming from the vehicle dynamic on the road profile. On working machineries, the vibration amplitudes in the same frequency range can be much higher due to irregular road profiles. Moreover, vibrations coming from a Diesel engine for NRMM (Non Road Mobile Machinery) are higher compared to the ones coming from an ICE used in the automotive field, requiring specific attention. Vibrations transmitted down to cell level can lead to premature failures due to mechanical delamination and wear of the active materials on the electrodes' surfaces and of the separator. Thus, a mechanical failure of such elements can lead to short circuit and thermal runaway. Mechanical isolation of battery packs against vibrations, has been explored by several research activities [3.57]. Several patented solutions consider the adoption of dumping elements to deal with vibrations transmitted along the vertical axis of the chassis [3.58], [3.59]. Also, lateral dynamics must be considered in the design of the case structure to prevent undesired cell movements. This is the reason why proper rigid spacers are used to block cells' relative motion within each module as well as rigid separators prevents modules movements inside the battery pack structure. Spacers' materials for cells are usually both electrically and thermally insulating to prevent undesired short circuits in case of impact and heat exchange between adjacent cells in case of an isolated cell failure. Finally, attention must be paid in screwed connections between cells' collectors and copper bus bars that physically connects them in series or parallel configurations. Vibrations can unfasten these joints leading to an increase in resistance or, in the worst case, an opening of the electrical circuit. In this case, usual precautions against spontaneous unfastening of threaded joints caused by vibrations can be adopted. Different is the case of mechanical fatigue life of these elements, especially for bus bars. Stresses induced by vibrations transmitted through the connections with the external case and with the cells inside can bring to crack propagation until a complete fatigue failure is reached. In this case, proper isolation and mechanical design of these elements can prevent undesired failures.

A more complex topic is the protection of the battery pack against mechanical abuses as impacts. Apart from proper design of absorbing elements, lots of attention must be put on the features that can prevent escalation of more dangerous events. First, if some cells are damaged as a result of an impact, the hot gasses deriving from possible local thermal runaway must be released in the atmosphere to prevent failure propagation. Moreover, the designed leakage point must be directed to not affect people safety in the moment when they are leaving the vehicle.

As briefly shown above, several fields of expertise are involved in the design of a safe and performing battery pack. Lots of efforts have been put in research and development of modern battery packs in order to meet new standards specific for this relatively young field [3.57]. However, still low attention is given by the scientific community to the application in NRMM field due to the early stage of its electrification process. Although several similarities between the two applications, NRMMs require specific design due to the wider range of possible loading scenarios that can be encountered during their operating life. The environmental harshness to which the battery packs of these machines would be subjected can be way different from the automotive case and would require properly designed solutions.

3.6 Lithium - Ion cells modelling and characterization

Lithium Ion batteries have superior performance compared to other chemistries. However, they must operate within their SOA to safely deliver electrical power. As mentioned before, their behaviour is strongly affected by temperature up to the point irreversible destructive chain reactions can be triggered if not well managed. The need of a BMS constantly aware of the cells' state has pushed the scientific community towards the development of mathematical models able to describe Li-Ion cells behaviour. Most of the relevant parameters/indicators that are defined for a certain state of the battery, are not directly measurable quantities. Thus, mathematical models are used to derive these pieces of information from other measurable quantities.

The non-linear behaviour of a Li-Ion cell can be appreciated in Figure 3.12, where the constant discharge behaviour is shown.

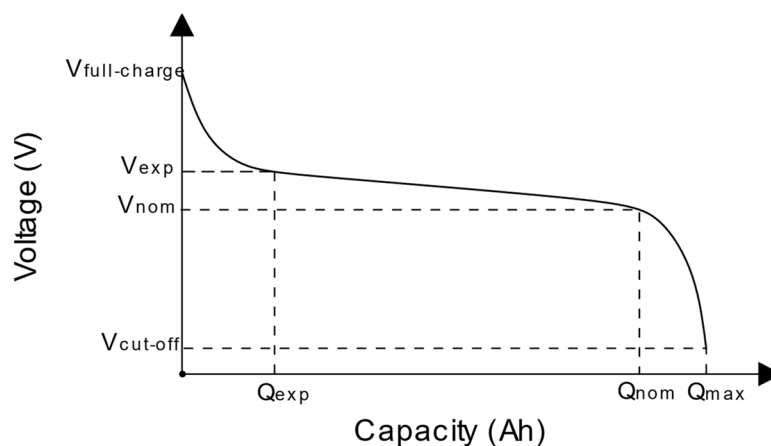


Figure 3.12 Lithium Ion discharge curve (1C): Voltage – discharge capacity.

Manufacturers prescribe the voltage operating range between $V_{\text{full-charge}}$ and $V_{\text{Cut-off}}$ when the maximum capacity has been already delivered. Usually, it is prescribed to not completely discharge the cell but to stop the power delivery when the 20% SoC is reached (or 80% DoD). This helps the battery life at the cost of a minor available capacity. The real range of interest is between V_{exp} and V_{nom} where the battery delivers most of the stored energy despite small variations in terminal voltage. The use of mathematical models to represent this behaviour is useful to increase the accuracy of the battery state estimation starting from measurements with a certain accuracy and noise.

From the electrical point of view, there are several type of modelling approaches described in the literature. Among them it is worth to mention Electrochemical Models (EM) and Equivalent Circuit-based Models (ECM). The first category focuses the attention in modelling the physical electrochemical phenomena occurring inside the cell, involving the active materials, the electrolyte, the electrodes and the separator elements [3.60], [3.61]. To describe this dynamic system, highly non-linear differential equations are used increasing both the accuracy and the required computational effort. EM models are widely adopted in the scientific community especially when the attention is on the design of cells' components and high enough computational resources are available. However, such high-end resources are not compatible with modern BMS for storage systems. In this case, low computational effort must be a requirement for battery models that have to run in Real-Time on "low cost" hardware platforms to allow proper decision making. This is the reason why ECM models have been widely studied in the last years [3.62], [3.63]. ECM models focus the attention on the main macroscopic phenomena and aim to describe their dynamic behaviour by mean of a lumped parameters modelling approach. The battery is described with an electrical circuit where resistor, capacitors and ideal voltage sources are combined to describe the relevant phenomena.

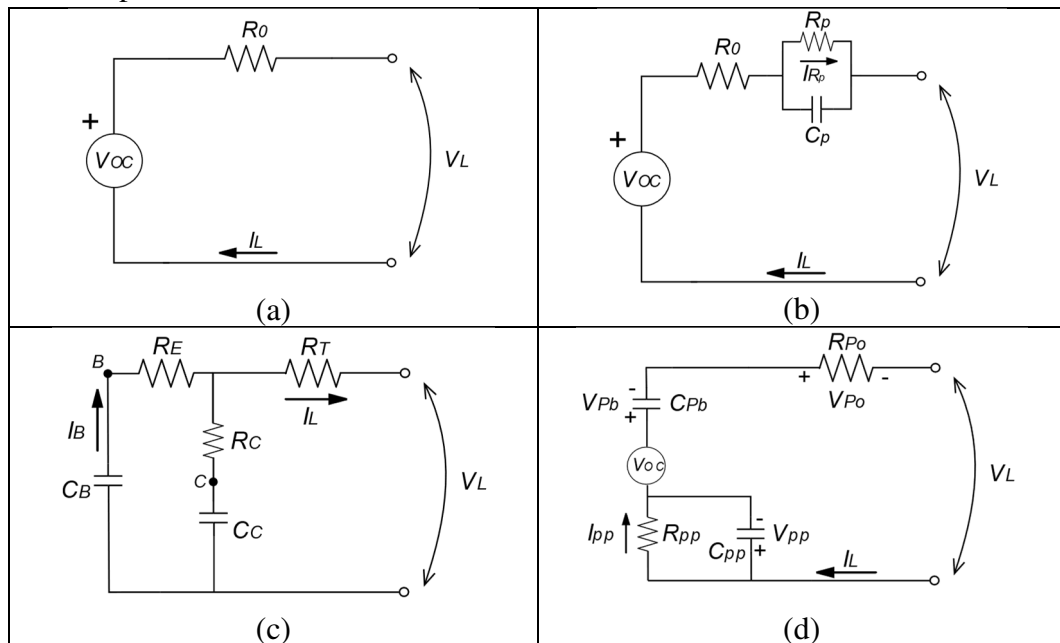


Figure 3.13 Equivalent circuit models: a) Rint, b) Thevenin, c) RC, d) PNGV.

In Figure 3.13a, the Rint model designed by the Idaho National Laboratory is shown. It consists of a series of an ideal voltage source describing the V_{OC} and a resistor R_0 to describe the internal resistance of the cell. The first one is mainly affected by the cell SoC, showing also some dependencies with extreme temperatures (unusual working conditions if proper thermal management strategies are adopted). The second is strongly affected by temperature which accelerates or slows down chemical reactions but shows also some variations with the SoC. The Thevenin model is shown in Figure 3.13b. It is the most widely adopted ECM when it comes to battery states estimation due to its ability to well describe the cell's dynamic behaviours. An ideal voltage source is used to describe the V_{OC} -SoC relation of the battery. R_0 describes the ohmic part of the internal battery resistance while the branch with R_P and C_P connected in parallel aim to emulate the battery's over-potential, thus its dynamic response. The more RC branches are used, the higher is the capability of the model to describe complex dynamic behaviours. Usually, no more than 3 RC branches are required especially for vehicles' applications. Although higher RC orders have higher accuracy, the increase in model performance not always justifies the increase in computational efforts. Figure 3.13c shows a two capacitances model designed by the battery manufacturer SAFT and the NREL. There are two main capacitors: C_B with higher capacitance is used to describe the storage capacity whereas the smaller C_C addresses surface effects on the electrodes. The resistor R_T describes the terminal resistance, something to consider especially in screwed connections working in high vibration environments. R_E and R_C are used to describe the cut-off resistance and the capacitive resistance. Lastly, the PNGV (Partnership for a New Generation of Vehicles) model shown in Figure 3.13d is another example of lumped parameters ECM that wants to describe physical characteristics of the battery. The V_{OC} here represents the maximum OCV at full charge while the capacitance C_{Pb} considers the OCV decrease with cell discharge. R_{P0} represents the ohmic resistance. R_{pp} and C_{pp} are the polarization resistance and capacitance in charge of representing the dynamic response of the cell. Several other ECM models are available in the literature, but most of the time they can be considered as derivation of these four simple models.

Batteries' thermal modelling is another important issue still discussed in the scientific community. Being able to predict battery thermal behaviour allows for temperature compensation of some ECM parameters (especially the Ohmic resistance), thus better SoC estimation. A battery thermal model must consider heat generation and accumulation inside the cell as well as its heat transfer mechanisms (conduction, convection, radiation) [3.64], [3.65]. It is commonly accepted to neglect internal convection mechanisms related to the electrolyte because of its very limited mobility. Thus, a common thermal model can be represented as in Equation (3.10)

$$\rho c_p \left(\frac{\partial T}{\partial t} + v \nabla T \right) \approx \frac{\partial (\rho c_p T)}{\partial t} = \nabla * \lambda \nabla T + q \quad (3.10)$$

where:

- ρ is the average (combined) density of the battery
- c_p is the average (combined) heat capacity per unit mass
- v is the velocity of the electrolyte
- λ is the average (combined) thermal conductivity along x, y and z direction
- q represents the heat generation

Another widely adopted approach is to consider the battery as a lumped body, with thermal properties uniformly distributed along all the directions. Under this assumption, Equation (3.10) can be simplified as follows

$$\frac{d(\rho c_p T)}{dt} = hA_s(T - T_\infty) + q \quad (3.11)$$

where:

- h is the heat transfer coefficient for convection
- A_s is the overall surface area exposed to the convective medium
- T_∞ is the temperature of the surrounding cooling medium

This approach is more accurate when the Biot number (Equation (3.12)) is lower than one.

$$Biot = \frac{hL_c}{\lambda} \quad , \quad L_c = \frac{Volume}{Surface\ area} \quad (3.12)$$

The energy balance equations shown above need further information about the heat generation term. There are two main contribution to the term q : reversible entropy and irreversible heat generation. The first term is related to the entropy changes related to electrochemical reactions inside the battery. It can be positive or negative depending on the net balance between endothermic and exothermic chemical reactions. The irreversible heat is related to the polarization of the active material and to the resistance of the active material and the electrolyte to ions movements (Joule effect). Several models can be found in literature for the heat generation term. Some can be linked to electrochemical models due to their focus on the active material structures [3.60]. A simplified heat generation model was proposed by Bernardi et al. [3.66].

$$q = I(V_{OC} - V_{batt}) - I \left(T \frac{dV_{OC}}{dT} \right) \quad (3.13)$$

The model shown in Equation (3.13) considers the heat generation related to the deviation from the thermodynamic equilibrium condition represented by the OCV both for the irreversible and reversible term.

3.6.1 Coupled thermo-electric model of a prismatic Lithium Ion cell

As stated at the beginning of this chapter, the applicability of a battery technology on industrial vehicles requires specific knowledge that goes beyond the actual state of the art. The very demanding loading scenarios related to NRMM applications, can put more stress on lithium cells than the current studies focused on the automotive field have shown. However, results of these studies can be considered as valuable starting point for further and more sectorial investigations.

The research activity on lithium ion batteries related to this PhD thesis was mainly meant at determining an efficient and effective battery model able to perform state estimations with loading scenarios derived from the specific industrial case of an orchard tractor (chapter4). For this reason, the coupled thermo-electric model battery model shown in Figure 3.14 was designed

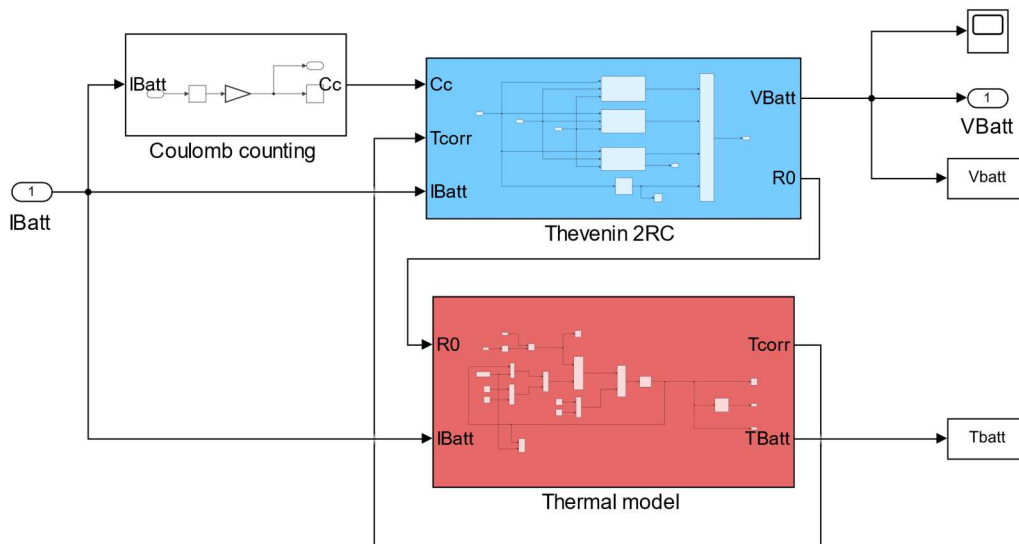


Figure 3.14 Thermo-electric battery model.

It consisted of three main sections:

- 1) The current integrator (Coulomb Counting)
- 2) The electric Equivalent Circuit Model (Thevenin 2RC)
- 3) The thermal model of the battery

The model took the cell current as input variable and estimate the cell voltage and mean temperature. The Coulomb counting section performed the integration in time of the input current (I_{Batt}) evaluating the actual SoC in terms of used capacity (C_c in Ah). The SoC evaluation is required to evaluate the actual ECM parameters from look up tables. The electric ECM model considered is shown in detail in Figure 3.15. It was an extended Thevenin model where 2RC branches (also known as dual polarization model) were adopted as best compromise between accuracy and computational efforts [3.62]-[3.63], [3.67].

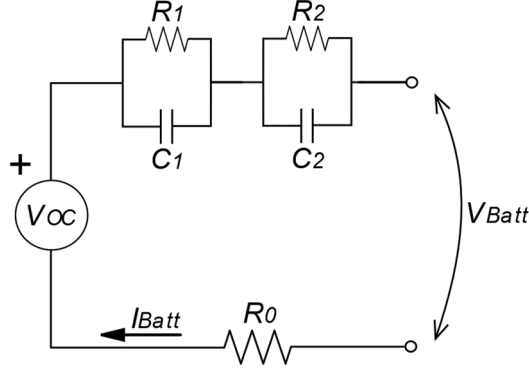


Figure 3.15 Thevenin model, 2RC.

Using standard Kirchhoff laws, the cell voltage can be expressed by considering the voltage drops across all the lumped elements as stated in the following equations

$$\frac{dV_1}{dt} = -\frac{V_1}{\tau_1} + \frac{I_{Batt}}{C_1} \quad (3.14)$$

$$\frac{dV_2}{dt} = -\frac{V_2}{\tau_2} + \frac{I_{Batt}}{C_2} \quad (3.15)$$

$$V_{Batt} = V_{OC} - R_0 I_{Batt} - V_1 - V_2 \quad (3.16)$$

where:

- V_{OC} is the cell OCV
- R_0 represents the Ohmic resistance
- R_i, C_i are the resistances and capacitances of the RC_i branch
- $\tau_i = R_i C_i$ are the time constants of the RC_i branch

Each parameter depended on the actual cell's SoC and temperature. In the proposed model, the SoC effect was taken into account considering look-up tables for each parameter. In this model, temperature influence was considered only on the resistances of the ECM. As shown in several works, internal resistance rapidly increases at lower temperatures and decreases at higher ones. For this reason, a correction factor T_{corr} was used to properly adapt the identified parameters at different temperatures.

The temperature correction factor can be evaluated if cell temperature is known. Unfortunately, in real applications it is very expensive to have temperature sensors for each cell in a battery pack. Usually, few temperature sensors are adopted to catch the average temperature of each module. Thus, it is necessary to implement a proper thermal model to estimate at least the mean temperature inside each cell. In the proposed thermo-electric model, the lumped thermal model in Equations (3.11) and (3.13) was used as shown in Figure 3.16.

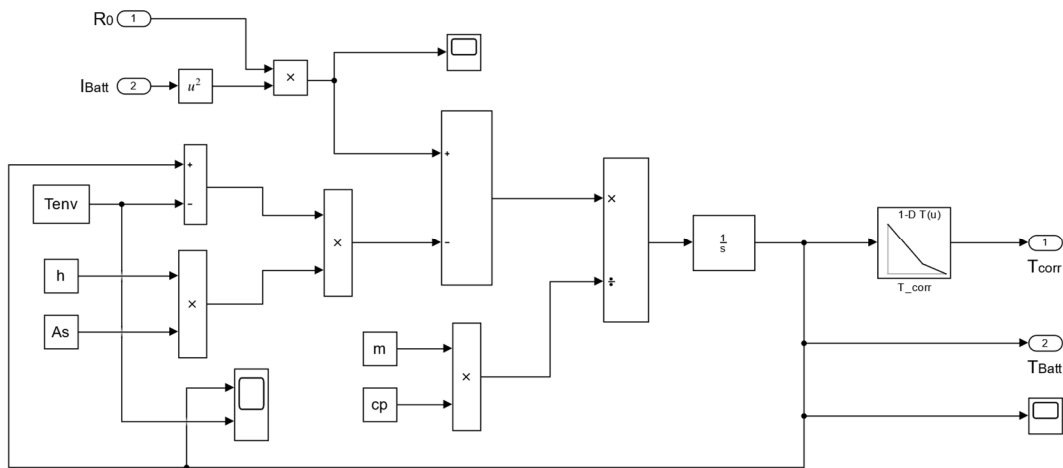


Figure 3.16 Thermal model implementation

For the purpose of this work, the V_{OC} changes with temperature thus the reversible heat exchange were neglected in the model due to the limited temperature excursions during the tests also at the highest continuous discharge current prescribed by the manufacturer. These assumptions are thus acceptable if proper thermal management is considered.

3.7 Battery testing activities

In this section, the main experimental activities done for the characterization of a prismatic Li-ion cell are shown. The main standard testing procedures available today are derived from the automotive field [3.68], [3.69]. Due to the lack of specific testing activities for heavy duty vehicles, this work started from the actual state of the art.

3.7.1 Battery testing system setup

The high demand for electric technology in vehicles' application has increased the need for deeper knowledge on battery systems. Electric performance, safety and longevity are the main priorities leading the scientific and industrial community research activities on Li-Ion cells. Standard testing procedures have been proposed depending on the specific chemistry and format of the cell (cylindrical, pouch or prismatic). These procedures consist of specific load history to be applied to the Cell Under Test (CUT) to evaluate performance both on the discharging and charging phases at different level of SoC.

Special testing equipment are required to investigate battery performance according to standard testing procedures. They mainly consist of a discharging unit (Electronic Load-EL), a charging unit (Power Supply-PS), a controller with a user interface and a data-logger. An EL is an electronic unit able to perform four different discharging modes:

- Constant Current (CC) when the load applied to the CUT is controlled to sink always the defined set-point current no matter of its actual voltage;

- Constant Voltage (CV) when the load applied to the CUT is controlled to maintain the terminal voltage equal to the predefined set-point voltage;
- Constant Power (CP) when the load applied to the CUT is controlled to sink the defined set-point power from the battery according to its actual voltage;
- Constant Resistance (CR) when the load applied to the CUT is controlled to sink a current proportional to its actual voltage. The proportionality is maintained regulating the sunk current according to the predefined “resistance” set-point.

A PS is an electronic device designed to apply a certain charging profile to the CUT. Several studies focused the attention on the drawbacks of not properly charging a Li-Ion Cells [3.70]. This phase is very critical when it comes to battery safety and cycle life. The actual trend is to speed up this phase in order to reduce vehicles’ “refuelling time” with respect to standard petrol engines vehicles. Very good results have been obtained in this direction. However, the main risk of such fast charging profiles is the acceleration of ageing mechanisms within the batteries. This is the reason why cell manufacturers prescribe very stringent charging characteristics on cells’ datasheets. The best, commonly accepted charging profile is the CC-CV (Constant Current - Constant Voltage) shown in Figure 3.17.

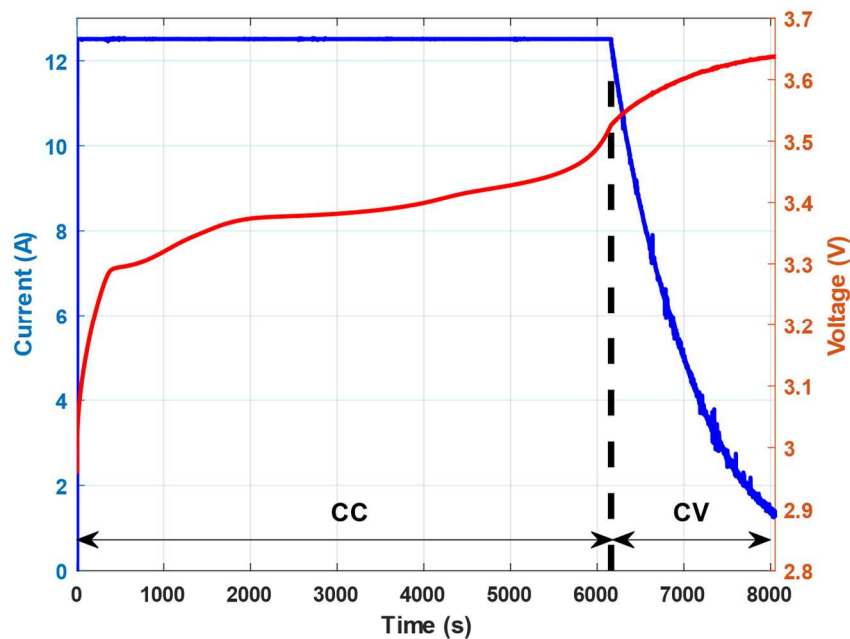


Figure 3.17 CC-CV charging procedure.

In the CC phase, the power supply controls the charging current to maintain the predefined set-point. Manufacturers usually prescribe 0.5-1C or 0.5-1 times the nominal capacity (or C-rate). This phase continues until the cell voltage reaches the prescribed $V_{full-charge}$. At this stage the PS switch to the CV mode where the current is regulated to maintain the same voltage. The charging current is stopped if it drops below a prescribed percentage of the nominal C-rate (usually $C/20$).

Using together an EL and a PS properly controlled allows the user to apply predefined charging-discharging profiles. Several industrial manufacturers propose integrated multichannel solutions where several EL/PS units are controlled

simultaneously to perform the user defined testing procedures. In this work, the testing equipment was designed and built using off-the-shelf hardware units for laboratory applications. The main reason is the freedom given by a custom solution when it comes to specific workloads of the testing equipment. These customizations usually increase the overall cost of the testing equipment. In Table 3.4 the main components of the testing setup shown in Figure 3.18 and are summarized.

Component	Manufacturer	Model
Electronic Load (EL)	Elektro-Automatik	EA-EL 9080-400
Power Supply (PS)	AimTTi	QPX-600DP
Controller Real-Time	National Instruments	NI PXIe 8840
Input/Output module	National Instruments	NI PXIe 6363
Software	National Instruments	LabVIEW/Custom

Table 3.4 Battery testing system components

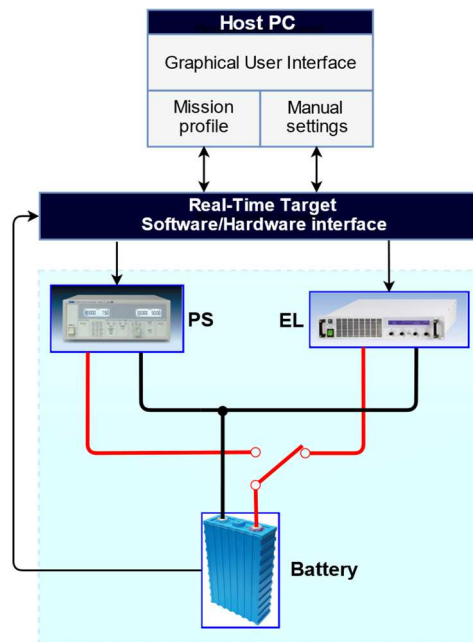


Figure 3.18 Battery testing system [3.67].

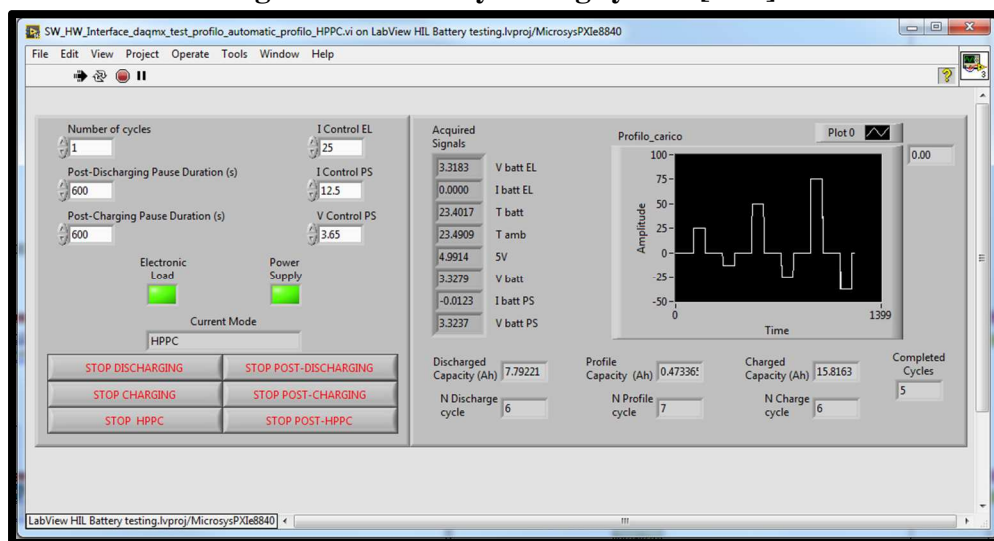


Figure 3.19 Graphical User Interface NI LabVIEW [3.67]

Further details about the control algorithm and software design can be found on the journal paper [3.67].

3.7.2 Description of the Li-Ion prismatic cell under test

For the characterization of the numerical model, an LFP prismatic cell was considered. In Table 3.5 the main characteristics given from the manufacturer are reported.

Specification	
Chemistry	LFP/C
Format	Prismatic
Dimensions (mm)	70x180x27
Nominal Capacity	25 Ah
Cut-off Voltage	2.0 V
End of Charge Voltage	3.65 V
End of Charge Current	C/20
Internal resistance	$\approx 4m\Omega$
Max continuous discharging current	3C

Table 3.5 CUT key specification

The available cell was already been used for previous research activities thus, some preliminary testing activities were performed to state the actual level of ageing. First, a series of 3 charge-discharge cycles with constant current (0.5C) were performed to brake the passivation layer inevitably formed on the active materials due to long shelf periods [3.71]. When the measured capacity became stable enough, several constant current cycles with 0.5C charging current and from 1 up to 3C discharging current were performed to fix the current capabilities of the CUT.

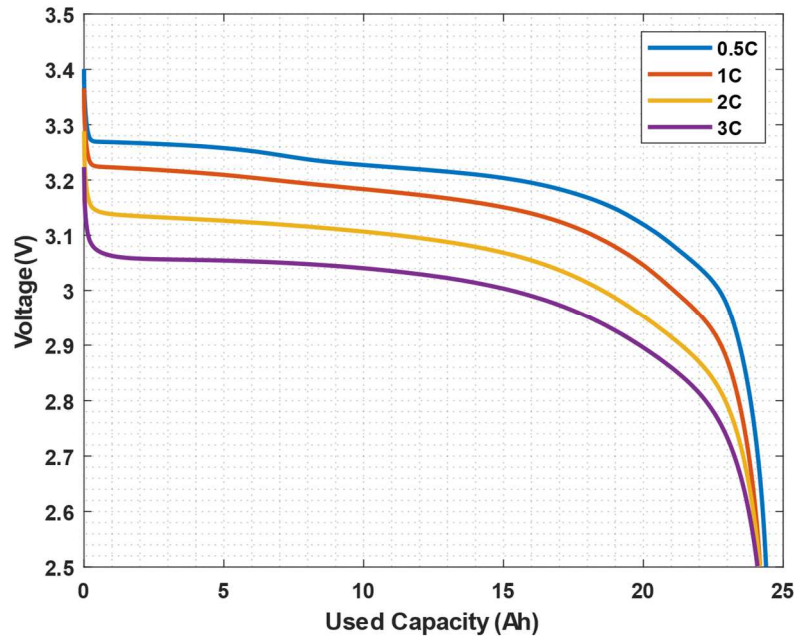


Figure 3.20 Constant Current discharge: capacity evaluation.

The tests were conducted at room temperature (23 °C average) which was controlled by the laboratory air conditioning system. The tests revealed that the current capacity of the CUT was 24 Ah or the 96% of its nominal capacity. This value was then considered in all the following analysis neglecting ageing effects due to the lower number of cycles involved in all the characterization activity.

3.7.3 Open Circuit Voltage Characterization

The OCV is the closest measurable quantity to the real SoC of the cell. However, it may take several hours for a battery to reach the equilibrium point after a single discharge pulse. To speed up testing procedures for OCV evaluation, several methods have been proposed in literature. In this work the method proposed in [3.72] was considered. A total of 4 testing cycle were performed. The first pair (Figure 3.21) consisted of a train of discharging pulses at 0.5C of period 42 minutes with a discharging time of 12 minutes and a rest time of 30 minutes.

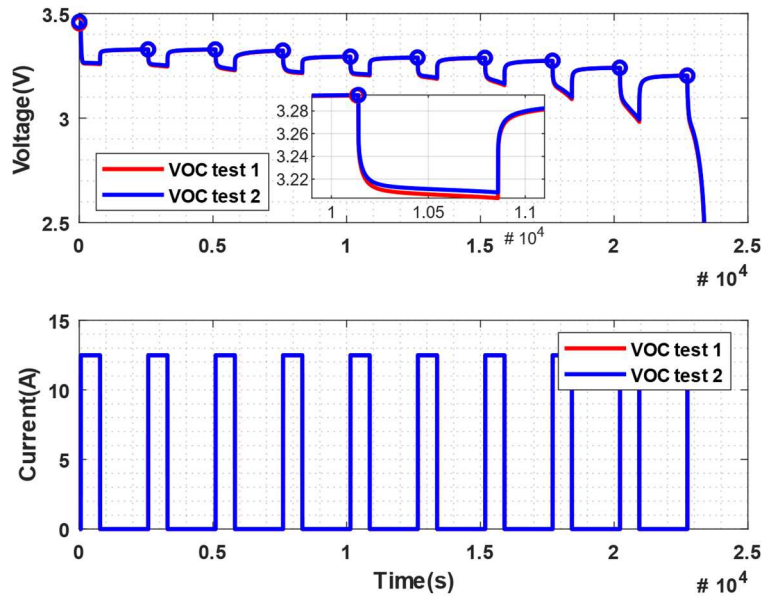


Figure 3.21 VOC discharge test.

The second (Figure 3.22) pair consisted of a train of charging pulses at 0.5C of period 42 minutes with a discharging time of 12 minutes and a rest time of 30 minutes (at least until the $V_{full\text{-}charge}$ was reached).

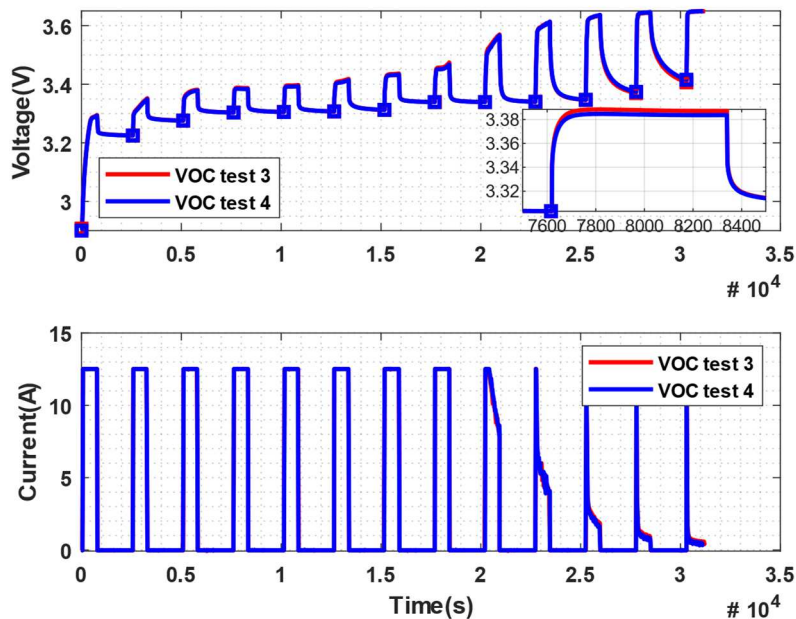


Figure 3.22 VOC charge test.

According to the method in [3.72], the local minima of the charging curves and the local maxima of the discharging ones are not the real OCV breakpoints due to a not long enough rest time. However, the authors proved that these points tend to get closer for higher resting times. For this reason, the real OCV curve was considered as the mean value of the previously identified breakpoints as shown in Figure 3.23.

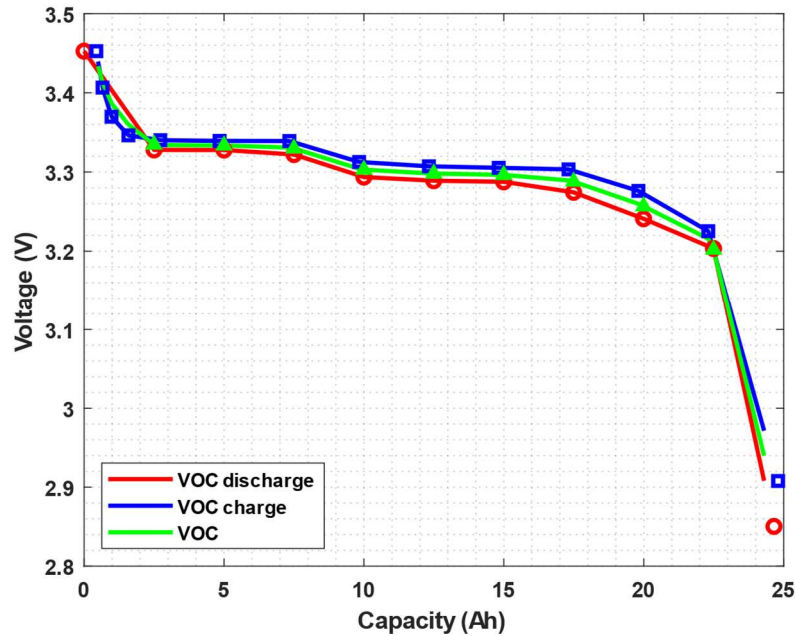


Figure 3.23 Voc evaluation.

The discharging and charging curves were analysed with respect of the discharged/charged capacity. The testing procedures were designed in such a way that each pulse would have discharged or charged 10% of the cell nominal capacity. Thus, the obtained Capacity - Voc curve can be considered a good starting point for SoC estimation.

3.7.4 Parameters identification and model validation

Once the OCV was determined, it was time to identify the other parameters of the thermo-electric battery model shown in Figure 3.14. Parameters used for the lumped thermal model are shown in Table 3.6. They were identified starting from data available in the literature for similar prismatic LFP cells [3.73], and then iteratively changing them to best fit experimental data for the specific CUT.

Parameter	Value
Mass m (kg)	0.663
Surface area A_s (m^2)	0.0376
Average heat capacity c_p ($\frac{J}{kg K}$)	1000
Average heat transfer coefficient h ($\frac{W}{m^2 K}$)	10

Table 3.6 Thermal model parameters

Due to special laboratory testing conditions (natural convection, low control on room temperature) the tuning for the heat transfer coefficient h was relatively easy. However, for more accurate results in case of an external cooling system, specific studies should be done to identify the proper mean value of h . Moreover, more complex 3D thermal model with lumped parameters like the one shown in [3.73] can be considered. The coupled architecture of the numerical models will still be maintained.

Parameters of the electrical model were identified with the help of an optimization tool built in the Matlab/Simulink® environment. The estimation problem can be summarised in the following steps.

1) Definition of an experimental data set

Data coming from the same tests used to evaluate the V_{oc} curve were considered as reference data set.

2) Definition of the model parameters to be estimated

The model was parametrized in terms of resistances (R_0, R_1, R_2) and time constants (τ_1, τ_2). For each parameter, a range of acceptable values were defined to speed up the estimation process. Non-negative values were considered for all the parameters. Resistances were searched in the range of some $m\Omega$. The two time constants represent a fast (τ_1) and a slow (τ_2) dynamic response. The former was set to be below 100 s the latter to the order of a few hours (the time required to reach the equilibrium condition).

3) Definition of the cost function

Like in every estimation problem, the tool adjusted the specified model parameters in order to have a simulated response y_{sim} as close as possible to the measured response y_{ref} , given the same stimulus (the battery current). Defined the error function

$$e(t) = y_{ref}(t) - y_{sim}(t) \quad (3.17)$$

the tool changed model parameters to minimize a certain cost function of the error. In this case, the Sum Squared Error cost function in Equation (3.18) was chosen.

$$F(x) = \sum_{t=0}^{t_N} e(t) \times e(t) \quad \text{With N the number of samples of the data set} \quad (3.18)$$

4) Definition of the optimization method

Strictly speaking, an optimization problem may consist in a minimization problem, a feasibility problem (of a solution with respect of some specified constraints) or in a mixed case of the previous ones. In this case, the estimation problem was reduced to a minimization problem to be solved with the Nonlinear Least Square method.

Table 3.7 summarized the identified model parameters, whereas Figure 3.24 and Figure 3.25 show the overall performance on the testing data and on the same type of pulsed excitation but at 2C respectively.

Capacity	VOC	$R_0(m\Omega)$	$R_1(m\Omega)$	$\tau_1(s)$	$R_2(m\Omega)$	$\tau_2(s)$
0	3.4975	0.0060	0.0089	24.1869	0.0010	234
2.5	3.3347	0.0032	0.0010	33.3268	0.0032	3099
5	3.3335	0.0032	0.0016	34.8426	0.0025	1426
7.5	3.3297	0.0036	0.0018	87.1105	0.0043	1746
10	3.3029	0.0032	0.0015	31.1599	0.0010	2791
12.5	3.2980	0.0035	0.0016	51.2465	0.0035	3053
15	3.2964	0.0033	0.0022	39.7024	0.0032	1908
17.5	3.2878	0.0041	0.0021	40.4590	0.0057	2005
20	3.2566	0.0036	0.0050	36.6400	0.0018	3.444
22.5	3.2013	0.0048	0.0068	46.7824	0.0010	961
25	2.8381	0.0058	0.0077	52.9739	0.0245	501

Table 3.7 Electric model parameters

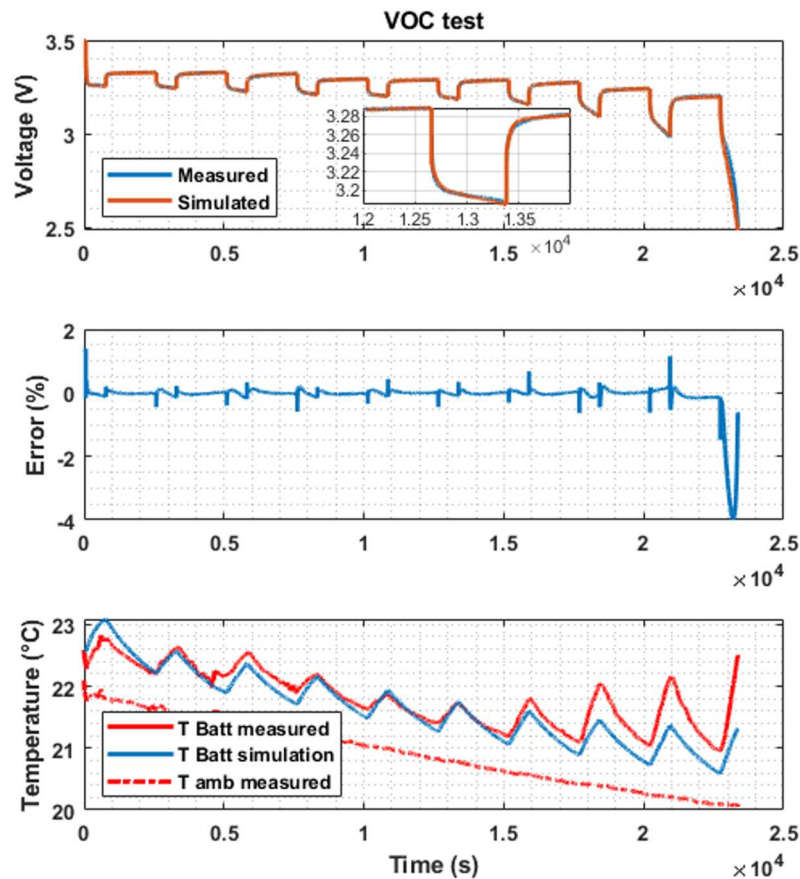


Figure 3.24 Model response and experimental data VOC test.

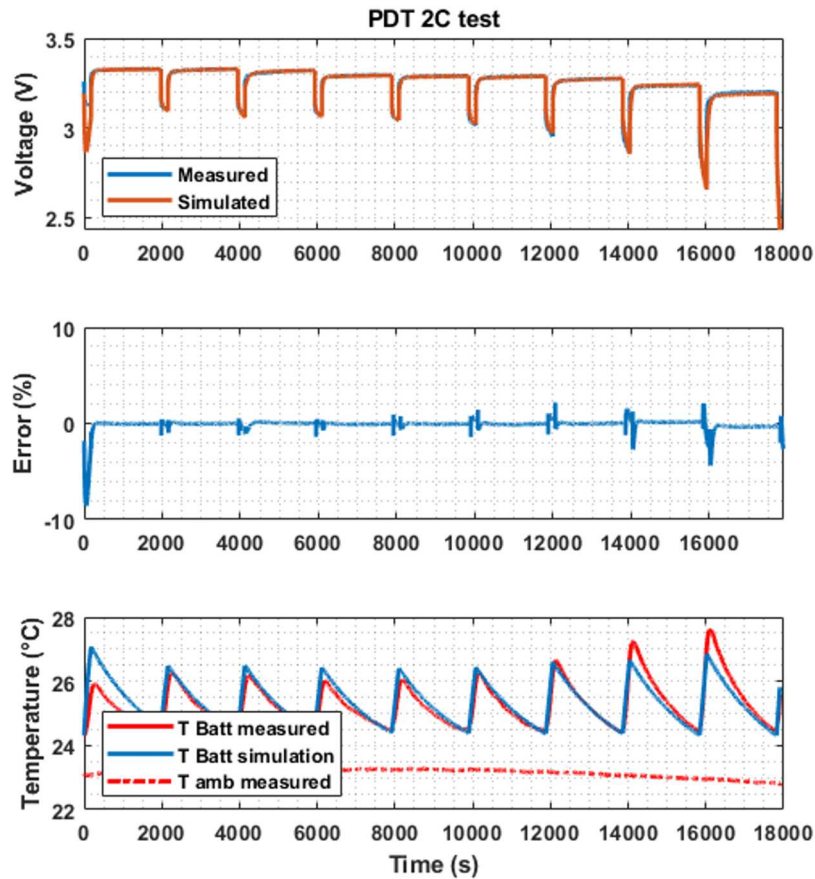


Figure 3.25 Model response and experimental data for a pulsed discharge test at 2C.

The parameter estimation process was done on all the look-up tables representing the relationship between the model parameters and the SoC (or available capacity). Results showed good model performance in representing battery voltage and temperature on two different case studies. The first one was the Pulsed Discharge Test (PDT) described in the previous section for V_{OC} identification. The second case is a PDT with discharge current at 2C. In both cases, the model showed very low average error (± 2) in the SoC range between 95% and 10%. At the limit of its useful range the model error increased due to the high non-linear behaviour in this range and the low number of breakpoints in the V_{OC} look-up table. This one was in fact evaluated every 10% SoC. A higher resolution of this table would decrease the error in these regions.

The model was indeed tested on several standard testing procedures. In Figure 3.26 and Figure 3.27 the main results in terms of average error in voltage and temperature evaluation are shown. Pulsed Discharge Tests showed very good results with an RMS error below the 1%. This is particularly relevant because these tests had very often rest periods (30 minutes between each pulse), so a low error in these phases is representative of a good match between the real OCV curve and the identified V_{OC} . Thus, a good SoC estimation can be expected just relying on the V_{OC} back-calculation starting from the instantaneous battery current measurement.

Very interesting results were also obtained from the DST test [3.67], a dynamic profile defined for the automotive application that was here used as a representation of a more realistic use case. Special attention is needed on the analysis of the Constant Discharge Tests (CDT). As can be seen in Figure 3.28 for the case CDT_2C, the RMS error on the voltage estimation was mainly related to the high error in the first 10% of SoC (from 100 to 90 % SoC). Again, is reasonable to think that with a more detailed V_{OC} curve, the accuracy of the estimation in this region can be improved.

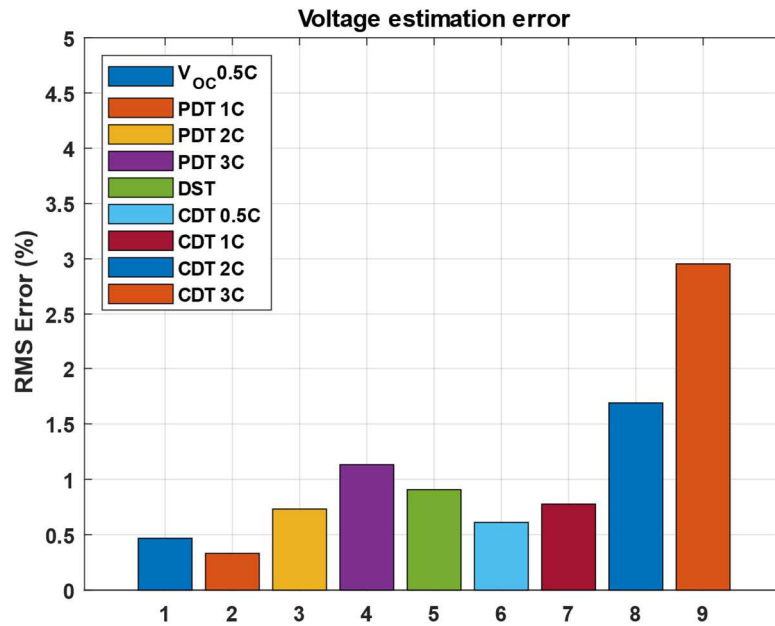


Figure 3.26 RMS error on voltage estimation for several standard tests

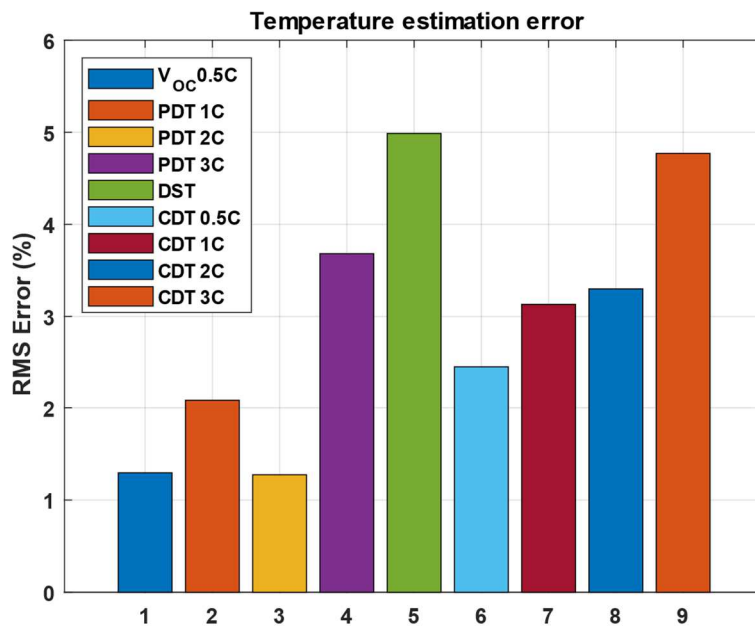


Figure 3.27 RMS error on temperature estimation for several standard tests

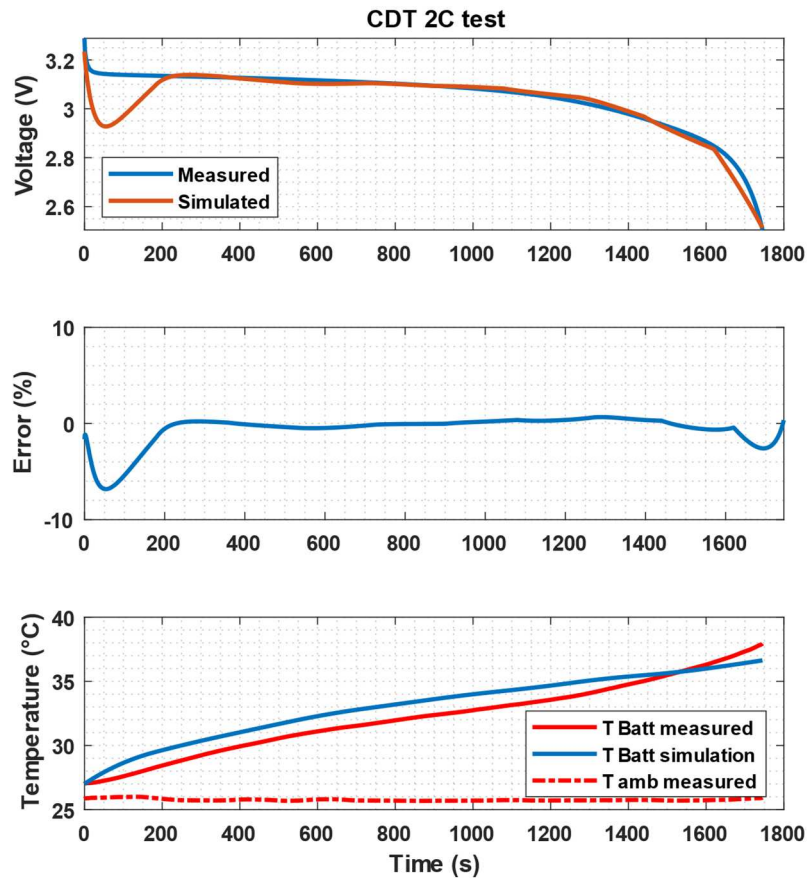


Figure 3.28 Model response and experimental data for a Constant Discharge Test at 2C.

From the thermal point of view, on all the tests the RMS error stayed below the 5% or within the range of ± 1.3 °C. Considering the simplification coming from the lumped thermal model approach and the usual order of magnitude of standard temperature sensors for BMS applications, the results were considered quite satisfactory compared to the low computational effort required.

3.8 Conclusions

In this chapter a brief review of energy storage was given with particular attention to battery-based technologies for vehicles applications. Among the different chemistries, lithium ion based electrochemical cells have shown the greater potential with their high power and high energy densities. Performance are strictly related to the chemical characteristics of the active materials used for the anode and the cathode. On the other hand, safety is still a major deal since if cells are not properly used and maintained with the help of cooling devices and BMSs which continuously monitor their activity. Battery cells monitoring is a serious deal to extract the best performance in a safe way. There is still a high attention of the scientific community about the state determination of a cell during its operating life. The SOC, SOH and SOP (SOF) estimation plays a crucial role when it comes to

optimize battery usage and program correctly maintenance. From the system design point of view, still lot of work can be done regarding the battery pack level. What was highlighted from this research was the lack of specific indication and standardization about battery pack design and performance analysis for heavy duty applications. Most of the scientific contributions derive from the automotive field which of course has totally different loading scenarios both from the electrical (performance) and from the mechanical (vibrations, harshness,...) point of view compared to industrial applications. In this work an LFP prismatic cell was studied and characterized. This chemistry is currently the most stable available and will probably be the most highly adopted on working machineries in the near future. The cell was characterized by mean of standard testing cycles derived from the automotive field. Although some of them present higher dynamics, is the author opinion that they are still not adequate enough for heavy industrial applications. As it will discussed in the following chapters, working machines have more severe loading scenarios and very different boundary conditions which could affect performance and safety (vibrations above all). Keeping these considerations in mind the battery model was still developed according to standard testing procedure. The parameter characterization showed a good level of accuracy between experimental and numerical data. The developed battery model will be implemented in the vehicle model of a hybrid orchard tractor presented in the next chapter. Although based on standard testing procedures, the relatively low discharge power which would affect the battery pack admits an electrical performance characterization of the type considered in this case. However, further investigations on performance with more specific mechanical working conditions should be considered to enhance model performance.

References

- [3.1] International Electrotechnical Commission (IEC), “Electrical Energy Storage”, White Paper, 2011
- [3.2] M. Aneke, M. Wang, “Energy Storage technologies and real life applications – A state of the art review”, *Applied Energy*, 179, 350-377, 2016
- [3.3] C. Zhang, Y.L. Wei, P.F. Cao, M.C. Lin, “Energy storage system: Current studies on batteries and power condition systems”, *Renewable and Sustainable Energy Reviews*, 82, 3091-3106, 2018.
- [3.4] S.O. Amrouche, D. Rekioua, T. Rekioua, S. Bacha, “Overview of energy storage in renewable energy systems”, *International Journal of Hydrogen Energy*, 41, 20914-20927, 2016
- [3.5] M. Hannan, M.M. Hoqueb, A. Mohamedb, A. Ayobb, “Review of energy storage systems for electric vehicle applications: Issues and challenges”, *Renewable and Sustainable Energy Reviews*, 69, 771-789, 2017.
- [3.6] K. Pielichowska, K. Pielichowski “Phase change materials for thermal energy storage”, *Progress in Materials Science*, 65, 67-123, 2014
- [3.7] T.B. Reddy, “Linden’s Handbook of Batteries, Fourth Edition”, McGraw-Hill Education, 2011
- [3.8] Q. Xu, T.S. Zhao, “Fundamentals for flow batteries”, *Progress in Energy and Combustion Science*, 49, 40-58, 2015.
- [3.9] B. Pollet, I. Staffell, J.L. Shang, “Current status of hybrid battery and fuel cell electric vehicles: From electrochemistry to market prospects”, *Electrochimica Acta*, 84, 235-249, 2012.
- [3.10] C. Liu, Y. Wang, Z. Chen, Q. Ling, “A variable capacitance based modeling and power capability predicting method for ultracapacitor”, *Journal of Power Sources*, 374, 121-133, (2018).
- [3.11] P. Tixador, “Superconducting Magnetic Energy Storage Status and Perspective”, *IEEE/CSC & ESAS EUROPEAN SUPERCONDUCTIVITY NEWS FORUM*, 2008.
- [3.12] S. Tie, C.W. Tan “A review of energy sources and energy management system in electric vehicles”, *Renewable and Sustainable Energy Reviews*, 20, 82-102, 2013.
- [3.13] G.J. May, A. Davidsonb, B. Monahov, “Lead batteries for utility energy storage: A review”, *Journal of Energy Storage*, 15, 145-157, 2018
- [3.14] L. Ouyang, J. Huang, H. Wang, J. Liu, M. Zhu, “Progress of hydrogen storage alloy for Ni-MH rechargeable power batteries in electric vehicles: A review”, *Materials chemistry and Physics*, 200, 164-178, 2017
- [3.15] C.H. Dustmann, “Advances in ZEBRA batteries”, *Journal of Power Sources*, 127, 85-92, 2004.
- [3.16] G. Zubi, R. Dufo-López, M. Carvalho, G. Pasaoglu, “The lithium-ion battery: State of the art and future perspectives”, *Renewable and Sustainable Energy Reviews*, 89, 292-308, 2018.
- [3.17] B. Scrosati, J. Garche, “Lithium batteries: Status, prospects and future”, *Journal of Power Sources*, 195, 2419-2430, 2010.
- [3.18] B Scrosati, K. M. Abraham, W. Van Schalkwijk, J. Hassoun, “Lithium Batteries Advanced Technologies and Applications”, *John Wiley & Sons*, 2013.
- [3.19] X. Feng, M. Ouyanga, X. Liua, L. Lua, Y. Xiaa, X. Hea “Thermal Runaway mechanism of lithium ion battery for electric vehicles: A review”, *Energy Storage Materials*, 10, 246-267, 2018.
- [3.20] Y. Wu, S. Saxena, Y. Xing, Y. Wang, C. Li, W.K.C. Yung, M. Pecht, “Analysis of manufacturing induced defects and structural deformations in lithium ion batteries using computed tomography”, *Energies*, 11(4), 925-947, 2018.
- [3.21] N Williard, W. He, C. Hendricks, M. Pecht, “Lessons learned from the 787 Dreamliner issue on lithium ion battery reliability”, *Energies*, 6, 4682-4695, 2013.
- [3.22] M.J. Loveridge, G. Remy, N. Kourra, R. Genieser, A. Barai, M.J. Lain, Y. Guo, M. Amor-Segan, M.A. Williams, T. Amietszajew, M. Ellis, R. Bhagat, D. Greenwood, “Looking Deeper into the Galaxy (Note 7)”, *Batteries*, 4(1), 3, 2018.
- [3.23] L. Lu, X. Han, J. Li, J.g Hua, M. Ouyang, “A review on the key issues for lithium ion battery management in electric vehicles”, *Journal of Power Sources*, 226, 272-288, 2013.
- [3.24] J. Jiang, C. Zhang, “Fundament and Application of Lithium-ion Batteries in Electric Drive Vehicles”, Wiley, 2015
- [3.25] R. Xiong, L. Li, J. Tian, “Towards a smarter battery management system A critical review on battery state of health monitoring methods”, *Journal of Power Sources*, 405, 18–29, 2018.
- [3.26] Hauser, R. Kuhn, “High voltage battery management systems BMS for electric vehicles” in *Advances in Battery Technologies for Electric Vehicles*, Woodhead Publishing, 2015
- [3.27] J Qi, D.D.C. Lu, “Review of battery cell balancing”, *Australasian Universities Power Engineering Conference, AUPEC 2014*, 2014
- [3.28] V. Duong, H.A. Bastawrous, K.W. See, “Accurate approach to the temperature effect on state of charge estimation in the LiFePO4 battery under dynamic load operation”, *Applied Energy*, 204, 560–571, 2017.
- [3.29] M. Cheng, Y.S. Lee, M. Liu, C.C. Sun, “State of charge estimation with aging effect and correction for lithium ion battery”, *IET Electr. Syst. Transp.*, 5 (2), 70–76, 2015.
- [3.30] Z. Li, J. Huang, B.Y. Liaw, J. Zhang, “On state of charge determination for lithium ion batteries”, *Journal of Power Sources*, 348, 281-301, 2017.
- [3.31] M.A Hannan, M.S.H. Lipub, A. Hussainb, A. Mohamed, “A review of lithium ion battery state of charge estimation and management system in electric vehicle applications: Challenges and recommendations”, *Renewable and Sustainable Energy Reviews*, 78, 834–854, 2017.
- [3.32] J. Cannarella, C.B. Arnold, “State of health and charge measurements in lithium ion batteries using mechanical stress”, *Journal of Power Sources*, 269, 7-14, 2014.
- [3.33] L.C. Casals, B.A. García, C. Canal, “Second life batteries lifespan Rest of useful life and environmental analysis”, *Journal of Environmental Management*, 232, 354–363, 2019.

- [3.34] M. Lipu, M.A. Hannan, A. Hussain, M.M. Hoque, P.J. Ker, M.H.M. Saad, A. Ayob, "A review of state of health and remaining useful life estimation methods for lithium ion battery in electric vehicles challenges and recommendations" *Journal of Cleaner Production*, 205, 115-133, 2018
- [3.35] M. Berecibar, I. Gandiaga, I. Villarreal, N. Omar, J. Van Mierlo, P. Van den Bossche. "Critical review of state of health estimation methods of li ion batteries for real applications", *Renewable and Sustainable Energy Reviews*, 56, 572–587, 2016.
- [3.36] H. Wang, E.Lara-Curzio, E.T. Rule, C.S. Winchester, "Mechanical abuse simulation and thermal runaway risks of large format Li-ion batteries", *Journal of Power Sources*, 342, 913-920, 2017.
- [3.37] Weng, X. Feng, J. Sun, H. Peng "State of Health monitoring of lithium ion battery modules and packs via incremental capacity peak tracking", *Applied Energy*, 180, 360–368, 2016
- [3.38] L. Zheng, J. Zhu, D.D.C. Lu, G. Wang, T. He, "Incremental capacity analysis and differential voltage analysis based state of charge and capacity estimation for lithium ion batteries", *Energy*, 150, 759-769, 2018.
- [3.39] L. Wang, X. Zhao, L. Liu, C. Pan, "State of health estimation of battery modules via differential voltage analysis with local data symmetry method", *Electrochimica Acta*, 256, 81–89, 2017.
- [3.40] X. Han, M. Ouyang, L. Lu, J. Li, Y. Zheng, Z. Li "A comparative study of commercial lithium ion battery cycle life in electrical vehicle: Aging mechanism identification", *Journal of Power Sources*, 251, 38-54, 2014.
- [3.41] P. Ladpli, F. Kopsaftopoulos, F.K. Chang, "Estimating state of charge and health of lithium ion batteries with guided waves using built in piezoelectric actuators", *Journal of Power Sources*, 384, 342–354, 2018.
- [3.42] Farmann, D. U. Sauer "A comprehensive review of on board State of Available Power prediction techniques for lithium ion batteries in electric vehicles", *Journal of Power Sources*, 329, 123-137, 2016
- [3.43] F. Sun, R. Xiong, H. He, "Estimation of state of charge and state of power capability of lithium battery considering varying health conditions", *Journal of Power Sources*, 259, 166-176, 2014.
- [3.44] L. Yong, W. Lifang, L. Chenglin, W. Lingfei, L. Junfeng, G. Yanjie, "Effects of temperature on dynamic characteristics of Liion batteries in electric vehicle applications", ITEC Asia-Pacific 2014
- [3.45] K. An, P. Barai, K. Smith, P.P. Mukherjee "Probing the thermal implication in mechanical degradation of lithium ion battery electrodes", *Journal of The Electrochemical Society*, 161 (6), 1058-1070, 2014.
- [3.46] Aris, B. Shabani, "An experimental study of a lithium ion cell operation at low temperature conditions", *Energy Procedia*, 110, 128 – 135, 2017.
- [3.47] J. Yao, F. Wu, B. Wu, X. Qiu, C. Yang, N. Li "Electrochemical performance and kinetics of LiFePO₄-C cathode in a low temperature electrolyte", *World Electric Vehicle Journal*, 4, 2010
- [3.48] M. Petzl, M. Kasper, M.A. Danzer, "Lithium plating in a commercial lithium ion battery: A low temperature aging study", *Journal of Power Sources*, 275, 799-807, 2015
- [3.49] Y. Kikuchi, M. Mitsui, Y. Nakayama, K. Tojima, "Apparatus and method for controlling state of charge/discharge of battery of hybrid car", EP0985570, 2000
- [3.50] Zhu, J. Mathews, B. Taenaka, P. Maguire, "Method and system for a vehicle battery temperature control", US7154068B2, 2006.
- [3.51] F. Kong, R. Kostecky, G. Nadeau, X. Song, K. Zaghbi, K. Kinoshita, F. McLarnon, "In situ studies of SEI formation", *Journal of Power Sources*, 97-98, 58-66, 2001.
- [3.52] D Abraham, E.P. Roth, R. Kostecky, K. McCarthy, S. MacLarend, D.H. Doughty, "Diagnostic examination of thermally abused high power lithium ion cells", *Journal of Power Sources*, 161, 648–657, 2006.
- [3.53] S. Arora, "Selection of thermal management system for modular battery packs of electric vehicles A review of existing and emerging technologies", *Journal of Power Sources*, 400, 621–640, 2018.
- [3.54] R. Schröder, M. Aydemir, G. Seliger "Comparatively assessing different shapes of lithium ion battery cells", *Procedia Manufacturing*, 8, 04-111, 2017.
- [3.55] L. H. Saw, Y. Ye, A.A.O. Tay, "Integration issues of lithium ion battery into electric vehicles battery pack", *Journal of Cleaner Production*, 113, 1032-1045, 2016.
- [3.56] M.J. Brand, S.F. Schuster, T. Bach, E. Fleder, M. Stelz, S. Gläser, J. Müller, G. SEXTL, A. Jossen, "Effects of vibrations and shocks on lithium-ion cells", *Journal of Power Sources*, 288, 62-69, 2015.
- [3.57] S. Arora, W. Shen, A. Kapoor, "Review of mechanical design and strategic placement technique of a robust battery pack for electric vehicles", *Renewable and Sustainable Energy Reviews*, 60, 1319–1331, 2016.
- [3.58] T. Higashino, K. Saito, T. Motohashi, "Battery pack with covering member and vehicle with the battery pack", US8642204, 2014
- [3.59] M. Iwasa, S. Ogata, H. Kadota, T. Hashimura, N. Mori, "Vehicle battery mounting structure", US8561743, 2013
- [3.60] S X Tang, L. Camacho-Solorio, Y. Wang, M. Krstic, "State of Charge estimation from a thermal electrochemical model of lithium ion batteries", *Automatica*, 83, 206–219, 2017.
- [3.61] S. Pramanik, S. Anwar, "Electrochemical model based charge optimization for lithium ion batteries", *Journal of Power Sources*, 313, 164-177, 2016.
- [3.62] X. Hu, S. Li, H. Peng, "A comparative study of equivalent circuit models for Li-ion batteries", *Journal of Power Sources*, 198, 359– 367, 2012.
- [3.63] Farmann, D.U. Sauer "Comparative Study of reduced order equivalent circuit models for on board state of available power prediction of lithium, ion batteries in electric vehicles", *Applied Energy*, 225, 1102–1122, 2018.
- [3.64] Q. Wang, B. Jiang, Y. Yan, "A critical review of thermal management models and solutions of lithium ion batteries for the development of pure electric vehicles", *Renewable and Sustainable Energy Reviews*, 64, 106–128 2016.
- [3.65] S. Panchal, I. Dincer, M. Angelin-Chaab, R. Fraser, M. Fowler, "Thermal modelling and validation of temperature distributions in a prismatic lithium ion battery at different discharge rates and varying boundary conditions", *Applied Thermal Engineering*, 96, 190–199, 2016.

- [3.66] Bernardi, E. Pawlikowski, J. Newman, "A general energy balance for battery systems", *J Electrochem Soc*, 132, 5–12, 1985.
- [3.67] Vergori, F. Mocera, A. Somà, "Battery modelling and simulation using a programmable testing equipment", *Computers*, 20–43, 2018.
- [3.68] G.Hunt, "USABC Electric Vehicle Battery Test Procedures Manual" *United States Department of Energy: Washington, DC*, USA, 1996.
- [3.69] "FreedomCAR Battery Test Manual for Power-Assist Hybrid Electric Vehicles" DOE/ID-11069; *National Engineering and Environmental Laboratory: Idaho Falls, ID*, USA, 2013.
- [3.70] Y. Gao, J. Jiang, C. Zhang, W. Zhang, Z. Ma, Y. Jiang, "Lithium ion battery aging mechanisms and life model under different charging stresses", *Journal of Power Sources*, 356, 103–114, 2017.
- [3.71] P. Keil, S.F. Schuster, J. Wilhelm, J. Travi, A. Hauser, R.C. Karl, A. Jossen, "Calendar Aging of Lithium-Ion Batteries: Impact of the graphite anode on capacity fade", *Journal of The Electrochemical Society*, 163 (9), 1872–1880 2016.
- [3.72] S. Abu-Shark, D. Doerffel, "Rapid test and non linear model characterisation of solid state lithium ion batteries", *Journal of Power Sources*, 130, 266–274, 2004.
- [3.73] R Rizk, H. Louahlia, H. Gualous, P. Schaetzel, "Experimental analysis and transient thermal modelling of high capacity prismatic lithium ion battery", *International Communications in Heat and Mass Transfer*, 94, 115–125, 2018.

Chapter 4

Modelling of an electrified architecture for agricultural applications

Industrial vehicles are machines designed to accomplish simple or more complex productive tasks. They are usually employed in heavy duty applications like in construction, agriculture, handling, forestry and so on. Productivity, reliability and robustness are the main design requirements for these types of vehicles. From the vehicle architecture point of view, the main difference between an industrial vehicle and a car is the use of the mechanical power coming from the engine. A car uses the energy coming from the primary energy source mainly to move/transport people or goods. For industrial vehicles, transportation may be just one of several tasks the machine is asked to accomplish. Through specific power output mechanisms, these machines can also move external tools produced by other vendors using their own energy source. The complexity in the energy management of an industrial vehicle requires specific attention in the design process of an electrified architecture. Each application has different requirements in terms of peak and average power. Some may prefer the boost capability of a parallel architecture. Others could take advantage from the steady state working condition of the thermal engine like in a series configuration. More complex architectures are instead required if particular features like a Continuously Variable Transmission (CVT) are desired. In this chapter, an orchard tractor is considered as use case to study an electrified architecture on a working machine which is traditionally used both for transportation and as energy source for external tools used in orchards. Several aspects will be covered, from the experimental activities required to characterize the machine working conditions to the modelling of the traditional and of an electrified architecture. Performance comparisons based on the same basic activities as well as for simplified working cycles.

4.1 Use case definition: study of an agricultural tractor

Industrial machines cover a wide range of application field, from construction to agriculture, handling and others. Each field has specific characteristics that must be analysed to design a proper electrified architecture. In this work, the attention was focused on an agricultural tractor. Agricultural tractors are machines originally designed to deliver high torque to pull trailers on the road or ploughs in the fields. Nowadays, they are also seen as mobile power generators to provide power for special tools, also called implements, designed for specific working tasks (Figure 4.1).

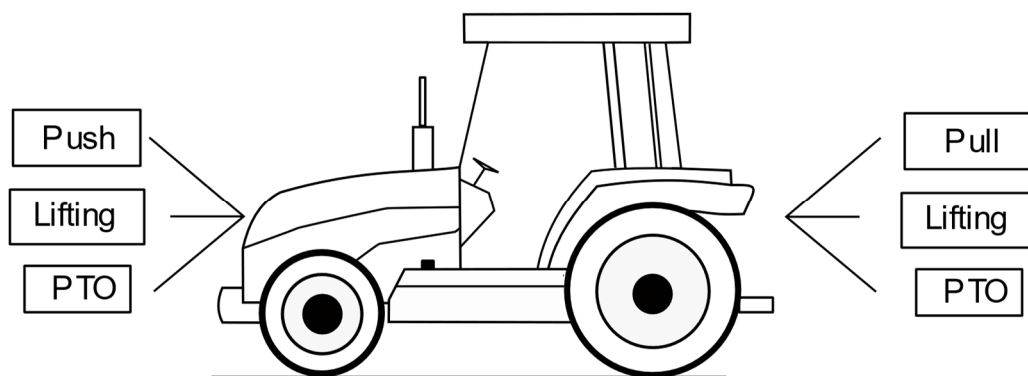


Figure 4.1 A modern tractor and its main functions

Depending on their characteristics and structural design, traditional tractors can have several classifications. Considering the type of tractive element there are:

- Wheel tractors (with four or more wheels)
- Crawler tractors with tracks (rubber or metal based)
- Walking tractors or power tillers (two wheels machines for field operations where operators drive them walking behind them)

Wheeled tractors are the most widely adopted in agriculture although some applications require the use of crawler tractors due their higher tractive performance. Among wheeled tractors, depending on the destination of use it is possible to distinguish between:

- General purpose tractors. These machines are usually considered when several field activities like ploughing, arrowing, harvesting and transportation on wide areas are the main daily activities. Due to the heavy working loads, these machines are equipped with high power Diesel engines. Special tyres with high rolling diameter and wide contact area are used to increase the tractive capabilities, thus the effectiveness of the power delivered by the engine.
- Row crop tractors. These tractors are mainly used for crop cultivations. To avoid crop damage, they are designed with higher ground clearance.

Moreover, they can come with different tyre sizes to best fit the inter row distance.

- Special purpose tractors. Specific applications like orchards, cotton fields, gardening require smaller tractors (due to the lower power requirements) but with a high degree of customization, especially in the flexibility for implements interfacing.

All these tractors' classes have the need to transfer power to special implements/equipment to make the work done. To pull them and efficiently use the power delivered by the engine, special drawbars (Figure 4.2a) or hitch systems (Figure 4.2b) are designed. Although these are just mechanical devices to transmit pulling forces, they can affect the tractive performance of the machine if the resultant of the forces is not properly oriented [4.1], [4.2].

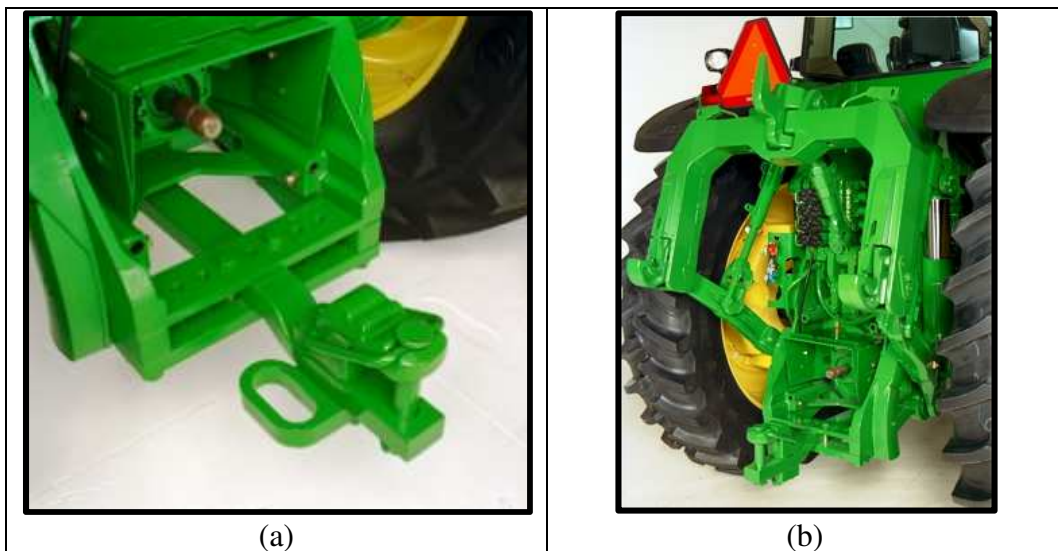


Figure 4.2: a) Drawbar structure, b) Three points hitch system

Nowadays it is common to see both the devices on tractors to give more flexibility in implements interfacing. The most common way to transmit mechanical power from the engine to the implement is by mean of a Power Take Off (PTO) connection (Figure 4.3).

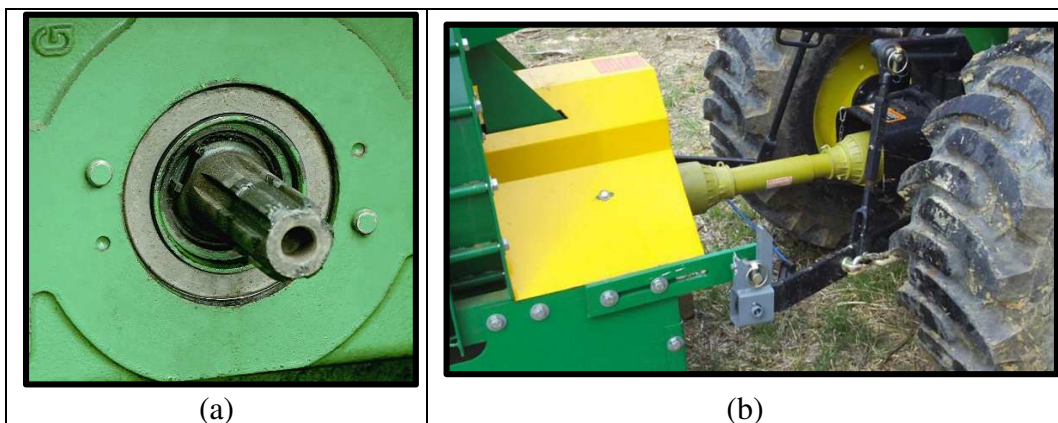


Figure 4.3: a) PTO output, b) PTO coupling shaft

From the early stages of tractor evolution, the PTO has become more and more a standard for power transfer [4.3]. There are specific requirements on the rotational speed, geometries, shielding and protection elements of these power connections. The original reference speed for PTO operations was set at 540 rpm, but some modern implements are also designed with a nominal PTO speed of 1000 rpm. Tractors manufacturers usually design flexible solutions to have these two standard speeds on the PTO shaft. High power tractors are usually equipped with a gearbox that allows both for 540 and 1000 rpm. The reduction gear set is thought to allow the engine to operate at maximum power speed. Nowadays, two more solutions can be found on tractors: 540E and 1000E. They are essentially different gear sets that allow the user to choose between an engine operating point in the region of maximum power output or a point of minimum fuel consumptions (perfect for low power implement applications).

Another way to transfer power to an auxiliary tool is by using a hydraulic power connection. Through a hydraulic pump directly connected to the engine shaft, hydraulic tools can receive the required power. Compared to a mechanical PTO, this power connection requires additional elements like pipelines, valves and a proper heat exchanger to properly and safely transfer hydraulic.

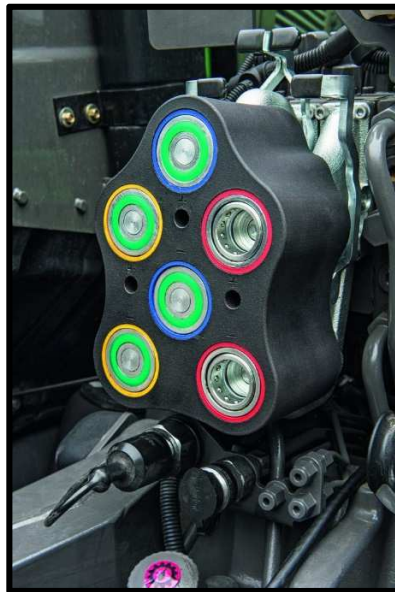


Figure 4.4: Connectors for hydraulic auxiliary tools

As discussed in [4.4], not all the power delivered by the tractor can be used for working operations. For example, considering an on field pulling activity (e.g ploughing), the engine power will be used to compensate for:

- Powertrain internal losses
- Hydraulic losses (especially for those basic system with no load sensing devices)
- Slippage
- Rolling resistance (view as main resistance against the tractor movement).

Considering all these contributions, the power required by on board auxiliaries (mainly cabin thermal conditioning) and the current wear condition of the tractor the effective power available for working operations can range between 50-75% of the actual engine power output.

The electrification of a tractor architecture allows for improvements in the overall efficiency of the machine. First, less fuel will be used to provide the same mechanical power. The use of electric machine can open the powertrain to more efficient layout in terms of number of gear reduction stages to have certain working speeds. The flexibility given by electric architectures and the high responsiveness of electric systems can also help in the development of advanced traction control systems. Another interesting improvement related to electrified powertrains will be the possibility to supply electric power to attached implement instead of using hydraulic systems. This has a dual advantage: it allows to improve the overall efficiency both on the tractor and the implement side; it allows for better control of implement performance. An electric driven implement would benefit from the higher transmission efficiency of an electric network. At the same time, the higher level of control of electric drives can increase the level of effectiveness of the implement itself. As an example, one application that would benefit from this characteristic is the seeding where higher precision in seeds deposition would translate in a higher degree of use of the cultivation field.

4.2 Experimental analysis on tractor performance

To design an electric architecture for an agricultural tractor, it is necessary to identify its fields of application and understand the actual machine behaviour under a characteristic set of working loads. In this study, the attention focused on a specialized tractor for orchard applications. As explained before, specialized tractors are thought to be used in specific application with lower power requirements compared to general purpose tractors. Moreover, the characteristics of the application fields require custom solution in the mechanical design of the tractor structure. As for the case study, orchard tractors usually need to have:

- small rear and front width to approach the narrowest orchard rows;
- small vehicle wheelbase for higher turning capability;
- low ground clearance and low overall height to be able to pass below tree branches.

The type of implements used on these machines cover essentially the main operations needed in orchards. Among the most used tools there are: trailers for transportation, shredders, rotary harrows, atomizers. Each tool, thus working scenario, have a specific working load. The first step of the analysis done in this chapter was exactly to study the load characteristics of these common applications by mean of experimental on field measurements of the tractor behaviour. The focus

was on engine performance since a new electrified architecture must at least cover actual power performance.

4.2.1 Methods

To characterize the tractor daily activities, the attention was focused on the measurements of engine performance during on field operations. To do that, some relevant engine data were collected reading them on the CAN BUS network of the tractor.

The CAN (Controlled Area Network) protocol was originally designed by Robert Bosch GmbH in the early 80's [4.5],[4.6]. The protocol structure allows for communication of several nodes on the same bus, physically made by a pair of twisted cables. Its main features can be summarized as follows:

- It is a serial networking technology which requires only two wires, namely CAN_High and CAN_Low (usually abbreviated in CAN_H and CAN_L)
- Has a maximum data rate of 1Megabit per second
- Each message (frame) has a maximum data load of 8 bytes
- Each frame is identified with a well defined message identifier (ID)
- The structure of the message ID defines also the priority of the message. If more nodes try to send a message on the bus at the same time, the frame with the highest priority automatically prevents the other to be sent.
- The protocol supports two types of identifiers lengths, 11 bit (standard) and 29 bit (extended)

The CAN protocol was initially designed for automotive applications and still represent the main protocol on this field. On top of the CAN protocol, higher level protocols were then designed to meet requirements for heavy duty applications. One of them is the SAE J1939 standard [4.7],[4.8]. The main characteristics of this standard can be summarized as follows:

- It was originally thought for heavy duty working vehicles and for fleet management
- It is a higher communication protocol that is built on top of the physical CAN layer protocol
- The prescribed baud rate is fixed at 250 Kilobit per second
- It uses the extended 29-bit identifier already available on the CAN protocol
- It allows a maximum of 30 nodes on the network and a maximum of 253 controller applications. An application does not necessarily coincide with a controller. One single controller unit can manage several applications
- It supports bidirectional node communication and broadcast messages
- Has a maximum message lengths of 1785 bytes (sent with multiple frames)
- Defines a set of Parameter Group Numbers (PGNs) to address predefined vehicle parameters

The SAE standard groups parameters depending on the type of information they transport and on the source they are generated by. Commonly used parameters are all classified within a Suspect Parameter Number (SPN) that gives information about the type of data, its length, resolution, offset and possible range.

In this work, the attention focused on specific parameters broadcasted by the engine ECU on the CAN Bus network. In particular, the accelerator pedal signal was acquired to have the reference speed set by the driver. Nowadays, tractors and many others working machines are equipped with engines with a speed controller that controls the fuel rate to follow the desired working speed. Thus, this signal together with the actual engine speed and percentage load were acquired to have comprehensive picture of the engine performance on each work load. These parameters were acquired with a CAN BUS protocol analyser (Figure 4.5a) connected to the vehicle network as a new node with the help of a J1939 adapter (Figure 4.5b). The measurement device was set to the listen – only mode in order to monitor the messages flow without interfering with the stream of information. This option was considered by the author mandatory in order to guarantee the safety of the measurement activity. All the data were acquired with the help of a portable personal computer, with a specifically developed software.

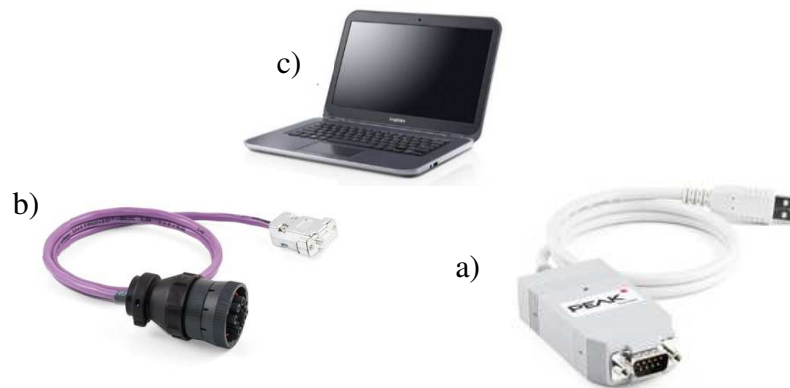


Figure 4.5 Data acquisition setup: a) CAN Bus protocol analyser, b) J1939 to DB9 adapter, c) Personal computer for data storage

4.2.2 Field tests and data processing

The measurement activities were performed on an orchard tractor which main characteristics are summarized in Table 4.1.

Mass	2500 kg
Nominal power	75 kW @ 2300 rpm
Vehicle wheelbase	1900 mm
Max vehicle width	1850 mm
Number of possible gear ratios	36
Top speed	40 km/h
Minimum speed	0.4 km/h

Table 4.1 Main characteristics of the orchard tractor under test.

Measurements were focused on evaluating tractor performance on a set of common working scenario. A set of 4 tractor activities were considered

- Transportation. The tractor was equipped with a trailer with a tare mass of 1400 kg connected using the rear drawbar. Two sets of tests were performed. The first series consisted in a set of accelerations from still up to the tractor maximum speed followed by a set of partial deceleration/acceleration (always up to the maximum speed). In this case no additional material was added to the trailer, thus the tractor pulled just the weight of the trailer itself. The second type of tests consisted of the same driving scenario but with the maximum allowed load: its total mass reached 6000 kg during these tests. Tests were performed on a flat paved road to simulate usual heavy transportation from the field to the company stocking facilities. Measurements were taken with the engine at its nominal working temperature. Cold start characterization was not the scope of the tests but needs further investigations for a more detailed analysis on limit working scenarios.

In Figure 4.6 an extract from the first series of tests is shown. The first plot shows the dynamic response of the engine to a given reference speed. Apart from the very first moments where the driver needed to shift gear from standstill start, once the clutch was fully engaged the responsiveness of the engine to the speed controller stimulus was determined by the system dynamic. The inertia of the entire system plus the sum of all the resistance contributions discussed in the previous section like powertrain losses, rolling resistance, some aerodynamic contribution and auxiliaries losses determined the engine rpm evolution. The second plot represents an important feedback broadcasted by the engine on the CAN Bus network. It represents the Actual Engine Percentage Load or the percentage estimation of the actual Torque output compared to the maximum available Torque output at the same rotational speed. Although the error affecting this parameter estimation, its monitoring allows to map the working load of the application. To satisfy the acceleration request from the driver, the engine speed controller forced the engine to output all the available power to accelerate the system. Then, as it will explored and discussed in the next sections, the actual load for steady state travel was always lower thanks also to the low aerodynamic resistance and the overall good rolling performance of the tyres (both on the tractor and trailer side). The knowledge of such data is crucial for the design of new architectures (also with more traditional technologies): new powertrains must be capable to give at least the same peak power performance to satisfy the driver/operator needs.

In Figure 4.7, the same type of driving scenario was applied to the trailer transportation at its maximum load (trailer total mass = 6000 kg). The higher

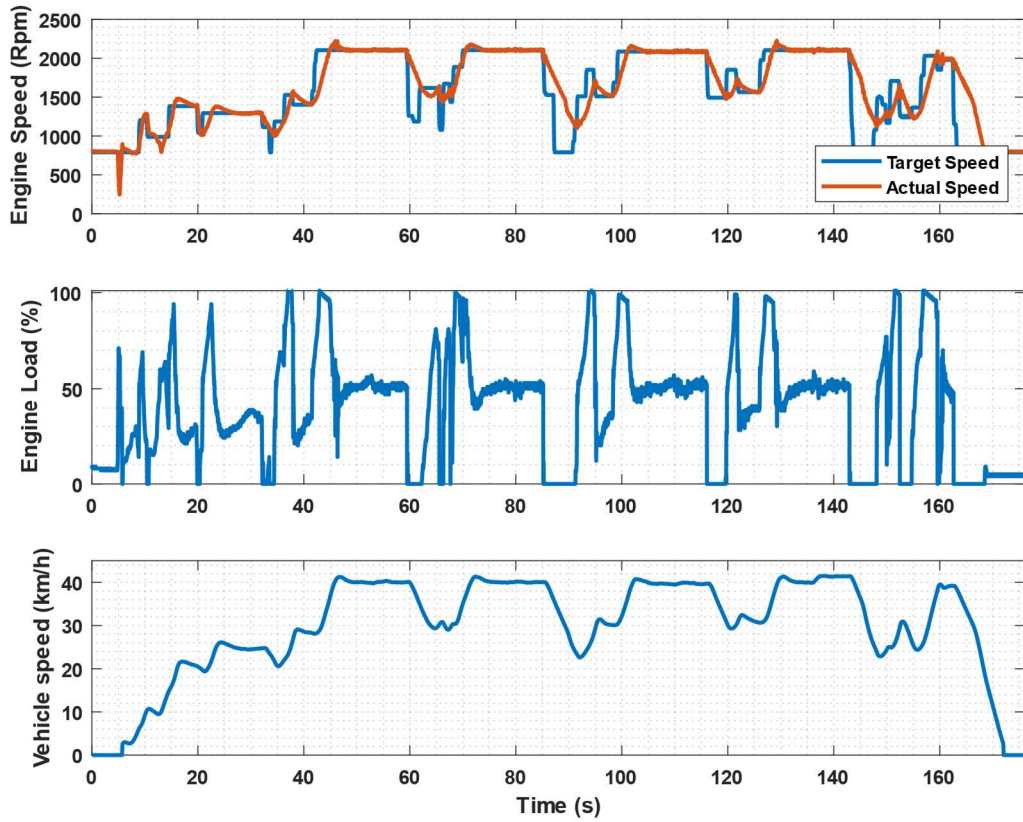


Figure 4.6 Transportation test – empty trailer 1400 kg

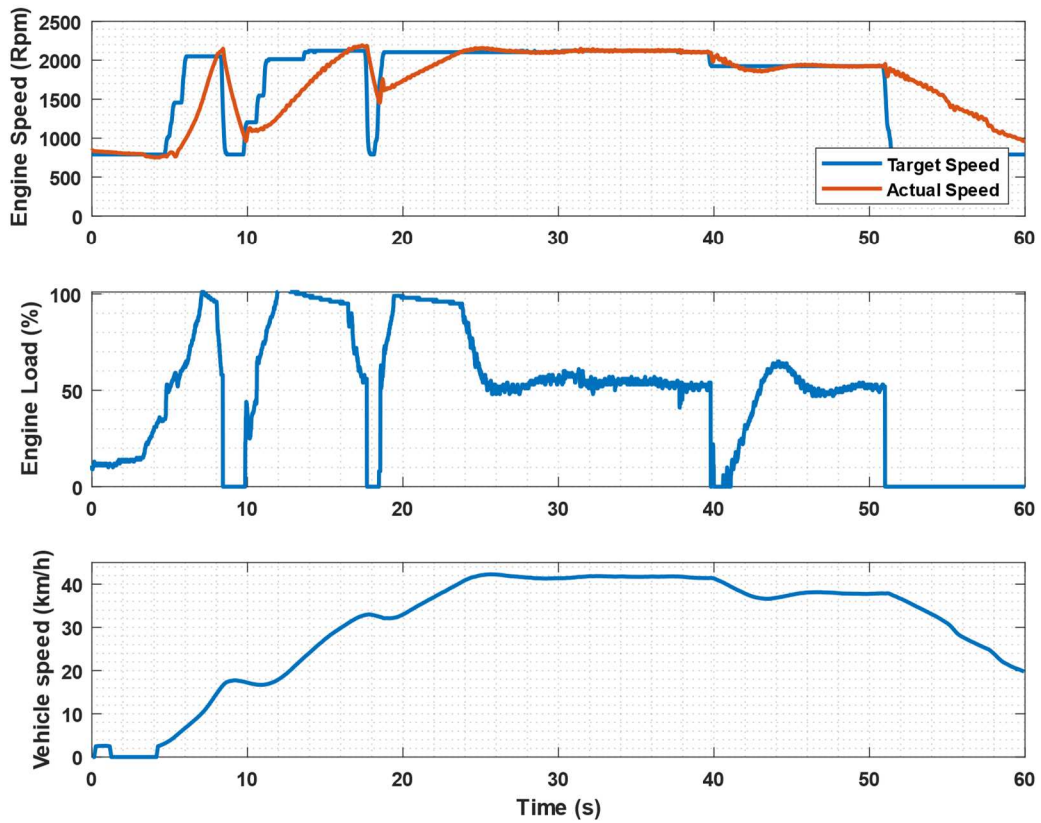


Figure 4.7 Transportation test – fully loaded trailer 6000 kg

trailer load slightly affected engine performance compared to the first type of tests. Average engine load at steady 40 km/h show higher values but in the order of 5-10%. Acceleration time was slightly higher, but the overall experience showed very little differences between the two set of tests. Looking at this first dataset, engine size is surely adequate to satisfy peak power demand in transportation, but it is oversized with regard to the steady state working load.

- Shredding. Orchard tractors are very often equipped with shredding tools for green maintenance operations. These tools consist in a series of rotating cutting elements moved by the PTO. The tests were performed considering a PTO speed of 540 rpm thus, with an engine speed around 2100 rpm and a mean working speed of 5 km/h. Considering the hardest grass encountered in the various tests (shown in Figure 4.8) the mean working load was essentially constant and equal to the 50% of the available power. Variations were mainly related to the irregularities of the terrain where the tests were performed. Thus, looking at the results of this working scenario, the installed engine power is oversized compared to the effective working load of the application.
- Rotary harrow. Rotary harrows are another group of very commonly used tools on orchard tractors. The tool consists of a series of rotating metal elements that are pushed against the terrain by means of a hydraulic actuator in order to move and mix its very first layer. This operation is essential to guarantee a proper air and nutrients distribution on the terrain layers mainly involved in the birth and growth of the plants.

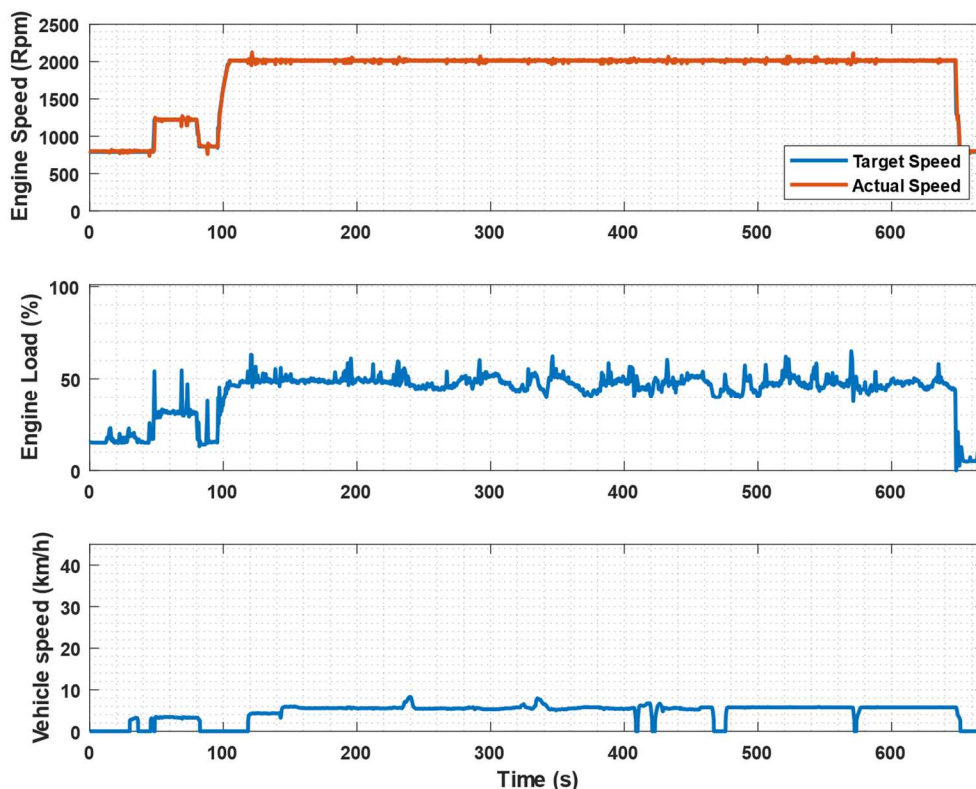


Figure 4.8 Shredding test – PTO 540 rpm



Figure 4.9 Rotary harrow test – PTO 540 rpm



Figure 4.10 Atomizer test – PTO 540

Tests with this equipment were performed using the PTO speed 540 rpm, an engine speed of 2100 rpm and a working speed of 3.4 km/h (Figure 4.9). From the engine load data, it is clear the heaviness or the working load. The diagram shows the setup phase ($t < 300$ s) and a series of three terrain rows to be harrowed. Once the vehicle was completely on steady working conditions (from $t = 300$ s up to the end), the engine had a mean working load of 80% at each row to be worked. It is worth to mention that the type of terrain worked during these tests was not in ordinary conditions. Previous rains wetted the clayey terrain making it even harder to be worked. As the driver suggested, usual common sense for these cases is to wait a couple of days after the rain in order to let the terrain dry. However, this unusual working condition can happen, thus the system should be able to operate. The engine load showed a variability of $\pm 10\%$ depending on the local working conditions encountered by the rotary harrow.

- Atomizer. An atomizer is a particular type of pulled sprayer which allows for efficient fertilizer and pesticides deposition on the plants. The power coming from the PTO is used to pressurize a mixture of water, fertilizer and/or pesticides which are then sprayed on an air flow coming from a centrifugal or axial fan. For the specific tests a centrifugal fan atomizer was used, with a PTO speed of 540 rpm, an engine speed of 2100 rpm and a working speed of 3.4 km/h (Figure 4.10). The working load was practically constant at 70% with the slight variations related to terrain asperities. From separate tests on single components of the atomizer, it was possible to identify the fan as the major power demanding element of the tool. To cover the widest area possible, the required air flow to be guaranteed can vary from 6000 up to 80000 m³/h for axial fans and from 3000 up to 20000 m³/h for centrifugal fans [4.4].

Several considerations can derive from the presented experimental results. First, a new powertrain architecture for a traditional tractor should be able to cover peak power demand of its typical working scenarios. Apart from acceleration in transportation, the analysed tractor activities did not use the full power of the engine for steady state operations. Thus, the engine is oversized, leading to generally higher fuel consumptions. A good practice would be to have an optimized engine able to cover the heaviest steady state working load and to compensate variations in power demand with a more responsive system. An electric motor could satisfy those requirements and in the following sections a numerical model of an electrified orchard tractor is presented.

4.3 Modelling and performance analysis of an electrified architecture for an orchard tractor

As discussed in the previous sections modern agricultural machines are usually designed with oversized power units to be able to overcome peak power demands

of the possible working scenarios. To meet this design requirement Diesel engines' nominal power must match the identified peak power demand. The most efficient way to use Diesel engines is to let them work in steady state conditions, possibly near their nominal power point. Although engine oversizing is a practical solution to meet customers' needs, this practice is very inefficient. This is becoming a serious problem which manufacturers are starting to deal with especially with the upcoming legislations on pollutant emissions for NRMM (see chapter 1). Up to now, the use of engine gas aftertreatment systems has been the common practice to meet legislation requirements. With yearly lower limits on pollutant emissions these systems are increasing in costs and sizes, creating a real concern also for their integration on the vehicle. This is the main reason that is pushing manufacturers in evaluating alternative architectures like the ones with electric components. More efficient powertrains meet emissions requirements and allow for new functionalities not allowed by traditional architectures.

The knowledge gained with the investigation activities on the main applications for an orchard tractor was used to propose a new electrified architecture. The proposed solution will be implemented in a numerical model of a tractor to study the applicability of the solution. First, the numerical model of the traditional vehicle was built and validated with the experimental data shown before. Then, on the same vehicle model structure an electric system was implemented, testing the new machine under the same working conditions.

4.3.1 Modelling of a tractor

Modelling the system behaviour of an entire tractor is a quite demanding task. A comprehensive numerical model of a traditional tractor should cover at least the following aspects:

- Vehicle and trailer (if present) dynamics
- Gearbox and clutch behaviour
- Engine
- PTO loads
- ECU control logic
- Driver behaviour.

Considering also the need for implementation of an electric system, to face the multi-domain nature of the problem a standard equation-based simulation approach was considered not flexible enough. Thus, a Physical Network (PN) modelling technique was used to model the physical system (vehicle dynamics, mechanical components and connections, ...) while the control architecture and all the related state machines were developed with the standard equation-based approaches. The tractor model shown in Figure 4.11 was built within the Matlab/Simulink environment, using the Simscape libraries to model the PN [4.9].

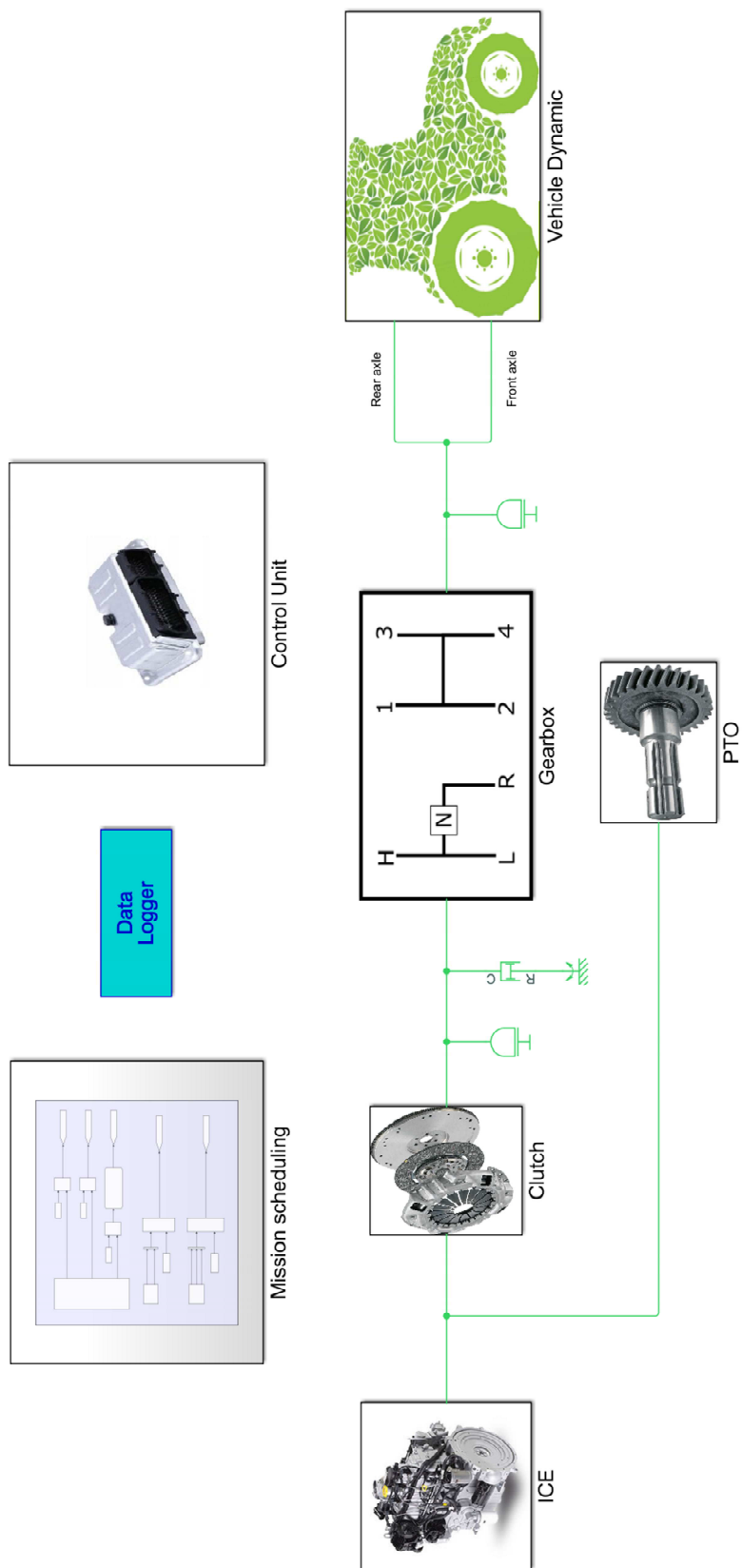


Figure 4.11 Numerical model of a traditional tractor architecture

In a PN each “block” modelling a physical component is characterized by physical ports that allow for energy exchange among all the elements of the system/network. Block ports from all the physical domains are characterized by two main variables: Through and Across variables are summarized in Table 4.2 for the main domains of interest. The product of a Through variable and an Across variable is always a power contribution. Thus, an energy balance-based approach allows for practical multi-domain simulations.

Physical Domain	Across Variable	Through Variable
Mechanical rotational	Angular velocity	Torque
Mechanical translational	Linear velocity	Force
Electrical	Voltage	Current
Thermal	Temperature	Heat flow
Hydraulic	Pressure	Flow rate

Table 4.2 Through and across variables in a physical network model.

The first subsystem modelled was the tractor vehicle model shown in Figure 4.12. It consisted in a block modelling the 1D longitudinal dynamic of the vehicle together with four blocks for wheels behaviour. Power from the transmission block splits between the front and rear axle where two differentials manage the power distribution among the wheels. Starting from the schematic representation in Figure 4.11, the chosen 1D longitudinal model of the tractor body satisfies equations (1-6) where:

- a and b are the horizontal ($\beta = 0$) distances between the centre of gravity (CG) and the front and rear axles
- h is the CG height from the ground ($\beta = 0$)
- m and g are the mass of the vehicle and the gravitational acceleration
- β is the road slope angle
- V_x is the vehicle longitudinal speed
- F_d is the aerodynamic drag force as $F_d = 0.5\rho C_d A V_x^2 * sign(V_x)$, ρ air density, C_d drag coefficient, A frontal cross sectional area of the vehicle
- F_{xf} and F_{xr} are the contact forces between the wheels and the ground on the longitudinal direction (front and rear axle)
- F_{zf} and F_{zr} are the normal contact forces between the wheels and the ground (front and rear axle)

$$m \dot{V}_x = 2(F_{xf} + F_{xr}) - F_d - mg \cdot \sin\beta \quad (4.1)$$

$$F_{zf} = \frac{-h(F_d + mg \cdot \sin\beta) + b \cdot mg \cdot \cos\beta}{2(a + b)} \quad (4.2)$$

$$F_{zr} = \frac{+h(F_d + mg \cdot \sin\beta) + a \cdot mg \cdot \cos\beta}{2(a + b)} \quad (4.3)$$

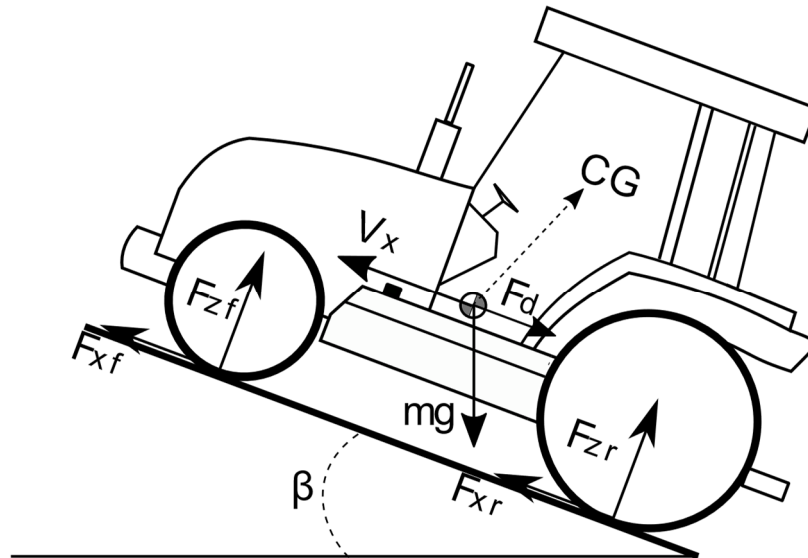


Figure 4.12 1D longitudinal tractor dynamic model

The vehicle dynamic model can be solved only if further information are provided about the wheel-ground contact. For this reason, four wheel contact models' blocks were considered. These blocks consisted of a friction-based tire model, where the use of static and dynamic friction coefficients determine the maximum traction torque. Once the maximum static torque is reached, slip between the wheel and the ground is evaluated and the effective tractive torque is calculated with the dynamic friction coefficient. The used tire model provided also a way to consider rolling resistance by mean of a constant rolling coefficient. For the purpose of this analysis this tyre model was considered accurate enough. More complex model can be implemented if further analysis on the tractive force are required.

Once the vehicle model showed kinematic consistency between geometric properties (tire rolling radius) and the tractor declared top speed, the equivalent gearbox was modelled Figure 4.13. It consisted of a series of gear couplings and "logical clutches" to change the engine speed achieving the desired vehicle working speed. Each gear ratio was modelled with a *Simple gear* block which simulated the engagement between two gears. The output of each gear was connected in parallel to the gearbox output shaft, while the input to the related logic clutch. Here the PN modelling approach showed its modelling flexibility. Each gear block was by default disconnected from the gearbox input shaft but once the related logic clutch was closed on the desired gear block, the power from the input shaft could follow the selected path. As a real clutch, the logic clutch model connects its input and output shaft by mean of friction and a certain normal pressure applied to the friction disks. To model powertrain losses a dissipative element was added in parallel to the power path of the gearbox. As previously investigated for other industrial vehicle applications [4.10]-[4.11], transmission power losses were modelled with a quadratic function of the actual vehicle speed (or equivalently to the actual rotational speed of the engine).

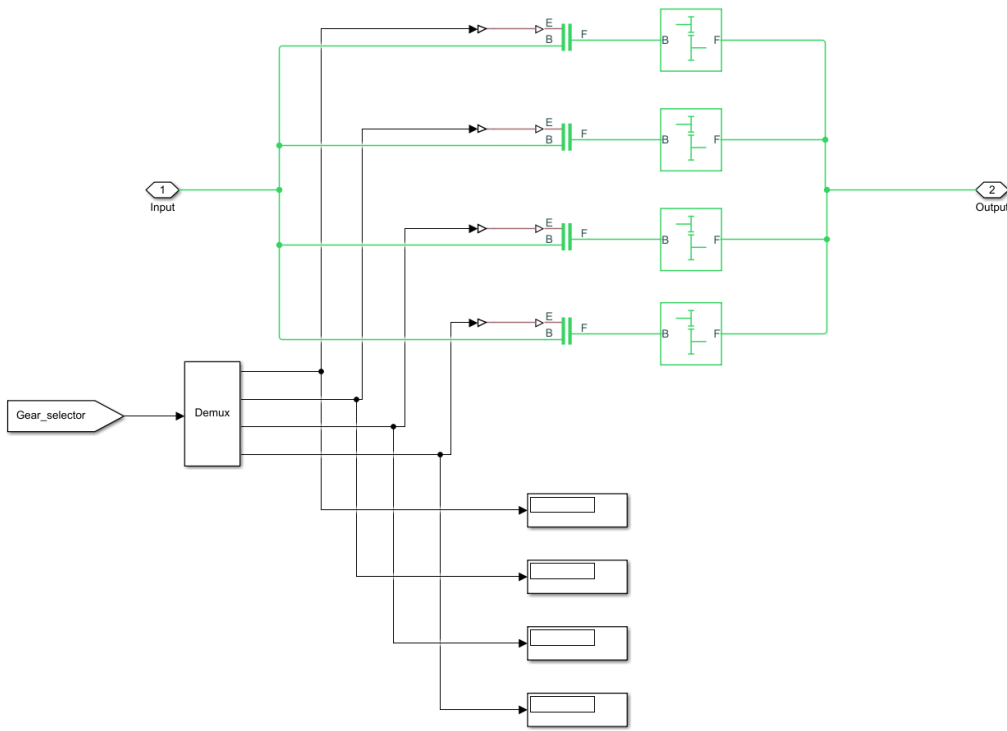


Figure 4.13 Gearbox model with logic clutches

Once the gear ratios of the gearbox model were determined to meet the vehicle working speeds in all the different tests, the clutch model was defined. Torque transmission was guaranteed by a clutch disk model. The use of a quadratic law for the dynamic friction coefficient with respect to the slip between the input and output shaft allowed to simulate the engagement phenomena. The plate pressure was determined by a normalized clutch signal between 0 and 1 linearly mapped into a pressure applied to the clutch disks

The engine model consisted of a power demand function that provided the maximum available power for a given engine speed. A throttle input between 0-1 given by the driver/engine controller determined the fraction requested of the total available power. Then, the engine torque was simply calculated as the ratio between the actual power and speed. The Diesel engine power demand function was expressed by a third order normalized polynomial form

$$p(w) = 0.6526w + 1.6948w^2 - 1.3474w^3 \quad (4.4)$$

The power function was normalized in terms of speed and power. In particular, given the maximum power P_{max} , the speed at maximum power Ω_0 , the maximum speed Ω_{max} and the stall speed Ω_{min} :

$$w = \frac{\Omega}{\Omega_0} \quad (4.5)$$

$$T = \frac{P_{max}}{\Omega_0} \frac{p(w)}{w} \quad (4.6)$$

If the actual engine speed Ω was in the range $[\Omega_{min}, \Omega_{max}]$, the normalized speed was calculated with (4.5). Thus, from the normalized power function (4.4) the actual engine torque was calculated with (4.6). Starting from the nominal data of

the engine in Table 4.1, and considering $\Omega_{min} = 750 \text{ rpm}$ and $\Omega_{max} = 2350 \text{ rpm}$ an the equivalent engine map shown in Figure 4.14 was determined.

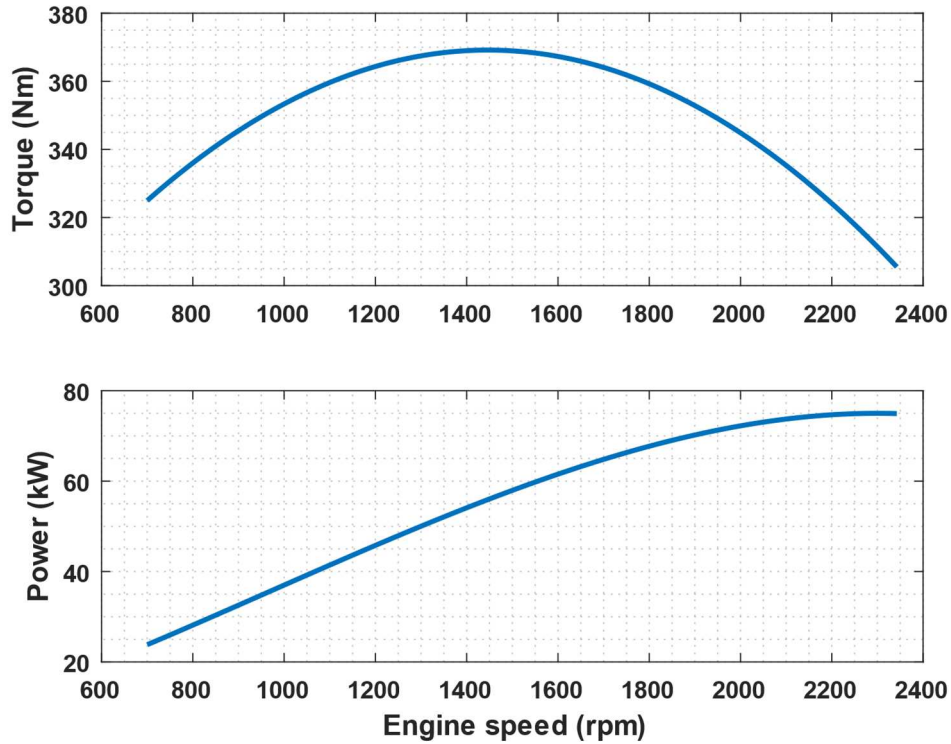


Figure 4.14 Equivalent polynomial engine map

According to [4.12], engine fuel consumption was evaluated as

$$Q_F = (0.0434 \cdot X + 0.019) \cdot P_{nom} \quad (4.7)$$

$$Q_R = Q_F \cdot [1 - (N - 1) \cdot (0.45 \cdot X + 0.877)] \quad (4.8)$$

where:

- Q_F is the diesel fuel consumption at partial load and full throttle (gal/h)
- Q_R is the diesel fuel consumption at partial load and reduced throttle (gal/h)
- X is the actual engine load expressed as the ratio of the actual engine output power over the maximum power available at the same speed (decimal)
- P_{nom} is the nominal engine power (hp)
- N is the ratio between the actual engine speed and the nominal speed at which P_{nom} is evaluated

This formulation derives from fuel consumption measurements done by the Nebraska Tractor Test Laboratory on more than 500 diesel engine tractors. Although it gives an approximation of the real fuel consumption, at the time of this study this formulation was considered for the correlation with the engine size (nominally related to P_{nom} for standard Diesel engines), with the actual engine load (X) and with the actual working speed range (N). The same fuel consumption model was used when modelling both the traditional and the hybrid architecture.

The engine model was supplemented by two different controllers. The Idle speed controller was in charge of governing the engine at its minimum speed to prevent shutdown in case of standstill start. Then the speed controller in Figure 4.15, was in charge of tracking the desired engine speed coming from the driver model. The speed controller consisted in a simple PI controller that depending on the error between the reference speed assigned by the driver with the accelerator pedal and the actual engine speed, changed the normalized throttle signal for the engine model. Due to the non-linearity of the engine map, the proportional and integral gain of the PI controller were given as Look up tables of the actual engine speed. In this way, a more realistic responsiveness of the engine was achieved.

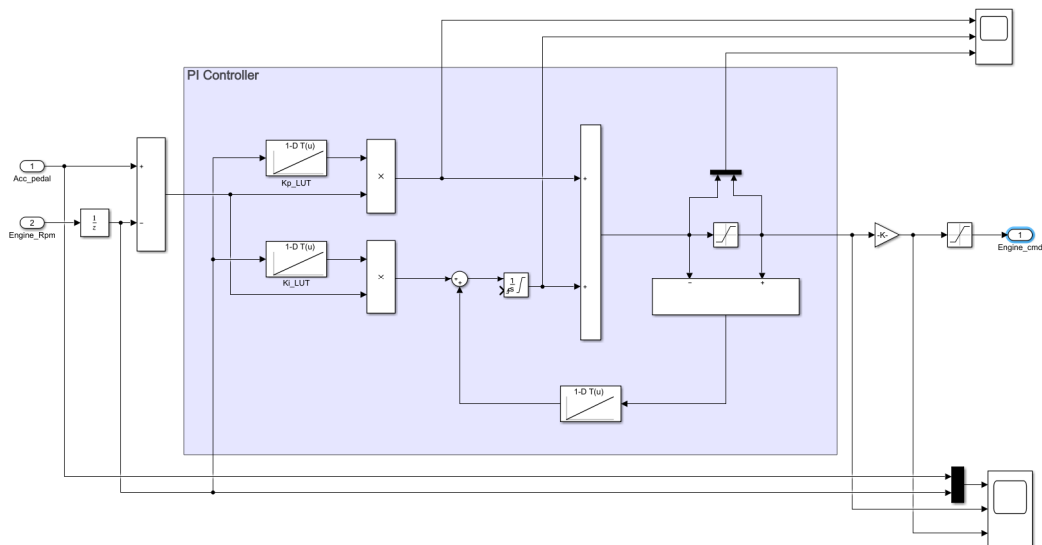


Figure 4.15 Engine speed controller

The last critical subsystem to be modelled inside the tractor was the PTO load. The power demand from this component strongly depends on the implement and application under investigation. Due to the lack of information about internal mechanisms of the implement and external working conditions (terrain conditions,...) a data-driven approach was adopted to simulate PTO loads. In principle, if the numerical model was capable of matching the engine load during not PTO operations (essentially transportation) thus the measured engine load data during PTO tests could give an estimation of the actual PTO load also in not stationary operations. Thus, a PI controller was in charge of tracking the engine load during PTO simulations on the traditional architecture, adapting the applied resistance to match experimental data (as it will be shown in the next session).

The so built tractor model required four inputs for each simulation to represent the driver behaviour and the working conditions. The signals to be given at each simulation were:

- The accelerator pedal/engine speed reference
- A pedal clutch signal
- A sequence of engaged gears

- An engine load data table for PTO simulations.

Given these inputs, simulation output and the measured data (from which the input signal were derived), should have matched in a properly designed model. The solver used for these simulations was set to use the Euler method with a fixed time step of 0.01 s to simulate the fastest control message on the CAN BUS network.

4.3.2 Simulation and validation of the model

Model validation had been a three-step process which aim was to set up the three important subsystems of the model: the engine speed controller, the tractor (and trailer) longitudinal dynamic model and the PTO model. The first step focused on the engine speed controller. The test considered to set up the model was the acceleration test with the trailer at its maximum load which was characterized by a highly dynamic power demand. From test data shown in Figure 4.7, the input signals for the numerical simulation were derived (Figure 4.16). As engine speed reference, the same input given by the driver was assigned to the model to replicate the desired working speed. Unfortunately, no information on the clutch signal and on the actual gear were available on the recorded data. Thus, the actual gear ratios were derived based also on the notes given by the driver during the tests. Then, the clutch signal and gear shifts were designed according to the analysis of the engine speed data and the actual vehicle speed: whenever the same engine speed corresponded to a different vehicle speed, a gear shift had happened.

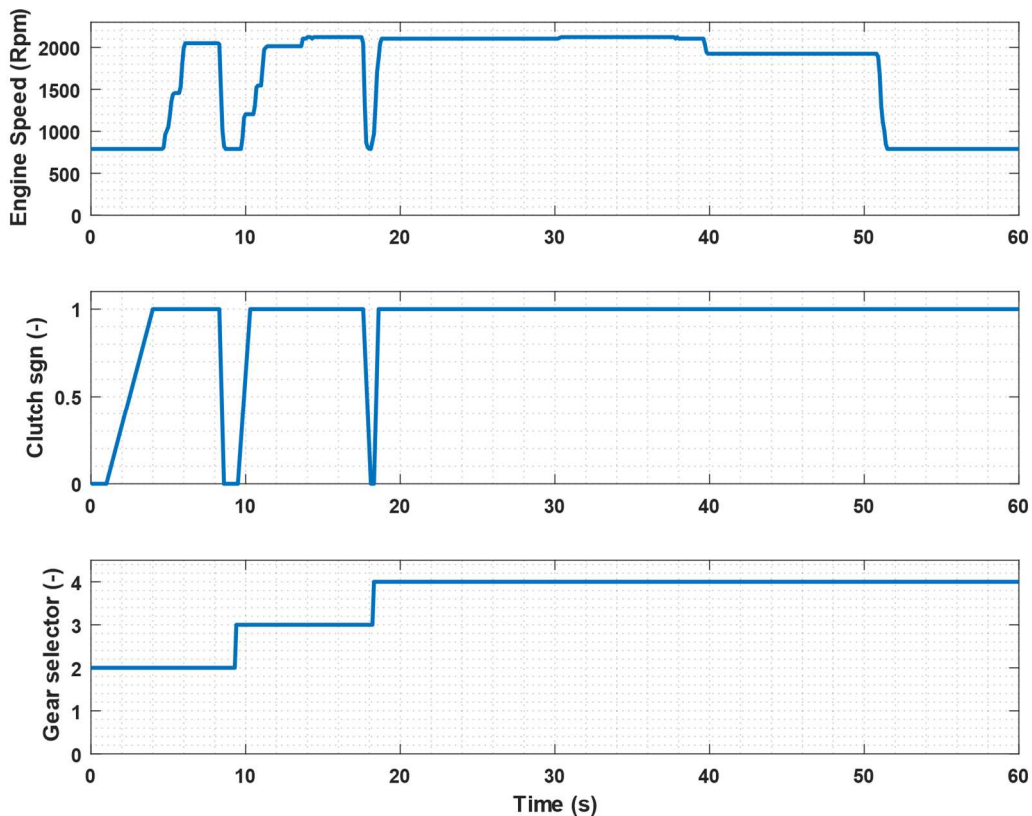


Figure 4.16 Model input signals: transportation test – trailer 6000 kg

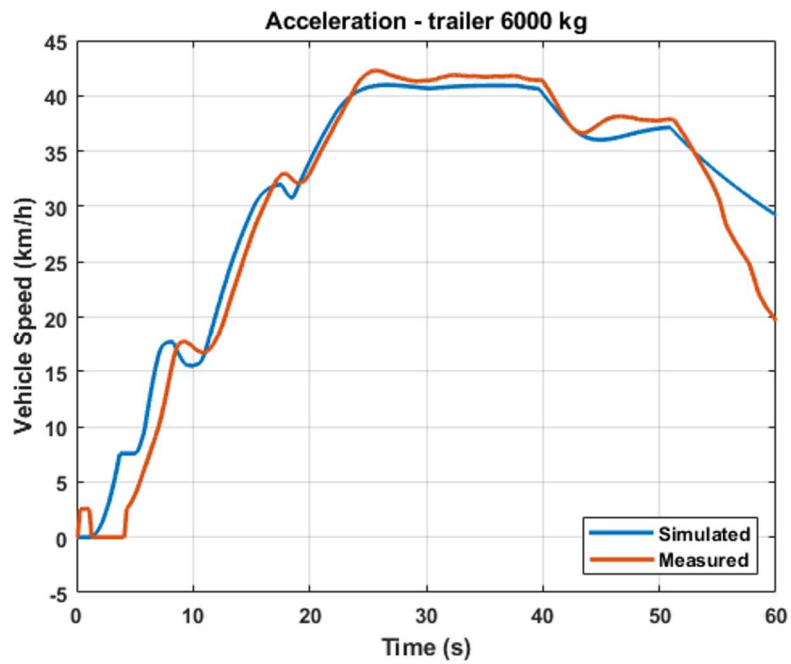


Figure 4.17 Vehicle speed comparison: Model vs Experimental data

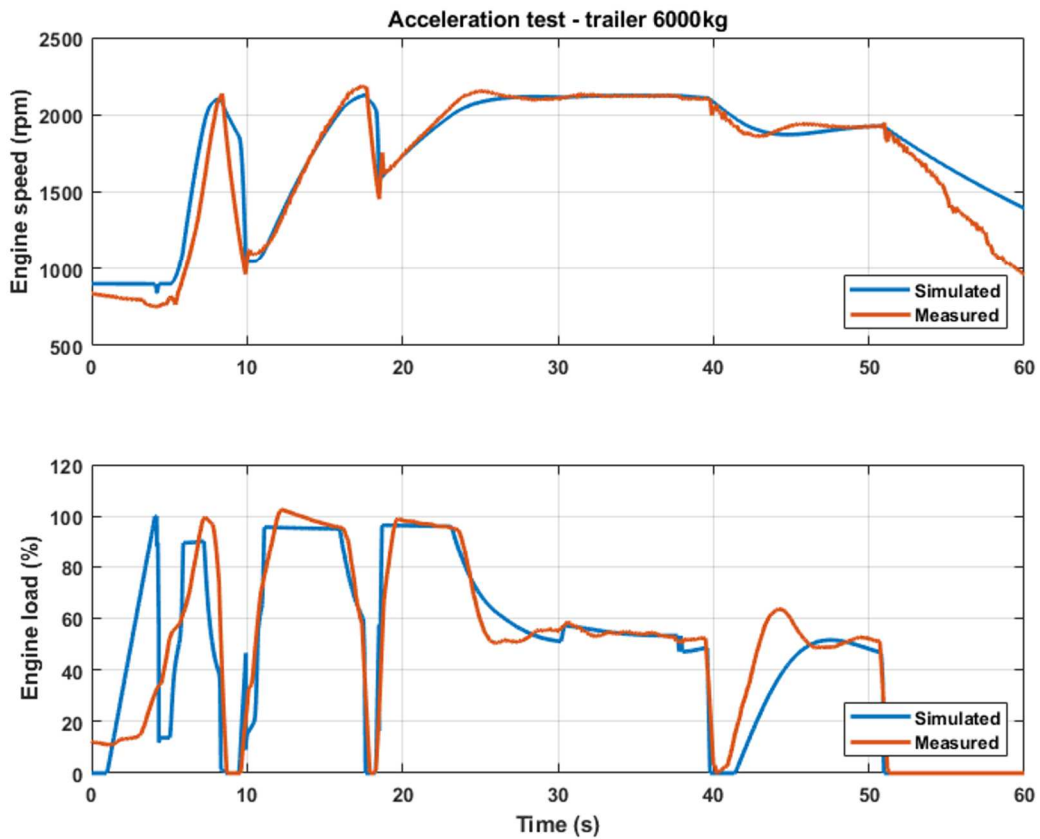


Figure 4.18 Engine performance comparison: Model vs Experimental data

In Figure 4.17-Figure 4.18, the main numerical results of the simulation are reported. Vehicle speed showed a good agreement between simulated results and measured data. These results validated the geometric parameters of the vehicle and trailer model (rolling radii), as well as the inertia properties and the overall resistance felt during the acceleration. The good results in the gear shifting timing validated also the clutch and gear ratio scheduling that were specifically designed from the available data.

It is worth to mention that the discrepancy between the simulated deceleration and the measured one from $t=50$ s up to the end of the simulation are related to the use of brakes by the driver. Since no data on the brake pedal signal nor GPS data were recorded, brakes were not included in this model. Looking more in detail at the behaviour of the numerical model, the engine speed showed good agreement between simulated and measured data. These validates both the engine model and the designed speed controller of which any data was available. Finally, the good agreement between the measured engine load and the same quantity calculated from the simulated actual engine performance gave a good feedback on the vehicle and trailer behaviour translational model.

Further investigations were needed to ensure the translational model of the tractor was accurate enough. Thus, the transportation test in Figure 4.6 with the empty trailer (tare mass of 1400 kg) was simulated. As for the previous test, the accelerator pedal signal was taken directly from the CAN BUS data while the clutch and the gear selector signals were derived (Figure 4.19).

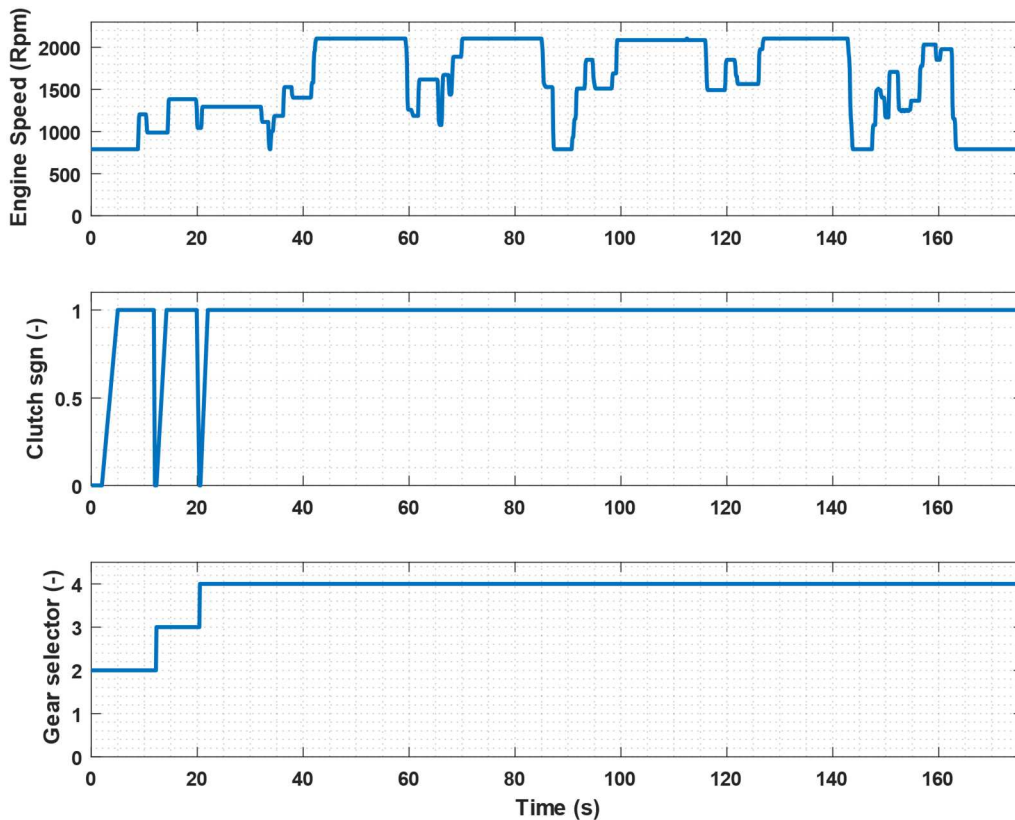


Figure 4.19 Model input signals: transportation test – trailer 1400 kg

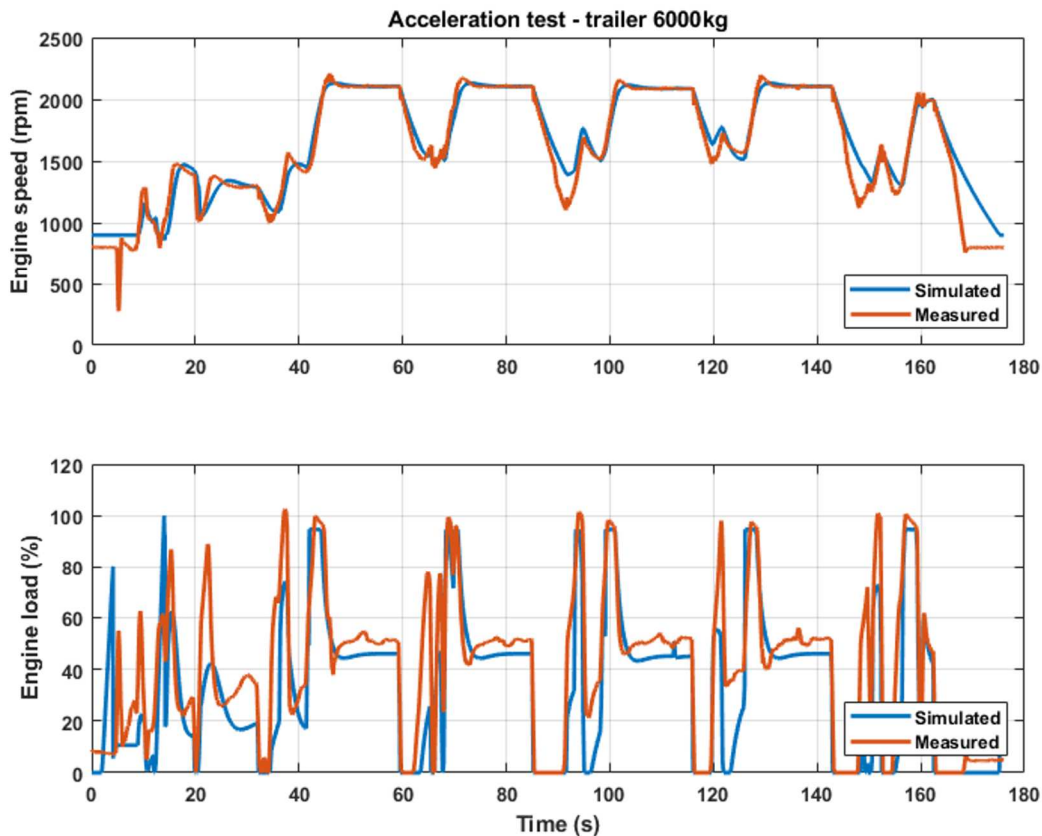


Figure 4.20 Engine performance comparison: Model vs Experimental data

Simulation results showed again good agreement between the vehicle and engine measured speeds and those obtained from the numerical model (always considering the absence of braking during real deceleration). Figure 4.20 shows only the engine speed comparison since the longitudinal vehicle was already validated before in terms of maximum speed. There were some appreciable differences in the engine load when dealing with accelerations from standstill. Higher accordance between simulated and measured engine load was present once the fourth gear and the clutch signals were constant. Thus, differences were mainly related to the scheduled clutch signal that evidently did not match well in the early acceleration stages. However, for the purpose of this analysis, the engine load estimation during longitudinal motion was considered accurate enough.

Once the longitudinal model of the tractor was validated, the PTO loads had to be characterized. As explained in the previous section, no data were available on the mechanisms of the considered implements. Thus, a reverse data-driven approach was considered. Having a good representation of the engine load for tractor longitudinal motion and engine losses from the previous numerical simulations, the model was run in order to find what was the percentage of the measured engine load related to the actual PTO load. This was possible because of how the PTO subsystem was modelled. The resistance torque value to be applied was determined by a feedback loop between the actual engine load of the model and the measured engine load at the same time instant. This comparison was

possible thanks to the fact that the model run with the same input signals of the real tractor.

In Figure 4.21-Figure 4.22 the case of the Atomizer work load is shown. The PTO feedback loop and experimental data allowed to determine the PTO power during the session. To measure the characteristics of the load, after the minimum and maximum power related to the specific activity were stated, the mean power and the standard deviation of the data distribution were evaluated approximating the behaviour to a normal distribution. This method allowed to evaluate, for each PTO working scenario a loading table (Table 4.3). The peak index represents the ratio between the maximum and the mean power demand. High values for the standard deviation and for the Peak index represented high variability of the work case.

	Atomizer	Shredder	Rotary harrow
Min	34.5	12	35
Max	40	26	52
Mean (Normal distribution)	36	19	44
Standard deviation	1	2	3
Peak index	1.11	1.37	1.18

Table 4.3 Statistics of the considered PTO working scenario – Power (kW).

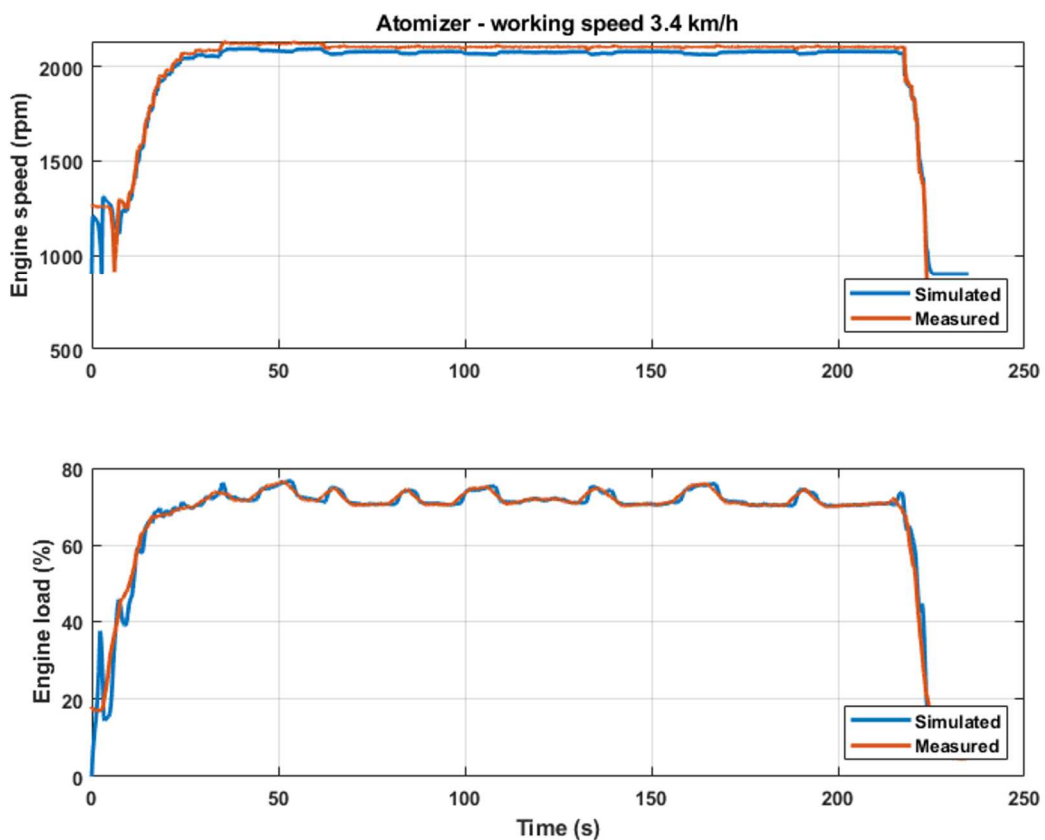


Figure 4.21 Engine performance comparison: Model vs Experimental data

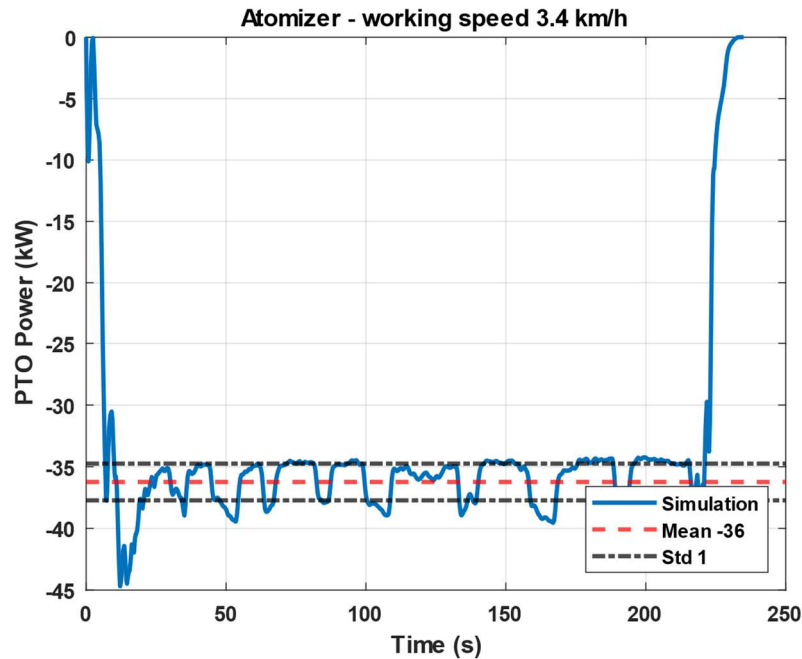


Figure 4.22 PTO equivalent load

4.3.3 Identification of an electrified architecture for an orchard tractor

When designing an electrified architecture for a working machine, the goal must be to achieve better efficiency of the overall system without compromising the usability/productivity of the current solution. This design constraint is mandatory to successfully propose the new machine to the market. Higher efficiency means higher fuel economy, thus lower operating costs. However, if the price for these improvements is the functionality of the machine itself, the technological result could remain a mere exercise in style.

The extensive experimental activity done on a specialized orchard tractor allowed to define and understand the characteristics of the main working scenarios which these machines are designed for. From the previous analysis, it was obtained that:

- The current tractor architecture used all the available installed power only during the 0-40 km/h accelerations. However, once the top speed was reached, the engine was committed with just half of its maximum capability to maintain the vehicle and the full loaded trailer at the top speed.
- The most energy consuming tasks recorded were PTO related. Some activities have very low power demands, others (like the atomizer and the rotary harrow) can ask up to 70% of the current engine capabilities for long periods of time (also several hours).

From this analysis, the engine resulted oversized for continuous working loads but worked great when it was time to pull heavy loads on the road (transient operations) or some PTO implements on the field. A full electric solution, although probably the easiest to implement, is not really practical for a full working day due to the actual limitations on Energy Storage System capabilities (see chapter 3 for more details). Thus, a hybrid solution is a more viable solution also for integration in the current vehicle architecture with relatively low impact at the system level.

Looking at the basic hybrid architectures showed in chapter 2 two possible solutions can be considered for the specific case study: a series or a parallel one. More complex solutions can be also adopted with overall higher improvements, but they would require a deeper re-design of the current system. If a series architecture is considered it is possible to state that:

- Decoupling the engine from the driveline, it could be easier to control it in order to maximize its efficiency, improving fuel efficiency thus reducing pollutant emissions.
- The use of an electric machine directly connected to the driveline could reduce the total number of gear ratios required to reach the target working speed. However, the flexibility of electric motors is not enough to satisfy the high torque required for pulling loads. Thus, a gear selector or some other types of gear reductions would be still required to cover all the possible operating ranges.
- The availability of a battery pack could allow some full electric operations. Its size would determine how long a certain task could be accomplished in full electric mode.
- The electric machine attached to the driveline must provide the same peak power and torque capabilities of the standard diesel engine. Considering well established technologies, like induction motors or permanent magnets synchronous motors, the size of the electric motor and of the electric generator could require a high level of structural changes on the current vehicle.
- Two electric machines require two electronic units, two sets of connectors and cables. These elements determine an overall higher volume of the electric system.
- The Hybrid Control Unit (HCU) must manage together the ICE, and two electric machines (one as a generator, one as a motor). The control software complexity and critical issues are directly correlated to the number of subsystems to be managed.

This brief analysis highlighted several pros and cons about the adoption of a series architecture on a specialized tractor like the one studied in this work. If a parallel architecture is considered, it is possible to say that:

- The direct coupling of the engine to the driveline reduces the degrees of freedom for efficiency optimization. However, the use of an electric

machine can help the engine in those transient operations where usually thermal engines show their lower efficiency.

- The connection of the engine to the driveline requires at least the same number of gear ratios of the standard architecture. If no additional clutches are added, the electric motor would operate always in synergy with the diesel engine thus, gear ratios are mandatory to keep the engine running at the right speeds allowing low vehicle working speeds.
- Depending on the positioning of the electric motor in the driveline layout, full electric sessions may or may not be allowed if no other clutches are introduced. Otherwise, the ICE would be dragged in full electric working operations.
- The size of the electric motors depends on the size of the adopted diesel engine since the mechanical coupling would add the power from the two sources. The greater is the ICE downsizing, the higher would be the performance required to the electric motor.
- A parallel architecture would require less electric/electronic components, leading to an overall lower volume of the electric subsystem.
- The HCU is asked to manage only two systems, one ICE and one EM, lowering the complexity of the control software architecture.

Knowing pros and cons of both the possible solutions, the parallel hybrid architecture was chosen as the one to be investigated. The main reason was that, according to the author opinion, this type of solution could be easier to implement on an existing tractor architecture. Thus, efforts in this direction could lead to a practical and realistic (from an industrial point of view) solution to be adopted. One of the goals of the investigation was also to understand if the implementation of such architecture could allow a certain downsizing of the Diesel engine, without sacrificing vehicle's capabilities.

4.3.4 Modelling of the electric hybrid architecture

The implementation of the hybrid parallel architecture in the tractor model consisted in three steps:

- Implementation of an electric motor which could add power to the main mechanical path of the driveline
- Modelling of a battery pack to supply electric power to the drive and the motor
- Implementation of a control algorithm to manage the electric unit

The PN modelling technique used for the traditional tractor allowed to easily integrate the electric system on the mechanical layout defined and validated before. In Figure 4.23 the new model layout is shown. Interconnections between physical systems are realized with a balance of the instantaneous power. A connection of the electric motor shaft to the engine output shaft had the effect to add or subtract power

to the main driveline depending on the sign of the torque applied. When connecting two mechanical elements, rotational speeds of each system were automatically constrained to be equal (an across variable cannot change without a physical element that allow for relative motion). Thus, the first step focused mainly on the identification of the mechanical performance of the Servomotor model which final characteristics are reported in Table 4.4. Electric motor characteristics were determined based on a new Diesel engine. For the purpose of this study, the ICE was chosen with the same nominal speed of the one currently installed, but with a nominal power of 54 kW (72% of the current installed nominal power). The reason for this choice was to push the engine to more efficient loading conditions (reducing oversizing effects) being sure to cover peak power demands with the electric system. The total installed power of the hybrid power-unit was indeed greater than the nominal power of the current one.

	Value
Nominal speed (rpm)	2300
Nominal power (kW)	30
Maximum torque (Nm)	130
Nominal efficiency	95%

Table 4.4 Electric motor characteristics.

A battery pack model was required in order to propel the vehicle and to evaluate the actual state of charge of the electric system. As explained more in detail in chapter 3, a battery pack is the result of a proper combination, in series and/or parallel, of elementary lithium ion cells which determine its total voltage and capacity. The battery pack model developed for this study consisted of a series connection of 192 elementary cells, modelled according to the Equivalent Circuit Model (ECM) described in chapter 3. With this configuration, all the cells were discharged with the same current. Two modelling strategies were considered. The first consisted of a complete battery pack model where for each simulation the ECM was solved 192 times at each integration time step (essentially for each cell). This modelling approach showed high potentiality, especially in testing of battery management system strategies. However, for the purpose of the analysis shown in this chapter, the simplified battery model shown in Figure 4.24 was considered. The ECM model was implemented just for one cell. Its actual voltage was measured and sent to an ideal voltage source after being amplified of 192 times. Thus, the right side of the PN was directly connected to the electric drive to supply power. The current delivered by the ideal voltage source was constantly measured and fed back to an ideal current source deputed to discharge the single cell on the left PN branch according to the real power demand. In this way, the benefits of the ECM model in terms of power delivery and state of charge evaluation could still be included in the system level model but the computational effort was way lower than the full battery pack model.

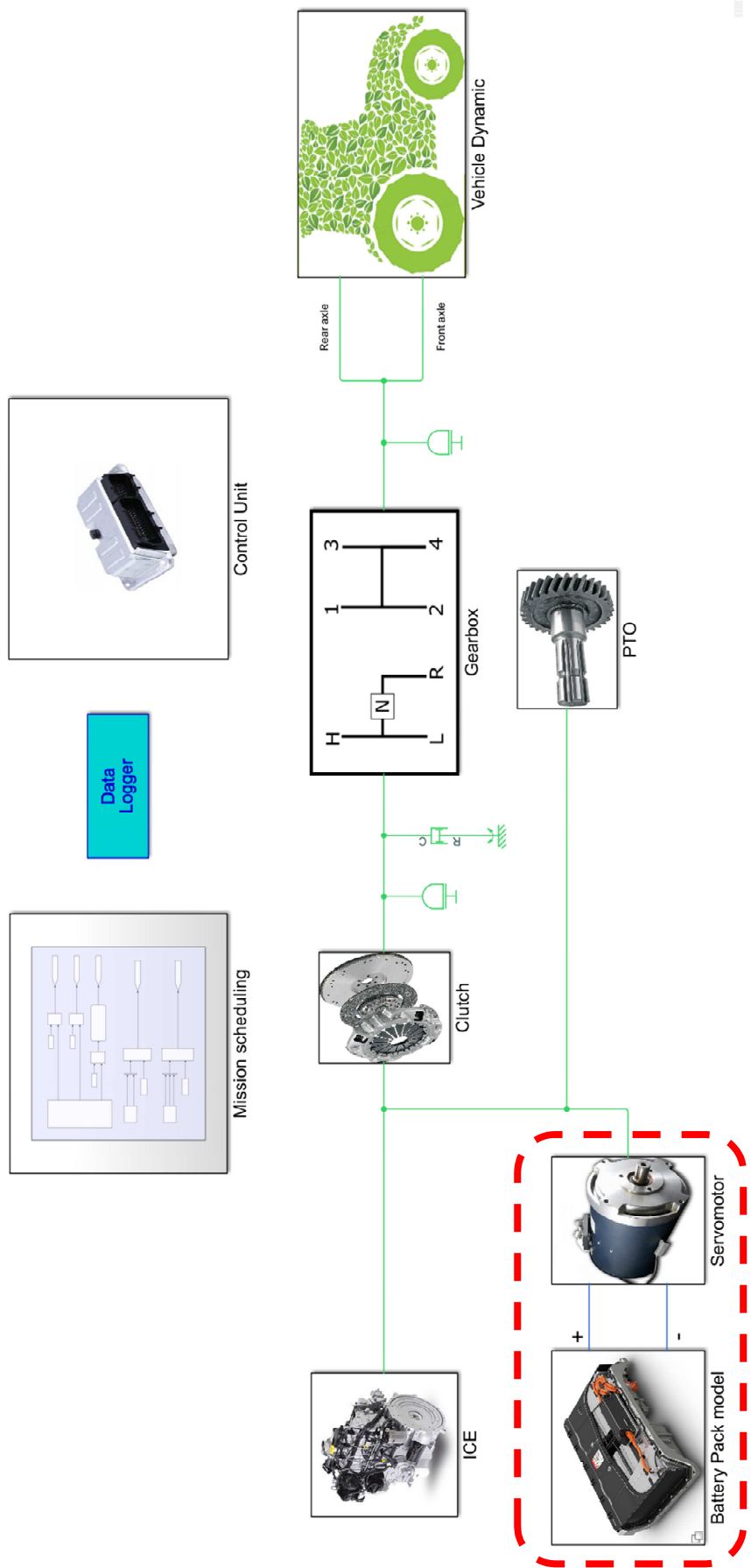


Figure 4.23 Physical network model of the hybrid parallel architecture

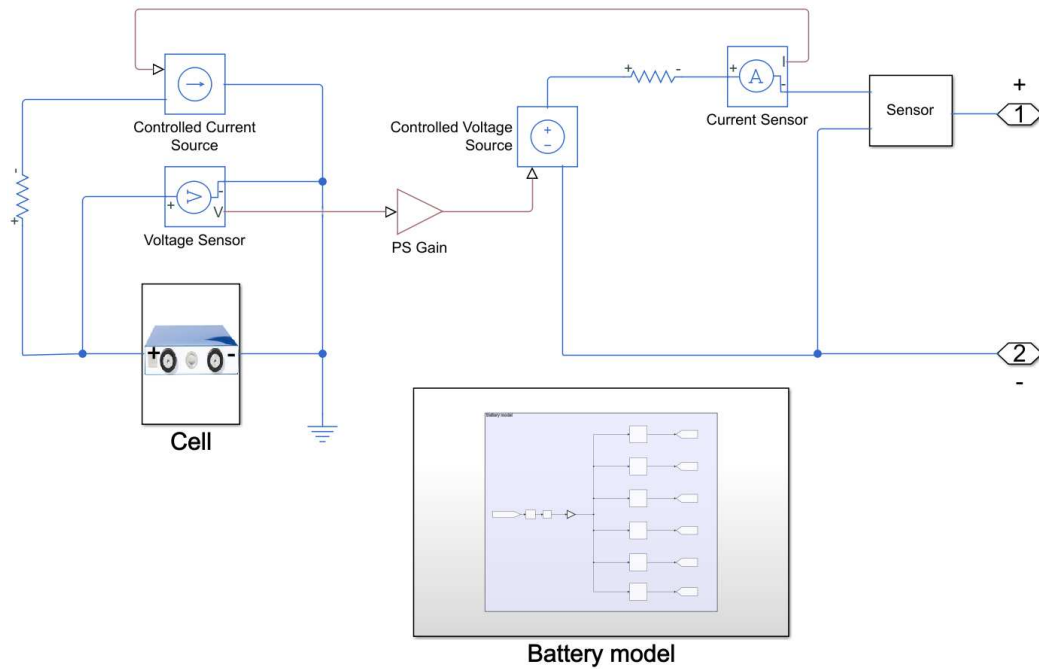


Figure 4.24 Physical network model of the battery pack

The last element to be modelled was the electric system controller, or Hybrid Control Unit (HCU). The HCU control strategy should be able to satisfy peak power demand as the traditional architecture using the new two power sources in the most convenient way. Moreover, to maximize the usage of the ICE, the strategy should be able to rely as far as possible on the power deliverable by the thermal unit. This point was crucial: as far as the ICE remained the main source of energy, the vehicle could count on a greater and quicker rechargeable storage system. Thus, this approach could allow also to optimize the battery pack size reducing its impact on the vehicle structural architecture. The more the system could rely on the thermal energy source, the more it would be capable of completing an entire working day. The control strategy implemented and investigated in this work can be described as follows.

- The system was thought in a Master-Slave configuration, where the ICE was the master node and the electric motor the slave one. This approach was considered because it could allow the implementation of the electric subsystem without major changes in the Electronic Control Unit (ECU) strategy of the Diesel engine. This could allow to use off the shelf engines reducing the cost related to customization. In the master slave configuration, HCU was the supervisor that determined the working conditions of the thermal engine actuating accordingly the electric motor.
- Diesel engines in working machines like the tractor of this study, are speed controlled. Thus, if the electric motor supplied additional power without an actual need, the ECU would reduce the amount of fuel in order to deliver less power and meet the speed reference. Here the need of a master – slave configuration. The electric motor should supply power depending on the

actual loading condition of the thermal engine to minimize the use of the electric energy stored in the battery pack.

To meet these requirements, the following algorithm was implemented in the controller shown in Figure 4.25 :

- A PID controller was in charge of reading the same speed reference given to the Diesel engine and its actual rotational speed and commanding a signal input for the electric motor
- An Observer constantly monitored the actual engine load and weighted the PID signal accordingly to a polynomial function. As discussed in the next section, the higher the order of the polynomial function, the lower was the energy taken from the battery pack to accomplish a certain task. However, the responsiveness of the electric system decreased as well.
- The signal of the controller was then converted in a 0-100 % range to be given to the electric motor drive controller for torque modulation.

The different weighting functions could be also considered as associated to several modes between which a user could chose if more power or more fuel economy are desirable (ECO – Boost modes).

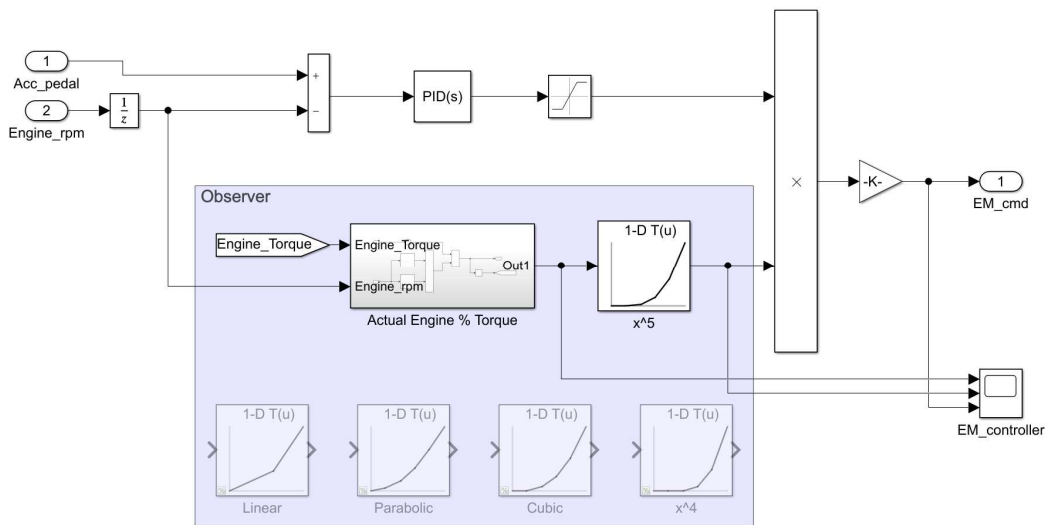


Figure 4.25 Electric motor controller

4.3.5 Performance analysis of the hybrid architecture

To evaluate performance of the hybrid architecture, the same load profiles measured and used to test the tractor model in the previous sections were used with the new hybrid powertrain. The aim of these investigation was to prove the power capabilities of the electrified architectures in typical loading scenarios of a specialized orchard tractor. These tests were used also to properly set up the electric motor controller to meet the peak power demand but also to minimize electric energy usage. For all the tests, the same driver input signals (speed reference, clutch

signal and gear selector) used to validate the tractor model were given to the hybrid power unit. The speed controller of the ICE had the same control logic of the previous case: it took the driver input speed reference and modulated the output power of the engine to match the desired speed. It is worth to mention also that no changes were applied to the ICE speed controller. The main reason is that the goal of this simulation was to demonstrate the capabilities of the Master – Slave configuration with the Load Observer control algorithm when coupled with off-the-shelf components from other manufacturers. Finally, for the purpose of this analysis a downsized Diesel engine with nominal power of 54 kW at 2300 rpm was considered. The main reason was the fact that this threshold allowed to stay in the power range 37-56 kW range prescribed by the new Stage V regulation that will enter in action in 2020. Thus, the overall emissions of the hybrid power unit would had been lower than the ones of the standard architecture.

In Figure 4.26-Figure 4.29, performance results of two architectures on the main activities studied in this work are reported. The acceleration test with maximum trailer load was chosen as a good candidate to represent a high transient load where the power unit must provide the same peak power capabilities of the traditional architecture. Using the same driver input signals, the new hybrid unit performed as well as the traditional tractor, as desirable from a user point of view. The vehicle speed plot is not shown here since the drivetrain and the vehicle model were the same thus, results in terms of top speeds were in accordance to actual the engine speed. What is worth to highlight is the combined power delivery of the power unit. Once the high transient phase of the acceleration was finished the contribution coming from the electric motor decreased drastically thanks to the observer work. In this way, the main source of energy was always the Diesel engine in steady state operations. Two benefits derived from this: the electric energy stored in the battery pack was wisely used and the thermal unit worked at higher loads where engines usually show better efficiency.

The most critical working loads for an electrified architecture are the ones with high average power demand, especially for hybrid architectures with downsized thermal engines. It is worth to mention that those tests were performed with the same PTO load derived before from the standard tractor model. The PTO torque evaluated with that model was then used as resistance torque applied to the PTO shaft of the hybrid unit. In terms of power capabilities, the power unit performed as well as the traditional powertrain. The HCU controller managed well the power split between the two power sources, preferring the thermal engine as the main one. Looking at the three PTO tests, a 27% (average) reduction in fuel consumption was registered with the downsized engine. The reasons for this improvement were mainly related to:

- Lower fuel consumption of the downsized thermal unit
- Higher overall efficiency of the hybrid power unit
- The efficient work of the electric motor controller
- The availability of stored electric energy in the battery pack.

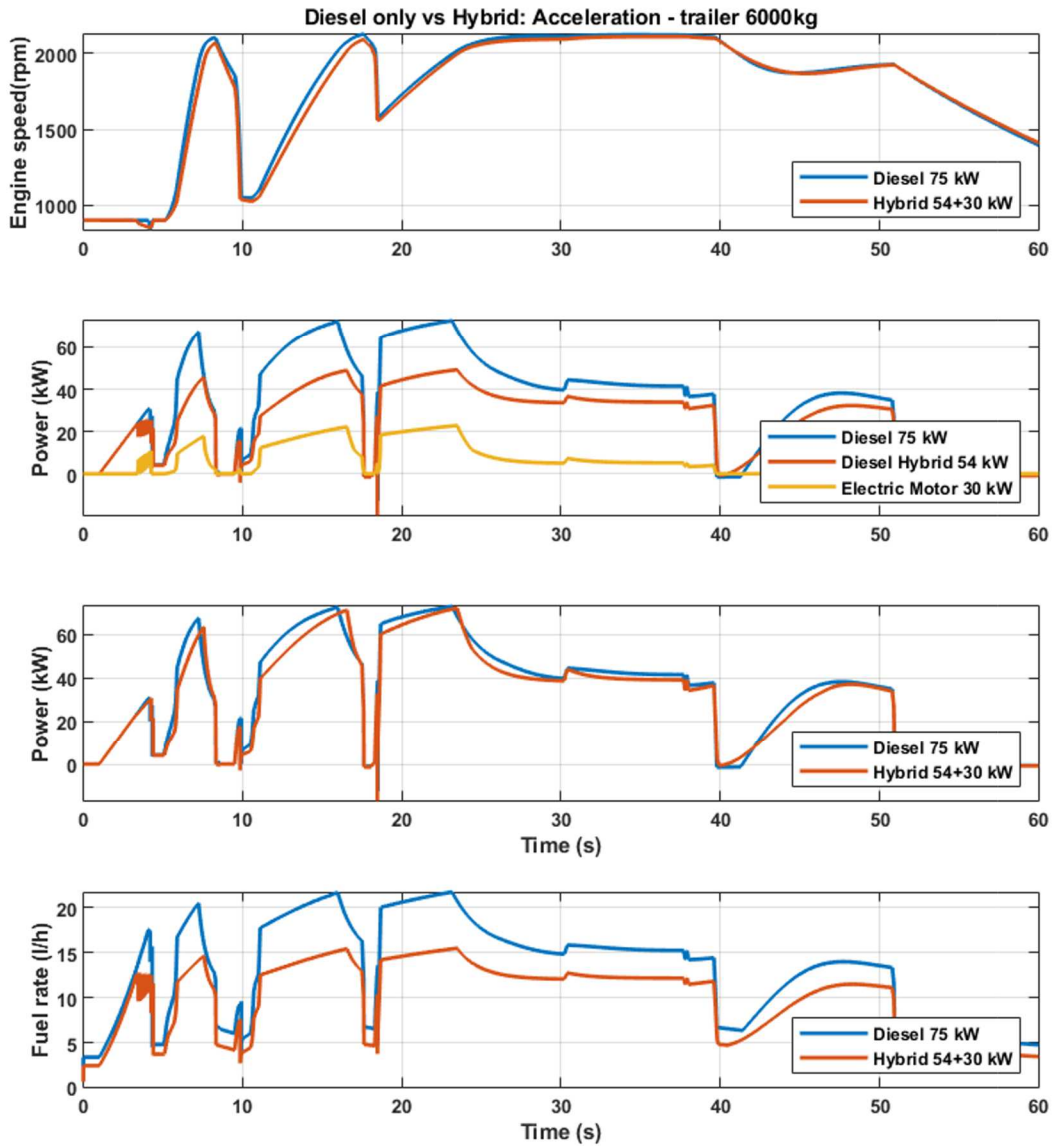


Figure 4.26 Power units performance comparison in the trailer test (max load)

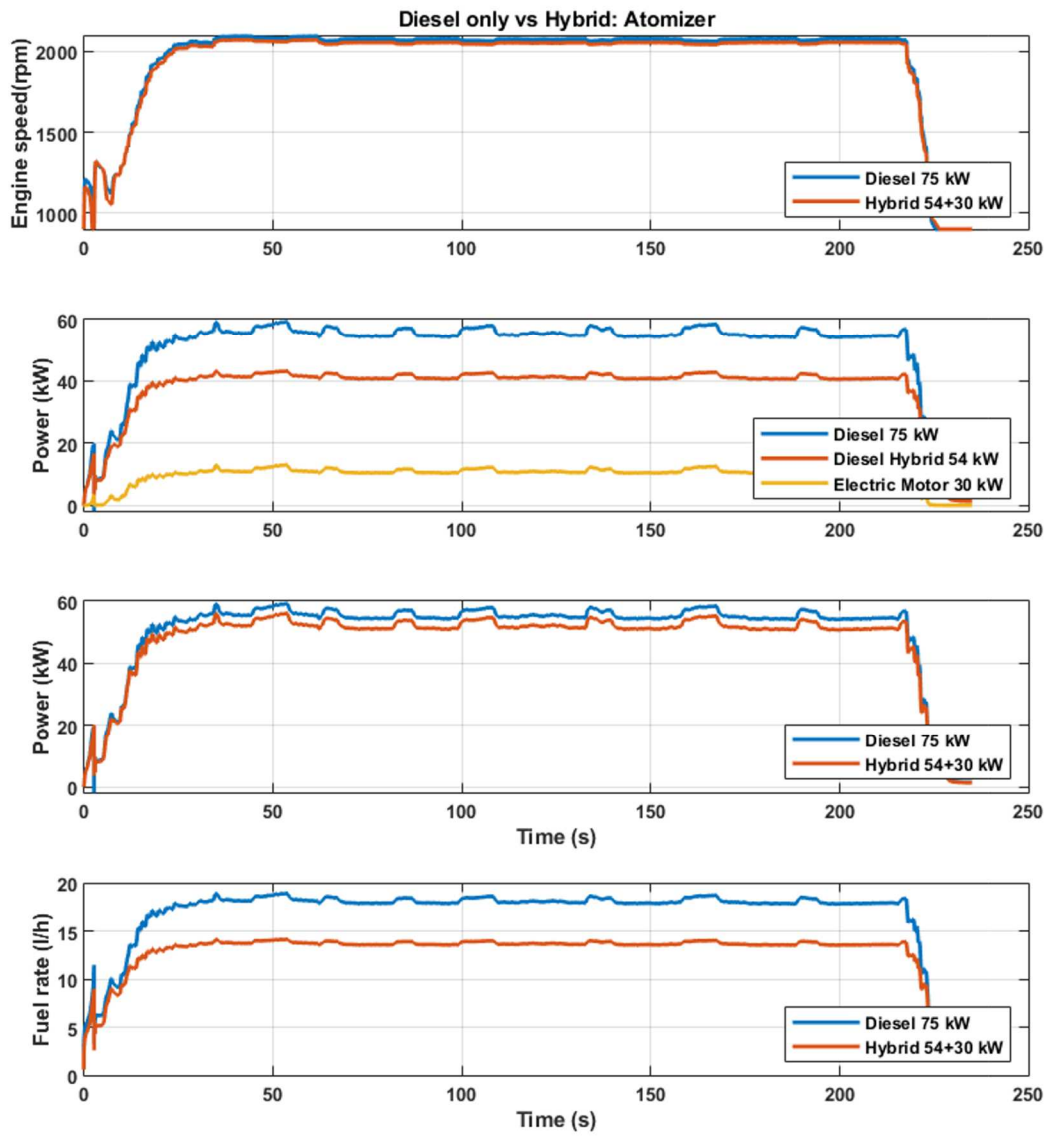


Figure 4.27 Power units performance comparison in the Atomizer test (mainly PTO load)

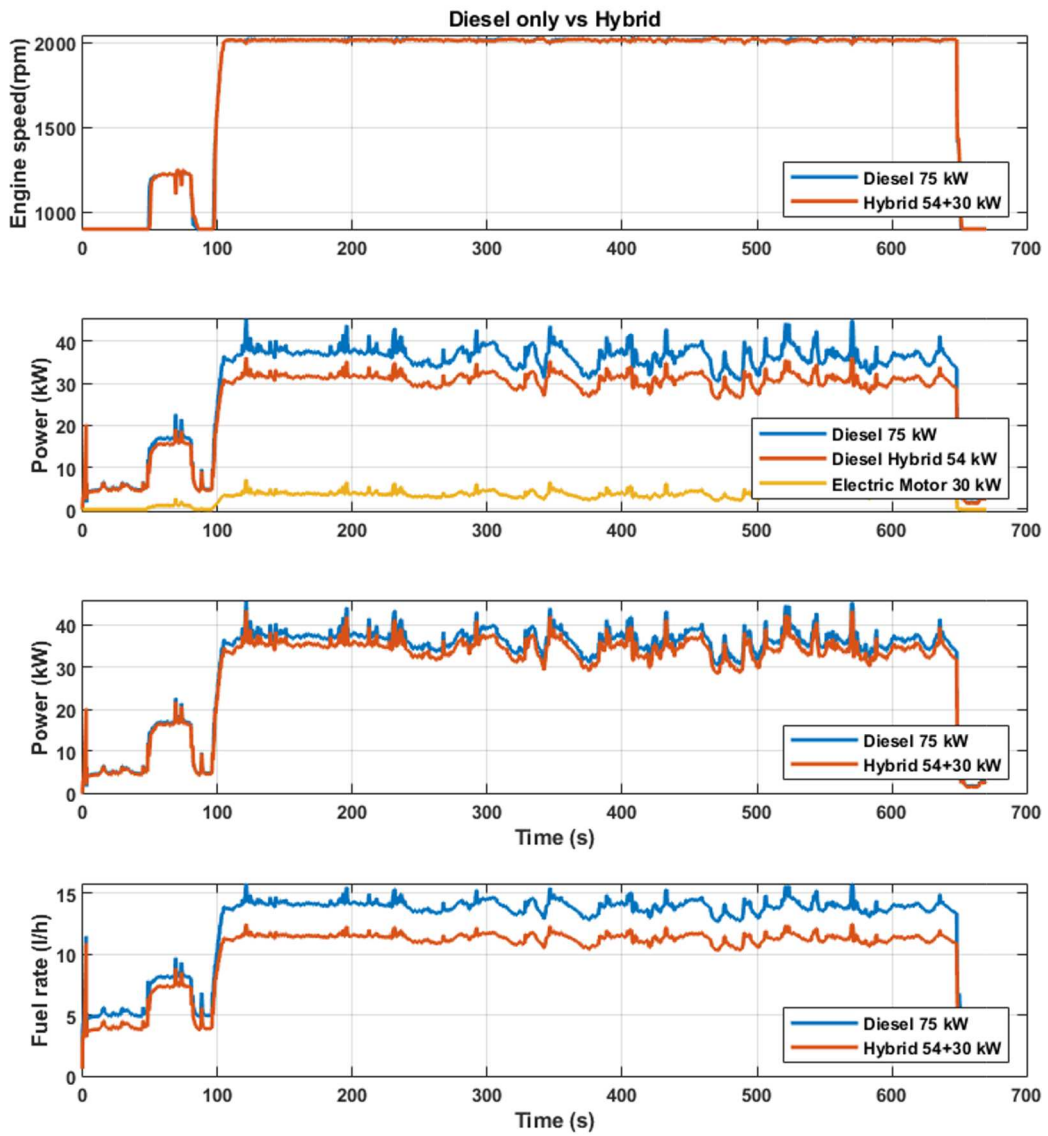


Figure 4.28 Power units performance comparison in the Shredder test (mainly PTO load)

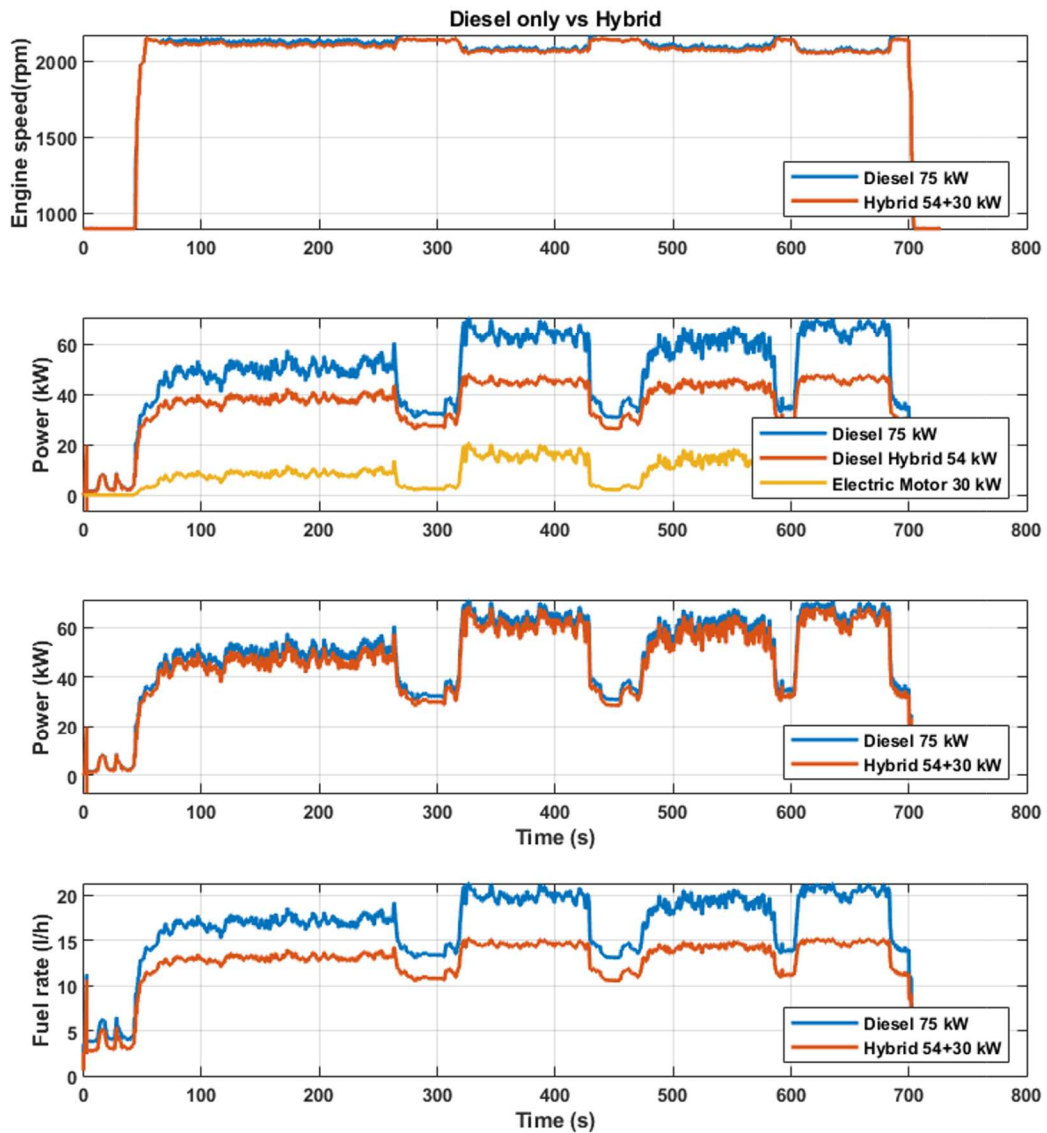


Figure 4.29 Power units performance comparison in the Rotary Harrow test (mainly PTO load)

In Table 4.5, it is possible to appreciate the overall improvements of the hybrid architecture compared to the traditional one. The total amount of energy requested by each power unit to accomplish the same task was evaluated as follows:

- For the traditional architecture, the total amount of energy consumed was evaluated as the energy of the fuel litres that were burnt to accomplish the task
- For the hybrid architecture, the total amount of energy consumed was the sum of the energy consumed by the thermal unit (evaluated as above) and the energy taken by the electric drive from the battery pack.

The values reported in the table below refers to the amount of energy consumed to accomplish the simulated task thus, depends on the working time measured during the experimental test.

	Trailer 6000 kg	Trailer 1400 kg	Atomizer	Shredder	Rotary harrow
Working Time (h)	0.017	0.05	0.065	0.18	0.2
Traditional (ICE)	2.3	5.5	11.9	25.2	36
Hybrid (ICE+EM)	1.8+0.13= =1.93	4.3+0.2= =4.5	9.1+0.9= =10	20.6+0.8= =21.4	27.2+2.5= =29.7
Delta (%)	-17%	-18%	-16%	-15%	-17%

Table 4.5 Power unit Energy consumption (kWh): comparison traditional vs hybrid.

4.3.6 Performance comparison on working cycles

In this section, results obtained from the numerical model of the hybrid architecture were used to understand the real daily capabilities of the proposed hybrid architecture. The overall improvements in the amount of energy required to accomplish certain tasks were strongly related to the amount of electric energy stored in the battery pack. This energy allowed the electric motor to help the smaller engine to satisfy the same peak power demand of the traditional tractor. The boosting process happened with a higher overall efficiency of the electric unit, amplifying the benefits of the downsized engine in terms of lower fuel consumption per unit of work done (for unit of work is intended the task to be accomplished). However, this architecture suffers those working loads with high mean power demand, typical scenario for most PTO activities.

In Table 4.6 the main results obtained from simulations were extended and normalized over 1 hour of working time. For the purpose of this analysis, a generic value E_{nom} kWh battery pack was considered. The size of the battery pack will be determined according to the most frequent working scenario that the tractor would face during its life. The table shows also the amount of energy taken from the

battery pack, that in this context is the “weaker” element of the chain in terms of endurance capabilities. For the purpose of this analysis, also charging capabilities of the battery pack must be considered. As suggested on the lithium ion cells datasheet from the manufacturer, the chosen cells can be charged with a current of 0.5C (or half of its nominal capacity). For the sake of simplicity, it is possible to approximate this quantity to half of the nominal energy of the cell thus $0.5 \cdot E_{nom}$ kWh. This charging strategy allows to consider a normalized charged energy of $0.5 \cdot E_{nom}$ kWh/h according to the definition itself of the charge rate.

	Trailer 6000 kg	Trailer 1400 kg	Atomizer	Shredder	Rotary harrow
Normalized Energy (ICE)	112	106	140	114	136
Normalized Energy (EM)	8.12	4.2	13.8	4.4	12.5

Table 4.6 Hybrid unit normalized energy consumption for 1 hour of work (kWh/h)

Let consider a first working scenario for a specialized tractor described as follows:

- 8 working hours, divided in two groups of 4 hours (8-12, 13-17)
- A working cycle consisting of: 45 % of transportation with no extra load (trailer empty – 1400 kg); 45 % of transportation with full load (trailer full – 6000 kg); 10 % of Idle time where the tractor is not really working but it is not useful to turn the engine down (not efficient)
- 1 hour of charging time during the lunch break.

According to this working scenario there would be:

- 3.6 hours of transportation at full load
- 3.6 hours of transportation with empty trailer
- 0.8 hours of idling
- 1 hour of break.

Thus, the amount of energy the battery should have can be easily found according to the balance equation between used and charged energy

$$8.12 \cdot 3.6 + 4.2 \cdot 3.6 - 0.5 \cdot E_{nom} \cdot 0.8 - 0.5 \cdot E_{nom} = 0 \quad (4.9)$$

From which $E_{nom} \approx 50 \text{ kWh}$

If the nominal voltage of the battery pack is considered

$$V_{pack} = 192 \cdot V_{cell} = 192 \cdot 3.2 \approx 615 \text{ V} \quad (4.10)$$

The required capacity of the cell can be found as

$$C = \frac{E_{nom}}{V_{pack}} \approx 80 \text{ Ah} \quad (4.11)$$

The obtained capacity is the minimum required to satisfy a daily working cycle focused on transportation like the one described above.

A battery pack based on the transportation oriented working scenario would easily cover a full working day of shredding with 90% of work time and 10 % of idle. This type of working scenario would not require charging the battery pack during lunch time. Different are the cases when the atomizer or the rotary harrow are considered. Let suppose to have the same working cycle viewed before for the shredder implement both for the atomizer and the rotary harrow. In the first case, there would be:

- $13.8 \cdot 7.2 = 99.4 \text{ kWh}$ of energy required for the implement
- $25 \cdot 0.8 = 20 \text{ kWh}$ of energy that could be recharged during idle phases (for example when refilling the atomizer tank)
- 25 kWh of energy charged during lunch time

With a proper scheduling, there would be a lack of 5 kWh at the end of the working day. Not having this amount of energy means not being able to accomplish the task (to water the plants in the field) properly which could affect the products quality. This type of working scenario is the most critical, but it is also not a daily activity. Thus, the occasional nature of this process could suggest to slightly increment the charging rate in order to fill the energy gap and completing the working day. As demonstrated in the automotive case, fast charging up to 80% SOC is possible if proper cooling is guaranteed during this process.

Similarly, it is possible to analyse the working scenario were the rotary harrow is attached to the tractor. Considering the same working cycle there would be:

- $12.5 \cdot 7.2 = 90 \text{ kWh}$
- $25 \cdot 0.8 = 20 \text{ kWh}$ of energy that could be recharged during idle phases (for example when setting up the tool during the day)
- 25 kWh of energy charged during lunch time

With this scenario, the proposed energy management scheduling is enough to cover the entire working day, without considering fast charging.

From the above analysis, it is clear that a 50 kWh battery pack is the minimum threshold if a downsized Diesel engine is considered. Of course, the feasibility of the proposed architecture strongly depends on how, such a battery pack can be, integrated on a current tractor architecture. Usually, specialized tractors are characterized by a very small size factor, thus the on-board integration would be a quite challenging task. However, it is worth to mention that the use of a downsized engine would free some space on the tractor architecture because of smaller dimensions and the lower number of exhaust gas after-treatment systems required to meet the new stage V regulation. Moreover, proper investigation should be

considered on the emissions of the new power unit. As demonstrated before, the amount of fuel burnt for work unit is lower, thus also bigger engines could satisfy the same emissions regulation of the 54 kW engine. This could suggest to slightly increase the nominal power of the adopted diesel engines to reduce the size of the battery pack without the need of emissions devices required for bigger engines.

4.4 Conclusions

In this chapter a numerical model of a hybrid architecture for a specialized tractor was developed. This study started from an extensive experimental campaign where performance of a traditional orchard tractor were measured on the field while performing some of the most common working tasks for these type of machines. This activity allowed both to collect data and to understand the driver expectations regarding the machine performance. From this knowledge a numerical model of a traditional tractor architecture was developed. The model was developed according to the physical network approach that allowed to identify subsystems that would have been in common with the new electrified architecture. The longitudinal vehicle model, the PTO model and the engine speed controller behaviour were validated using experimental data. The vehicle speed, the engine speed and actual load were considered as the main parameters of interest to be compared to the tractor ones recorded from the vehicle CAN BUS. Once the traditional tractor model was validated, a hybrid parallel architecture was investigated according to a critical analysis with pros and cons against a series architecture. The numerical model was then expanded including the electric subsystem (electric motor, battery pack and electric motor controller). The hybrid architecture investigated in this study considered a downsized Diesel engine compared to a traditional one. The goal of the investigation was to understand the peak power capabilities of the new hybrid power unit, used on the same vehicle architecture (with a Master slave configuration between the thermal engine and the electric unit) and to evaluate the required size of the battery pack in order to satisfy typical daily working cycles. As main design reference, a transportation working cycle was considered to size the cell capacity of the battery pack. Then the so obtained battery pack was analysed according to other working cycles, mainly centred on PTO working operations. The main results of this work highlighted the good peak power capabilities of the electric system, with a control logic able to minimize the intervention of the electric unit under low working loads. However, for the nominal engine power considered, some PTO working scenarios (like the atomizer one) are particularly energy demanding, thus specific charging strategies must be adopted to ensure the accomplishment of the working task. It is worth to mention that these types of activities are not scheduled on a daily base so a proper rapid charging strategy can be considered. The most critical point when dealing with the implementation of an electrified architecture is the vehicle integration of all the components. The battery pack must be properly designed to minimize the overall volume, which most of the time is a critical aspect on specialized tractors as the one studied in this work. However, the downsizing of

the engine would free some space both for its smaller size and for the lower amount of gas after-treatment systems required to satisfy Stage V regulations.

References

- [4.1]. F.J. Sonnen. “Drawbar performance of high powered farm tractors with rear wheel and four wheel drive”, *Journal of Terramechanics*, 6, 7-21, 1969.
- [4.2]. Polcar, “Drawbar pull and its effect on the weight distribution of a tractor”, *Acta Universitatis Agriculturae et Silviculturae Mendelianae Brunensis*, 65 (17), 145-150, 2017.
- [4.3]. ISO Standard 500-1:2014, “Agricultural tractors – Rear mounted power take-off types 1, 2, 3, and 4—Part1: General specifications, safety requirements, dimensions for master shield and clearance zone”, 2014.
- [4.4]. L. Bodria, G. Pellizzi, P. Piccarolo, “Meccanica e Meccanizzazione Agricola”, *Edagricole*, 2013.
- [4.5]. ISO 11898-1:2015, “Road vehicles -- Controller area network (CAN) -- Part 1: Data link layer and physical signalling”, 2014.
- [4.6]. W. Voss, “A Comprehensible Guide to Controller Area Network”, *Copperhill Technologies Corporation*, 2005.
- [4.7]. SAE Standard J1939, “Serial control and communications heavy duty vehicle network – Top level document”, *SAE International*, 2012.
- [4.8]. W. Voss, “A Comprehensible Guide to J1939”, *Copperhill Technologies Corporation*, 2008.
- [4.9]. Mathworks, “Getting started with Simscape”, *Mathworks.com*, 2018.
- [4.10]. Somà, F. Mocera, F. Bruzzese, E. Viglietti, “Simulation of dynamic performance of electric hybrid heavy working vehicles”, *Eleventh International Conference on Ecological Vehicles and Renewable Energies (EVER)*, 2016.
- [4.11]. Somà, F. Bruzzese, F. Mocera, E. Viglietti, “Hybridization factor and performance of hybrid electric telehandler vehicle”, *IEEE Transactions on Industry applications*, 52(6), 5130-5138, 2016.
- [4.12]. R. Grasso, J.V. Perumpral, D. Vaughan, G.T. Roberson, R. Pitman, “Predicting Tractor Diesel Fuel Consumption”, *Virginia Cooperative Extension*, 2010

Chapter 5

Hardware – In – the – Loop bench testing for hybrid electric vehicles and control strategies

The electrification of NRMM can impact positively on their efficiency, improving the overall emissions of pollutant elements coming from several fields (construction, agriculture, handling, ...). The use of electric machines as mechanical power sources enhances the overall vehicle performance and capabilities. The specific field of application determines the architecture topology. Depending on the on-board electric power availability, the level of electrification (measured with the Hybridization Factor) increases. A full electric architecture would be the ideal solution for almost any ground vehicle. It is simpler both in terms of design and manufacturing process and it is relatively simple to control and integrate with other on-board technologies. However, with the exception of a limited number of applications, the actual state of the art of electric technology and in particular of lithium-ion batteries does not allow the widespread diffusion of full electric architectures. Today, hybrid solutions are the most viable alternative to traditional powertrains for off road vehicles. Hybrid topologies are more complex compared to full electric ones. The benefits related to more complex architectures go from efficiency improvements to the enhancement of new features and capabilities not available with traditional ones. Proper application-oriented control strategies are required on the supervisor controller of the hybrid system to achieve the best performance. In this chapter, results presented in chapter 4 were used to develop a control strategy for a hybrid parallel architecture of an orchard tractor. The application software deployed on an automotive control unit was tested on a scaled bench of the hybrid powertrain considered. The control system was tested on working scenarios derived from experimental measurements to have indications on the performance achievable by such architecture with a downsized diesel engine.

5.1 Design and development of the HIL bench

Hybrid and electric vehicles are complex mechatronic systems which require multidisciplinary knowledge during all the development stages. Using the definition of a system given by the International Council on System Engineering (INCOSE) [5.1][5.1], hybrid electric vehicles can be defined as constructs where “*several elements together are able to produce results not obtainable by each element alone*”. Control electronics is the key to integrate and manage such a variety of components (mechanical, electrical, hydraulic, ...) to meet design requirements. Using the System Engineering (SE) approach, the electrification of a working vehicle may be approached as follows:

- Definition of the typical working scenarios thus identifying the need of the final user
- Design of the system starting from the requirements of high-level subsystems down to those of the smaller ones
- Manufacturing and integration at system level of each subsystem
- Verification and Validation (V&V) of each subsystem and the overall result.

The procedure described above is also known in literature as the V-model diagram (Figure 5.1) and is the schematic representation of the SE approach [5.2]-[5.3]. It is not a straight path. Several iterations may be required to match system requirements. Feedbacks from the V&V stage are used to make the appropriate changes to the initial design. Although this method provides a structured way from the early design to the system release, it may lead to higher costs if the number of iterations and prototypes to verify is directly related. This is the reason why more developed engineering approaches have been included in the V-model to reduce to the minimum possible the number of prototypes required.

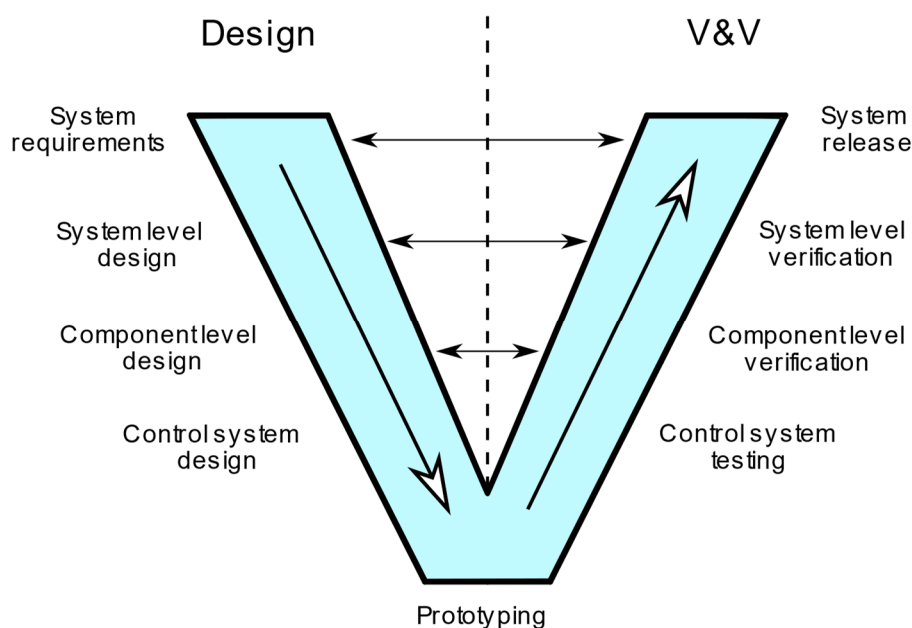


Figure 5.1 V-diagram and system engineering approach

First, it is worth to mention the Model Based Design (MBD) approach [5.4]. Modelling the system or also just a part of it allows to simulate several operating working conditions. Simulations can reduce the dependency from prototyping when it comes to understand the behaviour of the system. The MBD concept was born to meet the need for design standardization of embedded systems. However, the philosophy behind it can easily adapt on other fields of application. Although simulation is a powerful tool, models cannot replicate perfectly the real world. The efforts required to increase model fidelity at a certain point grow exponentially and still would not match entirely with the real phenomena. This is one of the reasons why on top of the MBD approach, Model In the Loop (MIL), Software In the Loop (SIL) and Hardware In the Loop (HIL) simulations were introduced [5.5]-[5.1][5.8]. With MIL, the early MBD process is addressed. The system and its control logic are modelled within the same simulation environment. What was shown in Chapter 3 can be addressed as a MIL simulation. The system plant (the hybrid tractor architecture) and its control logic (Master-Slave configuration ICE+EM) were developed and studied for given working scenarios and driver inputs. The SIL simulation is more related to the actual C code generated from the control logic. The actual hardware inside most modern Vehicle Control Units (VCUs) can be programmed by C-code software deployed with specific compilers and flashed on the controller memory. The SIL simulation wants to simulate the response of the C-code corresponding to the control algorithm to be sure that the behaviour matches the MIL results. At this point the control application is ready for hardware implementation and the VCU must be tested together with other subsystems. Here is where HIL comes in. Often, it is not necessary to have the full prototype of the entire system to prove the functionality of a subsystem. The Device Under Test (DUT) can be connected to just a subset of physical components of the system. The other ones, or the interactions with them and other external factors can be simulated on a Real Time (RT) system and given as input signal to the DUT. The RT simulation must constantly read the signals from the DUT and from the rest of the simulation environment and provide them with the proper actuation commands and/or feedback signals.

As described in [5.9] and shown in Figure 5.2, HIL simulations for hybrid and electric systems can be developed at different system levels:

- *Signal level*. The DUT is the controller board. The entire system in terms of mechanical components, power electronics, electric machines and batteries is simulated on a Real Time operating system. The DUT is tested and validated according to its behaviour under well-defined system signals [5.10]-[5.15].
- *Power level*. In this case, both the controller and the power electronics are tested. The simulation environment must be able to produce power signals at the interface with the electronic drive and/or electric components as well as electric feedback signals for the controller. Power flow to and from the electronic DUT is regulated using proper electronic loads or power supplies

guided by the RT system simulation. In the same way signals are provided to the control board [5.16]-[5.19].

- Mechanical level. The vehicle powertrain is considered. The mechanical subsystem is connected to another mechanical machine that will be actuated by the RT simulator to act as a load or as a mover according to the working scenario. This is the most complete type of HIL simulation because covers the control part, the electric and electronic subsystems and the mechanical powertrain. It can provide a good understanding of the designed vehicle just simulating it on a static bench [5.20] - [5.1][5.26].

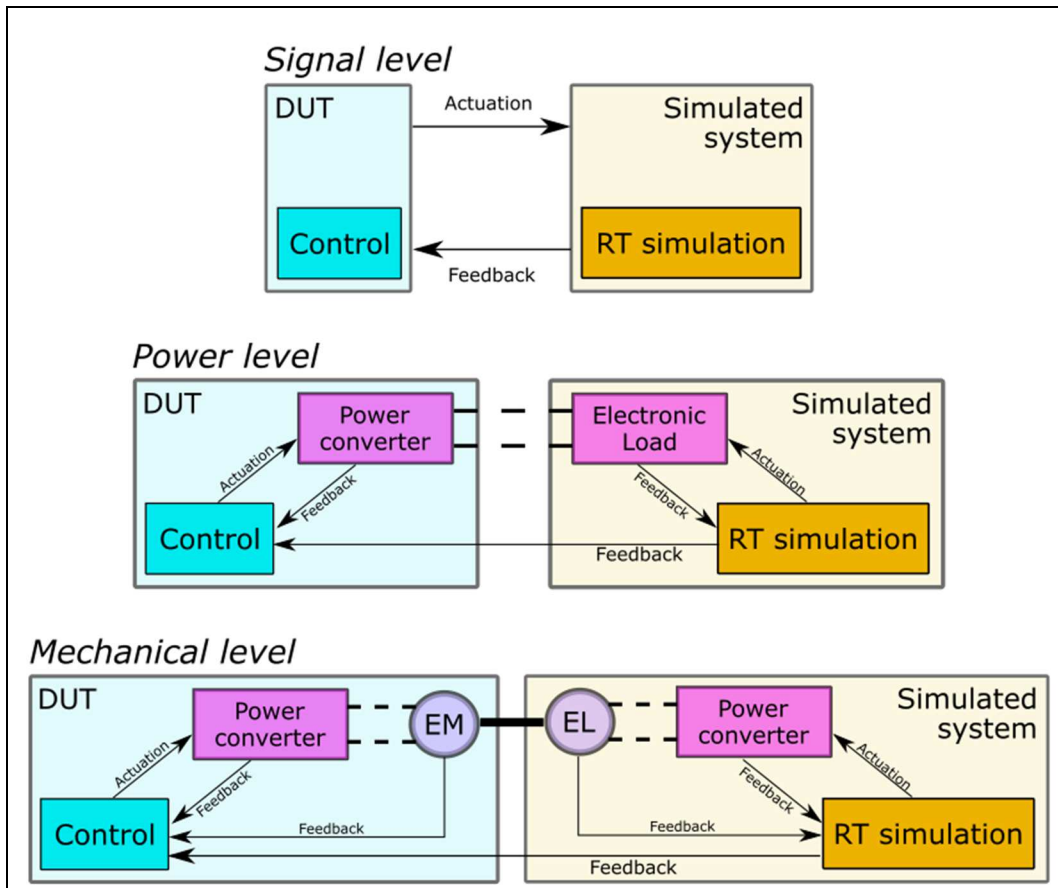


Figure 5.2 Hardware-In-the-Loop simulations

In this chapter, the control strategy for the orchard tractor hybrid was tested on a properly designed test bench for HIL simulation. The goal was to study performance of the control strategy when deployed on real hardware and included on a mechatronic system. The scaled electromechanical hardware was of the same type than other systems developed by the research group in previous work [5.1][5.27]. Thus, the controller would experience the same feedbacks of a real electric powertrain. In the following sections the HIL bench will be described in its hardware and software aspects.

5.1.1 Electro-mechanical layout

The HIL bench developed in this activity was meant to replicate a scaled version of a hybrid electric orchard tractor powertrain with a parallel configuration. As shown in Figure 5.3 and Figure 5.4, the mechanical layout consisted of three permanent magnets synchronous machines: two of them were actuated as electric motors (ICE, EM) the third one instead as an electric generator (Eg or Load). ICE and EM were connected by mean of an electromagnetic clutch which allowed to easily couple and decouple the first two electric machines. The adoption of the clutch was mainly considered to allow HIL simulations of full electric configurations where just one of the two electric motors is required. Moreover, in-opera transitions between full electric and hybrid mode can be tested with this configuration. However, for the purpose of the analysis of this work the clutch was used mainly in its engaged state. Between the power unit (ICE+EM) and the Load simulator a torque transducer was placed to measure the instantaneous torque. EM, the sensor and the Load were connected with a pair of helical “flexible” couplings to compensate for small misalignment in the overall layout. Three custom brackets were designed to support the electric machines and constraint them to the working bench by mean of several M5 screws (not shown in the pictures).

The electro-mechanical system was powered by a low voltage lithium-ion battery pack (40 V) to prevent any possible accidental electric shock. In the proposed layout, the generator acted as a mechanical load applied to the two motors. Part of the subtracted energy was sent back to the battery pack which powered the system, while the remaining part was dissipated into heat. In this way also the overall power consumption of the bench was optimized. Each electric motor was actuated by a Power Converter Unit (PCU) which was in charge of converting the electric energy available on the Dc Bus into a three-phase sinusoidal current and actuating in torque or speed controlled mode the electric machines. The PCUs were all bidirectional, allowing for energy flow from and to the battery pack. Thus, also regenerative braking from one of the two electric motors can be simulated as well.

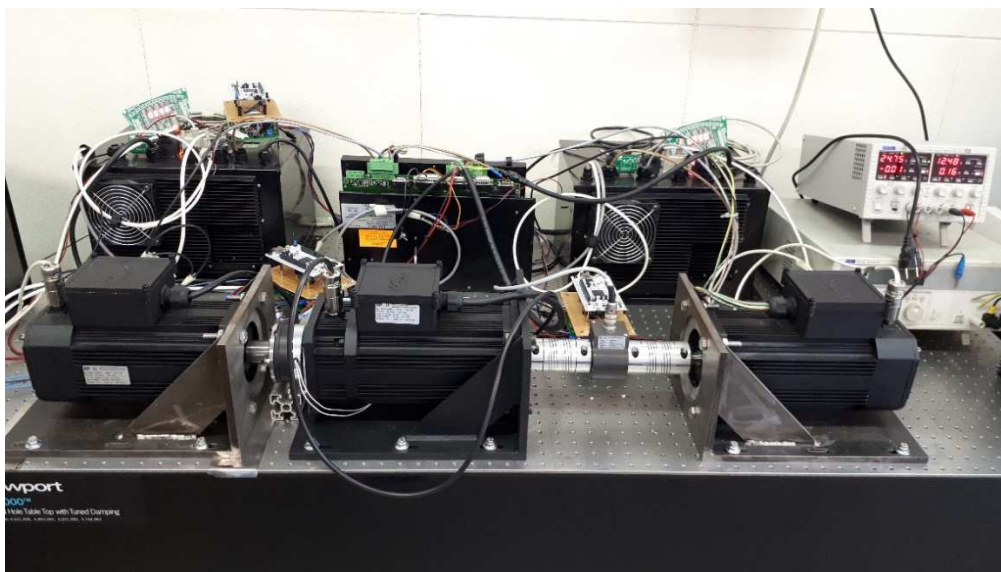


Figure 5.3 HIL Bench

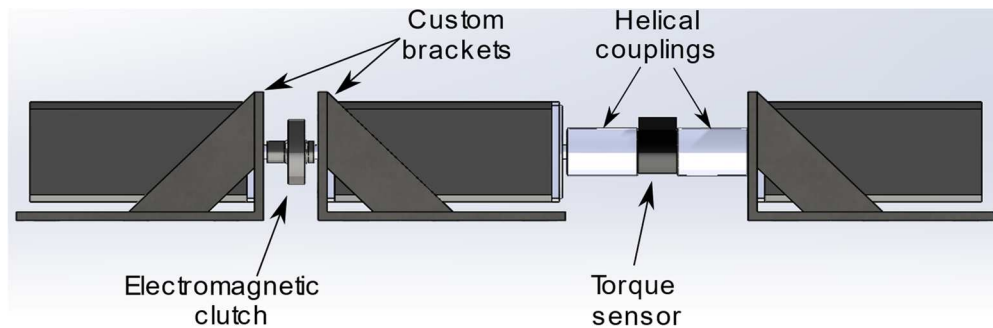
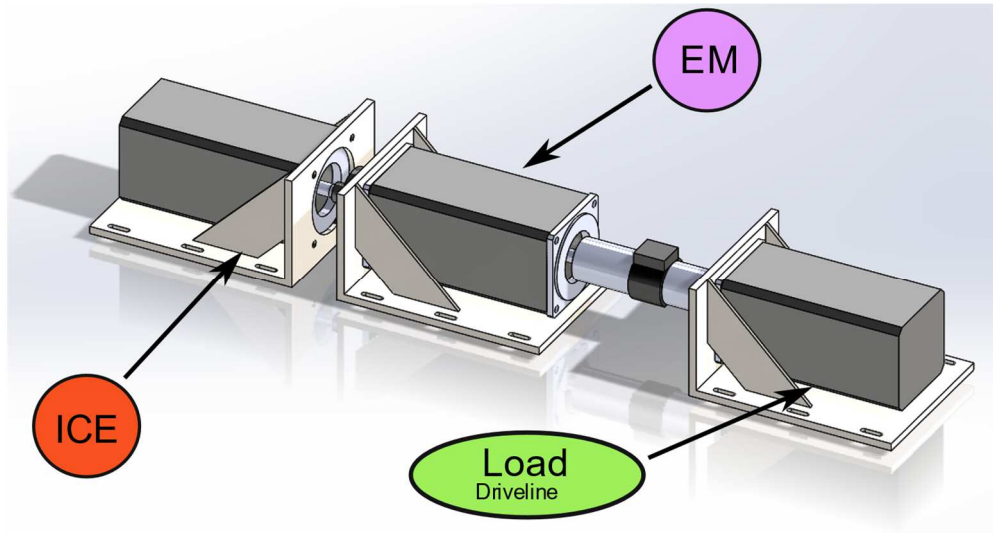


Figure 5.4 HIL Bench: mechanical couplings

In Table 5.1 the main characteristics of the electric machines are reported. The machine simulating the driveline load was manufactured to produce higher torque at the bench nominal speed. In this way several working scenarios could be covered by the same device. About the nominal speed and the Back ElectroMotive Force (BEMF) of these machines, its peak value ($V_{peak} \approx 1.41 BEMF_{VRMS}$) was slightly higher of the voltage Dc-Bus (45 V vs 40V). This meant a real maximum speed of 730 rpm, high enough for the scaled speed range used in the testing activity.

Property	Em ₁ (ICE)	Em ₂ (EM)	Eg (Load)
Nominal speed (rpm)	800	800	1000
BEMF @ Nominal speed (Vrms)	32	32	32
Nominal Torque (Nm)	12	12	17
Nominal Current (Arms)	17	17	32
Peak Torque (Nm)	24	24	34
Peak Current (Arms)	34	34	64

Table 5.1 Electric machines characteristics

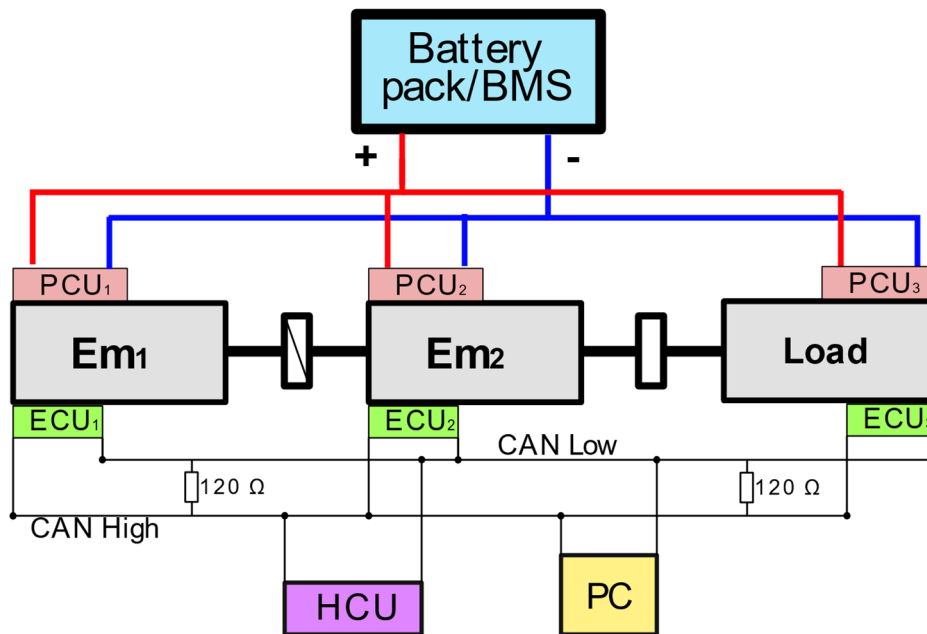


Figure 5.5 HIL Bench Layout

5.1.2 Control architecture and CAN BUS implementation

In Figure 5.5, the overall HIL bench layout is shown. Each electrical machine was actuated by an inverter which took or gave back power to the “high voltage” line connected to the battery pack. Each inverter was controlled by a custom designed Electronic Controller Unit (ECU) like the one shown in Figure 5.6. The board consisted of a digital and an analogue section connected to exchange signals and data. The analogue section was designed to accomplish the following tasks:

- *Acquisition and conditioning* of feedback measurements from the system, in particular the actual motor speed read by the PCU and the supplied motor current
- *Conditioning and amplification* of the control signal given in output by the Microcontroller of the digital section to provide useful analogue signals for the PCU
- *Manual control* by mean of an analogue rotary potentiometer for set up operations
- *CAN BUS interface* to properly connect the CAN BUS controller of the control board to the CAN BUS network of the bench.

The digital section mainly consisted of a Microcontroller Development Board from St-Microelectronics (mod. NUCLEO F767ZI). This board provided access to the powerful STM32-F767ZI microcontroller with the 32-bit ARM Cortex M7 architecture running at a maximum frequency of 216 MHz. Apart from the high computational capabilities provided by this development board (thanks also to the dedicated floating-point unit FPU), it was chosen for some peripherals features that

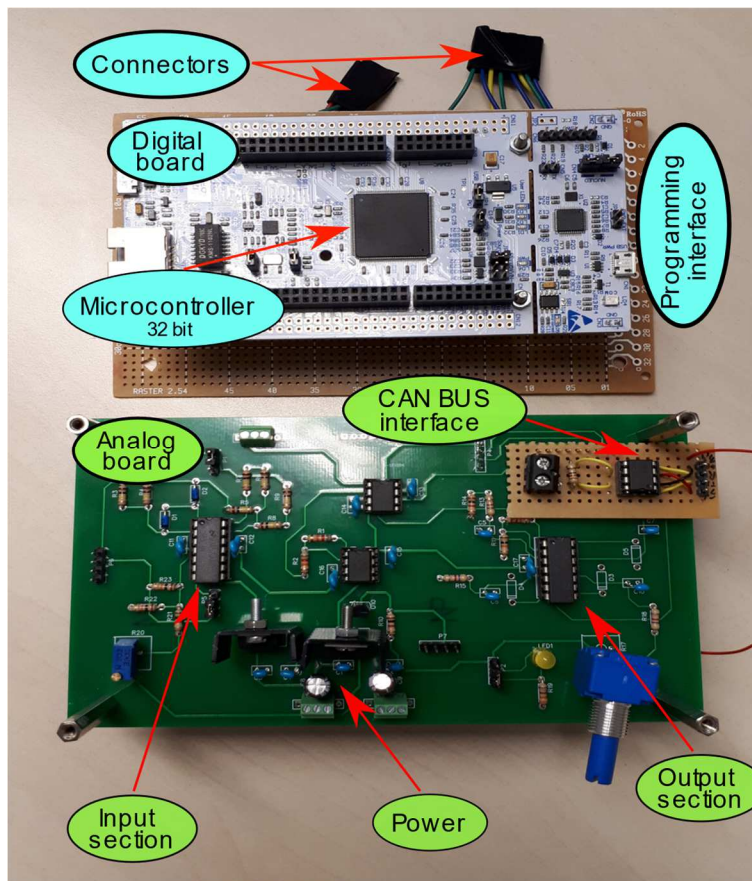


Figure 5.6 ECU custom board: digital and analogue sections

well suited this project. Among them, it is worth to mention:

- 3 x 12-bit Analog-to-Digital Converters (ADCs) able to provide up to 2.4 Mega Samples Per Seconds (MSPS), on a total of 24 channels (3ADCs x 8channels)
- A Direct Memory Access (DMA) controller with up to 16, CPU independent, streams to memory blocks
- Up to 13 x 16-bit timers
- 3 CAN Bus communication interfaces

The 12-bit ADCs were required by the application due to the limited range of the feedback analogue signals provided by the PCUs. Other common development boards available on the market provide 10-bit ADCs, with an overall resolution of 3.2 mV if a 3.3 V supply is considered. In this case, the 12-bit ADC allowed for a higher resolution of 0.8 mV ($\approx \frac{3.3 \text{ V}}{4096 \text{ bit}}$) which was more appropriate to the 0-1V range of the analogue signals from the PCUs for the specific scaled application. Thanks to the DMA, data acquisition was essentially organized as a continuous stream of ADC values directly to the programmed memory position without affecting the CPU workload. This approach is particularly useful in deterministic algorithm (see below) to help the CPU meeting the time constraints of the application. Among the available timers, two of them were used:

- A timer with an updating frequency of 1 kHz, mainly used for the main system application timing management
- A timer with an updating frequency of 10 kHz as main source for the PWM control signal.

The slower timer was used to count precisely 1 ms of elapsed time. This time unit was then used to temporize the main loop of the application. Every time the timer fired up, a counter was incremented by one unit. Whenever the counter reached the value of 10, the main application could start. It is worth to mention that this timing strategy can be applied only if the main application is guaranteed to last less than 10 ms. Otherwise, more complex scheduling strategies should be considered to meet timing requirements. The second timer was used to generate a Pulse Width Modulation (PWM) signal (Figure 5.7). The PWM cycle timer was set to fire every 0.1 ms (10 kHz). Within this time interval, 100 divisions allowed to modulate the duty cycle (T_{on}/T_{off}) of the PWM signal. This modulation technique allowed to describe the slower, time variant control signal (with a period of 10 ms) just using a train of pulsed signals.

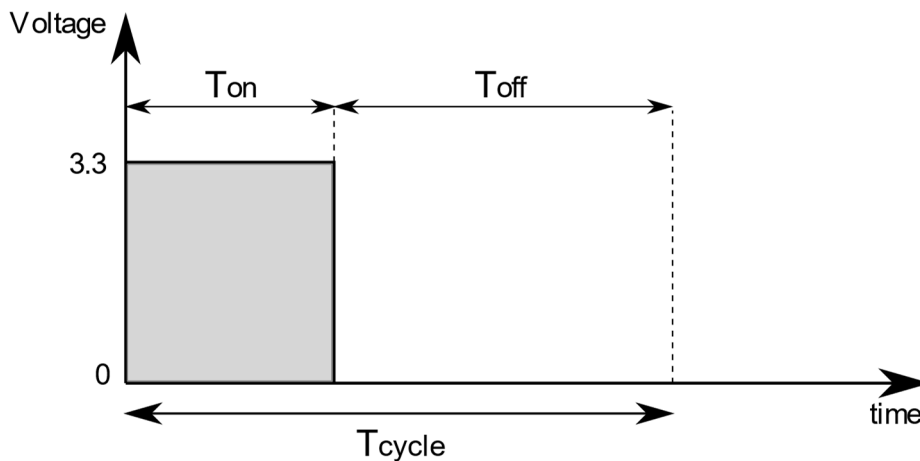


Figure 5.7 PWM control signal

To smooth the control signal a low pass filter on the analogue board was implemented by mean of an RC stage like the one shown in Figure 5.8. For given values of the resistance (R in Ω) and the capacitance (C in F), the cut-off frequency of the low pass filter can be evaluated as

$$f_{cut-off} = \frac{1}{2\pi RC} \quad Hz \quad (5.1)$$

Thus for $f_{cut-off} = 330 \text{ Hz}$, lower enough compared to the control signal period of 10 ms, and a capacitance of 100 nF a resistance of 4.8 k Ω was obtained. A commercial resistor of 4.7 k Ω was considered for a final $f_{cut-off} \approx 340 \text{ Hz}$.

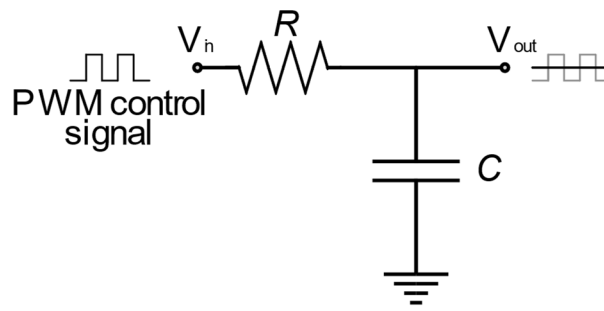


Figure 5.8 RC low pass filter of the control signal

Finally, the CAN BUS controller of the STM32-F767ZI allowed the development of a communication protocol between the different components of the bench. Since the PCUs didn't have a CAN communication interface, the custom ECU added this capability to each unit. As explained in the previous chapters, the CAN BUS is a low-level communication protocol which uses a pair of twisted wires to transmit messages between nodes on the same network at a maximum speed of 1 Mbit/s. In the specific case of the developed HIL bench, each node of the network shown in Figure 5.5 required custom firmware development, thus a custom high-level communication protocol was designed. Thanks to the experience gained on the SAE J1939 standard during the experimental campaign on the orchard tractor, the custom CAN BUS protocol was structured according to the specification of this standard. Thus, a BaudRate of 250 kbit/s was considered together with the 29-bit extended format for the message identifier. Then, a set of message structures were identified to be sure to share all the relevant information on the network. In Table 5.2 - Table 5.3, the main messages and related data fields are reported. Due to the central role of the CAN BUS communication on this HIL bench, each ECU firmware was designed with a clear workflow in mind which can be summarized in the following points:

- Reading control messages from the CAN BUS network, giving at each data field the correct meaning
- Given the reference signal, elaborating numerically the proper control signal according to the feedback measurements from the PCU
- Sending the PWM control signal to the PCU
- Sending on the CAN BUS network a monitoring message with the main information about the actual condition of the specific unit.

Property	Bytes	Range	Status
Actual Engine Load (%)	1	[-100, +100]	-
Engine speed (rpm)	2	[0,800]	-
Control mode	2 bits	-	- Speed - Torque

**Table 5.2 Monitoring message structure
(According to J1939 standard definitions)**

Property	Bytes	Range	Status
Speed reference (rpm)	2	[0,800]	-
Torque reference	1	[-100, +100]	-
Control mode	2 bits	-	- Speed - Torque

**Table 5.3 Control message structure
(According to J1939 standard definitions)**

As in real vehicles, the speed reference was evaluated according to two possible inputs: a potentiometer manually actuated (as the vehicle pedal by the driver) directly read by the Hybrid Control Unit (HCU); a message sent over the CAN BUS by a more advanced potentiometer with an on-board CAN Controller able to send the same numerical information according to the specific standard of the network. To automate the testing procedure and include the driver input in the simulation environment, a frame with [0,100] % data field value was sent by the PC connected to the CAN BUS network by mean of an active CAN analyser (the same discussed in chapter 4). This message simulated an active potentiometer actuated by the driver according to the desired working speed. It is worth to mention that these systems with their basic monitoring software are usually able to send static messages over the network (periodic messages but with the same data fields). To overcome this limitation a specific software was developed to talk to the physical hardware and send time dependent data. To meet the strict timing requirements of the control messages (10 ms) which would had affected the control loops involved on the bench, the C software was developed on a Linux based Operating System (OS). In this OS, the effective task scheduling allowed to meet the desired timing requirements. Moreover, the Linux Kernel comes with an interface (a Socket) to talk to CAN BUS hardware like the CAN analyser. Through this socket the communication was handled in the same way as it is usually possible to talk to other standard peripherals in a personal computer (like the ethernet hardware). With the same approach, also the control signal for the electric Load was sent by the Linux machine. Reading the actual ICE and EM load from the CAN BUS, the software evaluated the correct Torque to be applied to simulate the working operations of the tractor (derived from the experimental tests and given in terms of percentage engine load at given speed). In this way the determination of the input signal of the system and the external working conditions became something on which the control boards were not involved in, but which affected their behaviour. According to the HIL definitions given in the previous sections, this HIL simulation set up was at mechanical level since all the main components involved on the final powertrain were included in the simulation environment (although in scaled versions in terms of power output). This setup allowed to test the control algorithm behaviour having feedbacks from physical hardware which could be used on a real prototype of the proposed architecture.

Since the main function of the control board was programmed to run every 10 ms, monitoring messages were sent back on the network with the same frequency

by each ECU. This could create a conflict on the CAN BUS network. However, message arbitration [5.1][5.28] - [5.1][5.31] defined in the CAN BUS protocol, prevented at hardware level this from happening. The priority of a message is defined by the first bits within the message identifier itself. Usually, control messages have the highest priorities, while monitoring messages the lowest and in this case, the same approach was adopted on the custom protocol.

The ECUs firmware were developed to allow two control modes: Speed and Torque control. The control signal that each ECU sent to its paired PCU defined the maximum current allowed to and from the electric machine, thus the mechanical torque that could be provided. The Torque control mode defined in the ECU firmware was in charge of translating the numerical information read from the CAN BUS with the proper control message into a physical signal for the PCU. The value +/- 100 % of the torque reference was split into two information: the desired torque and the direction of application. The first parameter was used to modulate the PWM signal duty cycle. The second one, to switch on the analogue board between the stages able to provide positive or negative signals (+/-10 V) for the PCU. Regarding the speed control mode, used on the ICE simulator, it consisted of a PI control loop which compared the CAN BUS reference speed and the actual motor speed provided by the PCU. Although the possibility to actuate positive and negative torque (as explained above) the ICE speed control loop was designed to provide only positive torque, as on real off-road vehicles' engines. To design the PI controller a numerical model of the plant at its full load was developed. Starting from experimental measurements of a step response in full load condition (Full torque from standstill), a second order transfer function (5.2) with delay was identified as appropriate model for the system.

$$H(s) = \frac{K}{(T_1s + 1)(T_2s + 1)} e^{-\tau s} \quad (5.2)$$

Parameter	Value
K	575
T ₁	0.0756
T ₂	0.0755
τ	0.121

Table 5.4 Plant model parameters

Using the parameter estimation toolbox provided by the Matlab/Simulink environment, the plant parameters were estimated. Results are reported in Table 5.4. The Plant transfer function was then used to tune the ICE PI speed control loop in the numerical environment. In Figure 5.9, results of the PI controller tuning in the numerical model are shown and compared to the actual performance of the same parameters implemented on the PI controller of the ECU. Results were considered good enough for the slow dynamic of the real engine speed controller. However, since the numerical model of the plant and the PI tuning were performed in a full load condition, two identical tests with the same speed reference but lower loads were performed (Figure 5.10). The real system experienced overshoots during these

tests, but the controller was able to quickly recover from these conditions without any sign of instability. The PI controller set up was thus considered accomplished.

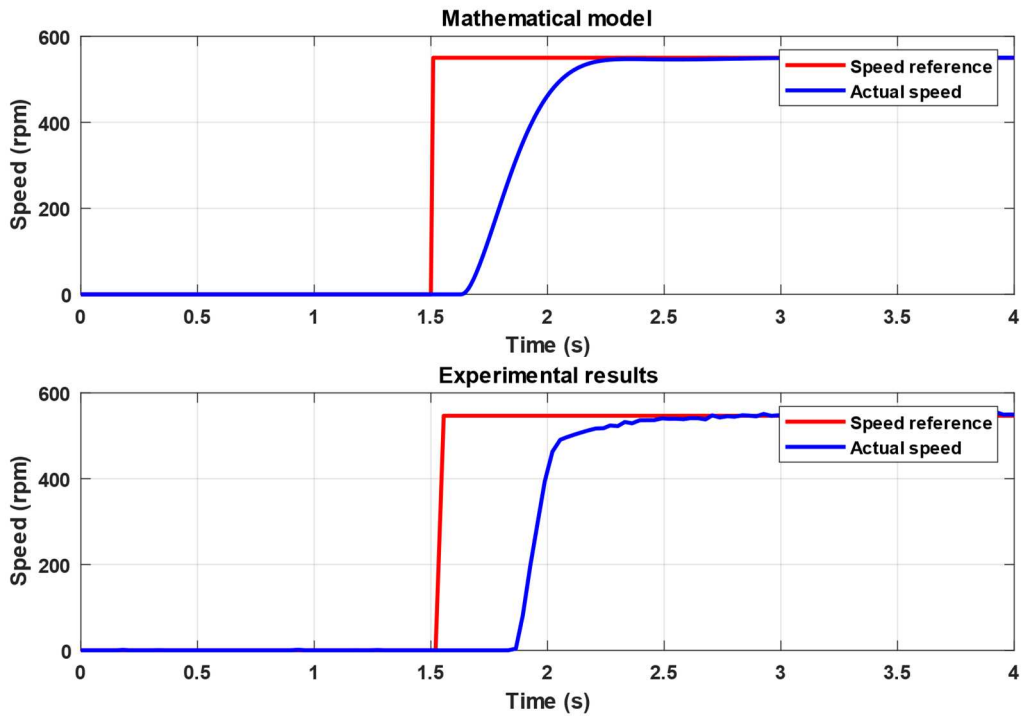


Figure 5.9 PI speed controller response of the ICE electric drive (full load)

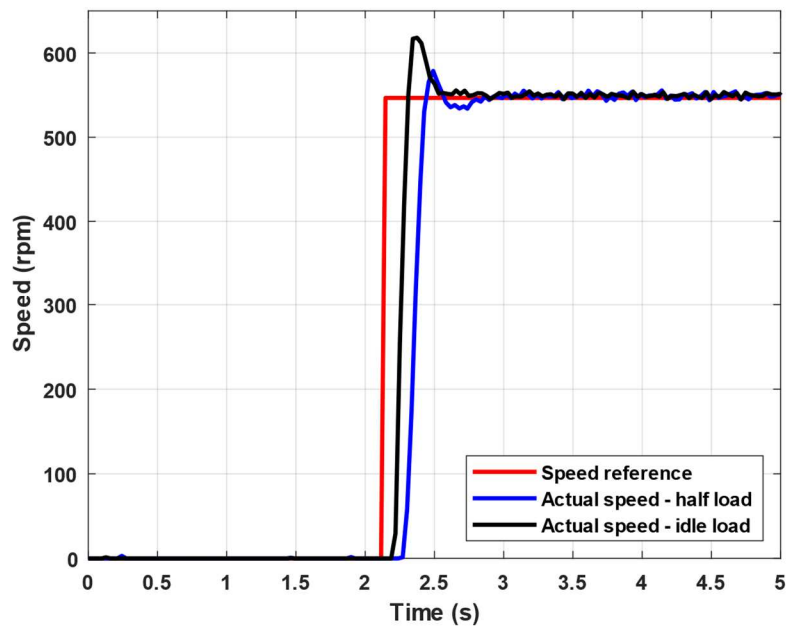


Figure 5.10 PI speed controller response of the ICE electric drive (medium and low load)

5.2 The Hybrid Control Unit

On modern vehicles, ECUs are in charge of controlling different parts and aspects of the system and/or coordinating a certain number of subsystems (nodes) connected on the same communication network. Nowadays, also on the simplest vehicle possible, at least one ECU is used to control the internal combustion engine and some basic vehicle functions. Moving to more complex systems it is common to find a network of control units where each node is in charge of controlling/actuating one particular subsystem. In these cases, especially on off-road vehicles, a centralized (usually proprietary) controller oversees the management of the entire system. In this case is common to address this control unit as the Vehicle Control Unit (or VCU). This embedded system is usually the most powerful controller in the network because of the number of physical interfaces he must manage and of the system level control strategies that must be performed. All the driver inputs are processed by this unit as well as the vehicle level functions (lights switching on-off, indicators and gauges on the vehicle dashboards) and diagnostics. This centralized unit allows for better division of tasks. Critical systems like the ABS or the traction control must not be overloaded with not safety related tasks. Moreover, this approach allows manufacturers to use off the shelf solutions for these critical functions, developed by specialized companies. The centralized approach, with a VCU acting as a “supervisor” of the overall system is more and more relevant when hybrid units are considered. As already discussed, in a hybrid architecture the electric subsystem requires its own control units. If the hybrid architecture proposed for the orchard tractor is considered, at least the following control units can be expected:

- A control unit to manage the power converter of the electric machine
- According to the battery pack layout, at least one BMS for each battery module and in some cases one master unit which managed the lower level controllers.
- A control unit for charging management.

The higher architecture complexity, the higher the number of additional control unit required. Other electric machines would require other control units to interface the PCUs to the vehicle network. If other mechanical devices must be integrated in the vehicle architecture, additional controllers may be required. In such a complex scenario, the benefits of a centralized vehicle controller known in this case as Hybrid Control Unit (HCU) are clear. Each subsystem would be developed independently but already prepared for vehicle integration and to receive actuation commands by a system supervisor. On the HCU the best energy or performance management strategies would be implemented to best fit the driver working requests to the actual working condition.

The HIL bench developed provided a good simulation and testing environment for the HCU. Its main role was to read the driver input signals (the commands sent over the CAN BUS network by the PC which simulated the driver) to interpret them

and send the correct commands to the ICE and the EM unit. On the HCU the control strategy developed and simulated in chapter 4 (Figure 5.11), was implemented to test the behaviour on physical hardware. The control strategy considered the ICE as the Master node of the mechanical driveline and EM as a slave unit. Depending on the working conditions, if the engine could not handle the applied load the electric unit was able to provide a power boost using the electric energy stored in the battery pack. The engine speed reference and the actual one were elaborated by the HCU in a speed control loop. The output was then fed into the Load observer block where a polynomial function weighted it according to the actual engine load before giving in output the torque reference for the EM. The bench was designed to prove the feasibility of the control strategy in the case of a downsized engine as simulated in the previous chapter. The Load observer was mandatory to minimize the amount of energy taken from the electric system. The ICE must remain the main energy source because of the limited amount of electric energy available during working operations.

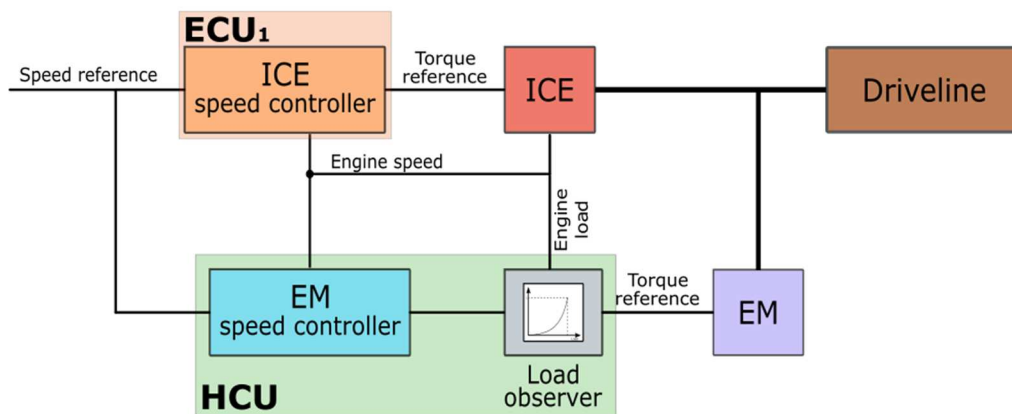


Figure 5.11 Master-slave control strategy with engine Load observer

Another important feature managed by the HCU was the engagement or disengagement of the electromagnetic clutch. A feature not really involved for the study reported on this chapter but already available for further testing activities.

5.2.1 Development and hardware implementation of the control algorithm

The control strategy was developed on an HCU from the manufacture ECOTRONS (Figure 5.12). It was a control unit based on the NXP MPC5744 microcontroller, provided with several features required in automotive and industrial applications. The main ones were:

- A 12/24 V supply voltage to cover the most common low voltage systems available today
- 15 x 12bit analogue input channels for sensors acquisition

- 17 digital output channels
- 28 channels to drive small and medium loads as the several auxiliaries on the vehicle
- -40 - +85 °C temperature range and a protection grade IP67 for the harshest environments
- 3 independent CAN BUS lines
- A preloaded Bootloader with the possibility to program the microprocessor through the CCP and XCP protocol.



Figure 5.12 Hybrid Control Unit

One of the reasons that suggested the use of this unit was the specific toolchain required to develop the software for the control board. Together with the hardware platform, the manufacturer provided also a Matlab/Simulink library to develop the software application on this environment and then generate the binary code to be flashed on their hardware through a dedicated software. This allowed to use the control algorithm developed for the simulations in chapter 4. The software architecture shown in Figure 5.13 consisted of six main sections:

- *Definition of the actual target hardware.* This section allowed the code generator to map the software functions to the specific peripherals of the hardware.

- CAN BUS setup. In this section all the relevant information regarding the configuration of the three CAN BUS lines were defined. In the specific case the CAN_B and CAN_C line were effectively involved. The CAN_B line was the one connected to the bench CAN BUS network to communicate the HCU control messages. The CAN_C line was the CAN BUS line used as the calibration/debug and programming line. For the two CAN BUS channels different protocols were considered. For the CAN_B line a specific structure in a Matlab file was defined with the main data fields of the control and monitoring messages the HCU was involved in. Similarly to the most widely used .dbc files for CAN BUS messages definitions, this file contained the correct map of each bit of the 8 data fields (8 bytes) expected by the J1939 protocol. In this way, the numerical value of the input and output signals could be provided in a more useful decimal format. The CAN BUS read/write functions used the Matlab file defined before to translate these values into suitable data fields for the CAN BUS network.
- Power management settings. This section allowed to define some settings for the wake up functions of the HCU. There were two main ways to wake the control unit:
 - Using the dashboard KEY signal as in most of the ECU for vehicle applications. This mode was the most adopted during the tests.
 - Using the CAN BUS line, waking up the HCU if any message is received by the CAN BUS controller.
- Non Volatile Memory (NVM). In this section it was possible to define critical parameters or other information which would not be lost at each KEY cycle. The main information stored permanently were related to variable types definitions and to parameters of the main application which were not object of any calibration.
- Calibration parameters. In this section, calibration parameters were defined. At the design stage, some data fields were addressed as relevant in determining the overall response of the control loop and that would have required some adjustment after being flashed on the HCU memory. The definition of calibration parameters is a common practice also in industrial applications because memory chips of these control units have a limited amount of writing cycles. Frequent uploads of the software which requires a complete erase of the memory slots dedicate for the software application deployment, would reduce drastically the total life of the hardware itself. Thus, the definition of calibration parameters is a good practice if the structure of the software is well defined and just changes of the overall response must be addressed.
- Application software. This was the section where the main application was contained. A Real-Time OS included during the code generation, scheduled the different part of the application depending on timing constraints and dependency from other signals

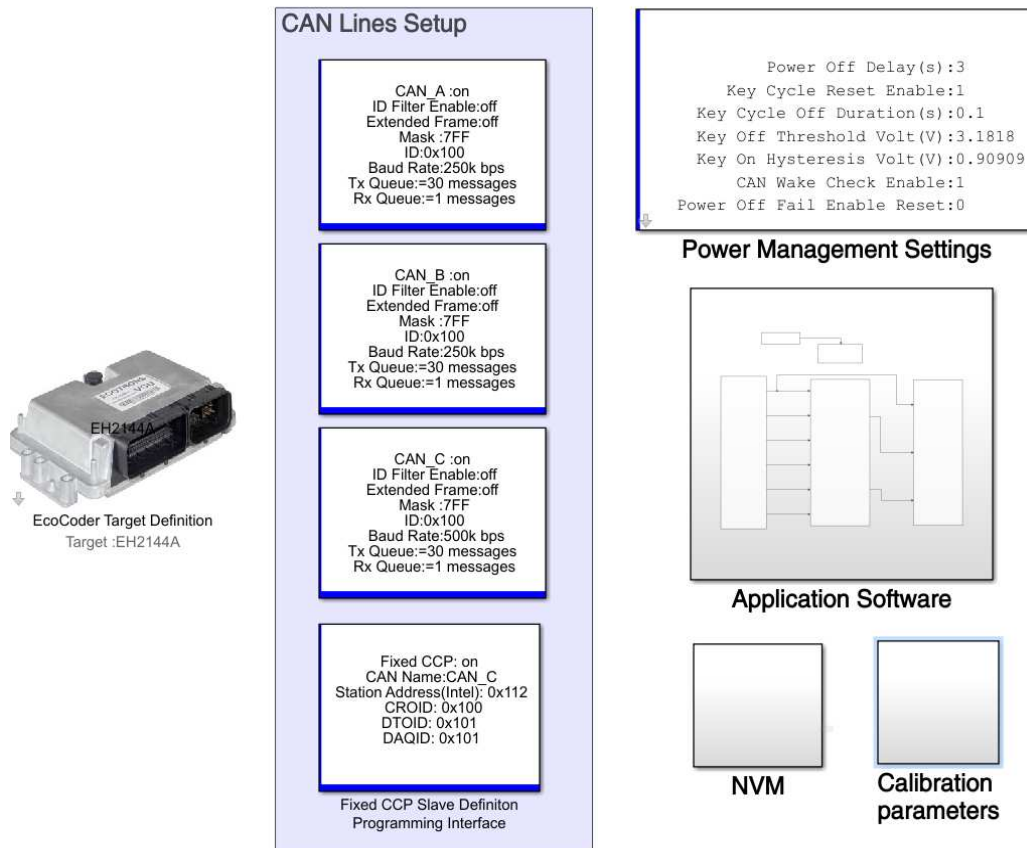


Figure 5.13 HCU software architecture

The Application software (Figure 5.14) was developed with a linear flow architecture. The *Input signals* section was in charge of collecting the relevant signals for the application acquiring both analogue and digital signals as well as CAN BUS parameters according to the specific messages structure file defined before. These signals were then passed to a *Processing* section where the main control algorithm was developed as well as other auxiliary functions. The processed signals determined two main outputs: the ICE speed reference and the EM torque reference. These signals were then processed inside the Output signals block to be transmitted over the CAN BUS network. Also the clutch digital signal read from the dedicated physical switch was used in this last section to engage or disengage the electromagnetic clutch.

The HCU *Processing* function was developed as shown in Figure 5.15. As already discussed, it consisted of a speed controller in charge of determining an actuation command according to the error between the ICE speed reference and the actual ICE speed. At the same time, the actual engine load was used to determine a weight factor for the *PI_Controller* actuation command. To smooth the observer response, the engine load value was filtered using a moving average window of 5 data points with a similar effect compared to a low pass filter. The combination of the *PI_Controller* and *Load Observer* output gave the actuation command of the EM. The final EM torque reference was established in the mode selection block. The clutch signal was interpreted by the processing unit as a driver request for the

Full electric mode. Thus, if that signal was High, the electromagnetic clutch was disengaged, and the reference torque read in the input signals section (from the CAN BUS or from the Pedal) was used instead of the actuation command from the *PI_Controller*.

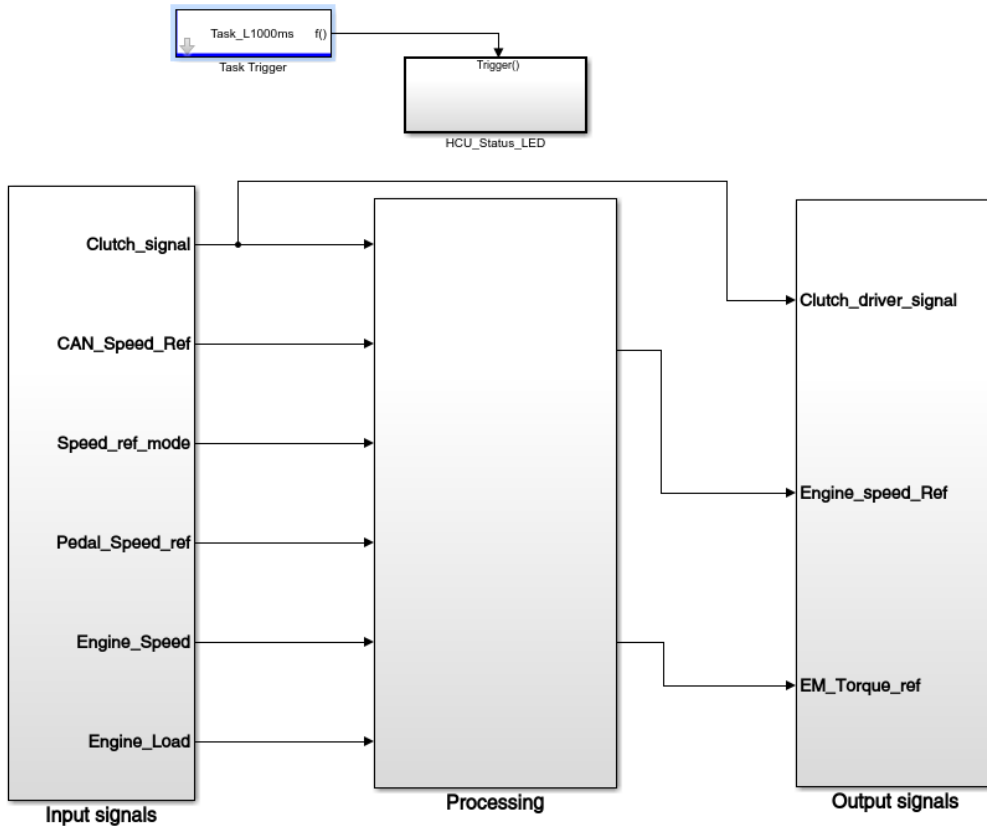


Figure 5.14 HCU Application architecture

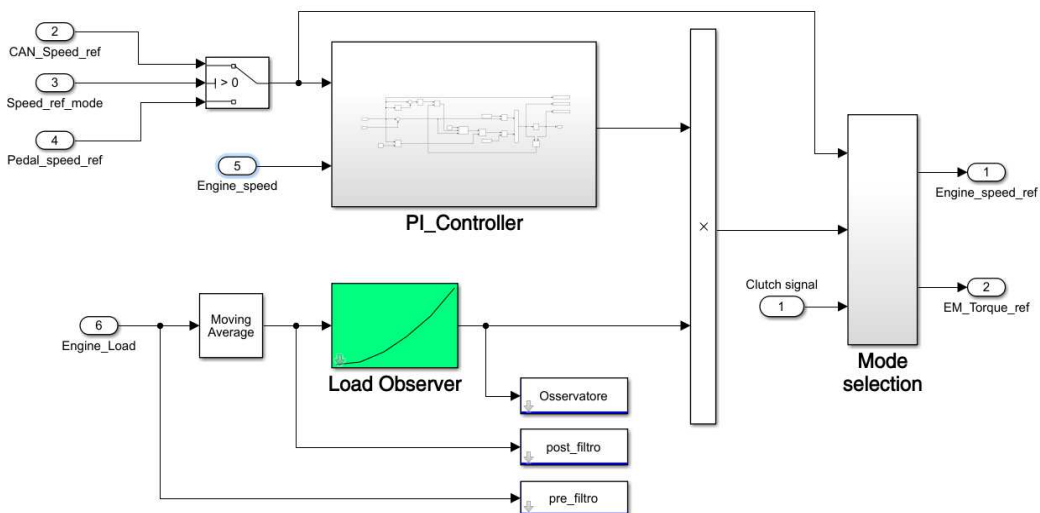


Figure 5.15 HCU Processing function

5.3 Experimental tests

Once the software development of the ECUs and of the HCU was concluded, the system was mechanically characterized before the HIL testing activity (discussed in the next section). The main point was to determine the real mechanical performance of the bench to provide the RT system with the correct data to apply accordingly the load and speed profiles of the working case studies. The overall goal of the experimental tests was to prove the feasibility of the hybrid parallel architecture with downsized Diesel engine and its control strategy over a set of real working scenario. Thus, to reproduce the same mechanical behaviour with the set of motors available on the bench the following strategy was adopted:

- The amount of maximum power of the ICE electric machine was limited electronically with a specific setup option on its PCU which defined the maximum motor current (I_{mot}) allowed. This condition was considered equivalent to the 75 kW Diesel engine of the traditional tractor. During simulation tests of the traditional architecture EM was not actuated and left free to spin. Thus, apart from the amount of energy required to rotate the rotor shaft, the power from ICE was primarily absorbed by the Load. The Load PCU was thus set accordingly to match the ICE nominal power output. This setup was kept the same during the hybrid tests in order to apply the same load scenarios to the new configuration.
- For tests of the hybrid configuration, the motor current limit of the ICE's PCU was scaled according to the ratio 54/75 between the nominal power of the downsized Diesel engine and the standard one (as studied in chapter 4). Accordingly, the power limit for EM was set to be 30/75 of the power limit for ICE. During hybrid simulations, the Load took both the power coming from ICE and from EM. However, stated that its power configuration in those set of simulations was the same of the ones done with the standard Diesel engine like setup, the applied load was the same for both the experimental activities.

To be consistent with this testing strategy, the two electric machines (ICE, EM) were characterized according to the applied load. To do that, the faster internal speed control loop of PCUs was used to fix the reference speed at which the maximum load had to be evaluated. In Table 5.5 - **Table 5.7** results of the characterization activity are reported. Tests were performed with the following procedure:

- 1) Fixed the maximum $I_{mot_{ICE}}$ current in its PCU (the maximum current allowed for the ICE motor), the maximum $I_{mot_{Load}}$ was determined in order to have a 100 % brake reference (Brake_ref) when the maximum $I_{mot_{ICE}}$ was reached. In this way the maximum brake torque (100% signal) was coupled to the maximum possible torque from ICE

- 2) For each speed step, the Brake_ref was increased from 0 up to the maximum value which guaranteed the speed control of the PCU to meet the speed requirement within a speed tolerance of 10 rpm.
- 3) At this point the $I_{mot_{ICE}}$, the signal $I_{mot_{ADC,ICE}}$ from ECU₁ and the torque measured by the torque sensor were recorded.

Speed	Brake_Ref [%]	Imot (Arms)	Imot_ADC (bit)	Torque (Nm)
150	100	17	260	7.3
250	100	17	260	7.1
350	100	17	260	7
450	100	17	260	6.9
550	83	15	220	5.9
650	56	10	160	4.4

Table 5.5 ICE mechanical characteristics (75 kW equivalent)

Speed	Brake_Ref [%]	Imot (Arms)	Imot_ADC (bit)	Torque (Nm)
150	74	13	195	5.3
250	71	13	185	5.1
350	69	12	180	5.1
450	64	12	175	4.6
550	58	11	165	4.3
650	49	9	140	3.7

Table 5.6 ICE mechanical characteristics (54 kW equivalent)

Speed	Brake_Ref [%]	Imot (Arms)	Imot_ADC (bit)	Torque (Nm)
150	64	10	165	4.6
250	64	10	158	4.6
350	64	10	155	4.6
450	64	10	152	4.6
550	64	10	145	4.6
650	44	7	102	3.4

Table 5.7 EM mechanical characteristics (30 kW equivalent)

Once the Brake_Ref table was fixed according to the 75 kW equivalent configuration, the ICE_{54kW} and EM were characterized as well with the same approach. The Load PCU set up was no more changed to have the same braking conditions as the first characterization test. One important information acquired during this activity was also the measured motor current read by the ECU ADC. The main reason is that this value was representative of the maximum torque at a specific rotational speed, thus could be used as a map to trace the actual engine load

on each electric machine. Of course, the map for ICE were updated when testing the 75 kW or the 54 kW equivalent systems. It is worth to mention the nonlinear behaviour of the relation $I_{mot}/\text{Torque} - \text{Speed}$. Due to the BEMF induced on the stator coils, the limited DC voltage on the bus prevented higher torque to be available at high rotational speed. A higher DC voltage should guarantee a flatter Speed-Torque relation because the DC Bus could “push” current more easily in the stator coils at the same rotational speed.

5.3.1 HIL tests

The HIL testing activity was organized as two set of simulations where the same loading scenarios were applied to the standard architecture and to the hybrid one to understand if the second was able to perform tasks as well as the first one. Testing scenarios were derived from the experimental data acquired on field from the tractor under test as mentioned in chapter 4. Two input were required for the bench: the engine speed and the brake load. Using equation (5.3) the measured engine speed was linearly mapped from the operating speed range of the Diesel engine (900-2300 rpm) to the operating ICE range (100-650 rpm).

$$Speed_{ref_{ICE}} = \frac{100}{650} \cdot \left(100 + \frac{550 (n_{Diesel} - 900)}{1400} \right) \quad (5.3)$$

The second input for the bench was the Brake actuation signal for the load. In this case, depending if the traditional or hybrid simulation was chosen, a different approach was required. When simulating the traditional architecture at each simulation instant the actual engine load feedback from ICE was read from its CAN BUS monitoring message. Then, the correct torque to be applied was evaluated with a closed control loop which compared the ICE actual engine load with the engine load measured during the experimental activity. This approach, also used in the simulation model described in chapter 4, allowed to replicate some working scenarios like the PTO operations where the lack of information about the internal mechanism of the implement and of the external conditions of the terrain prevented the design of a more detailed numerical model. Since the bench focused the attention on the power unit, the main goal was to be sure that each of the two case studies would had felt the same working condition. During simulations of the hybrid architecture, another approach was used to generate the Brake reference signal. From the ICE engine load (54 kW equivalent) and from the EM actual load (30 kW equivalent), the overall equivalent load of the power unit was evaluated as the sum of the torque applied by each unit, normalized with the torque map registered for the 75 kW equivalent configuration. Although the total power of the hybrid unit was actually higher (84 kW equivalent) the goal was to control the system in such a way that it could cover the performance of standard architecture. Moreover, to optimize the battery usage, the less EM is involved, the smaller the actual battery

pack could be. Speed_ref_{ICE} and Brake_ref values were sent over the CAN BUS network by the Linux PC with a 10 ms period.

Three working scenarios were chosen as case studies from the ones studied in chapter 4: the atomizer test, the shredder test and the rotary harrow test. Their working load presented some specific characteristics where the hybrid architecture and the control strategy performance should be studied. On the Atomizer test, the high mean power request could drain the on-board battery too quickly if the Diesel engine is not properly involved as primary source of energy because of unnecessary contributions of the electric motor. On the other hand, on the Shredder test, where the mean power is relatively low, the action of the electric motor should be as low as possible (always for battery optimization). Finally, on the Rotary Harrow tests peak performance capabilities of the hybrid system can be evaluated with engine load values close 95% (traditional architecture) in some working point.

The three working scenarios were tested in both configurations: traditional architecture (Diesel 75 kW) and hybrid parallel (Diesel 54 kW + Electric Motor 30 kW). The input data for the HIL bench were always the ICE speed and the brake actuation command. In Figure 5.16 - Figure **5.18**, results of the HIL simulation of the traditional architecture are shown. This set of tests was performed to evaluate how the brake command matched with the ICE performance. Since the system was speed controlled, and far from saturated conditions, the ICE was always able to cover the applied brake torque. Apart from the small delay between the actuation command of the brake and actual ICE load, test results showed a good match between these two quantities. Thus, the input data were also given to the hybrid parallel configuration to study how the system would had behaved to the same applied load. Due to the physical limitations of the real system, the Load observer was tested with a quadratic weighting function. Higher polynomial degrees would optimize battery consumption. However, these functions showed poor system response, thus the quadratic one was chosen as best trade-off between performance and energy consumption. In Figure 5.19 - Figure **5.21** results of the HIL simulation are reported. In these tests, studying performance of the control algorithm deployed on the HCU was the main goal. In the Atomizer test, the power request was split between the two power sources with ICE at 75% and EM at 25% of their maximum capabilities. This meant that the primary source of power for this demanding task would be the ICE with a partial contribution from the electric motor. This result was mainly related to the specific Load observer curve used. A higher order of the polynomial function would had increased the ICE Load, leading to a lower percentage of the energy taken from the battery pack. However, the Load observer curve must be designed also considering the overall performance of the system. In a real tractor, and more in general for off-road industrial vehicles, Diesel engines are designed to withstand continuous working loads around 70-80%. Although higher loads are possible due to the power reservoir of the engine, continuous full load operations would certainly reduce the total mechanical life span of the engine (considering wear, bearings life, sealing components and others). Thus, the best trade-off between engine performance and stored energy must be found. However,

if the Diesel engine is specifically designed for this type of working scenario, higher continuous engine load operations could be considered.

The Shredder test was the lower demanding test due to an overall average engine load of the traditional engine of 50 %. Since the engine of the hybrid architecture has a nominal power equal to the 72 % of the traditional one, it had the capability to satisfy the load with a very low contribution from EM (around 15% of its maximum capability). Also in this case, a Load observer curve specifically designed for the real machine could reduce this quantity. Results coming from this test (also from the simulated one) can suggest to specifically calibrate the Load observer curve of the real tractor according to the specific working cycle. Depending on the tasks the user should accomplish, several Load observer curves could be defined in order to prefer a lower electric energy consumption or a higher power boost (ECO - BOOST). These curves could be tested in HIL benches like the one developed in this work to study the stability of the system with the different curves. Finally, the Rotary Harrow test helped in understanding system and control performance during high power working conditions. Since both the machines were below their saturation conditions thanks to their joint work, the speed reference was well followed although the heavy applied load. This load required high involvement of the Diesel engine with peak engine load around 95%. However, the continuous operating load was mainly between 85-90%. As mentioned before, this working condition is very demanding from the mechanical point of view. Thus, a more aggressive load observer curve chosen by the user could provide a higher power contribution lowering the ICE load. Of course, this would require a proper design of the electric energy reservoir in order to complete the working cycle.

The Master-slave configuration of the proposed architecture with a Load observer control algorithm showed good stability in all the proposed tests, crucial requirement for real machines. The electric system followed the speed control of the ICE with a weighted speed control loop running on the HCU. The weighting function for EM showed good peak power capabilities but could unnecessarily drain the battery pack energy. Thus, several modes of operation should be provided to the user in order to let him choose the most suitable configuration for the specific task. Also, the possibility to completely exclude the electric system should be considered. If the tasks are not particularly power demanding, the user could prefer to use the main engine as the only power source. This could be the case for most of the shredding activities as well as for the main road operations which do not involve highly loaded trailers. The smaller engine could easily accomplish the task in a more efficient way (higher mean load compared to the traditional Diesel), thus with lower fuel consumption and pollutant emissions. Similarly, some small tasks can be accomplished by the electric system if a proper clutch (in the bench the electromagnetic one was adopted, but every electronically actuated clutch can fit as well) disengage the Electric motor from the Diesel engine. This was the reason why the electric motor was sized for 30kW although in hybrid conditions its involvement could be way lower. The limiting factor to the type of possible full electric operations would be the installed battery pack since the HCU could easily be programmed drive the electric unit both in speed and in torque.

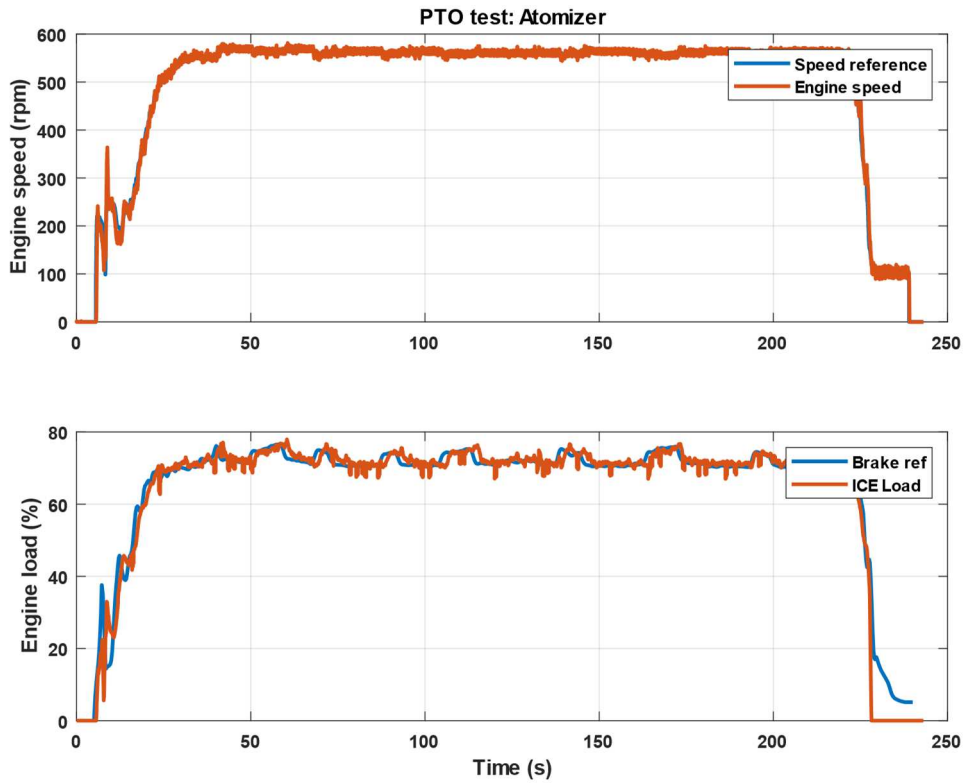


Figure 5.16 Atomizer test – Diesel 75 kW (equivalent)

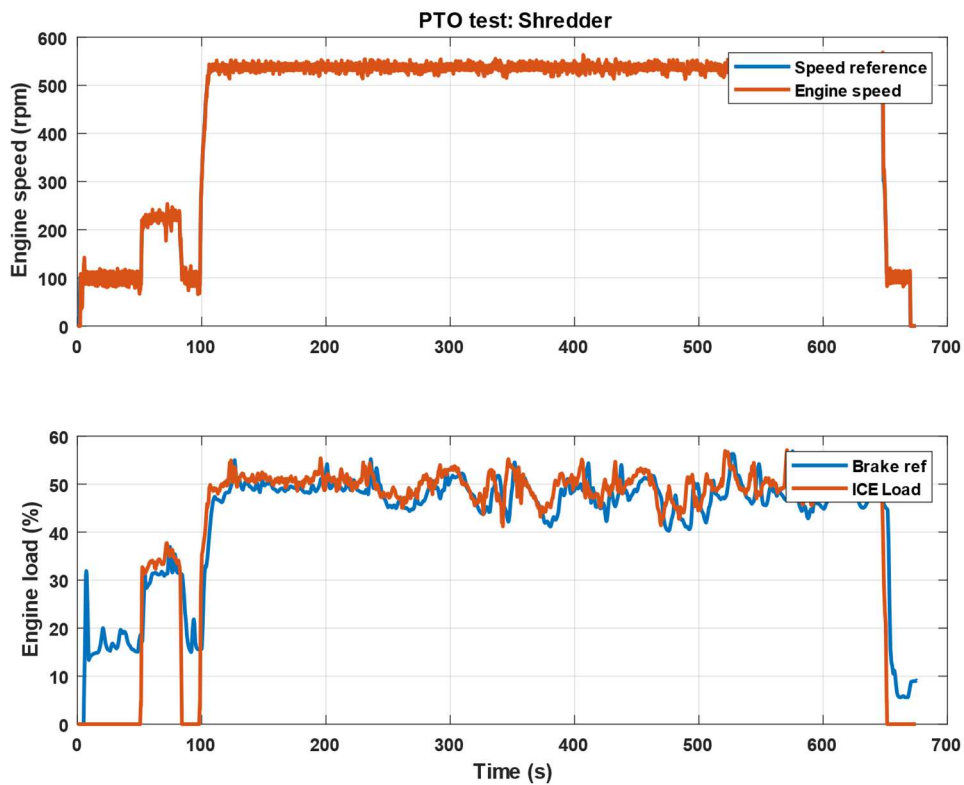


Figure 5.17 Shredder test – Diesel 75 kW (equivalent)

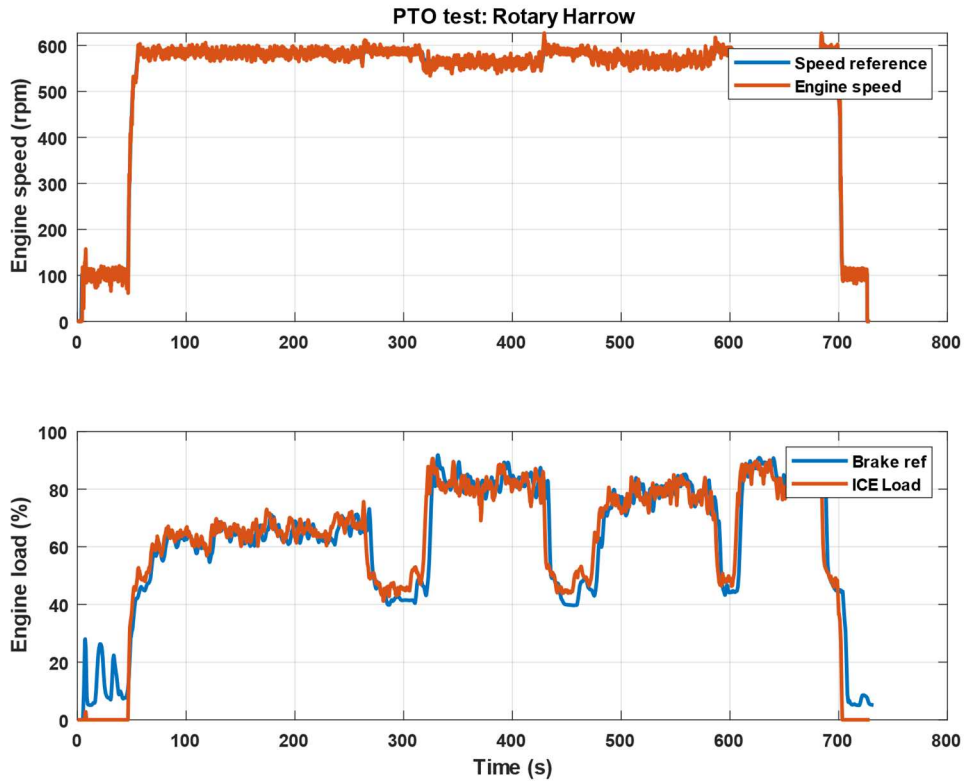


Figure 5.18 Rotary Harrow test – Diesel 75 kW (equivalent)

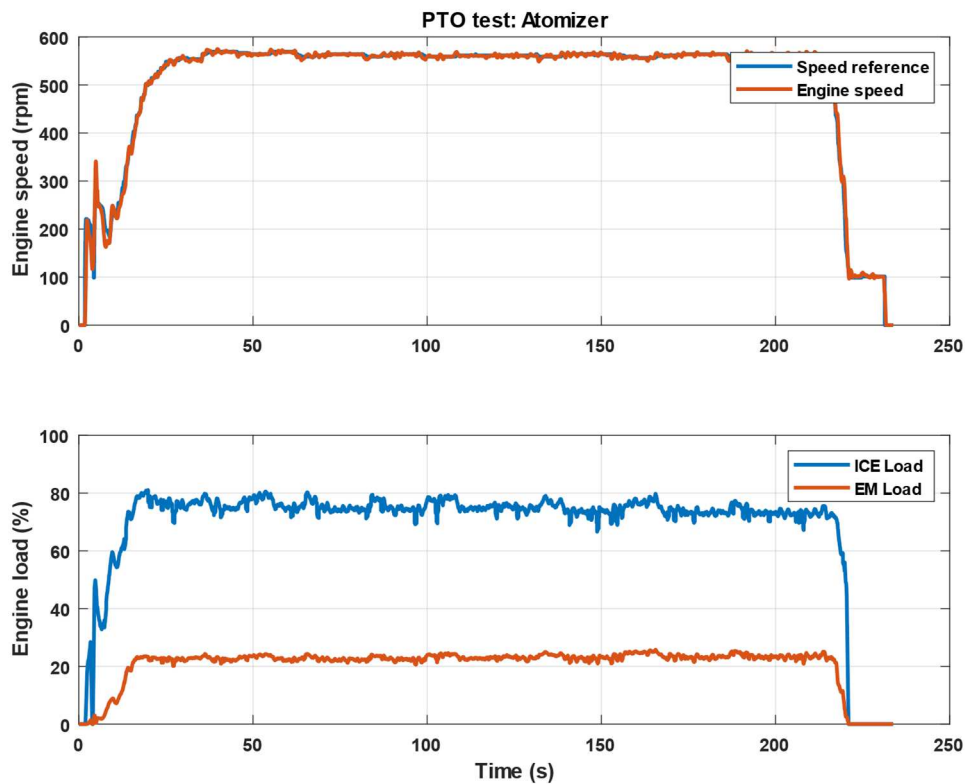


Figure 5.19 Atomizer test – hybrid parallel

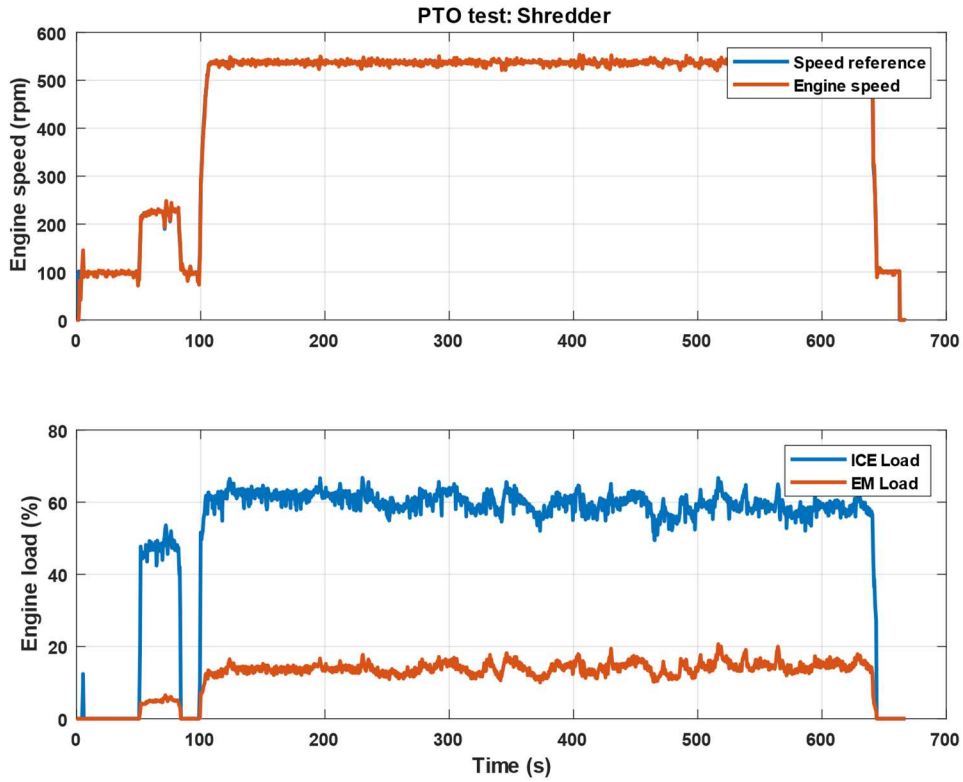


Figure 5.20 Shredder test – hybrid parallel

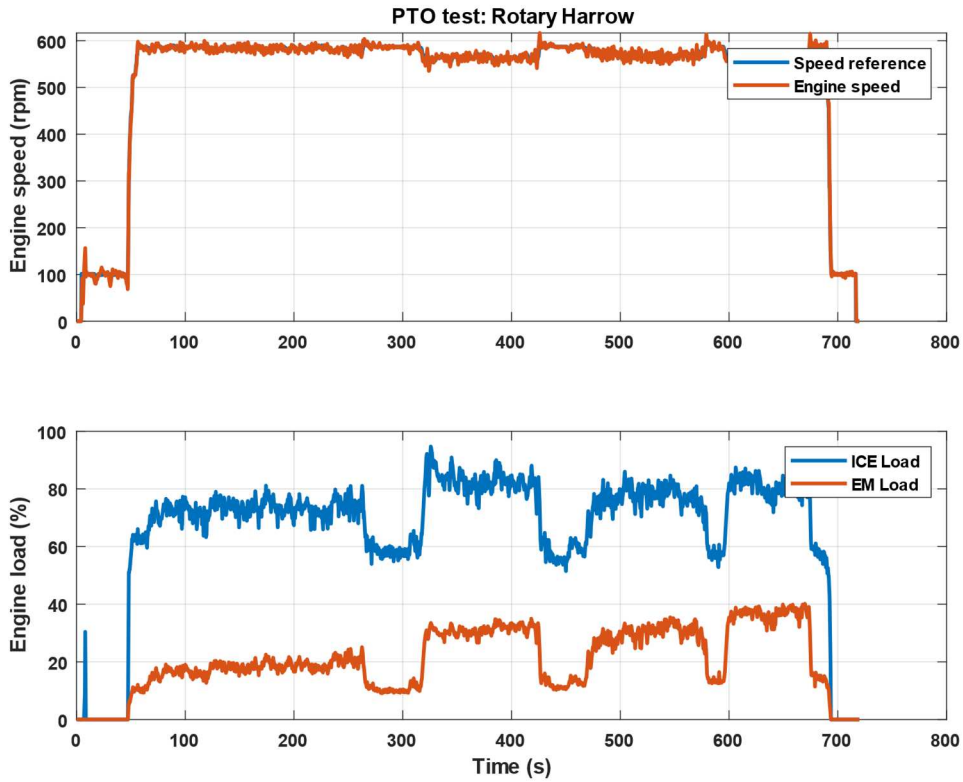


Figure 5.21 Rotary Harrow test – hybrid parallel

5.4 Conclusions

In this chapter the HIL bench developed to test the hybrid architecture for an orchard tractor proposed in the previous chapters was shown. The bench goal was to prove the feasibility of this topology under specific working loads derived from on field measurements. The hybrid architecture consisting of two power sources (the ICE and the EM) was reproduced in a scaled version in the lab (Mechanical level HIL bench). The bench can be considered mechanically equivalent to a hybrid solution to be implemented on a real hybrid tractor since both ICE and EM are actuated to supply power on the same shaft. The HIL bench was mainly meant for proving the feasibility of the Master-Slave control algorithm on real working scenario. This approach allows for plug & play solutions where the electric system is applied to the existing architecture without requiring any changes to the engine ECU control paradigm. The electric system must follow the speed loop of the downsized Diesel engine in order to provide the extra power when needed in those operations where the traditional Diesel engine was highly involved. The Load observer function implemented on the HCU which oversaw EM control, allowed to optimize the electric energy use during the considered working conditions. However, the design of this weighting functions is something that should also consider the overall mechanical system capabilities. The more the battery pack is involved during working operations, the lower would be the engine load but the bigger the capacity would be to fulfil the entire working day. Thus, the best trade off must be found according to most common working scenarios of the machine. Moreover, also with this level of detail it is not possible to optimize the wide range of operations with a single Load observer curve. Thus, the user should be able to choose between different operating modes depending on the specific working task. In some cases, the electric system could be also not necessary thus, it could be completely turned off preserving the battery pack for more demanding tasks as well as its life span. The HIL bench testing activity is mandatory when dealing with such complex system before the real vehicle implementation as also suggested by the system engineering approach. In this case, real hardware implementation allowed to exclude some Load observer curves successfully simulated on the PC but with not satisfactory performance on Real Time systems.

References

- [5.1] INCOSE, “About Systems Engineering”, <https://www.incose.org/about-systems-engineering>.
- [5.2] C. Haskins, “Systems Engineering Handbook - A guide for system life cycle processes and activities”, *INCOSE*, 2006.
- [5.3] NASA, “System Engineering Handbook”, *NASA Center for AeroSpace Information*, 2007.
- [5.4] G. Gaviani, G. Gentile, G. Stara, L. Romagnoli, T. Thomsen, A. Ferrari, “From conception to implementation: A model-based design approach”, *IFAC Proceedings Volumes*, 37(22), 29-34, 2004.
- [5.5] J. Nibert, M. E. Herniter, Z. Chambers, “Model-Based System Design for MIL, SIL, and HIL”, *World Electric Vehicle Journal*, 5, 1121-1130, 2012.
- [5.6] M. Shedeed, M. G. Elshafey, M. Sobh, S. Hammad, “A Mechatronic CAN Based Functional design and verification unified approach”, *IFAC Proceedings Volumes*, 42(19), 450-456, 2009.
- [5.7] National Instruments, “Accelerating the Product Development Lifecycle with Faster Test: Navigating the V Diagram”, 2018. [Online]. Available: <http://www.ni.com/white-paper/54936/en/>, [Accessed: 24- Feb- 2019].
- [5.8] H. Gao, T. Zhang, H. Chen, Z. Zhao, K. Song, “Application of the X in the loop testing method in the FCV hybrid degree test”, *Energies*, 11(2), 433 – 456, 2018.
- [5.9] A. Bouscayrol, “Different types of hardware in the loop simulation for electric drives”, *2008 IEEE International Symposium on Industrial Electronics*, 2008.
- [5.10] D. Ramaswamy, R. McGee, S. Sivashankar, A. Deshpande, J. Allen, K. Rzemien, W. Stuart, “A case study in Hardware In the Loop testing: Development of an ECU for a Hybrid electric vehicle”, *SAE Technical Paper*, 2004.
- [5.11] A. Mouzakitis, D. Copp, R. Parker, K. Burnham, “Hardware In the Loop system for testing automotive ECU diagnostic software”, *Measurement and Control*, 42(8), 238-245, 2009.
- [5.12] P. Waeltermann, “Hardware In the Loop: the technology for testing electronic controls in vehicle engineering”, www.dspace.com.
- [5.13] Speedgoat, AGCO “Fendt Automated testing of tractor controllers using Hardware in the Loop test benches”, www.speedgoat.com.
- [5.14] S. Raikwar, L.J. Wani, S. A. Kumar, M. S. Rao, “Hardware In the Loop test automation of embedded systems for agricultural tractors”, *Measurement*, 133, 271-280, 2019.
- [5.15] L. Wang, Y. Zhang, C. Yin, H. Zhang, C. Wang, “Hardware In the loop simulation for the design and verification of the control system of a series parallel hybrid electric city bus”, *Simulation Modelling Practice and Theory*, 25, 148-162, 2012.
- [5.16] A. Bouscayrol, W. Lhomme1, P. Delarue1, B. Lemaire-Semail1, S. Aksas “HIL simulation of electric vehicle traction systems using energetic Macroscopic representation”, *IECON 2006 - 32nd Annual Conference on IEEE Industrial Electronics*, 2006.
- [5.17] C. Mayet, P. Delarue, A. Bouscayrol, “Hardware In the Loop simulation of traction power supply for power flows analysis of multi-train subway lines”, *IEEE Transaction on Vehicular Technology*, 66 (7), 5564-5571, 2017
- [5.18] S. Lee, J. Cherry, B. Lee, J. McDonald et al., "HIL Development and Validation of Lithium-Ion Battery Packs," *SAE Technical Paper*, 2014.

- [5.19] F. Mocera, E. Vergori, A. Somà, “Study of battery performance with Hardware In the Loop simulation of a working vehicle”, 2018 Thirteenth International Conference on Ecological Vehicles and Renewable Energies (EVER), 2018.
- [5.20] F. Mocera, A. Somà, “Study of a Hardware-In-The-Loop bench for hybrid electric working vehicles simulation”, *2017 Twelfth International Conference on Ecological Vehicles and Renewable Energies (EVER)*, 2017.
- [5.21] C. Lin, L Zhang, “Hardware In the Loop simulation and its application in electric vehicle development”, *IEEE Vehicle Power and Propulsion Conference (VPPC)*, 2008.
- [5.22] L. Gauchia, J. Sanz, “Hardware In the Loop simulation platform for energy systems in hybrid electric vehicles”, *2008 IEEE International Symposium on Industrial Electronics*, 2008.
- [5.23] H. Zhang, Y. Zhang, C. Yin, “Hardware In the Loop simulation of robust mode transition control for a series parallel hybrid electric vehicle”, *IEEE Transactions on Vehicular Technology*, 65(3), 1059-1069, 2016.
- [5.24] Y. Zhang, S. Lu, Y. Yang, Q. Guo, “Internet distributed Vehicle In the loop simulation for HEVs”, *IEEE Transactions on Vehicular Technology*, 67(5), 3729-3739, 2018.
- [5.25] A. Abdelrahman, K.S.Algarny, M.Z. Youssef, “A novel platform for powertrain modelling of electric cars with experimental validation using Real Time Hardware In the Loop”, *IEEE Transactions on Power Electronics*, 33(11), 9762-9771, 2018.
- [5.26] P. Fajri, R. Ahmadi, M. Ferdowsi, “Control approach based on equivalent vehicle rotational inertia for motor dynamometer test bench emulation of electric vehicles”, *2013 International Electric Machines & Drives Conference*, 2013.
- [5.27] F. Mocera, A. Somà, “Working Cycle requirements for an electrified architecture of a vertical feed mixer vehicle”, *Procedia Structural Integrity*, 2018.
- [5.28] ISO 11898-1:2015, “Road vehicles -- Controller area network (CAN) -- Part 1: Data link layer and physical signalling”, 2014.
- [5.29] W. Voss, “A Comprehensible Guide to Controller Area Network”, Copperhill Technologies Corporation, 2005.
- [5.30] SAE Standard J1939, “Serial control and communications heavy duty vehicle network – Top level document”, SAE International, 2012.
- [5.31] W. Voss, “A Comprehensible Guide to J1939”, Copperhill Technologies Corporation, 2008

Conclusions and future works

In this work the design of a hybrid architecture for an orchard tractor and its control logic was discussed. The idea started from the general need of new powertrain architectures that is involving all the industrial fields of working machines. To meet new regulations on pollutant emissions and provide machines able to perform as well as the traditional ones, the scientific community and industrial research and development groups are focusing the attention on new architectures based on full electric or hybrid electric topologies. The reason relies on the possibility of downsizing, or eliminate in some special cases, traditional Internal Combustion Diesel Engines. As discussed in Chapter 1, these power units represented the state of the art for industrial machines propulsion because of their efficiency and reliability. However, performance come at the price of high pollutant emissions especially in terms of NO_x and Particulate Matter. This is the reason why in the last decade several gas after-treatment systems have been widely adopted to meet regulations on the amount of pollutants measured at the outlet pipe. However, the Stage V regulation will define new stricter thresholds which will lead to bigger after-treatment systems. The volume they occupy is essentially dead volume in terms of on-board capabilities, because no extra-features are added from the productivity point of view. Thus, new solutions that will use the same volume but adding new capabilities would rather be appreciated.

The hybrid electric architecture proposed in this thesis for an orchard tractor is the result of comprehensive review of the actual state of the art of two major topics: a comprehensive review of what was already been proposed in the industrial field in terms of topologies to understand pros and cons of the solutions when applied in specific fields of applications; a review of energy storage solutions to understand the actual capabilities of such systems both in terms of performance capabilities and design constraints. These reviews were the starting points for the development of the two mathematical models proposed in Chapters 3 and 4. First, the mathematical model of a Lithium-Ion cell was developed by mean of a Dual Polarization Equivalent Circuit Model integrated with a thermal model of the battery used to correct online cell parameters due to the effects of temperature. The proposed model was characterized with a set of standard testing activities proposed in literature. However, to the author opinion these standard procedures (derived from the automotive field) should be fully discussed in future works. When it comes to the application on working machines, battery packs would be affected by different working loads and external conditions, thus automotive derived testing procedures may be not representative enough.

The battery model developed in Chapter 3 was then used in Chapter 4 within the hybrid electric model of the orchard tractor. The activity discussed in Chapter 4 started from the on-field measurements of the traditional tractor performance. Using data derived from the Diesel engine output on the CAN BUS line of the vehicle, it was possible to characterize its working load during some representative daily activities. The proposed parallel hybrid electric architecture should have performed at least as the traditional architecture from which measurements were derived. The

proposed hybrid system considered a downsized Diesel engine with an auxiliary electric motor to provide the extra power when required. In this way the engine size resulted optimized compared to the standard work load of the machine. In case an extra power demand, the electric motor could help using the electric energy stored in the battery pack. The control algorithm developed was focused on the concept of a plug and play solution which could easily adapt to off the shelf components in terms of traditional diesel engines. The logic behind the control strategy consisted of a Load Observer function. Looking at the actual engine load, its main goal was to preserve as much as possible the electric energy used in order to keep the thermal engine as primary energy source due to its faster refuelling. Moreover, this approach would use in a more effective way the full power capabilities of the engine that would no more be oversized. The proposed architecture was simulated with the same working loads of the traditional tractor modelled in order to compare the overall results for given workloads. In all the simulated scenarios an improvement in the efficiency of the operations was highlighted. Moreover, once the architecture was defined and validated, a set of possible daily working cycles were defined and analysed to find the best solution in terms of on-board storage capacity to meet a full day activity.

Finally, the proposed architecture was replicated and tested in a Hardware-In-the-Loop bench configuration as discussed in Chapter 5. The architecture was replicated both in terms of physical and electrical component involved as well as of control architecture. In fact, a dedicated CAN BUS protocol was developed to simulate the real control scenario where actuation commands would be constrained to specific periodic messages defined by a standard protocol which affects the controller parameters design process. The complete architecture was tested according to three working scenarios derived from the analysis performed in Chapter 4. Specific software was developed both to control each single motor controller as well as to replicate the driver behaviour during working conditions. What was highlighted from the experimental activity was the need for different Load Observers maps in order to optimize very different working scenarios. Sometimes, these tractors are oversized for most of the daily activities. What was highlighted from the experimental measurements was the possibility to use just the downsized engine for most of the common activities. Thus, if two or more Load Observer functions could be used for low and high-power applications (chose both automatically or manually according to the user preferences) a higher level of performance optimization could be easily reached. The bench highlighted and proved the possibility to cover with the new architecture peak performance of the traditional system, optimizing electric energy performance according to the instantaneous working load of the diesel engine.

The activity done in this Doctoral Thesis starts from a real need for more efficient and functional powertrain architectures. The proposed solution of the hybrid orchard tractor was developed considering the possibility to adapt this new hybrid power unit to a traditional vehicle architecture with the lowest possible impact on the vehicle layout. However, if the motor and its power electronic unit do not have a high impact on the machine layout, the battery pack integration would

require a considerable amount of on-board volume that surely would require some mechanical redesign of the chassis. The proposed working cycles highlighted a certain amount of capacity to accomplish certain scenarios. However, the proposed scenarios can be seen as the worst case ones. Thus, for more light duty applications, a higher level of battery pack size optimization could be achieved. Moreover, if a higher power engine is used, the same control logic could reduce the amount of emissions and the total battery size if proper Load Observer functions would be designed. Thus, future works need to investigate how the combination of high power engines and electric machines would affect emissions without the use of special gas after-treatment systems. It is reasonable to think that the quicker response and flexibility of an electric machine could help in reducing pollutant emission especially in transient operations where Diesel engines perform the worst. Moreover, the proposed architecture was chosen as the most practical to be implemented on an existing mechanical layout due to the low number of elements involved. However, if a higher level of freedom in terms of layout is possible, the series architecture should be also investigated. Several advantages would derive from this type of architecture at the price of a more complex layout and control strategy. As an example, decoupling the driveline from the engine higher efficiency level could be achieved and most importantly, a lower number of gears would be required. In some cases, the gearbox could be totally replaced leading to a natural eCVT configuration.

